

For Reference

NOT TO BE TAKEN FROM THIS ROOM

Ex LIBRIS
UNIVERSITATIS
ALBERTAENSIS



THE UNIVERSITY OF ALBERTA

RELEASE FORM

NAME OF AUTHOR Ekwere J. Peters

TITLE OF THESIS Stability Theory and Viscous Fingering in
..... Porous Media

DEGREE FOR WHICH THESIS WAS PRESENTED Ph.D., Petroleum Engineering

YEAR THIS DEGREE GRANTED 1979

Permission is hereby granted to THE UNIVERSITY OF ALBERTA LIBRARY to reproduce single copies of this thesis and to lend or sell such copies for private, scholarly or scientific research purposes only.

The author reserves other publication rights, and neither the thesis nor extensive extracts from it may be printed or otherwise reproduced without the author's written permission.

THE UNIVERSITY OF ALBERTA

STABILITY THEORY AND VISCOUS FINGERING IN POROUS MEDIA

by



EKWERE J. PETERS

A THESIS

SUBMITTED TO THE FACULTY OF GRADUATE STUDIES AND RESEARCH
IN PARTIAL FULFILMENT OF THE REQUIREMENTS FOR THE DEGREE
OF DOCTOR OF PHILOSOPHY

IN

PETROLEUM ENGINEERING

DEPARTMENT OF MINERAL ENGINEERING

EDMONTON, ALBERTA

SPRING, 1979

THE UNIVERSITY OF ALBERTA
FACULTY OF GRADUATE STUDIES AND RESEARCH

The undersigned certify that they have read, and recommend to the Faculty of Graduate Studies and Research for acceptance a thesis entitled "Stability Theory and Viscous Fingering in Porous Media", submitted by Ekwere J. Peters in partial fulfilment of the requirements for the degree of Doctor of Philosophy in Petroleum Engineering.

ABSTRACT

Viscous fingering during immiscible displacement in porous media was studied as a problem of hydrodynamic stability to determine the range of displacement parameters for which the usual mathematical predictions of immiscible displacements may be undertaken with confidence. The necessary and sufficient conditions for the onset of instability were derived by perturbation theory. The resulting theoretical stability boundaries were verified by adverse mobility ratio displacements in cylindrical cores in the presence and absence of connate water saturation. Measurements conducted on the viscous fingers, which were successfully photographed with the aid of a fluorescent displacing water, permitted the estimation of the capillary parameter required for the quantitative prediction of the onset of instability.

Experimentally, instability, indicated by viscous fingering, was observed both in the presence and absence of connate water saturation. However, for the same fluids and porous media, the phenomenon occurred at a much lower rate in the absence of connate water than in the presence of connate water saturation. In both systems, the onset of instability was attended by a noticeable decline in the breakthrough oil recovery.

Theoretically, instability will occur whenever certain universal dimensionless groups exceed their critical values. In cylindrical and rectangular systems, the stability boundaries

are given by the inequalities:

$$\frac{(M - 1)(V - V_c)\mu_w D^2}{C^* \sigma K_{wr}} \leq 13.56$$

and

$$\frac{(M - 1)(V - V_c)\mu_w L_x^2 L_y^2}{C^* \sigma K_{wr} (L_x^2 + L_y^2)} \leq 9.87$$

In applying the stability tests, the velocities should be in cm/sec, viscosities in poise, lengths in cm, interfacial tensions in dynes/cm and permeabilities in cm². For the particular porous medium and fluids used in this study, the capillary constant, C*, was estimated as 5.45 in the absence of connate water saturation and 306.25 in the presence of connate water saturation.

ACKNOWLEDGEMENTS

The author acknowledges with gratitude the encouragement and guidance provided by Dr. D. L. Flock, who supervised this study.

Acknowledgements are also made to Dr. R. G. Bentsen, for his helpful comments and suggestions throughout the study; to Mr. G. T. Walsh, who designed the coreholders used in the experiments; to Mr. H. Schroeder, who processed the photographs taken during the course of the study; to Mrs. R. Mei, who typed the manuscript; and to AOSTRA and the Petroleum Aid to Education Fund, for their financial support.

Finally, the author is grateful to his wife, Unwa, and daughter, Eno, for providing the congenial family atmosphere that contributed to the successful completion of this study.

TABLE OF CONTENTS

CHAPTER	PAGE
1. INTRODUCTION	1
1.1 The Nature of the Problem	1
1.2 Notions of Stability Theory	3
1.3 Purpose and Scope of the Study	7
1.4 Organization of the Report	9
2. THEORY OF IMMISCIBLE DISPLACEMENT AND MODEL SCALING . .	12
2.1 Immiscible Displacement Equations	12
2.1.1 Darcy's Law for Two-Phase Flow	12
2.1.2 Continuity Equations	13
2.1.3 Other Equations	13
2.1.4 Homogeneous Incompressible Fluids	14
2.1.5 Saturation Equation	16
2.1.6 Fractional Flow Formula	18
2.1.7 Dimensionless Form of the Displacement Equations	18
2.1.8 One-Dimensional Displacement	22
2.1.9 Displacement Equation with Fractional Flow as Dependent Variable	23
2.1.10 Displacement Equation with Distance as Dependent Variable	26
2.2 Pertinent Solutions of the Displacement Equations	27
2.2.1 Unperturbed Saturation and Breakthrough Recovery Profiles	27

CHAPTER	PAGE
2.2.2 Buckley-Leverett Solution	31
2.3 Model Scaling	32
2.3.1 General	32
2.3.2 Scaling Principles for Immiscible Displacements	32
3. REVIEW OF RELATED RESEARCH	41
4. STABILITY THEORIES OF IMMISCIBLE DISPLACEMENT IN POROUS MEDIA	66
4.1 General	66
4.2 Stability Theory of Buckley-Leverett Displacements	66
4.2.1 Perturbation Equation for Fractional Flow	66
4.2.2 Lagrangian Formulation	68
4.2.3 Solution of the Linearized Fractional Flow Equation	71
4.2.4 Solution of the Linearized Lagrangian Equation	76
4.2.5 The Effects of Rate and Mobility Ratio on the Stability Problem	80
4.2.6 Summary	80
4.3 Extension of the Stability Theory of Chuoque et al	81
4.3.1 Cylindrical Systems	81
4.3.2 Rectangular Systems	87

CHAPTER	PAGE
4.3.3 Summary	87
5. EXPERIMENTAL EQUIPMENT AND PROCEDURE	89
5.1 Porous Media	89
5.2 Fluids	89
5.3 Pumping System	91
5.4 Pressure Recording System	91
5.5 Displacement Procedure	94
5.6 Retrieval and Photography of Core-Sections	95
6. EXPERIMENTAL RESULTS AND OBSERVATIONS	96
6.1 General	96
6.2 Displacement Records	100
6.2.1 No Connate Water Present	101
6.2.2 Connate Water Present	117
6.3 Breakthrough Recovery Data	130
6.3.1 Connate Water Present	130
6.3.2 No Connate Water Present	133
6.4 Quantitative Predictions	133
6.4.1 Estimation of C , C^* and σ^*	133
6.4.2 Estimation of the Finger Wavelength for Run 24	140
6.4.3 Prediction of the Onset of Instability	140
6.5 Scaling in the Presence of Viscous Fingering	142
6.6 Other Results	148
7. DISCUSSION	152
7.1 Stability Theories	152
7.1.1 The Buckley-Leverett Model	152

CHAPTER	PAGE
7.1.2 Extended Theory of Chuoke et al	154
7.2 Experimental Verification	157
7.2.1 Estimation of System Parameters	157
7.2.2 Prediction of the Onset of Instability	159
7.2.3 Qualitative Considerations	162
7.3 Model Scaling	165
7.4 Connate Versus Nonconnate Water Bearing Systems	168
7.5 Other Results	169
8. CONCLUSIONS AND RECOMMENDATIONS	172
8.1 Summary and Conclusions	172
8.2 Practical Application of the Results	174
8.3 Suggestions for Further Studies	175
* * *	
REFERENCES	177
BIBLIOGRAPHY	180
APPENDIX A. NUMERICAL SOLUTION OF IMMISCIBLE DISPLACEMENT EQUATIONS	185
APPENDIX B. RHEOLOGICAL PROPERTIES OF MODEL FLUIDS	208
APPENDIX C. COMPUTER PROGRAM FOR PROCESSING PRESSURE RECORDS FROM PAPER TAPE	211
APPENDIX D. RECOVERY AND PRESSURE DATA FOR RUNS 14 AND 28	214
APPENDIX E. EXPERIMENTAL RESULTS FROM THE LITERATURE	228

LIST OF TABLES

TABLE		PAGE
4.1	Zeros of Bessel Function, $J'_m(x)$	83
5.1	Fluid Properties at 21.5°C	90
6.1	Summary of Displacement Data with Connate Water Saturation	98
6.2	Summary of Displacement Data without Connate Water Saturation	99
6.3	Measured Finger Wavelengths - Run 23	138
6.4	Measured Finger Wavelengths - Run 11	139
6.5	Measured Wavelengths in CM - Run 24	141
6.6	Comparison of Onset of Instability in the Presence and Absence of Connate Water Saturation at a Viscosity Ratio of 102.5	142
A1	Saturation Profile at a Dimensionless Time of 0.1	195
A2	Saturation Profile at a Dimensionless Time of 0.2	197
A3	Saturation Profile at a Dimensionless Time of 0.3	199
A4	Saturation Profile at a Dimensionless Time of 0.4	201
A5	Saturation Profile at a Dimensionless Time of 0.5	203
A6	Saturation Profile at a Dimensionless Time of 0.6	205
A7	Breakthrough Recovery Predicted by One-Dimensional Numerical Simulator	207
B1	Summary of Viscometer Tests	209
B2	Verification of Darcy's Law	210
D1	Production History - Run 14	215
D2	Pressure History - Run 14	216
D3	Production History - Run 28	221
D4	Pressure History - Run 28	222

		PAGE
D5	Estimation of Flood Front Arrival at the Pressure Transducer	227
E1	Experimental Results from Wiborg (32)	229
E2	Experimental Results from Baird (33)	230
E3	Experimental Results from de Haan (30)	231

LIST OF FIGURES

FIGURE		PAGE
2.1	Typical Relative Permeability Curves	15
2.2	Typical Capillary Pressure Curve	15
2.3	Normalized Relative Permeability Curves	20
2.4	Normalized Capillary Pressure Curve	20
2.5	Typical Saturation Profiles Generated by One-Dimensional Numerical Simulator	29
2.6	Typical Recovery Behaviour Generated by One-Dimensional Numerical Simulator	30
2.7	Stationary Solution of the Fractional Flow Equation	33
5.1	Rheological Properties of Model Fluids	92
5.2	Verification of Darcy's Law	93
6.1	Model and Prototype Recoveries as Correlated by the Linear Scaling Coefficient. Connate Water Present	131
6.2	Model and Prototype Recoveries as Correlated by the Radial Scaling Coefficient. Connate Water Present	132
6.3	The Effect of Viscosity Ratio on Recovery. Connate Water Present	134
6.4	Model and Prototype Recoveries as Correlated by the Linear Scaling Coefficient. No Connate Water Present	135
6.5	Model and Prototype Recoveries as Correlated by the Radial Scaling Coefficient. No Connate Water Present	136
6.6	The Effect of Viscosity Ratio on Recovery. No Connate Water Present	137
6.7	Predicted Onset of Instability	143
6.8	Scaling Requirements for Instability. No Connate Water Present	144
6.9	Proposed Scaling Requirements for Instability. No Connate Water Present	145

	PAGE
6.10 Scaling Requirements for Instability. Connate Water Present	146
6.11 Scaled Onset of Instability	147
6.12 The Effect of Viscous Fingering on Oil Recovery History	149
6.13 Effect of Viscous Fingering on Frontal Movement Through Displacement System	151
7.1 Prediction of the Onset of Instability in the Studies by Wiborg (32) and Baird (33)	160
7.2 Prediction of the Onset of Instability in the Study by de Haan (30)	163
7.3 Comparison of Recovery Performance at Favourable Viscosity Ratios	170

LIST OF PHOTOGRAPHIC PLATES

PLATE		PAGE
6.1	Displacement Record, Run 20, No Connate Water Q = 2.5 cc/hour, Viscosity Ratio = 102.5	102
6.2	Displacement Record, Run 23, No Connate Water Q = 40 cc/hour, Viscosity Ratio = 102.5	105
6.3	Displacement Record, Run 24, No Connate Water Q = 200 cc/hour, Viscosity Ratio = 102.5	108
6.4	Displacement Record, Run 26, No Connate Water Q = 480 cc/hour, Viscosity Ratio = 102.5	111
6.5	Displacement Record, Run 27, No Connate Water Q = 1120 cc/hour, Viscosity Ratio = 102.5	114
6.6	Displacement Record, Run 33, No Connate Water Q = 10 cc/hour, Viscosity Ratio = 0.92	118
6.7	Displacement Record, Run 35, No Connate Water Q = 1120 cc/hour, Viscosity Ratio = 0.92	121
6.8	Displacement Record, Run 1, Connate Water Present Q = 2.5 cc/hour, Viscosity Ratio = 102.5	124
6.9	Displacement Record, Run 11, Connate Water Present Q = 1120 cc/hour, Viscosity Ratio = 102.5	127

NOMENCLATURE

A	System cross-sectional area
a	Core radius
C	Chuoque's constant
C^*	Constant of proportionality between the effective and the measured interfacial tensions
c_1, c_2	Signed principal curvatures of macroscopic interface
D	Core diameter
\vec{f}_w	Fractional flow vector
\bar{f}_w	Stationary fractional flow function
f_w^*	Fractional flow perturbation
g	Gravitational acceleration
IOIP	Initial oil in place
J	Leverett function
K	Absolute permeability
K_O^*	Normalizing permeability in the oil phase
K_W^*	Normalizing permeability in the water phase
K_{ro}	Relative permeability to oil
K_{rw}	Relative permeability to water
K_{or}	Permeability to oil at connate water saturation
K_{wr}	Permeability to water at residual oil saturation
L	Characteristic system length
L_x	Length in the x-direction
L_y	Length in the y-direction
M	End point mobility ratio
N_c	Ratio of capillary to viscous forces

N_g	Ratio of gravitational to viscous forces
n	Stability index
P_c	Capillary pressure
P_o	Pressure in the oil phase
P_w	Pressure in the water phase
p^*	Pressure perturbation
p	Perturbed pressure
Q	Volumetric injection rate
$R(r)$	Separated velocity potential
r	Radial coordinate
r_D	Dimensionless radial coordinate
S	Normalized water saturation
S_f	Normalized water saturation at the front
S_o	Oil saturation
S_{or}	Residual oil saturation
S_w	Water saturation
S_{wi}	Initial or connate water saturation
$T(t)$	Separated velocity potential
t	Real time
t_D	Dimensionless time
u_r, u_θ, u_x	Dimensionless velocities in the r, θ and x - directions of cylindrical coordinates
\vec{u}	Total superficial velocity vector
\vec{u}_o	Superficial velocity vector in the oil phase
\vec{u}_w	Superficial velocity vector in the water phase
u_x^*, u_y^*, u_z^*	Velocity perturbations in the x, y and z - directions of rectangular cartesian coordinates

V	Superficial velocity of the unperturbed interface
V_c	Critical superficial velocity
X, Y, Z	Dimensionless x, y and z - distances of rectangular cartesian coordinates
x, y, z	Rectangular cartesian coordinates
\bar{X}	Stationary solution of the displacement equation
X^*	Displacement perturbation
$X(x)$	Separated velocity potential
$Y(y)$	Separated velocity potential
$Z(z)$	Separated velocity potential
α	Angle system makes with the vertical
α_x	Eigenvalue or x -directed wave number
α_y	Eigenvalue or y -directed wave number
γ	Eigenvalue or wave number
η	Frontal perturbation
$\theta(\theta)$	Separated velocity potential
θ	Angular direction in cylindrical coordinates
$\cos\theta$	Cosine of oil-water contact angle measured through the water phase
λ	Wavelength of Fourier component of disturbance
λ_c	Critical wavelength of disturbance
λ_m	Most probable wavelength of disturbance
μ_o	Oil viscosity
μ_w	Water viscosity
π	3.14159...
ρ_o	Oil density
ρ_w	Water density

$\Delta\rho$	Water-oil density difference
Σ	Summation
σ	Water-oil interfacial tension
σ^*	Effective or pseudo-interfacial tension
τ	Normalized dimensionless time
Φ	Perturbed velocity potential
ϕ	Porosity

CHAPTER 1

INTRODUCTION

1.1 THE NATURE OF THE PROBLEM

The displacement of one fluid by another in a porous medium forms the basis of most enhanced oil recovery processes in the petroleum industry. Whether it be a waterflood, a steamflood, a polymerflood, or a surfactantflood, in every case, one fluid is called upon to displace another in an efficient manner.

Frequently, the displacing fluid is less viscous than the displaced fluid. This arrangement has long been recognized as unfavourable to the displacement efficiency. In addition to this inherent inefficiency, the less viscous displacing fluid may "shoot" through the porous medium in the form of macroscopic fingers, grossly bypassing the resident fluid, thus resulting in a general impairment of the displacement effort. This channelling phenomenon, which is distinct from that which may be legitimately attributed to permeability stratification or other gross inhomogeneities in the system, has come to be known as viscous fingering.

Although it is generally recognized that an adverse viscosity ratio is a necessary condition for viscous fingering, it is by no means a sufficient condition. Other factors, such as the displacement rate, the gravitational forces, the capillary forces and even the system geometry play some role in the occurrence of the phenomenon. The complex interaction of these variables to create viscous fingering has historically been studied using stability

concepts, following the identification of fingering as a form of hydrodynamic instability by Engelberts and Klinkenberg (1).

Instability raises several practical and theoretical concerns. Viscous fingering results in the premature breakthrough of the displacing fluid, creating in effect a pipeline from the injection to the production point. At the theoretical level, instability would seriously undermine the validity of the mathematical predictions of the displacement behaviour. Although the numerical solutions of the equations of immiscible displacement have been perfected in recent years, the forecasts from these solutions will be seriously in error if the displacements being modelled are unstable. Furthermore, the conventional scaling procedure based on the assumptions of stable displacements may no longer be sufficient to relate laboratory results to field prototypes in the presence of instability.

A systematic study that would result in the identification of the stability boundaries during immiscible displacements will therefore be of practical and theoretical value. First, it will provide guidance on the choice of displacement parameters to ensure a stable and efficient displacement. Second, it will delineate the region of flood operation within which the mathematical predictions may be applied with confidence. Finally, such a study would lead to universal scaling groups that will permit the prediction of prototype behaviour using model results in the face of instability. The identification of the stability boundaries during immiscible displacements forms the broad objective of the present study.

1.2 NOTIONS OF STABILITY THEORY

Although no universal definition of stability exists, a common theme seems to permeate all stability definitions. It is the quality of being immune to small disturbances (2). For example, certain flow patterns in hydrodynamics which are possible in theory are often unrealizable in practice over certain ranges of flow parameters because of their inability to sustain themselves against the small but inevitable disturbances that occur in physical systems. Such flows are therefore classified as unstable. It is with the differentiation of the stable from the unstable configurations of the permissible mode of operation that stability theory is concerned (3).

A stability analysis is usually motivated by the observation that the mathematical model of the process being studied appears to correlate well with the physical process over some range of the system parameters, but fails to do so at others. Stability theory then assumes that the potential for this departure of the physical process from the mathematical prediction is inherent in the governing mathematical equations and may be revealed by an appropriate stability analysis. Stability analysis therefore seeks to bridge the gap between theory and reality when both appear to be at odds.

The steps involved in conducting a stability analysis using perturbation concepts may be summarized as follows (4). First, an unperturbed state whose stability is being studied is specified. This will be in the form of a mathematical model of the functioning of the system under consideration. In the displacement of one fluid by another in porous media, the unperturbed behaviour is generally

modelled by systems of nonlinear partial differential equations. Next, the system is disturbed slightly from the unperturbed state, and the subsequent behaviour of the disturbance or perturbation observed over the course of time. Mathematically, this amounts to deriving the differential equations of perturbative terms introduced into the dependent variables of the partial differential equations of the unperturbed system, and studying the behaviour of their solutions over the course of time. Finally, the stability conclusion is drawn based on the behaviour of the perturbations. If the perturbations grow with time and become unbounded, then the unperturbed system is unstable. If the perturbations are damped with time, then the unperturbed system is stable. If the perturbations neither grow nor die out during the course of time, then a state of neutrality exists.

In some situations, there is often a close correspondence between the physical and mathematical aspects of the stability analysis. In such situations, both the unperturbed state and the perturbations take on concrete physical meanings. For example, it is easy to appreciate the growth of a perturbation leading to instability when a cone balanced on its apex tumbles to its side when slightly disturbed. In more complex situations, such as flow through porous media, the correspondence between the mathematical and the physical aspects of the stability analysis is not as close. One has to stretch one's imagination to appreciate the significance of a pressure, a velocity, a fractional flow or a saturation perturbation. In these situations, the stability analysis often

unavoidably takes on the appearance of an exercise in mathematical manipulations, which may seem to have little to do with a physical process. Be this as it may, the stability analysis is still valid. The connection between the mathematical analysis and instability in the real system is preserved inasmuch as the equations from which the stability analysis originates constitute an adequate model of the physical process. In simple as well as complex systems, instability must of course be signalled by a recognizable physical symptom in the real process. In the previous example, the cone will fall on its side catastrophically to signal instability whereas in the case of displacements in porous media, viscous fingers will develop as a mark of instability.

The steps involved in conducting a stability analysis are easy to state but difficult to implement. This is because the resulting perturbation equations are usually highly nonlinear and as such are not easily amenable to analytical solutions. It is therefore often mathematically expedient to assume that the perturbations are infinitesimally small so that nonlinear terms may be neglected. This approximation results in a linear stability theory in contrast to a nonlinear theory which attempts to allow for finite perturbations. The linearized perturbation equations can then easily be transformed into an eigenvalue problem, the behaviour of the solution of which determines the stability classification. The result of the stability analysis is usually stated in the form that when certain critical values of the pertinent parameters are exceeded, the process becomes unstable and its behaviour can no

longer be adequately predicted by the existing mathematical model.

In the linear stability theory, certain terms of the original perturbation equations are neglected and the question naturally arises as to the influence of this approximation on the stability conclusion. For example, could the nonlinear terms, if retained, have reversed the stability conclusion? Lin (5) does not think so. It is clear that the conclusion cannot be reversed in the case in which the process is judged stable, for in this case, the infinitesimal perturbations become smaller still and as a result the assumption that led to the neglect of nonlinear terms remains valid throughout in time. In cases involving instability, Eckhaus (6) maintains that the nonlinear terms only serve to limit the growth of the perturbations to some finite magnitude, thus resolving the apparent contradiction of unbounded growth of an infinitesimal perturbation that is a common feature of the linear theory. A linear theory is therefore adequate if the objective is that of mere stability classification whereas a nonlinear theory would be necessary if the purpose is to predict the ultimate stationary character of the perturbations.

A number of stability theories have been proposed in the literature in an attempt to derive the conditions that promote instability and viscous fingering during immiscible displacement in porous media (7, 8, 9, 10). Of these, the theory of Chuoke, van Meurs and van der Poel (7) is considered the most authoritative. A major assumption of this theory and others is that of piston-like displacement. Yet the accepted mathematical model of immiscible

displacement in petroleum reservoirs, hereafter referred to as the Buckley-Leverett model (11), indicates that under conditions of adverse viscosity ratios in which viscous fingering is likely to occur, the displacement is anything but piston-like. These theories would therefore seem to be founded upon a doubtful model of the unperturbed process. The applicability of the theory of Chuoke et al. (7) even to the Buckley-Leverett type of displacement has not been fully explored. Instead, a few attempts have been made to derive the stability criteria based on the Buckley-Leverett equations, attempts that have only met with partial success due to mathematical difficulties (12, 13).

Furthermore, the experimental results of Chuoke et al. (7) indicated good agreement between their theory and observations in Hele-Shaw models and in porous media without connate water saturation. However, the experimental verification of their theory in porous media with connate water, which are more representative of petroleum reservoirs, was cursory and the results inconclusive. Also, since no clear stability boundaries emerged from their study, their results have not provided the much needed practical guidance to combat instability or even to predict its occurrence.

1.3 PURPOSE AND SCOPE OF THE STUDY

The identification of the stability boundaries during immiscible displacements was the broad objective of this study. Specifically, the purpose of the study was

- 1) to extend the theory of Chuoke et al. (7) in order to predict the onset of instability and viscous fingering during immiscible displacement;

- 2) to attempt a stability theory based on the Buckley-Leverett model in order to determine whether such a theory would yield conclusions different from those obtained from the theory of Chuoke et al.(7);
- 3) to experimentally capture viscous fingering in laboratory cores both to verify the stability conclusions and to study the influence of fingering on oil recovery; and
- 4) to investigate how the experimental recovery data so collected may be suitably scaled to permit the prediction of the recovery behaviour of one system based on the experimental data collected on another, in the presence of instability.

In recognition of the mathematical difficulties encountered by previous researchers, only a linear stability theory will be attempted for the Buckley-Leverett model. The theory of Chuoke et al. (7) will be extended to predict the onset of instability in rectangular as well as cylindrical systems. The efforts to experimentally capture viscous fingering will be devoted to obtaining photographic records of the displacement paths created by the injected water in laboratory cores, while the scaling investigation will be confined to seeking ways of presenting the experimental recovery data collected on two cores of the same material but of different dimensions so as to plot as one curve. The short core will be regarded as the model and the long core as the prototype. Parallel experimental data will be collected on cores with and without connate water saturation.

1.4 ORGANIZATION OF THE REPORT

As a prelude to the stability analysis, the theory of immiscible displacement in porous media is reviewed in Chapter 2. This theory is broadly referred to as the Buckley-Leverett model. The relevant equations are derived first in dimensional form and then in dimensionless form to give them the widest possible application. The process of casting the equations in dimensionless form known as inspectional analysis leads naturally to a discussion of model scaling which forms the second half of this chapter. After a brief comparison of the two methods of deriving the similarity laws, the dimensionless groups pertinent to the study at hand are derived by inspectional analysis.

The studies of previous researchers related to stability theory and viscous fingering during immiscible displacement are reviewed in Chapter 3. No attempt is made to review all that has been published on the subject. Instead, only those studies considered significant and relevant to the present one are reviewed. In particular, the theory of Chuoke et al. (7) is discussed in detail preparatory to its subsequent extension in Chapter 4.

Presented in Chapter 4 are the major theoretical contributions of this study. Using the immiscible displacement equations of Chapter 2 and the stability concepts of Chapter 1, a stability analysis based on the Buckley-Leverett displacement model is undertaken. The chapter concludes with a successful extension of the theory of Chuoke et al. (7).

The experimental set up and procedure employed in this study are outlined in Chapter 5. Because the core packing and flooding techniques are relatively standard and routine matters, they are only briefly discussed. What is not routine, however, is the technique developed in this study to capture viscous fingering in laboratory cores.

Presented in Chapter 6 are the experimental results in the form of tables, graphs and photographs of the paths created by the fluorescent displacing water. These photographic records clearly indicate viscous fingers where they exist. Brief comments are made about the trends in the experimental results. New scaling proposals are presented, and quantitative predictions regarding the onset of instability in certain displacement systems are undertaken.

The results of this study are discussed in Chapter 7 both from the theoretical and experimental standpoints. The present findings are compared with those of previous studies, and possible explanations of the experimental observations are offered. The necessary and sufficient conditions for instability and viscous fingering are stated in the light of the results of this study.

Summarized in Chapter 8, the last chapter of this report, are the major arguments, findings and contributions of this study. Specific conclusions are drawn about stability theories and viscous fingering during immiscible displacements in porous media. Also presented are concrete proposals for scaling laboratory recovery data collected on geometrically dissimilar cores both in the presence and absence of connate water saturation. Suggested areas

of further research are outlined to extend the present study, to fill in the experimental gaps and to do some of those things that were left undone at the conclusion of this study.

The references are restricted to those publications cited in the text of this report, while the bibliography contains other publications that were consulted during the course of this study but not specifically cited in the final report.

CHAPTER 2

THEORY OF IMMISCIBLE DISPLACEMENT AND MODEL SCALING

2.1 IMMISCIBLE DISPLACEMENT EQUATIONS

The partial differential equations of immiscible displacement in porous media are obtained by combining three types of equations - Darcy's law for multiphase flow, the equations of conservation of matter and the equations of state for the participating fluids.

2.1.1 Darcy's Law for Two-Phase Flow

The law of simultaneous flow of two immiscible fluids in porous media is given by a generalized form of Darcy's law. Let the two fluids be denoted as oil and water, where the water displaces the oil. For a homogeneous and isotropic porous medium, Darcy's law applied to the water and oil phases yields

$$\vec{u}_w = \frac{-K_w^* K_{rw}}{\mu_w} (\nabla P_w + \rho_w g \nabla z) \quad 2.1$$

and

$$\vec{u}_o = \frac{-K_o^* K_{ro}}{\mu_o} (\nabla P_o + \rho_o g \nabla z) \quad 2.2$$

The z-direction is positive upwards and K_w^* and K_o^* are as yet unspecified normalizing permeabilities used to define water and oil relative permeabilities. A common choice of normalizing permeability is the absolute permeability of the porous medium, but other choices may be more convenient.

There are fourteen dependent variables in Eqs. 2.1 and 2.2.

These are: $u_{wx}, u_{wy}, u_{wz}, u_{ox}, u_{oy}, u_{oz}, P_w, P_o, S_w, S_o, \rho_w, \rho_o, \mu_w$ and μ_o . To complete the mathematical formulation of the displacement model, eight more equations are required to supplement the six provided by Eqs. 2.1 and 2.2.

2.1.2 Continuity Equations

Two additional equations are obtained from the law of conservation of matter applied to the water and oil phases in a region free of sources and sinks.

$$\frac{\partial (S_w \rho_w \phi)}{\partial t} + \nabla \cdot (\rho_w \vec{u}_w) = 0 \quad 2.3$$

and

$$\frac{\partial (S_o \rho_o \phi)}{\partial t} + \nabla \cdot (\rho_o \vec{u}_o) = 0 \quad 2.4$$

2.1.3 Other Equations

The following equations of state apply:

$$\rho_w = \rho_w(P_w) \quad 2.5$$

$$\rho_o = \rho_o(P_o) \quad 2.6$$

$$\mu_w = \mu_w(P_w) \quad 2.7$$

$$\mu_o = \mu_o(P_o) \quad 2.8$$

Next, a capillary pressure is defined as

$$P_o - P_w = P_c(S_w) \quad 2.9$$

and the oil and water saturations must of course sum to unity:

$$S_o + S_w = 1 \quad 2.10$$

The above fourteen equations provide in principle a complete mathematical description of two-phase immiscible displacement as currently understood. To obtain solutions for the particular displacement situation of interest, the equations must be augmented with appropriate initial and boundary conditions for each of the dependent variables.

The rock-fluid interactive properties - relative permeabilities and capillary pressure functions - must be determined experimentally; alternatively, analytical models may be used. Typical relative permeability and capillary pressure curves are shown in Figures 2.1 and 2.2 in which the displacing water is the wetting phase and the absolute permeability of the porous medium, the normalizing permeability. The presence of connate water saturation in these curves at which the relative permeability and capillary pressure functions take on critical values, indicates that the theory of immiscible displacement outlined here is applicable only to connate water bearing systems.

2.1.4 Homogeneous Incompressible Fluids

If the fluids are homogeneous and incompressible, then the densities and viscosities are constant. Furthermore, in a non-deformable, homogeneous porous medium, the porosity is also constant. With these assumptions, the continuity equations simplify to

$$\phi \frac{\partial S_w}{\partial t} + \nabla \cdot \vec{u}_w = 0 \quad 2.11$$

and

$$\phi \frac{\partial S_o}{\partial t} + \nabla \cdot \vec{u}_o = 0 \quad 2.12$$

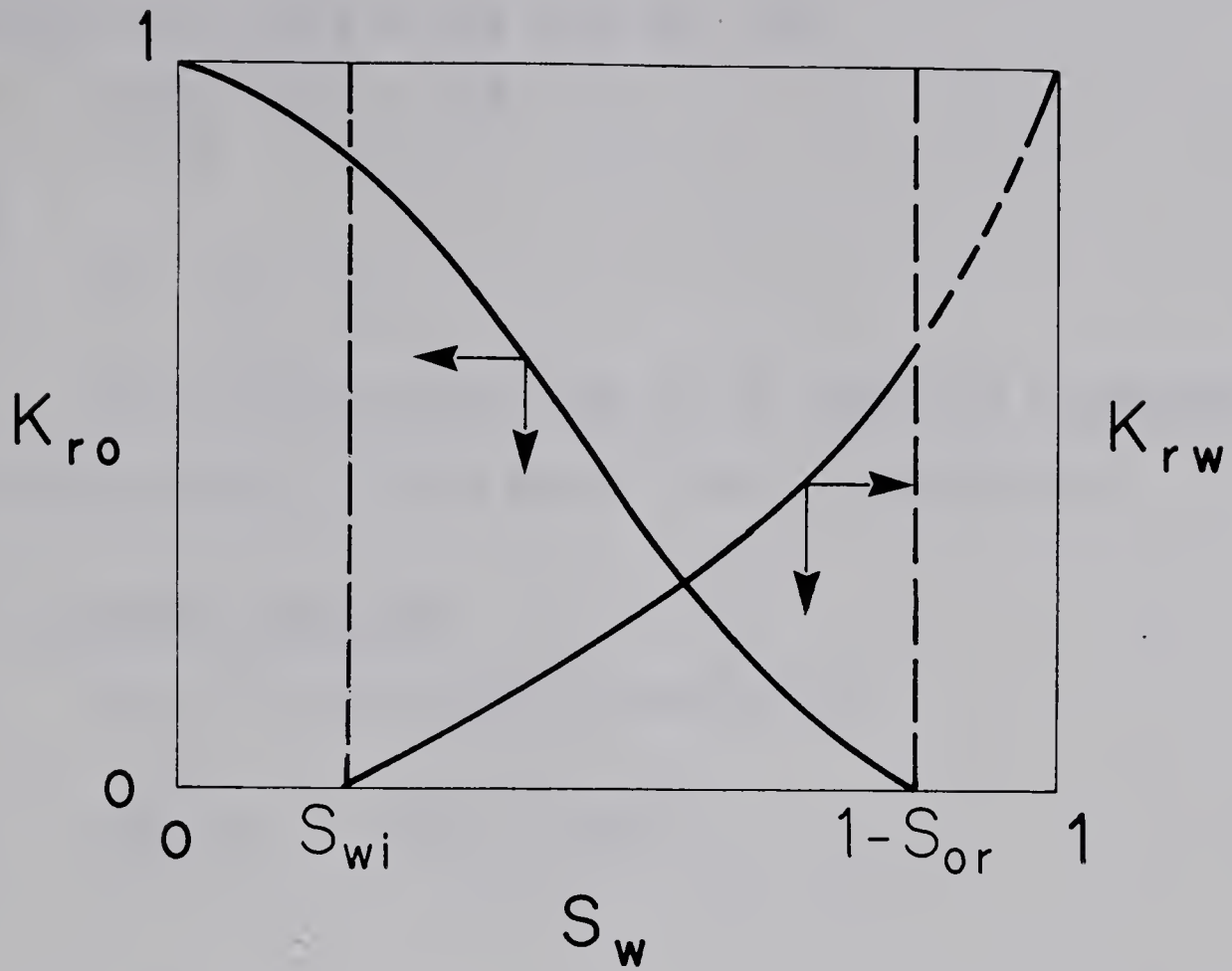
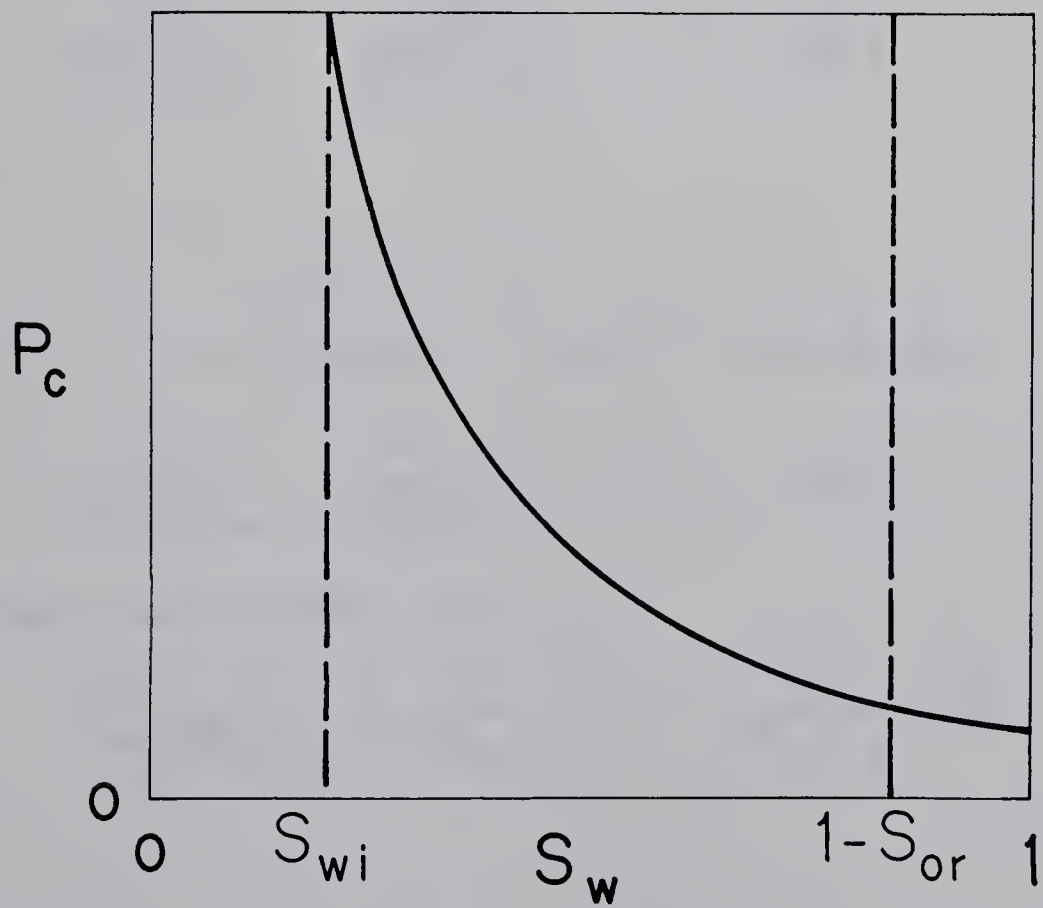


FIG.2.1 Typical Relative Permeability Curves

FIG. 2.2 Typical Capillary Pressure Curve



Adding Eqs. 2.11 and 2.12 and using Eq. 2.10

$$\nabla \cdot (\vec{u}_w + \vec{u}_o) = \nabla \cdot \vec{u} = 0 \quad 2.13$$

where

$$\vec{u} = \vec{u}_w + \vec{u}_o \quad 2.14$$

Various alternative forms of the immiscible displacement equations that will be found useful later are now derived.

2.1.5 Saturation Equation

Eqs. 2.1 and 2.2 may be rewritten as

$$\frac{\vec{u}_w}{K_w^* K_{rw} / \mu_w} = -(\nabla P_w + \rho_w g \nabla z) \quad 2.15$$

and

$$\frac{\vec{u}_o}{K_o^* K_{ro} / \mu_o} = -(\nabla P_o + \rho_o g \nabla z) \quad 2.16$$

Subtracting Eqs. 2.16 from 2.15 yields

$$\frac{\vec{u}_w}{K_w^* K_{rw} / \mu_w} - \frac{\vec{u}_o}{K_o^* K_{ro} / \mu_o} = \nabla P_c - \Delta \rho g \nabla z \quad 2.17$$

where

$$\Delta \rho = \rho_w - \rho_o \quad 2.18$$

Using Eq. 2.14 to eliminate u_o from 2.17, one obtains

$$\frac{\vec{u}_w}{K_w^* K_{rw} / \mu_w} - \frac{\vec{u} - \vec{u}_w}{K_o^* K_{ro} / \mu_o} = \nabla P_c - \Delta \rho g \nabla z \quad 2.19$$

which upon rearrangement leads to

$$\vec{u}_w \left[\frac{1}{K_w^* K_{rw} / \mu_w} + \frac{1}{K_o^* K_{ro} / \mu_o} \right] = \frac{\vec{u}}{K_o^* K_{ro} / \mu_o} + \nabla P_c - \Delta \rho g \nabla z \quad 2.20$$

Let

$$F_w(S_w) = \frac{K_w^* K_{rw} / \mu_w}{K_w^* K_{rw} / \mu_w + K_o^* K_{ro} / \mu_o} = \frac{MK_{rw}}{MK_{rw} + K_{ro}} \quad 2.21$$

where

$$M = \frac{K_w^* \mu_o}{\mu_w K_o^*}, \quad 2.22$$

then Eq. 2.20 becomes

$$\vec{u}_w = F_w \vec{u} + \frac{K_o^*}{\mu_o} F_w K_{ro} \nabla P_c - \frac{K_o^* \Delta \rho g}{\mu_o} F_w K_{ro} \nabla z \quad 2.23$$

Using Eq. 2.22, 2.23 can be written as

$$\vec{u}_w = F_w \vec{u} + \frac{K_w^*}{\mu_w} \frac{F_w K_{ro}}{M} \nabla P_c - \frac{K_w^* \Delta \rho g}{\mu_w} \frac{F_w K_{ro}}{M} \nabla z \quad 2.24$$

Substituting Eq. 2.24 into 2.11 gives

$$\phi \frac{\partial S_w}{\partial t} + \nabla \cdot (F_w \vec{u}) + \nabla \cdot \left(\frac{K_w^*}{\mu_w} \frac{F_w K_{ro}}{M} \nabla P_c \right) - \nabla \cdot \left(\frac{K_w^* \Delta \rho g}{\mu_w} \frac{F_w K_{ro}}{M} \nabla z \right) = 0 \quad 2.25$$

Noting that

$$\nabla \cdot (F_w \vec{u}) = F_w \nabla \cdot \vec{u} + \vec{u} \cdot \nabla F_w = \vec{u} \cdot \nabla F_w, \quad 2.26$$

Eq. 2.25 simplifies to

$$\phi \frac{\partial S_w}{\partial t} + \vec{u} \cdot \nabla F_w + \nabla \cdot \left(\frac{K_w^*}{\mu_w} \frac{F_w K_{ro}}{M} \nabla P_c \right) - \nabla \cdot \left(\frac{K_w^* \Delta \rho g}{\mu_w} \frac{F_w K_{ro}}{M} \nabla z \right) = 0 \quad 2.27$$

Since F_w , P_c , K_{ro} and K_{rw} are functions of S_w only, Eq. 2.27 may further be modified to give the desired saturation equation:

$$\phi \frac{\partial S_w}{\partial t} + \frac{dF_w}{dS_w} \vec{u} \cdot \nabla S_w + \nabla \cdot \left(\frac{K_w^*}{\mu_w} \frac{F_w K_{ro}}{M} \frac{dP_c}{dS_w} \nabla S_w \right) - \frac{K_w^* \Delta \rho g \nabla z}{\mu_w M} \frac{d}{dS_w} (F_w K_{ro}) \frac{\partial S_w}{\partial z} = 0 \quad 2.28$$

2.1.6 Fractional Flow Formula

Dividing every term of Eq. 2.24 by the modulus of the total velocity vector yields the fractional flow formula:

$$\vec{f}_w = \frac{\vec{u}_w}{|\vec{u}|} = F_w \frac{\vec{u}}{|\vec{u}|} + \frac{K_w^* F_w K_{ro}}{\mu_w |\vec{u}| M} \nabla P_c - \frac{K_w^* \Delta \rho g F_w K_{ro}}{\mu_w |\vec{u}| M} \nabla z \quad 2.29$$

Written in terms of the fractional flow, Eq. 2.11 becomes

$$\frac{\phi}{|\vec{u}|} \frac{\partial S_w}{\partial t} + \nabla \cdot \vec{f}_w = 0 \quad 2.30$$

Eq. 2.30 is a generalized form of the Buckley-Leverett (11) displacement model with the capillary term retained. This equation and modifications of it will play a dominant role in the stability theory developed in this study for connate water bearing systems.

2.1.7 Dimensionless Form of the Displacement Equations

When cast in dimensionless form, the immiscible displacement equations can be applied directly to either a laboratory model or to a field prototype. Moreover, the dimensionless parameters that emerge naturally from the process of nondimensionalization serve as scaling groups which may be employed to relate the results of laboratory displacements to those of the prototypes.

To facilitate the dimensionless formulation, the following dimensionless and normalized variables are defined. First, a dimensionless nabla is defined as

$$\nabla^* = L \nabla \quad 2.31$$

where

$$\nabla^* = \underline{i} \frac{\partial}{\partial X} + \underline{j} \frac{\partial}{\partial Y} + \underline{k} \frac{\partial}{\partial Z} \quad 2.32$$

and

$$X = \frac{x}{L}, \quad Y = \frac{y}{L}, \quad Z = \frac{z}{L} \quad 2.33$$

Next, a normalized water saturation is given by

$$S = \frac{S_w - S_{wi}}{(1 - S_{wi} - S_{or})} \quad 2.34$$

Finally, a capillary pressure curve based on a generalized Leverett's J-function (14) is defined as

$$P_c = \frac{\sigma \cos \theta}{\sqrt{K/\phi}} J(S_w) \quad 2.35$$

As a function of the normalized water saturation, the relative permeability and capillary pressure curves take on simpler limiting values when the permeabilities at irreducible fluid saturations, K_{wr} and K_{or} , are used to normalize the water and oil curves, respectively. Typical curves are sketched in Figures 2.3 and 2.4.

With the above definitions, the fractional flow formula, Eq. 2.29, takes on the following dimensionless form:

$$\vec{f}_w = F_w \frac{\vec{u}}{|\vec{u}|} + \left[\frac{\sigma \cos \theta K_{wr} \sqrt{\phi}}{|\vec{u}| \mu_w L \sqrt{K}} \right] \frac{F_w K_{ro}}{M} \frac{dJ}{dS} \nabla^* S - \left[\frac{K_{wr} \Delta \rho g}{|\vec{u}| \mu_w} \right] \frac{F_w K_{ro}}{M} \nabla^* Z \quad 2.36$$

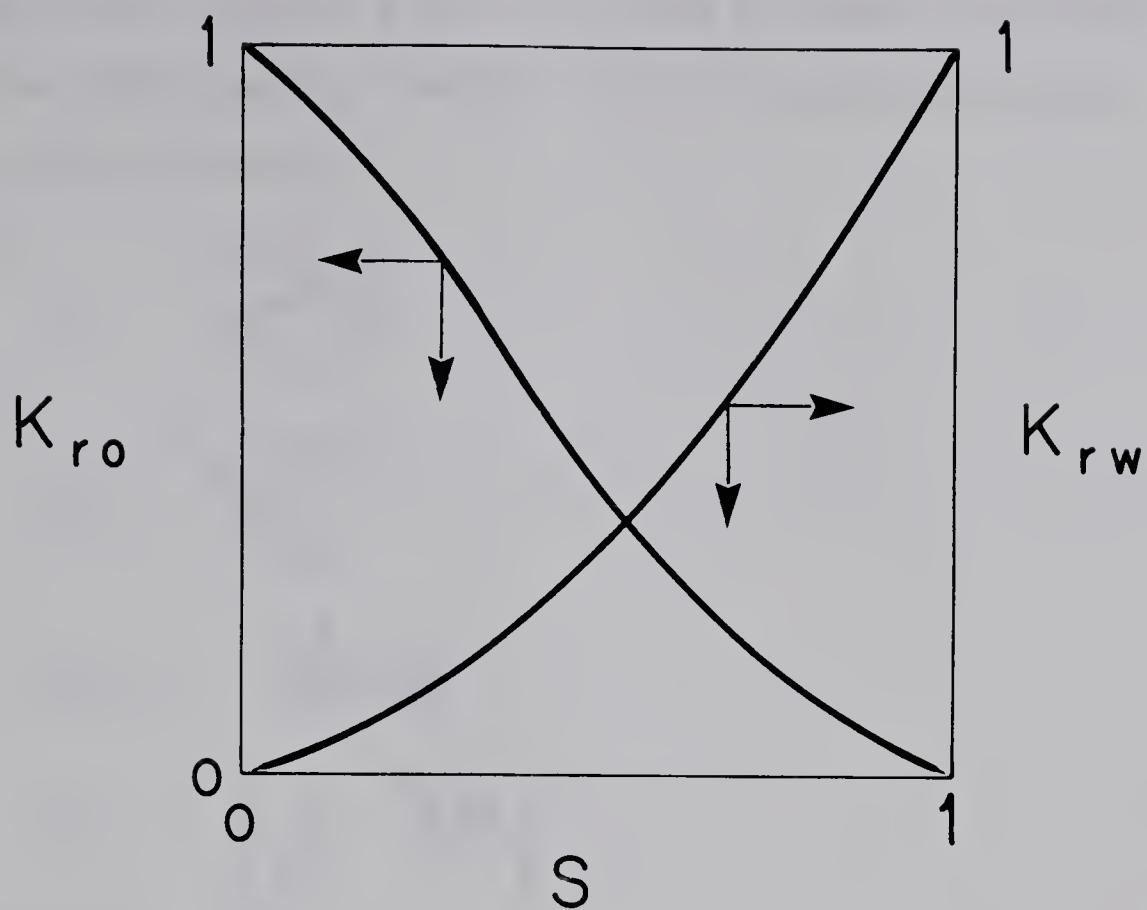
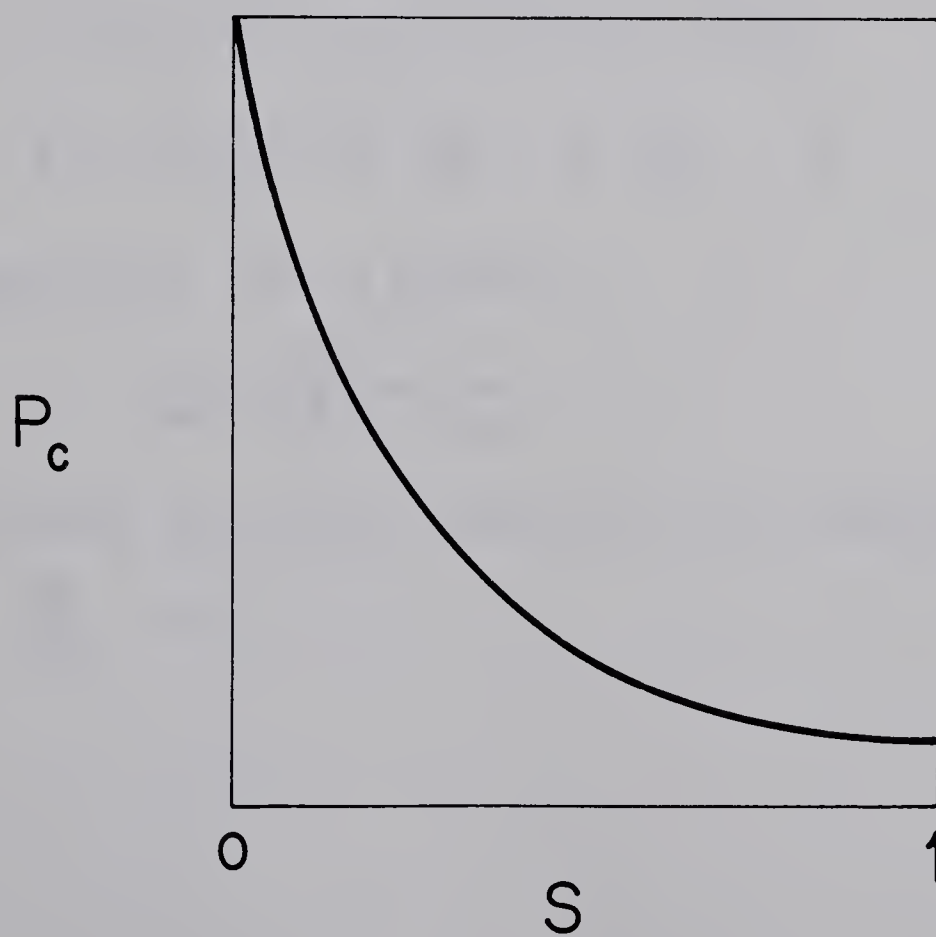


FIG.2.3 Normalized Relative Permeability Curves

FIG.2.4 Normalized Capillary Pressure Curves



Using a notation somewhat similar to those of Fayers and Sheldon (15) and Bentsen (16), one may identify the following dimensionless parameters and functions:

$$N_c = \frac{\sigma \cos \theta K_{wr} \sqrt{\phi}}{|\vec{u}| \mu_w L \sqrt{K}} \quad 2.37$$

$$N_g = \frac{K_{wr} \Delta \rho g \nabla^* Z}{|\vec{u}| \mu_w} \quad 2.38$$

$$C(S) = - \frac{F_w K_{ro}}{M} \frac{dJ}{dS} \quad 2.39$$

$$G(S) = \left[\frac{\vec{u}}{|\vec{u}|} - \frac{N_g K_{ro}}{M} \right] F_w \quad 2.40$$

With this notation, Eq. 2.36 takes on the compact form:

$$\vec{f}_w = G(S) - N_c C(S) \nabla^* S \quad 2.41$$

To complete the derivation of the dimensionless equations, Eq. 2.41 is substituted into Eq. 2.30 to obtain:

$$\phi \frac{(1 - S_{wi} - S_{or})}{|\vec{u}|} \frac{\partial S}{\partial t} + \frac{1}{L} \nabla^* \vec{f}_w = 0 \quad 2.42$$

If a dimensionless time is defined as

$$\tau = \frac{|\vec{u}| t}{\phi L (1 - S_{wi} - S_{or})}, \quad 2.43$$

Eq. 2.42 yields the desired dimensionless displacement equation

$$\frac{\partial S}{\partial \tau} + \nabla^* \vec{f}_w = 0 \quad 2.44$$

or in cartesian coordinates,

$$\frac{\partial S}{\partial \tau} + \frac{\partial f_{wx}}{\partial X} + \frac{\partial f_{wy}}{\partial Y} + \frac{\partial f_{wz}}{\partial Z} = 0 \quad 2.45$$

2.1.8 One-Dimensional Displacement

Displacement tests conducted in a laboratory core are essentially one-dimensional. Suppose that the unidirectional displacement is specified to be in an X-direction which makes an angle, α , with the vertical. Then,

$$\frac{\partial f_{wy}}{\partial Y} = 0, \quad \frac{\partial f_{wz}}{\partial Z} = 0 \quad 2.46$$

and

$$\frac{\partial f_{wx}}{\partial X} = \frac{\partial f_w}{\partial X} \quad 2.47$$

Furthermore, for a core of constant cross-section,

$$|\vec{u}| = \frac{Q}{A} = V \quad 2.48$$

Noting that $\nabla \cdot \vec{Z}$ is equal to $\cos \alpha$, and $\vec{u}/|\vec{u}|$ is unity in the X-direction, the one dimensional displacement equation becomes:

$$\frac{\partial S}{\partial \tau} + \frac{\partial f_w}{\partial X} = 0 \quad 2.49$$

and

$$f_w = G(S) - N_c C(S) \frac{\partial S}{\partial X} \quad 2.50$$

where

$$N_c = \frac{\sigma \cos \theta K_{wr} \sqrt{\phi}}{V_{\mu_w} L \sqrt{K}} \quad 2.51$$

$$N_g = \frac{K_{wr} \Delta \rho g \cos \alpha}{V_{\mu_w}} \quad 2.52$$

and

$$G(S) = \left[1 - \frac{N_g K_{ro}}{M}\right] F_w \quad 2.53$$

If the core is oriented horizontally, then

$$N_g = 0 \quad 2.54$$

2.1.9 Displacement Equation with Fractional Flow as Dependent Variable

The one-dimensional displacement equations, Eq. 2.49 and 2.50, have two dependent variables - normalized water saturation and the fractional flow of water. It is possible to transform these equations by repeated use of the chain rule into a partial differential equation with the fractional flow as the only dependent variable, normalized water saturation and dimensionless time being the independent variables. This transformation has been demonstrated in a recent paper by Bentsen (17).

In the repeated use of the chain rule, it is often advantageous to append subscripts to the partial differentials in order to clearly indicate which variables are held constant during the partial differentiation, and to drop the subscripts from the final equations at the conclusion of the derivation.

With this notation, Eq. 2.49 and 2.50 become

$$\left(\frac{\partial S}{\partial \tau}\right)_X + \left(\frac{\partial f_w}{\partial X}\right)_\tau = 0 \quad 2.55$$

and

$$f_w(X, \tau) = G(S) - N_c C(S) \left(\frac{\partial S}{\partial X}\right)_\tau \quad 2.56$$

The following functional relations are required:

$$S = S(X, \tau) \quad 2.57$$

$$X = X(S, \tau) \quad 2.58$$

and

$$f_w = f_w(S, \tau) \quad 2.59$$

From calculus, Eq. 2.59 and 2.57 yield

$$df_w = \left(\frac{\partial f_w}{\partial S}\right)_\tau dS + \left(\frac{\partial f_w}{\partial \tau}\right)_S d\tau \quad 2.60$$

$$dS = \left(\frac{\partial S}{\partial X}\right)_\tau dX + \left(\frac{\partial S}{\partial \tau}\right)_X d\tau \quad 2.61$$

Substituting for dS in Eq. 2.60 using Eq. 2.61,

$$df_w = \left(\frac{\partial f_w}{\partial S}\right)_\tau \left(\frac{\partial S}{\partial X}\right)_\tau dX + \left[\left(\frac{\partial f_w}{\partial S}\right)_\tau \left(\frac{\partial S}{\partial \tau}\right)_X + \left(\frac{\partial f_w}{\partial \tau}\right)_S\right] d\tau \quad 2.62$$

Thus,

$$\left(\frac{\partial f_w}{\partial X}\right)_\tau = \left(\frac{\partial f_w}{\partial S}\right)_\tau \left(\frac{\partial S}{\partial X}\right)_\tau \quad 2.63$$

and

$$\left(\frac{\partial f_w}{\partial \tau}\right)_X = \left(\frac{\partial f_w}{\partial S}\right)_\tau \left(\frac{\partial S}{\partial \tau}\right)_X + \left(\frac{\partial f_w}{\partial \tau}\right)_S \quad 2.64$$

Substituting Eq. 2.63 into Eq. 2.55, one obtains

$$\left(\frac{\partial S}{\partial \tau}\right)_X + \left(\frac{\partial f_w}{\partial S}\right)_\tau \left(\frac{\partial S}{\partial X}\right)_\tau = 0 \quad 2.65$$

Eq. 2.65 is a first order partial differential equation which can be solved by the method of characteristics. It is clear that the characteristic is given by

$$\frac{dX}{d\tau} = \left(\frac{\partial f_w}{\partial S}\right)_\tau \quad 2.66$$

along which

$$dS = 0 \quad 2.67$$

That is,

$$S = \text{constant} \quad 2.68$$

along the characteristic. This fact enables Eq.2.66 to be written as

$$\left(\frac{\partial X}{\partial \tau}\right)_S = \left(\frac{\partial f_w}{\partial S}\right)_\tau \quad 2.69$$

From Eq. 2.58,

$$dX = \left(\frac{\partial X}{\partial S}\right)_\tau dS + \left(\frac{\partial X}{\partial \tau}\right)_S d\tau \quad 2.70$$

Substituting Eq. 2.70 into 2.61

$$dS = \left(\frac{\partial S}{\partial X}\right)_\tau \left(\frac{\partial X}{\partial S}\right)_\tau dS + \left[\left(\frac{\partial S}{\partial X}\right)_\tau \left(\frac{\partial S}{\partial \tau}\right)_X + \left(\frac{\partial X}{\partial \tau}\right)_S\right] d\tau \quad 2.71$$

Thus,

$$\left(\frac{\partial S}{\partial X}\right)_\tau \left(\frac{\partial X}{\partial S}\right)_\tau = 1 \quad 2.72$$

Hence,

$$\left(\frac{\partial S}{\partial X}\right)_\tau = \frac{1}{\left(\frac{\partial X}{\partial S}\right)_\tau} \quad 2.73$$

provided $\left(\frac{\partial X}{\partial S}\right)_\tau$ is nonzero.

Using Eq. 2.73, Eq. 2.56 takes on the form:

$$f_w(S, \tau) = G(S) - N_c \frac{C(S)}{\left(\frac{\partial X}{\partial S}\right)_\tau} \quad 2.74$$

Differentiating Eq. 2.69 with respect to S and interchanging the order of the differentiation on the left hand side, leads to

$$\frac{\partial}{\partial \tau} \left(\frac{\partial X}{\partial S}\right)_\tau = \left(\frac{\partial^2 f_w}{\partial S^2}\right)_\tau \quad 2.75$$

Integrating Eq. 2.75 with respect to τ ,

$$\left(\frac{\partial X}{\partial S}\right)_\tau = \left(\frac{\partial X}{\partial S}\right)_{\tau=0} + \int_0^\tau \left(\frac{\partial^2 f_w}{\partial S^2}\right)_\tau d\tau \quad 2.76$$

From Eq. 2.74,

$$\left(\frac{\partial X}{\partial S}\right)_{\tau=0} = - \frac{N_c C(S)}{f_w(S,0)-G(S)} \quad 2.77$$

Substituting Eq. 2.77 into 2.76 yields

$$- \frac{N_c C(S)}{f_w(S,\tau)-G(S)} = - \frac{N_c C(S)}{f_w(S,0)-G(S)} + \int_0^\tau \left(\frac{\partial^2 f_w}{\partial S^2}\right)_\tau d\tau \quad 2.78$$

Differentiating Eq. 2.78 with respect to τ and rearranging gives

$$[f_w(S,\tau)-G(S)]^2 \frac{\partial^2 f_w}{\partial S^2} = N_c C(S) \frac{\partial f_w}{\partial \tau}, \quad 2.79$$

which is the required equation of displacement with the fractional flow of water as the only dependent variable and the normalized water saturation and the dimensionless time as the independent variables.

2.1.10 Displacement Equation with Distance as Dependent Variable

It is required in this formulation to make the distance travelled by the normalized water saturation the dependent variable while the saturation and dimensionless time remain the independent variables. This is the Lagrangian viewpoint of the displacement. This Lagrangian viewpoint is obtained by first differentiating Eq. 2.74 and rearranging as

$$[f_w(S,\tau)-G(S)]\left(\frac{\partial^2 X}{\partial S^2}\right)_\tau + \left[\left(\frac{\partial f_w}{\partial S}\right)_\tau - G'(S)\right]\left(\frac{\partial X}{\partial S}\right)_\tau + N_c C'(S) = 0 \quad 2.80$$

and then substituting Eq. 2.69 to obtain

$$[f_w(S,\tau)-G(S)] \frac{\partial^2 X}{\partial S^2} + \left[\left(\frac{\partial X}{\partial \tau}\right) - G'(S)\right]\left(\frac{\partial X}{\partial S}\right)_\tau + N_c C'(S) = 0 \quad 2.81$$

2.2 PERTINENT SOLUTIONS OF THE DISPLACEMENT EQUATIONS

Preliminary to the stability theory developed in this study, typical numerical solutions of the displacement equations were undertaken to gain insight into the unperturbed behaviour of the immiscible displacement model. Such a clear indication of the anticipated flood behaviour would serve to highlight the unusual experimental trends that have motivated the appeal to stability concepts to reconcile observations with theory.

Also presented in this section are the analytical stationary solutions of the fractional flow equation. These are the Buckley-Leverett solutions that will constitute the unperturbed behaviour for the proposed stability theory.

2.2.1 Unperturbed Saturation and Breakthrough Recovery Profiles

The one-dimensional immiscible displacement equation was integrated by a finite difference scheme, using the method of simultaneous solution, in order to simulate incompressible two-phase displacement in a laboratory core. The following rock-fluid properties were used:

$$K_{rw} = K_w/K_{wr} = S^2 \quad 2.82$$

$$K_{ro} = K_o/K_{or} = 1 - S^2 \quad 2.83$$

$$P_c = \frac{0.05}{1 - S_{wi}} [1 - S_w] \quad 2.84$$

The Fortran code for the simulator and the tabulations of the saturation and breakthrough recovery predictions are presented in Appendix A.

Figure 2.5 shows a typical evolution of the unperturbed saturation profile at various dimensionless times for a relatively high displacement rate. Each profile consists of a region of steep saturation gradients which constitutes the front, followed by a region of comparatively lower saturation gradients. It may be observed that at this rate, the front assumes a fixed shape soon after the initiation of the flood and thereafter propagates through the system at a uniform speed. The flood is then said to have stabilized at this rate.

This stabilization is further illustrated in Figure 2.6 which shows the theoretical variation of the breakthrough recovery with a dimensionless rate at mobility ratios of 1.9 and 8.1. The theory predicts a breakthrough recovery which increases with rate until stabilization for all mobility ratios; the higher the mobility ratio, the lower the recovery efficiency. Based on this theory, a subsequent decrease in the breakthrough recovery after stabilization would constitute an unusual behaviour to be investigated as a possible manifestation of instability.

It is important to draw a clear distinction between a stabilized flood and a stable flood. Stabilization represents the attainment of a stationary state of affairs whereas stability implies the attenuation of the small perturbations that arise during the course of the displacement. For instance, each of the breakthrough recovery profiles of Figure 2.6 which constitute the unperturbed flood behaviour, consists of two regions - an unstabilized region in which the recovery varies with rate and a stabilized region in

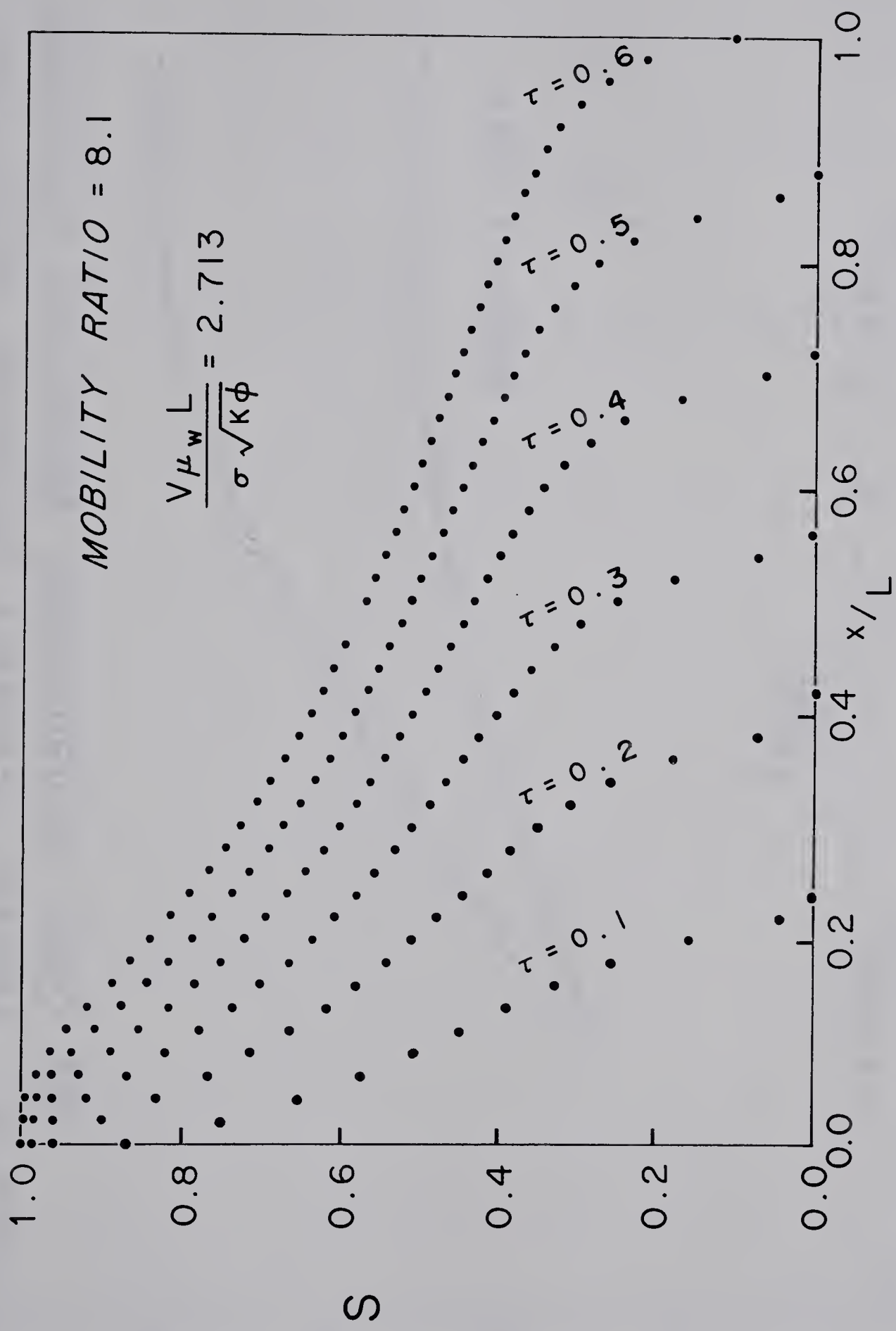
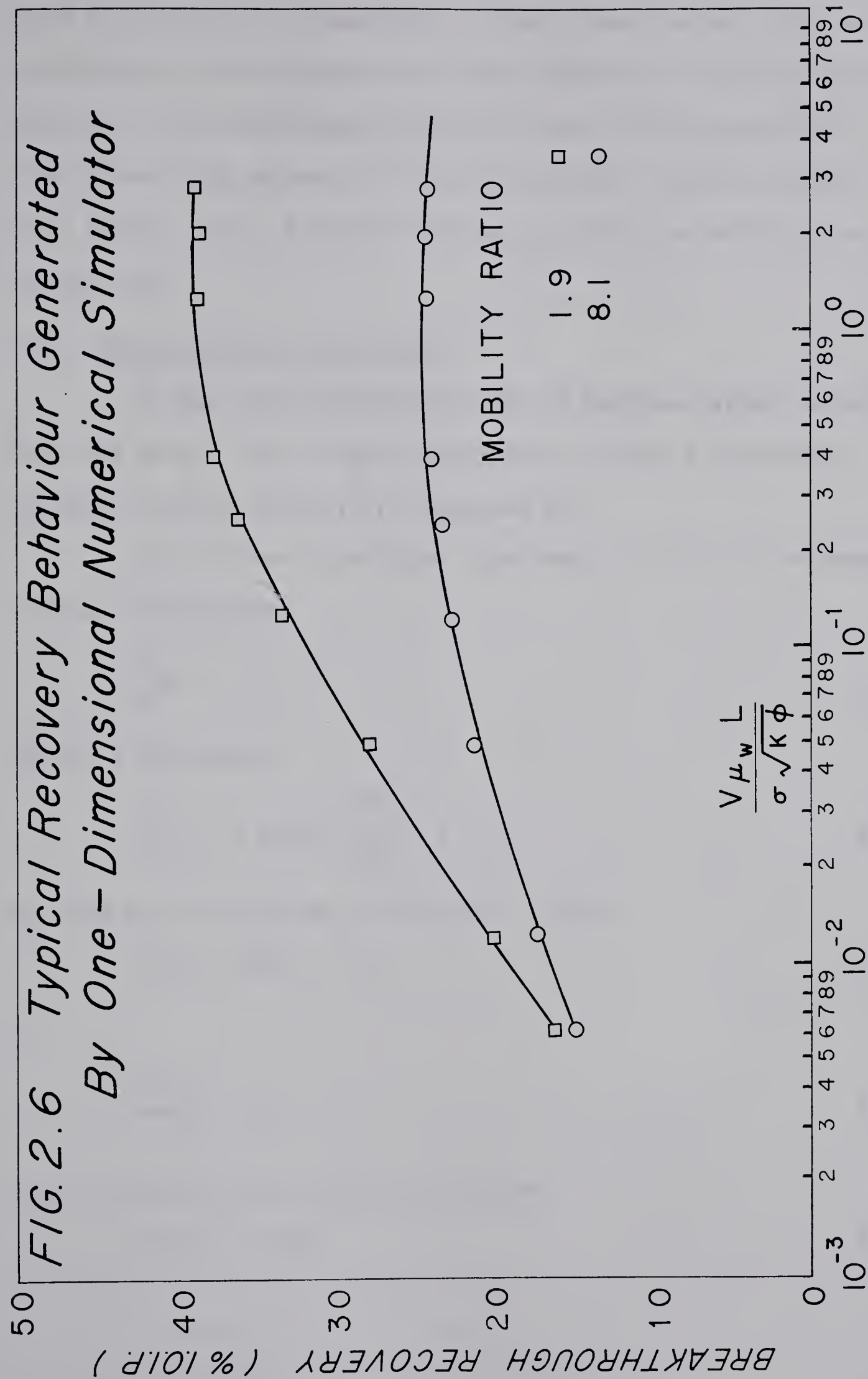


FIGURE 2.5 TYPICAL SATURATION PROFILES GENERATED BY ONE-DIMENSIONAL NUMERICAL SIMULATOR



which the recovery is independent of rate. Nevertheless, since no perturbations were introduced into the solutions of the differential equations of the displacement model (at least not intentionally), these unperturbed recovery profiles are also the limiting profiles for a stable flood. A stable flood may therefore be stabilized or unstabilized.

2.2.2 Buckley-Leverett Solutions

It has been demonstrated that the Buckley-Leverett solution, involving Welge's (18) tangent construction, is but a stationary solution of the fractional flow equation (17).

At stationary conditions, the fractional flow is independent of time. Accordingly,

$$\frac{\partial f_w}{\partial \tau} = 0 \quad 2.85$$

and Eq. 2.79 becomes

$$[\bar{f}_w(S) - G(S)]^2 \frac{\partial^2 \bar{f}_w}{\partial S^2} = 0 \quad 2.86$$

Eq. 2.86 may be satisfied in two ways. Either

$$\bar{f}_w(S) - G(S) = 0 \quad 2.87$$

or

$$\frac{\partial^2 \bar{f}_w}{\partial S^2} = 0 \quad 2.88$$

Eq. 2.87 leads to the stationary solution

$$\bar{f}_w(S) = G(S) \quad 2.89$$

while Eq. 2.88 indicates a linear relationship between \bar{f}_w and S . These two solutions may be suitably married at the front to yield one continuous stationary solution as shown in Figure 2.7. The solution will then consist of two parts. In the frontal zone,

$$\bar{f}_w(S) = \frac{\bar{f}_w(S_f)}{S_f} S \quad 0 < S < S_f \quad 2.90$$

and in the trailing zone behind the front,

$$\bar{f}_w(S) = G(S) \quad S_f < S < 1 \quad 2.91$$

These are the well known Buckley-Leverett solutions.

2.3 MODEL SCALING

2.3.1 General

Whenever possible, experimental results should be presented in a manner that makes them applicable to systems other than the one used to acquire the data. When the results are so presented, it is then possible to use the data collected on a laboratory system, the model, to predict the behaviour of another system, the one of actual interest, the prototype. To facilitate the predictions, it is first necessary to establish a set of relationships between the two systems. These relationships are usually known as scaling laws, modelling laws or similarity requirements.

2.3.2 Scaling Principles for Immiscible Displacements

In general, two methods may be used to derive the scaling laws: inspectional analysis which is based on the differential equations of immiscible displacement and dimensional analysis which is based on a knowledge of the pertinent variables affecting the displacement process.

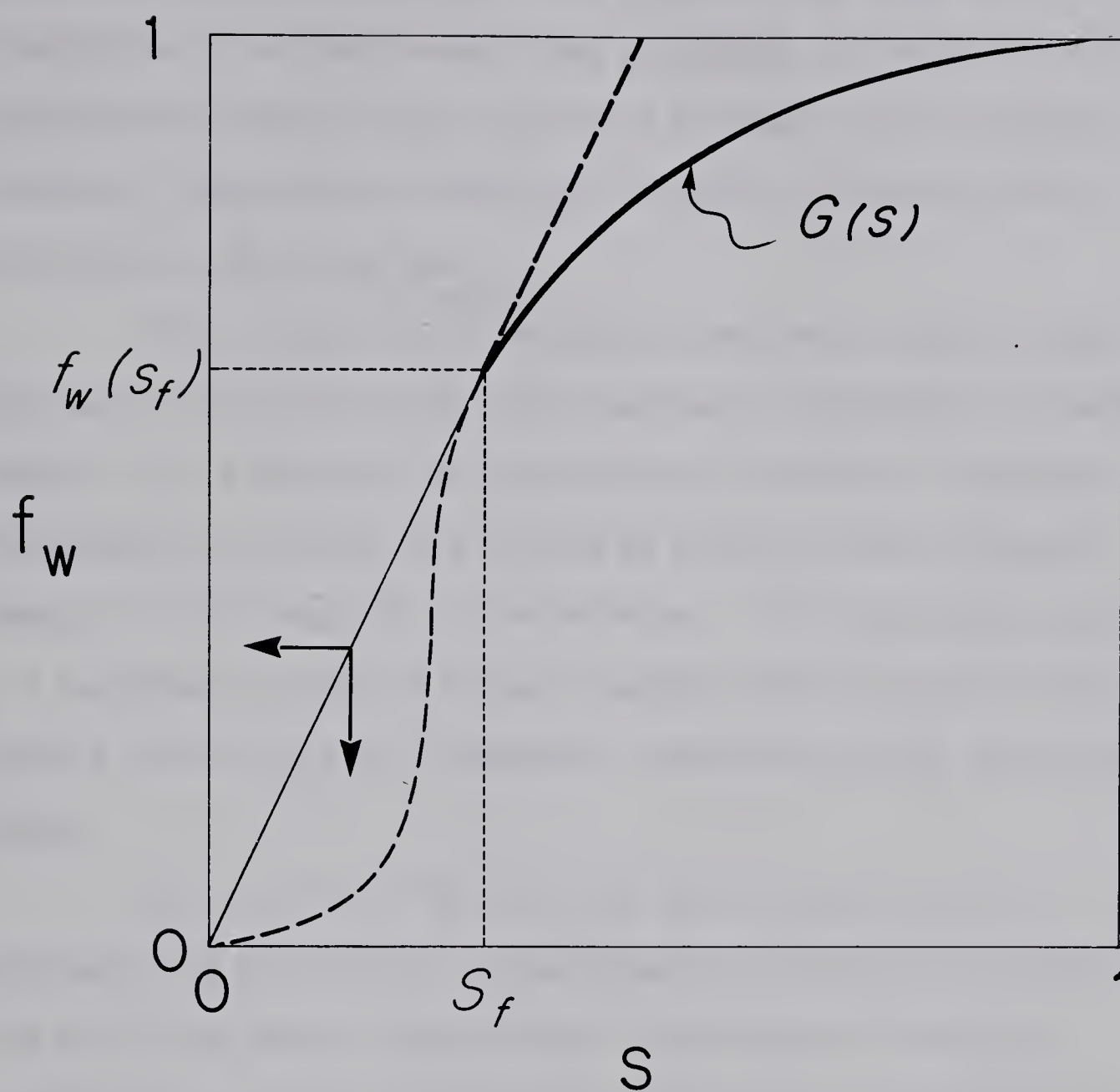


FIG. 2.7 Stationary Solution Of
The Fractional Flow Equation

The process of inspectional analysis consists of rendering the differential equations of the displacement together with the initial and boundary conditions into dimensionless forms by the introduction of suitable normalizing variables. The result of this nondimensionalization is the appearance of dimensionless dependent variables, dimensionless independent variables and dimensionless similarity or scaling groups.

Unlike inspectional analysis, dimensional analysis does not require that the process being modelled be expressed by equations. Instead, only a knowledge of the pertinent variables is required. The dimensionless groups are derived by requiring that the power products of the variables be dimensionless. This requirement results in a homogeneous system of linear equations, the solution of which yields a complete set of independent, though not unique, dimensionless groups.

Both methods of deriving the scaling laws have their advantages and limitations. Inspectional analysis usually gives rise to scaling groups whose physical significance is readily apparent, whereas the significance of some of the groups derived by dimensional analysis may be quite obscure. For example, based on the locations of the scaling groups in the dimensionless differential equations, it is easy to identify that a certain group is the ratio of viscous to capillary forces or gravitational to viscous forces. On the other hand, inspectional analysis, unlike dimensional analysis, does require a mathematical equation for the process under study. If such an equation is unavailable, inspectional analysis cannot

commence whereas dimensional analysis can still provide some guidance in setting up experiments to initiate a study. In any case, even when a differential equation is available, it is only the aspect of the phenomenon which is well understood that is usually modelled. As a result, the scaling groups derived from the equations may be incomplete. Dimensional analysis is therefore much more general, and in this generality lies the source of its strength and its weakness. When very little theory is available, dimensional analysis can be relied upon to provide initial guidance in setting up experiments. However, it is so general that the inclusion of superfluous variables in the list of pertinent variables will give rise to superfluous but no less legitimate scaling groups.

Extensive literature exists regarding the specific applications of the above methods for deriving the scaling laws of immiscible displacement. Ever since Leverett et al. (19) presented their model studies in which dimensionless groups were used to scale laboratory displacements to field prototypes, numerous studies have been undertaken that have greatly extended their initial efforts (1, 20, 21, 22, 23, 24, 25, 26, 27).

Engelberts and Klinkenberg (1) made extensive use of dimensionless groups obtained by dimensional analysis to study the influence of certain variables on immiscible displacements in laboratory cores. In addition, they employed the various groups as a general aid in presenting their experimental findings.

Rapoport (20) has presented a complete derivation of the scaling laws by inspectional analysis, while Greenkorn (26) has

presented a systematic method of deriving the scaling groups by dimensional analysis using matrix algebra. Geertsma et al.(22) have combined the advantages of the two methods by employing them in a complementary manner to derive a complete set of scaling groups for various displacement arrangements in porous media.

The relevant dimensionless scaling groups for the present study are best derived by inspectional analysis. Eq. 2.27 provides a convenient starting point for such a derivation. Let the oil and water densities be equal so that the gravitational term may be neglected. With this assumption, Eq. 2.27 becomes

$$\phi \frac{\partial S_w}{\partial t} + \vec{u} \cdot \nabla F_w + \nabla \cdot \left(\frac{K_w^*}{\mu_w} \frac{F_w K_{ro}}{M} \nabla P_c \right) = 0 \quad 2.92$$

Let a modified Leverett (14) function be defined as

$$P_c = \frac{\sigma^*}{\sqrt{K/\phi}} J(S_w) \quad 2.93$$

and K_w^* be equal to K . To describe the displacement in a horizontal cylindrical core, Eq. 2.92 is expanded in cylindrical (r, θ, x) coordinates to give

$$\begin{aligned} & \phi \frac{\partial S_w}{\partial t} + \left[u_r \frac{\partial S_w}{\partial r} + \frac{u_\theta}{r} \frac{\partial S_w}{\partial \theta} + u_x \frac{\partial S_w}{\partial x} \right] \frac{dF_w}{dS_w} \\ & + \frac{\sigma^* \sqrt{K\phi}}{\mu_w M} \left[\frac{1}{r} \frac{\partial}{\partial r} \left(r F_w K_{ro} \frac{dJ}{dS_w} \frac{\partial S_w}{\partial r} \right) + \frac{1}{r^2} \frac{\partial}{\partial \theta} \left(F_w K_{ro} \frac{dJ}{dS_w} \frac{\partial S_w}{\partial \theta} \right) \right. \\ & \left. + \frac{\partial}{\partial x} \left(F_w K_{ro} \frac{dJ}{dS_w} \frac{\partial S_w}{\partial x} \right) \right] = 0 \end{aligned} \quad 2.94$$

Next, the following dimensionless variables are defined:

$$r_D = \frac{r}{a} \quad 2.95$$

$$X = \frac{x}{L} \quad 2.96$$

$$\vec{U} = \frac{\vec{u}}{V} \quad 2.97$$

and

$$t_D = \frac{Vt}{\phi L} \quad 2.98$$

Substituting Eqs. 2.95 to 2.98 into Eq. 2.94 yields the required dimensionless equation:

$$\begin{aligned} \frac{\partial S_w}{\partial t_D} + \left(\frac{L}{D}\right) \left[2U_r \frac{\partial S_w}{\partial r_D} + 2 \frac{U_\theta}{r_D} \frac{\partial S_w}{\partial \theta} \right] \frac{dF_w}{dS_w} + U_x \frac{\partial S_w}{\partial X} \frac{dF_w}{dS_w} \\ + \left(\frac{L}{D}\right) \left(\frac{\sigma^* \sqrt{K\phi}}{V_{\mu_w} D} \right) \frac{1}{M} \left[\frac{4}{r_D} \frac{\partial}{\partial r_D} \left(r_D F_w K_{ro} \frac{dJ}{dS_w} \frac{\partial S_w}{\partial r_D} \right) \right. \\ \left. + \frac{4}{r_D^2} \frac{\partial}{\partial \theta} \left(F_w K_{ro} \frac{dJ}{dS_w} \frac{\partial S_w}{\partial \theta} \right) \right] \\ + \left(\frac{\sigma^* \sqrt{K\phi}}{V_{\mu_w} L} \right) \frac{1}{M} \frac{\partial}{\partial X} \left(F_w K_{ro} \frac{dJ}{dS_w} \frac{\partial S_w}{\partial X} \right) = 0 \end{aligned} \quad 2.99$$

The following dimensionless groups emerge from the inspectional analysis:

- (a) independent variables: r_D, θ, X, t_D ;
- (b) dependent variables: S_w, U_r, U_θ, U_x ;
- (c) similarity groups:

$$L/D, M, \sigma^* \sqrt{K\phi}/V_{\mu_w} D, \sigma^* \sqrt{K\phi}/V_{\mu_w} L, K_{rw}, K_{ro}, dJ/dS_w$$

Thus, if the similarity groups are the same in the model and the prototype, then the dependent variables will be the same in the two

systems at homologous points and time. If the model and the prototype consist of the same fluids and porous media, then the scaling requirements pertaining to the rock-fluid properties are always met. As a result, only the following similarity groups remain to be satisfied:

$$L/D, \sigma^* \sqrt{K\phi} / V_{\mu_w} D, \sigma^* \sqrt{K\phi} / V_{\mu_w} L$$

In these groups, σ^* is an unknown effective interfacial tension which accounts for the surface or capillary properties of the displacement system. Because of the different initial interfacial arrangements, it may be expected that σ^* will take on different values in systems with and without connate water saturations for the same fluids and porous media. It may also be inferred that σ^* will be higher in systems containing connate water saturation to reflect the increased capillary activities that will result from the presence of fluid/fluid interfaces throughout the system even prior to commencing the displacement. In the absence of any other guide, it will be assumed that σ^* is directly proportional to σ , with the constant of proportionality C^* being higher in systems with connate water saturation than in systems without connate water saturation. An experimental estimate of C^* , and hence σ^* , in the two systems will greatly enhance the understanding of the displacement mechanisms in the two systems.

The physical significance of the scaling groups is as follows. The ratio, L/D , ensures the geometric similarity between the model and the prototype. The remaining two groups are ratios of capillary to viscous forces. The group, $\sigma^* \sqrt{K\phi} / V_{\mu_w} L$, represents the

ratio of the capillary to viscous forces in the X-direction, that is, in the direction of the bulk motion. This group will therefore be termed the linear scaling group. The group, $\sigma^* \sqrt{K\phi} / V_{\mu_W} D$, on the other hand represents the ratio of viscous to capillary forces in the radial and angular directions, that is, in directions tranverse to that of the bulk motion. It will therefore be referred to as the radial scaling group.

A form of the linear scaling group, $V_{\mu_W} L / \sigma \sqrt{K\phi}$, is widely used in the literature to correlate laboratory displacement results (1, 28, 29, 30, 31, 32, 33). Used in this form, the group is essentially a dimensionless rate. It may be anticipated that if the displacement is essentially one-dimensional, as would be the case in a stable displacement or an unstable displacement dominated by tubular fingers, then this group will be a good correlating group for the model and the prototype recoveries even when the two systems are geometrically dissimilar. However, if the displacement is multi-dimensional in character, as in the case of an unstable displacement with tapering or conical fingers, the linear group may not be suitable for scaling the experimental results. Under this circumstance, the transverse or radial group, $V_{\mu_W} D / \sigma \sqrt{K\phi}$, may be a more appropriate scaling coefficient. Because this group is often lost due to linear flow assumption from the outset, it has not been widely used in the literature as a possible correlating group for presenting experimental results.

As the radial scaling group controls the transverse spreading of the injected fluid to prevent fingering, it may be

expected that the magnitude of this group will play a major role in the onset of instability. Based on the results of the inspectional analysis of the Buckley-Leverett model given by Eq. 2.99, it may be inferred that the onset of instability leading to viscous fingering in a core will involve a radial scaling coefficient of the form $V\mu_w D^2 / \sigma L \sqrt{K\phi}$.

For the present study, the dimensionless scaling groups will be employed for two purposes. First, the groups will be used to scale the model results in order to predict the prototype behaviour. To meet this objective, two cores of the same diameter but different lengths will be used to collect the experimental data. The short core could be regarded as the model and the long core as the prototype even in a laboratory setting. The model and the prototype are therefore geometrically dissimilar. The scaling objective will be accomplished by seeking the appropriate correlating group that will enable the data collected on the model and the prototype to plot as one curve over a wide range of displacement rates. Second, the dimensionless groups will be used as suitable variables in their own right to explore the influence of the displacement parameters on instability and viscous fingering in porous media both in the presence and absence of connate water saturation.

CHAPTER 3

REVIEW OF RELATED RESEARCH

The study of frontal instability and the associated phenomenon of viscous fingering during immiscible displacement in porous media was pioneered at Shell Production Research Laboratory, Amsterdam. Among the significant contributions from this research centre may be cited the studies of Engelberts and Klinkenberg (1), van Meurs (34), van Meurs and van der Poel (35), Chuoke, van Meurs and van der Poel (7), de Haan (30), and Hagoort (13).

The contributions from elsewhere included in this review are those of Rachford, Jr. (12), Perkins and Johnston (36), Kloepper (31), Wiborg (32) and Baird (33).

In keeping with the scope of the present study, this review is limited to immiscible displacements only. Consequently, the phenomenon of viscous fingering and the related stability theory in miscible systems are not reviewed.

In 1951, Engelberts and Klinkenberg (1) published the results of laboratory floods in an apparently homogeneous porous medium in which the displacing water was observed to channel through the displaced oil in the form of macroscopic fingers. Because this fingering was most severe in high oil-water viscosity ratio floods, the authors termed the phenomenon "viscous fingering".

Their tests, conducted on cylindrical homogeneous packs of coarse sand, initially fully saturated with oil, led to the following observations. At a viscosity ratio of one, the porous body was

uniformly invaded by the dyed displacing water over all the displacement rates studied. Furthermore, the displacement efficiency, as indicated by the pattern of water invasion at the conclusion of each test, improved with increasing displacement rate. At a viscosity ratio greater than one, the porous medium was relatively well invaded at low displacement rates. At high rates, the displacement was anything but uniform. Instead, it was haphazard with large sections of the porous medium uncontacted by the displacing water at the end of each test. This fingering pattern of water invasion worsened as the displacement rate increased. At intermediate rates, there was a transition from the relatively uniform water invasion of low rate to the severe fingering of high rate displacements.

These displacement patterns were also reflected in the breakthrough oil recovery profiles. For the displacements at a viscosity ratio of one, the breakthrough recoveries increased with rate. At viscosity ratios of 4 and 24, the recoveries were comparable to that at a viscosity ratio of one at low rates. At high rates, however, the recoveries decreased significantly because of viscous fingering with a marked transition from high to low recoveries at intermediate rates.

The observations of Engelberts and Klinkenberg (1) were confirmed by van Meurs (34) who developed a transparent displacement system that permitted direct visual observations of the displacement process. Photographs of the displacement patterns showed spectacular fingering at a viscosity ratio of 80, and no fingering at a viscosity ratio of one.

Based upon these observations van Meurs and van der Poel (35) doubted the applicability of the relative permeability concepts of the conventional theory of immiscible displacement to displacements dominated by viscous fingering. They accordingly developed a competing theory, tailored to viscous fingering. This theory, which parallels the conventional Buckley-Leverett theory in several respects, has received little or no recognition.

A common experimental condition in all of the above reported studies was the absence of connate water saturation in the displacement systems. Engelberts and Klinkenberg (1) justified the exclusion of connate water saturation as a simplification of the experimental condition, apparently in the belief that the absence of connate water was immaterial to the displacement process itself. Later studies were to demonstrate, however, that this belief was mistaken.

As the observed phenomenon of viscous fingering in nonconnate water bearing systems could not be satisfactorily attributed to permeability stratifications in the system because of the homogeneous nature of the controlled sand packs, Engelberts and Klinkenberg (1) identified the phenomenon as a manifestation of instability, a notion widely used in hydrodynamics to explain puzzling flow behaviour. In so doing, these authors set the stage for the theoretical treatment of viscous fingering by subsequent researchers as a problem of hydrodynamic stability.

Chuoque et al. (7) presented the first systematic theoretical study of viscous fingering from the stability standpoint. Using perturbation theory, they conducted a first order linear stability analysis of the displacement process and successfully derived the

conditions that would promote instability and viscous fingering.

Their mathematical stability theory, published in 1959, is still widely regarded as the most authoritative on the subject of immiscible displacement in porous media. In view of this wide acceptance, and because their original paper omitted some of the mathematical steps essential to a full appreciation of their contribution, their theory is reviewed here in greater detail than presented in the original paper. In addition to filling in the mathematical gaps, this expanded review highlights the inherent assumptions and limitations of their theory and thus helps to put it in proper perspective. Furthermore, the detailed mathematical derivations presented here prepare the ground for the extension of their theory, undertaken in the present study, to cylindrical coordinates, a more appropriate coordinate system for studying the stability of displacements in cylindrical laboratory cores.

It is important to realize from the outset that their stability theory was not based on the Buckley-Leverett model of immiscible displacement in porous media. Rather, it was founded on a piston-like displacement model in which the displacing fluid sweeps the displaced fluid ahead of it leaving behind only an immobile displaced fluid saturation. The authors appear to have been guided to this choice of unperturbed behaviour by a certain analogy that exists between piston-like displacement between parallel plates or Hele-Shaw models without a porous medium, and single phase flow of Newtonian fluids in porous media. Accordingly, they postulated the following hydrodynamic equations to describe the displacement: Darcy's law for single phase flow and the continuity equation for

incompressible flow:

$$\vec{u} = - \frac{K}{\mu} \nabla(p + \rho g z \cos \alpha) \quad 3.1$$

$$\nabla \cdot \vec{u} = 0 \quad 3.2$$

In Eq. 3.1, the z-direction is inclined at an angle α to the upward vertical.

The unperturbed displacement model may be specified as follows. Consider the situation in which water displaces oil at a constant superficial velocity, V , in the z-direction. Then the unperturbed equations in cartesian coordinates are:

$$u_x = 0 \quad 3.3$$

$$u_y = 0 \quad 3.4$$

$$u_z = V \quad 3.5$$

$$p = P \quad 3.6$$

Suppose that the displacement is slightly disturbed about the above unperturbed quantities. Then the perturbed velocities and pressure will be given by

$$u_x = 0 + u_x^* \quad 3.7$$

$$u_y = 0 + u_y^* \quad 3.8$$

$$u_z = V + u_z^* \quad 3.9$$

$$p = P + p^* \quad 3.10$$

Substituting Eqs. 3.7 to 3.9 into Eq. 3.1 gives

$$u_x^* = - \frac{K}{\mu} \frac{\partial p}{\partial x} \quad 3.11$$

$$u_y^* = - \frac{K}{\mu} \frac{\partial p}{\partial y} \quad 3.12$$

$$V + u_z^* = - \frac{K}{\mu} \left(\frac{\partial p}{\partial z} + \rho g \cos \alpha \right) \quad 3.13$$

where the perturbed pressure, p , has been retained in all the right

hand sides. Eqs. 3.11 to 3.13 may be combined into the one vector equation

$$\vec{u}^* = - \nabla \frac{K}{\mu} (p + \frac{\mu}{K} Vz + \rho g z \cos \alpha) \quad 3.14$$

if K is assumed to be independent of the space variables. Let a perturbed velocity potential be defined by

$$\Phi = \frac{K}{\mu} (p + \frac{\mu}{K} Vz + \rho g z \cos \alpha) \quad 3.15$$

Thus

$$p = \frac{\mu}{K} \Phi - \frac{\mu}{K} Vz - \rho g z \cos \alpha + P(t) \quad 3.16$$

where $P(t)$ is an arbitrary function of time. Eq. 3.15 becomes

$$\vec{u}^* = - \nabla \Phi \quad 3.17$$

Substituting Eq. 3.7 to 3.9 into Eq. 3.2 gives the continuity equation for the perturbed flow in terms of the velocity perturbations:

$$\nabla \cdot \vec{u}^* = 0 \quad 3.18$$

Substituting for \vec{u}^* in Eq. 3.18 using 3.17, one obtains the partial differential equation for the perturbed velocity potential

$$\nabla^2 \Phi = 0 \quad 3.19$$

Since all the normal velocity perturbations must vanish at the walls, the following boundary conditions must apply:

$$u_x^*(0,y) = - \frac{\partial \Phi}{\partial x}(0,y) = 0 \quad 0 < y < L_y \quad 3.20$$

$$u_x^*(L_x,y) = - \frac{\partial \Phi}{\partial x}(L_x,y) = 0 \quad 0 < y < L_y \quad 3.21$$

$$u_y^*(x,0) = - \frac{\partial \Phi}{\partial y}(x,0) = 0 \quad 0 < x < L_x \quad 3.22$$

$$u_y^*(x,L_y) = - \frac{\partial \Phi}{\partial y}(x,L_y) = 0 \quad 0 < x < L_x \quad 3.23$$

Eq. 3.19, together with the boundary conditions expressed by Eqs. 3.20 to 3.23, may be solved by the method of separation of variables. Let

$$\Phi(x, y, z, t) = X(x) Y(y) Z(z) T(t) \quad 3.24$$

Substituting Eq. 3.24 into 3.19 and dividing through by XYZT gives upon rearrangement,

$$\frac{X''}{X} = - \left(\frac{Y''}{Y} + \frac{Z''}{Z} \right) \quad 3.25$$

Since the left hand side of Eq. 3.25 is a function of x only, while the right hand side is a function of y and z only, the equation can only be satisfied if both sides are equal to a common constant, the separation constant. Thus,

$$\frac{X''}{X} = - \left(\frac{Y''}{Y} + \frac{Z''}{Z} \right) = - \alpha_X^2 \quad 3.26$$

Hence,

$$X'' + \alpha_X^2 X = 0 \quad 3.27$$

$$X'(0) = 0 \quad 3.28$$

$$X'(L_X) = 0 \quad 3.29$$

and

$$\frac{Y''}{Y} + \frac{Z''}{Z} = \alpha_X^2 \quad 3.30$$

A further separation of Eq. 3.30 and application of the boundary conditions yield

$$Y'' + \alpha_Y^2 Y = 0 \quad 3.31$$

$$Y'(0) = 0 \quad 3.32$$

$$Y'(L_Y) = 0 \quad 3.33$$

and

$$Z'' - \gamma^2 Z = 0 \quad 3.34$$

where

$$\gamma^2 = \alpha_x^2 + \alpha_y^2 \quad 3.35$$

Eqs. 3.27 to 3.34 constitute eigenvalue problems which have nontrivial solutions only for certain discrete values of the eigenvalues, α_x , α_y and γ . Mathematically, the eigenvalue, γ , is nothing more than a separation constant which takes on specific values depending on the x , y dimensions of the displacement system. It turns out that γ has a physical meaning in the context of the stability problem under consideration. When an arbitrary disturbance is decomposed into its Fourier components, the eigenvalues determine the wavelengths of these components, for

$$\lambda = 2\pi/\gamma \quad 3.36$$

The solutions of the above eigenvalue problems yield

$$X(x) = E_1 e^{\pm i\alpha_x x} \quad 3.37$$

$$\alpha_x = \frac{m_1 \pi}{L_x}, \quad m_1 = 1, 2, 3, \dots \quad 3.38$$

$$Y(y) = E_2 e^{\pm i\alpha_y y} \quad 3.39$$

$$\alpha_y = \frac{m_2 \pi}{L_y}, \quad m_2 = 1, 2, 3, \dots \quad 3.40$$

$$Z(z) = E_3 e^{\pm \gamma z} \quad 3.41$$

and

$$\gamma_{m_1 m_2}^2 = \frac{m_1^2 \pi^2}{L_x^2} + \frac{m_2^2 \pi^2}{L_y^2} \quad 3.42$$

where E_1 , E_2 and E_3 are arbitrary constants, while m_1 and m_2 are integers.

Substituting Eqs.3.37, 3.39 and 3.41 into Eq. 3.24, gives

$$\Phi(x,y,z,t) = E_1 E_2 E_3 e^{\pm \gamma z + nt \pm i(\alpha_x x + \alpha_y y)} \quad 3.43$$

where $T(t)$ has been expressed as an exponential function. The fact that Φ_o must be bounded at $z = \infty$ and Φ_w similarly bounded at $z = -\infty$, because flow far away from the interface is uniform, dictates the following solutions for the perturbed velocity potentials in the oil and water phases:

$$\Phi_o = B_1 e^{-\gamma z + nt + i(\alpha_x x + \alpha_y y)} \quad 3.44$$

and

$$\Phi_w = B_2 e^{+\gamma z + nt + i(\alpha_x x + \alpha_y y)} \quad 3.45$$

where B_1 and B_2 are arbitrary constants.

Two boundary conditions apply at the interface - the kinematic condition which requires equality of the normal velocity components in both phases and the dynamic condition which allows for capillarity at the interface.

Let the perturbed interface about $z = 0$ be given by

$$z - \eta(x,y,t) = 0 \quad 3.46$$

where η is a displacement perturbation to be determined. The kinematic condition requires that

$$\frac{D}{Dt} [z - \eta(x,y,t)] = 0 \quad 3.47$$

where

$$\frac{D}{Dt} = \frac{\partial}{\partial t} + \vec{u}^* \cdot \nabla$$

Hence,

$$\frac{\partial \eta}{\partial t} + u_x^* \frac{\partial \eta}{\partial x} + u_y^* \frac{\partial \eta}{\partial y} = u_z^* \quad 3.48$$

Eq. 3.48 is the nonlinear partial differential equation for the displacement perturbation, the solution of which will determine the stability classification. Before solving, Eq. 3.48 is first linearized by assuming that the second order quantities $u_x^* \frac{\partial \eta}{\partial x}$ and $u_y^* \frac{\partial \eta}{\partial y}$ are negligibly small in comparison to $\frac{\partial \eta}{\partial t}$ and u_z^* . The linearized equation becomes

$$\frac{\partial \eta}{\partial t} = u_z^* \quad \text{at } z = \eta \quad 3.49$$

From Eq. 3.17,

$$u_z^* = - \frac{\partial \Phi}{\partial z} \quad 3.50$$

Thus,

$$\frac{\partial \eta}{\partial t} = - \frac{\partial \Phi}{\partial z} \Big|_{z=\eta} \quad 3.51$$

Application of the kinematic condition to the water and oil zones leads to

$$\frac{\partial \eta}{\partial t} = - \frac{\partial \Phi_w}{\partial z} \Big|_{z=\eta} = - \frac{\partial \Phi_o}{\partial z} \Big|_{z=\eta} \quad 3.52$$

Now, from Eq. 3.45,

$$\frac{\partial \Phi_w}{\partial z} \Big|_{z=\eta} = \gamma B_2 e^{\gamma \eta + nt + i(\alpha_x x + \alpha_y y)} \quad 3.53$$

If $\gamma \eta$ is assumed nearly equal to zero, then

$$\frac{\partial \Phi_w}{\partial z} \Big|_{z=\eta} = \gamma B_2 e^{nt + i(\alpha_x x + \alpha_y y)} \quad 3.54$$

Similarly,

$$\frac{\partial \Phi_o}{\partial z} \Big|_{z=\eta} = -\gamma B_1 e^{nt + i(\alpha_x x + \alpha_y y)} \quad 3.55$$

From Eq. 3.52, it follows that

$$B_2 = -B_1 \quad 3.56$$

Thus,

$$\frac{\partial \eta}{\partial t} = \gamma B_1 e^{nt + i(\alpha_x x + \alpha_y y)} \quad 3.57$$

which may be immediately integrated to yield the displacement perturbation:

$$\eta(x, y, t) = \frac{\gamma}{n} B_1 e^{nt + i(\alpha_x x + \alpha_y y)} \quad 3.58$$

Next, the stability index, n , is related to the rock and fluid properties and the eigenvalues by application of the dynamic boundary condition:

$$(p_w - p_o)_{z=\eta} = \sigma^*(c_1 + c_2) + P_c(t) \quad 3.59$$

In Eq. 3.59, $P_c(t)$ accounts for the microscopic fluid/fluid capillary pressure drop; σ^* is a pseudo or effective interfacial tension between the fluids which in the case of displacement in parallel plates is equal to the measured fluid/fluid interfacial tension; c_1 and c_2 are the principal curvatures of the macroscopic interface separating the oil and water zones. For small frontal perturbations,

$$c_1 = -\frac{\partial^2 \eta}{\partial x^2} \quad \text{and} \quad c_2 = -\frac{\partial^2 \eta}{\partial y^2} \quad 3.60$$

Now, from Eq. 3.16

$$p_w = \frac{\mu_w}{K_{wr}} \Phi_w - \frac{\mu_w}{K_{wr}} Vz - \rho_w g z \cos \alpha + P_w(t) \quad 3.61$$

and

$$p_o = \frac{\mu_o}{K_{or}} \Phi_o - \frac{\mu_o}{K_{or}} Vz - \rho_o g z \cos \alpha + P_o(t) \quad 3.62$$

Substituting Eqs. 3.60, 3.61 and 3.62 into 3.59 gives

$$\left[\frac{\mu_w}{K_{wr}} \Phi_w - \frac{\mu_o}{K_{or}} \Phi_o \right]_{z=\eta} + \eta \left(\frac{\mu_o}{K_{or}} - \frac{\mu_w}{K_{wr}} \right) V + (\rho_o - \rho_w) g \eta \cos \alpha + \sigma^* \left(\frac{\partial^2 \eta}{\partial x^2} + \frac{\partial^2 \eta}{\partial y^2} \right) + P_w(t) - P_o(t) - P_c(t) = 0 \quad 3.63$$

By definition,

$$P_c(t) = P_w(t) - P_o(t) \quad 3.64$$

Substituting for Φ_w , Φ_o , η and $P_c(t)$ into Eq. 3.63 and assuming $\gamma \eta$ small, one obtains the characteristic equation:

$$\left(\frac{\mu_o}{K_{or}} + \frac{\mu_w}{K_{wr}} \right) n - \gamma \left[\left(\frac{\mu_o}{K_{or}} - \frac{\mu_w}{K_{wr}} \right) V + (\rho_o - \rho_w) g \cos \alpha \right] + \sigma^* \gamma^3 = 0 \quad 3.65$$

The stability index is then given by

$$n = \frac{\gamma \left[\left(\frac{\mu_o}{K_{or}} - \frac{\mu_w}{K_{wr}} \right) V + (\rho_o - \rho_w) g \cos \alpha \right] - \sigma^* \gamma^3}{\left(\frac{\mu_o}{K_{or}} + \frac{\mu_w}{K_{wr}} \right)} \quad 3.66$$

The sign of the exponent, n , determines the stability classification. A necessary and sufficient condition for instability is that n be positive. This condition is met whenever

$$\left(\frac{\mu_o}{K_{or}} - \frac{\mu_w}{K_{wr}} \right) V + (\rho_o - \rho_w) g \cos \alpha > \sigma^* \gamma^2 \quad 3.67$$

The above inequality may be expressed as a number of necessary and sufficient conditions for instability. It is convenient to define a critical velocity as

$$\left(\frac{\mu_o}{K_{or}} - \frac{\mu_w}{K_{wr}} \right) V_c + (\rho_o - \rho_w) g \cos \alpha = 0 \quad 3.68$$

$$\text{i.e. } V_c = \frac{K_{wr} \Delta \rho g \cos \alpha}{\mu_w (M - 1)} \quad 3.69$$

Subtracting Eq. 3.68 from 3.67, yields

$$\left(\frac{\mu_o}{K_{or}} - \frac{\mu_w}{K_{wr}}\right)(V - V_c) > \sigma^* \gamma^2 \quad 3.70$$

Substituting Eq. 3.36 into 3.70, the condition for instability becomes

$$\lambda > 2\pi \left[\frac{\frac{K_{wr}}{\mu_w} \sigma^*}{(M - 1)(V - V_c)} \right]^{1/2} \quad 3.71$$

Let a critical wavelength be defined as

$$\lambda_c = 2\pi \left[\frac{\frac{K_{wr}}{\mu_w} \sigma^*}{(M - 1)(V - V_c)} \right]^{1/2} \quad 3.72$$

The necessary and sufficient condition for instability expressed by Eq. 3.67 may now be stated in the following equivalent but more elaborate form:

$$V > V_c \quad 3.73$$

$$M > 1 \quad 3.74$$

$$\lambda > \lambda_c \quad 3.75$$

The three conditions must be met simultaneously if instability is to occur.

A close examination of Eq. 3.66 shows that the exponent, n , possesses a maximum at a certain eigenvalue, γ_m . This indicates the presence of a most probable wavelength in the stability problem. Differentiating n with respect to γ and equating to zero gives

$$\left[\left(\frac{\mu_o}{K_{or}} - \frac{\mu_w}{K_{wr}} \right) V + (\rho_o - \rho_w) g \cos \alpha \right] - 3\sigma^* \gamma^2 = 0 \quad 3.76$$

Introducing Eq. 3.36 into 3.76 and rearranging gives the most probable wavelength as

$$\lambda_m = 2\pi\sqrt{3} \left[\frac{\frac{K_{wr}}{\mu_w} \sigma^*}{(M-1)(V-V_c)} \right]^{1/2} \quad 3.77$$

Thus,

$$\lambda_m = \lambda_c \sqrt{3} \quad 3.78$$

In parallel plate models, σ^* is the interfacial tension between the fluids. In porous media, the value of σ^* is unknown. Assuming σ^* is proportional to σ , then

$$\sigma^* = C^* \sigma \quad 3.79$$

With this assumption, Eq. 3.77 becomes

$$\lambda_m = 2\pi\sqrt{3C^*} \left[\frac{\frac{K_{wr}}{\mu_w} \sigma}{(M-1)(V-V_c)} \right]^{1/2} \quad 3.80$$

Alternatively,

$$\lambda_m = C \left[\frac{\frac{K_{wr}}{\mu_w} \sigma}{(M-1)(V-V_c)} \right]^{1/2} \quad 3.81$$

where C , hereafter referred to as Chuoke's constant, is given by

$$C = 2\pi\sqrt{3C^*} \quad 3.82$$

The constant, C , may be determined by actual measurement of the most probable wavelength of instability, where such can be captured in an experiment.

In a horizontal system, the critical rate is zero; as a result, the rate condition for instability is always met. Whether instability actually occurs will therefore depend upon the fulfilment of the remaining two conditions. If it is assumed that the permeabilities at residual fluid saturations are equal to the absolute permeability

of the porous medium, then Eq. 3.81 becomes

$$\lambda_m = C \left[\frac{K\sigma}{(\mu_o - \mu_w)V} \right]^{1/2} \quad 3.83$$

while the conditions for instability reduce to

$$\frac{\mu_o}{\mu_w} > 1 \quad 3.84$$

and

$$\lambda > \lambda_c \quad 3.85$$

Chuoque et al. (7) conducted a number of experiments to verify their theory. Three displacement systems were studied; namely, an inclined Hele-Shaw model without a porous medium, van Meurs' (34) transparent model packed with glass powder in the absence of connate water saturation and the same model in the presence of connate water saturation.

In the parallel plate displacements, there was excellent agreement between the theoretical predictions and the experimental findings. At a viscosity ratio of 2.5, they observed a stable displacement front at rates below the critical predicted by Eq. 3.69. At rates higher than this critical, the displacement became unstable and viscous fingers developed at the front. The sinusoidal character of the fingers permitted direct experimental measurement of their average wavelength. Again, there was excellent agreement between the measured wavelength and the most probable wavelength predicted by Eq. 3.77. At still higher rates, more numerous fingers were formed with the consequent decrease in wavelength just as predicted by Eq. 3.77.

This close agreement between the theoretical predictions and the experimental results in parallel plate displacements was not altogether unexpected because the hydrodynamic equations (Eqs. 3.1 and 3.2) upon which the stability theory is founded constitute an accurate mathematical representation of flow between parallel plates.

In the displacements involving porous media in the absence of connate water saturation, viscous fingers were again clearly visible. In contrast to the parallel plate displacements, the fingering phenomenon was much more disorderly. Also, the sinusoidal character of the fingers was less apparent. As the oil viscosity increased, the fingers became more numerous in accordance with the trends predicted by the theory. Because the pseudo-interfacial tension, σ^* , is unknown for displacements in porous media, no a priori prediction of the most probable wavelength of instability could be undertaken. However, by experimentally measuring the average wavelength of the fingers as best they could, the authors fitted the experimental observations to the theory by calculating the constant C in Eq. 3.83. They obtained the best fit when C was about 30.

In the connate water bearing displacements, the results and observations were not as clear-cut. The authors showed a photograph of the displacement pattern with evidence of fingering obtained at an extremely high displacement rate. In contrast to the previous cases, the fingering lacked any definite pattern. As a result, the authors did not attempt any measurements that might lead to quantitative predictions of instability and viscous fingering in connate water bearing systems.

After conceding insufficient quantitative experimental data to test their stability theory in connate water bearing systems, Chuoke et al. (7) proceeded to comment significantly on the stability of such systems. They asserted that for a strongly water-wet system containing connate water saturation, the unknown pseudo-interfacial tension, σ^* , was likely to be high, a fact that would greatly limit the possibility of instability in such systems. Also, a high pseudo-interfacial tension may give rise to critical wavelengths far in excess of the model dimensions, with the consequence that instabilities, though present, cannot manifest themselves in spectacular ways.

These observations suggest the possibility that if the most probable wavelength of instability could somehow be measured and applied to Eq. 3.83, then one could fit the experimental observations to the theory and obtain a value of C much larger than in a comparable displacement in the absence of connate water. No such measurements and direct estimation of C have been undertaken, although some indirect calculations have been attempted with doubtful results (31, 32, 33).

Chuoke et al. (7) also addressed the question of scaling unstable displacements. To account for instability, they suggested that the ratio of the most probable wavelength to model width, λ_m/D , be scaled in addition to the usual scaling requirements for immiscible displacement. Based upon the observed oil recovery behaviour of their system, they recognized that strict equality of λ_m/D in model and prototype was not essential at all rates in order that one might predict the behaviour of the other. They identified the following

three regions of flood operation in which to study the scaling requirements.

If $\lambda_m/D \ll 1$, as in a high rate displacement, numerous fingers were formed with the result that the breakthrough recovery became essentially independent of rate or λ_m/D . In this range of operation, the λ_m/D in the model may differ from that in the prototype, yet the recovery from one will be equal to the other. Strict compliance with the scaling requirement is therefore not essential for predictive purposes.

Similarly, at the other extreme, if $\lambda_m/D \gg 1$, as in very low rate displacements, then the most probable wavelength will far exceed the model width. Because the instabilities cannot manifest themselves significantly under these conditions, the breakthrough recovery will again be independent of rate or λ_m/D . As before, strict scaling will not be required for the purposes of recovery predictions.

Sandwiched between the two extremes is the transition region in which the breakthrough recovery varies significantly with rate or λ_m/D . It turns out that this is the region in which λ_m/D is of the order of one. It is obvious that slight differences in λ_m/D between model and prototype could result in significantly different recoveries. It is therefore only in this region that the equality of λ_m/D between the model and the prototype must be enforced if one is to accurately predict the recovery of the other.

de Haan (30) also investigated the variation of breakthrough recovery with viscous fingering in displacement systems without

connate water saturation. Assuming C equal to 30, he calculated the dimensionless rates at which the critical wavelengths of the viscous fingers would equal his core diameter at viscosity ratios of 4 and 25. As expected from the previously discussed scaling requirements, the calculated rates were in the region of significant recovery variation with rate. This observation provided further confirmation of the validity of Chuoke's stability theory, at least, for displacements in the absence of connate water saturation.

Rachford (12), questioned the applicability of a stability theory based on a parallel plate displacement model to immiscible displacement in strongly water-wet systems containing connate water saturation. He argued that as the displacement in connate water bearing systems obeyed the Buckley-Leverett model, a stability theory that sought to explain any unusual displacement behaviour in such systems should be founded on the Buckley-Leverett equations. He attempted the first such stability analysis.

Introducing pressure perturbations into the Buckley-Leverett equations, Rachford (12) successfully derived the partial differential equations governing these perturbations. However, unable to cope with highly nonlinear equations with varying coefficients, he assumed the coefficients constant. Even so, he resorted to numerical techniques based on a few selected initial perturbations to obtain solutions. His stability theory, though based on the Buckley-Leverett equations, appears to be limited in two respects. First, the assumption of constant coefficients in place of varying ones is at best questionable. Second, the results of a stability analysis based on a few selected rather than arbitrary initial perturbations cannot be generalized.

These limitations notwithstanding, the author observed certain aspects of the stability of connate water bearing displacements worthy of note. He found no tendency towards instability in all the cases studied. Furthermore, high displacement rates and adverse viscosity ratios were beneficial to stability as the perturbations decayed most rapidly under these conditions. Based on these observations, he concluded that no additional scaling was required to account for instability in connate water bearing displacements, as no instability was evident in the cases studied.

Concerned by the apparent controversy in the literature regarding instability and viscous fingering during immiscible displacements, Perkins and Johnston (36) investigated the problem experimentally. Their displacement systems were similar to the three employed by Chuoke et al. (7).

In all the systems studied, no fingering occurred at favourable viscosity ratios. At adverse viscosity ratios, severe fingering was observed in both the Hele-Shaw model and the glass bead pack without connate water saturation. The bead pack with connate water saturation showed a behaviour that was remarkably different. Numerous small fingers developed at the inlet end of the system early in the displacement. They were, however, subsequently damped out to form a graded saturation distribution before they could advance far into the model, for the range of displacement rates studied. Because of the striking influence of connate water saturation on the displacement behaviour, the authors concluded that fingering studies that would be most meaningful with respect to water-wet reservoirs should be conducted on connate water bearing porous media.

As recently as 1974, Hagoort (13) considered certain stability questions in water-wet media containing connate water saturation as still unanswered. He therefore offered yet another stability theory for such systems. Like Rachford (12), he argued that the stability analysis should be based on the Buckley-Leverett displacement model. But after reviewing the characteristics of this model, he assumed a constant shock saturation behind the front, contrary to the requirements of the model for adverse mobility ratios. In addition to violating the material balance requirements for the displacement, this assumption effectively rendered his stability analysis equivalent to that of Chuoke et al. (7). It is therefore not surprising when Hagoort (13) concluded that the stability analysis based on piston-like displacements was directly applicable to Buckley-Leverett displacements.

His stability theory differed from that of Chuoke et al. (7) in two important respects. The mobility ratio condition for instability was based on a so-called shock mobility ratio rather than on the end point mobility ratio. The shock mobility ratio was defined as

$$M_s = \left[\frac{K_{or} K_{ro}(S_f)}{\mu_o} + \frac{K_{wr} K_{rw}(S_f)}{\mu_w} \right] / \frac{K_{or}}{\mu_o} \quad 3.86$$

In Chuoke's theory, the role of capillary forces in determining the wavelengths of instability emerged naturally as part of the stability analysis. In his theory, Hagoort (13) merely assumed that capillary forces determined the wavelength of the instability and used energy arguments to justify this assumption.

His stability conclusion therefore lacked the existence of a critical wavelength. Instead, he concluded that the displacement was unstable if the shock mobility ratio was greater than one, provided that the wavelength of the instabilities was smaller than the model width.

Since the shock mobility ratio is considerably lower than the end point mobility ratio, it is possible for the shock mobility ratio to be less than one even at very adverse end point mobility ratios. Hagoort (13) attributes the lack of instability in Rachford's (12) studies to such a condition. Although an end point mobility ratio of up to 23 was studied, the shock mobility ratio was less than one for all the cases examined.

The author conducted several adverse viscosity ratio displacements in the presence of connate water saturation to verify his theory. His major conclusion was to attribute a decrease of breakthrough recovery at high rate to instability for which the wavelength was sufficiently small to be accommodated in the model.

A similar decrease in breakthrough recovery at high displacement rates has been observed by Wiborg (32), Kloepper (31) and Baird (33). Although the decrease in recovery in these studies was attributed to instability and viscous fingering, no positive evidence of fingering was presented. Instead, attempts were made to calculate the constant C in Eq. 3.83 on the assumption that the stability theory of Chuoke et al. (7) was applicable to their connate water bearing systems.

Since no experimental records of fingering were available upon which to measure the wavelengths of any fingers that might be

present, C was estimated indirectly by assuming that the rate at which the decrease in recovery became noticeable marked the onset of fingering, and that at this rate, the critical wavelength of the fingers would equal the core diameter. But the theoretical calculations of de Haan (30) would seem to indicate otherwise. Using a value of 30 for C obtained by Chuoke et al. (7), he estimated the dimensionless rates at which the critical wavelength of instability would equal his core diameter at viscosity ratios of 4 and 25. The fact that the estimated rates were well into the regions in which the recovery had decreased significantly would seem to indicate a lack of correspondence between the rate of onset of recovery decrease, and the rate at which the critical wavelength of instability would equal the core diameter.

The difficulty of estimating the rate at which the critical wavelength of instability would equal the core diameter from the recovery data may in part account for the different estimates of C obtained in these studies. Wiborg (32) estimated C values of 27.7, 24.3 and 39.4 using three different oils; Kloefer (31), a value of 64; and Baird (33), values of 118 and 139 using two different oils.

A review of the literature has been undertaken to indicate the current state of the art in the treatment of viscous fingering as a problem of hydrodynamic stability in porous media. Two distinct displacement systems seem to have emerged depending on the presence or absence of connate water saturation in the porous body.

Chuoke et al. (7) have presented quantitative predictions of instability and viscous fingering in Hele-Shaw models and porous

media without connate water saturation. No quantitative predictions were presented for instability and viscous fingering in porous media with connate water saturation, which are closer to the conditions in petroleum reservoirs. Furthermore, the construction of stability theories specifically addressed to connate water bearing systems based on the Buckley-Leverett equations has met with only limited success in the face of what appears to be an insurmountable mathematical task.

Severe fingering has been demonstrated at adverse viscosity ratios in Hele-Shaw models and porous media in the absence of connate water saturation, thus confirming the inherent instability of the displacements in these systems. The displacement behaviour of systems with connate water saturation under similar conditions, remains something of an enigma. The reported damping of viscous fingers on these systems would seem to indicate the inherent stability of the displacements in such systems, yet the decrease in recovery at high rates documented by numerous investigators indicates instability here as well, perhaps an instability without conspicuous fingering.

The theoretical objectives of the present study were therefore twofold: first, to extend the theory of Chuoke et al. (7) in order to predict the onset of instability in cylindrical and rectangular systems both in the presence and absence of connate water saturation; second, to attempt a stability theory based on the Buckley-Leverett equations. Experimentally, it was the purpose of this study to capture viscous fingering in the presence and absence of connate water saturation in order to verify the various stability

theories, and to attempt quantitative predictions based on the measurements conducted on the fingers.

CHAPTER 4

STABILITY THEORIES OF IMMISCIBLE DISPLACEMENT IN POROUS MEDIA

4.1 GENERAL

The stability analysis of immiscible displacement based on the Buckley-Leverett equations is undertaken in this chapter. Also presented is an extension of the theory of Chuoke et al. (7) to predict the onset of instability in cylindrical and rectangular systems.

4.2 STABILITY THEORY OF BUCKLEY-LEVERETT DISPLACEMENTS

4.2.1 Perturbation Equation for Fractional Flow

The partial differential equation for the fractional flow of water (Eq. 2.79), together with the appropriate initial and boundary conditions are:

$$(f_w - G)^2 \frac{\partial^2 f_w}{\partial S^2} = N_c C \frac{\partial f_w}{\partial \tau} \quad 0 < S < 1 \quad 4.1$$

$$f_w(S, 0) = 1 \quad 4.2$$

$$f_w(0, \tau) = 0 \quad 4.3$$

$$f_w(1, \tau) = 1 \quad 4.4$$

Let \bar{f}_w be the stationary solution of the fractional flow equation.

$$(\bar{f}_w - G)^2 \frac{\partial^2 \bar{f}_w}{\partial S^2} = 0 \quad 4.5$$

$$\bar{f}_w(S, 0) = 1 \quad 4.6$$

$$\bar{f}_w(0, \tau) = 0 \quad 4.7$$

$$\bar{f}_w(1, \tau) = 1 \quad 4.8$$

If the stationary solution is subjected to a first order perturbation, then the perturbed fractional flow is given by

$$f_w = \bar{f}_w + f_w^* \quad 4.9$$

Substituting Eq. 4.9 into Eqs. 4.1, 4.3 and 4.4 gives

$$(\bar{f}_w + f_w^* - G)^2 \frac{\partial^2}{\partial S^2} (\bar{f}_w + f_w^*) = N_c C \frac{\partial}{\partial \tau} (\bar{f}_w + f_w^*) \quad 4.10$$

$$\bar{f}_w(0, \tau) + f_w^*(0, \tau) = 0 \quad 4.11$$

$$\bar{f}_w(1, \tau) + f_w^*(1, \tau) = 1 \quad 4.12$$

Substituting Eqs. 4.5 to 4.8 into 4.10 to 4.12 yields the following partial differential equation for the fractional flow perturbation:

$$(\bar{f}_w + f_w^* - G)^2 \frac{\partial^2 f_w^*}{\partial S^2} + (\bar{f}_w + f_w^* - G)^2 \frac{\partial^2 \bar{f}_w}{\partial S^2} = N_c C \frac{\partial f_w^*}{\partial \tau} \quad 4.13$$

$$f_w^*(0, \tau) = 0 \quad 4.14$$

$$f_w^*(1, \tau) = 0 \quad 4.15$$

In the frontal zone,

$$\frac{\partial^2 \bar{f}_w}{\partial S^2} = 0, \quad 0 < S < S_f \quad 4.16$$

and the perturbation equation becomes

$$(\bar{f}_w - G)^2 \frac{\partial^2 f_w^*}{\partial S^2} - N_c C \frac{\partial f_w^*}{\partial \tau} = -[2f_w^*(\bar{f}_w - G) + f_w^{*2}] \frac{\partial^2 f_w^*}{\partial S^2} \quad 4.17$$

$$f_w^*(0, \tau) = 0 \quad 4.18$$

$$f_w^*(S_f, \tau) = 0 \quad 4.19$$

To complete the mathematical formulation, an arbitrary initial perturbation is specified as

$$f_w^*(S, 0) = \alpha_1(S) \quad 4.20$$

Eqs. 4.17 to 4.20 constitute a nonlinear initial-boundary value problem for the fractional flow perturbation in the frontal zone of the Buckley-Leverett displacement model.

Behind the displacement front,

$$\bar{f}_w - G = 0 \quad S_f < S < 1 \quad 4.21$$

and the initial-boundary value problem for the perturbation takes on the form:

$$N_c C \frac{\partial f_w^*}{\partial \tau} = f_w^{*2} \frac{\partial^2 f_w^*}{\partial S^2} + f_w^{*2} \frac{\partial^2 \bar{f}_w}{\partial S^2} \quad S_f < S < 1 \quad 4.22$$

$$f_w^*(S_f, \tau) = 0 \quad 4.23$$

$$f_w^*(1, \tau) = 0 \quad 4.24$$

$$f_w^*(S, 0) = \alpha_2(S) \quad 4.25$$

where $\alpha_2(S)$ is an arbitrary initial fractional flow perturbation behind the displacement front.

4.2.2 Lagrangian Formulation

The stability of the Buckley-Leverett displacement may also be studied by introduction of perturbations into the Lagrangian form of the displacement equation. This equation together with a possible set of initial and boundary conditions is given by

$$(f_w - G) \frac{\partial^2 X}{\partial S^2} + \left(\frac{\partial X}{\partial \tau} - G' \right) \frac{\partial X}{\partial S} + N_c C' = 0 \quad 4.26$$

$$X(0, \tau) = \psi(\tau) \quad \tau > 0 \quad 4.27$$

$$X(1, \tau) = 0 \quad 4.28$$

$$X(S, 0) = 0 \quad 4.29$$

$$f_w(S, 0) = 1 \quad 4.30$$

$$f_w(0, \tau) = 0 \quad 4.31$$

$$f_w(1, \tau) = 1 \quad 4.32$$

The perturbed displacement is

$$X = \bar{X} + X^* \quad 4.33$$

Introducing Eqs. 4.33 and 4.9 into 4.26,

$$(\bar{f}_w + f_w^* - G) \left(\frac{\partial^2 \bar{X}}{\partial S^2} + \frac{\partial^2 X^*}{\partial S^2} \right) + \left(\frac{\partial \bar{X}}{\partial \tau} + \frac{\partial X^*}{\partial \tau} - G' \right) \left(\frac{\partial \bar{X}}{\partial S} + \frac{\partial X^*}{\partial S} \right) + N_c C' = 0 \quad 4.34$$

The unperturbed stationary solution satisfies

$$(\bar{f}_w - G) \frac{\partial^2 \bar{X}}{\partial S^2} + \left(\frac{\partial \bar{X}}{\partial \tau} - G' \right) \frac{\partial \bar{X}}{\partial S} + N_c C' = 0 \quad 4.35$$

Subtracting Eq. 4.35 from 4.34 yields the following perturbation equation:

$$(\bar{f}_w + G) \frac{\partial^2 X^*}{\partial S^2} + \left(\frac{\partial \bar{X}}{\partial \tau} - G' \right) \frac{\partial X^*}{\partial S} + \frac{\partial \bar{X}}{\partial S} \frac{\partial X^*}{\partial \tau} = - \left(f_w^* \frac{\partial^2 \bar{X}}{\partial S^2} + f_w^* \frac{\partial^2 X^*}{\partial S^2} + \frac{\partial X^*}{\partial S} \frac{\partial X^*}{\partial \tau} \right) \quad 4.36$$

At stationary or stabilized conditions,

$$\frac{\partial \bar{X}}{\partial \tau} = \frac{\partial \bar{f}_w}{\partial S} \quad 4.37$$

and

$$\frac{\partial \bar{X}}{\partial S} = - \frac{N_c C}{\bar{f}_w - G} \quad 4.38$$

Substituting Eqs. 4.37 and 4.38 into 4.36 gives upon rearrangement,

$$\begin{aligned}
 & (\bar{f}_w - G)^2 \frac{\partial^2 X^*}{\partial S^2} + (\bar{f}_w - G)(\bar{f}_w - G)' \frac{\partial X^*}{\partial S} - N_c C \frac{\partial X^*}{\partial \tau} \\
 & = - (\bar{f}_w - G) \left(f_w^* \frac{\partial^2 \bar{X}}{\partial S^2} + f_w^* \frac{\partial^2 X^*}{\partial S^2} + \frac{\partial X^*}{\partial S} \frac{\partial X^*}{\partial \tau} \right)
 \end{aligned} \tag{4.39}$$

Because the boundary conditions were not perturbed, the above perturbation equation will be subject to homogeneous boundary conditions of the form

$$X^*(0, \tau) = 0 \tag{4.40}$$

$$X^*(1, \tau) = 0 \tag{4.41}$$

As before, the interval $S(0, 1)$ may be divided into a frontal zone $S(0, S_f)$, and a trailing zone $S(S_f, 1)$. For these sub-intervals, the perturbation equations become

$$\begin{aligned}
 & (\bar{f}_w - G)^2 \frac{\partial^2 X^*}{\partial S^2} + (\bar{f}_w - G)(\bar{f}_w - G)' \frac{\partial X^*}{\partial S} - N_c C \frac{\partial X^*}{\partial \tau} \\
 & = - (\bar{f}_w - G) \left(f_w^* \frac{\partial^2 \bar{X}}{\partial S^2} + f_w^* \frac{\partial^2 X^*}{\partial S^2} + \frac{\partial X^*}{\partial S} \frac{\partial X^*}{\partial \tau} \right)
 \end{aligned} \tag{4.42}$$

$$X^*(0, \tau) = 0 \tag{4.43}$$

$$X^*(S_f, \tau) = 0 \tag{4.44}$$

$$X^*(S, 0) = \beta_1(S) \tag{4.45}$$

and

$$N_c C \frac{\partial X^*}{\partial \tau} = 0 \tag{4.46}$$

$$X^*(S_f, 0) = 0 \tag{4.47}$$

$$X^*(1, 0) = 0 \tag{4.48}$$

$$X^*(S, 0) = \beta_2(S) \tag{4.49}$$

where $\beta_1(S)$ and $\beta_2(S)$ are arbitrary initial perturbations.

The mathematical derivation of the perturbation equations is now complete. In general, the equations are nonlinear partial differential equations subject to homogeneous boundary conditions. Because of the nature of the stationary solutions of the Buckley-Leverett equations, the perturbation problems have divided naturally into two subintervals - a frontal zone and a trailing zone. To determine the stability or otherwise of the Buckley-Leverett displacement, these equations must now be solved, at least formally. The growth of the perturbations with time indicates instability, whereas a decay of the perturbations indicates stability.

4.2.3 Solution of the Linearized Fractional Flow Equation

The analytical solution of the nonlinear perturbation equation is in general difficult. If the perturbations are, however, assumed to be infinitesimally small, then the nonlinear terms may be neglected. The resulting linear equations are more amenable to analytical solutions.

In the frontal zone, the linearized fractional flow perturbation equation is

$$(\bar{f}_w - G)^2 \frac{\partial^2 f_w^*}{\partial S^2} - N_c C \frac{\partial f_w^*}{\partial \tau} = 0 \quad 0 < S < S_f \quad 4.50$$

together with the auxiliary conditions expressed by Eqs. 4.18 to 4.20. Eq. 4.50 may be solved by the method of separation of variables. Let

$$f_w^*(S, \tau) = F(S)T(\tau) \quad 4.51$$

Substituting Eq. 4.51 into 4.50 and separating variables leads to the following two ordinary differential equations:

$$T' + \frac{\lambda}{N_c} T = 0 \quad 4.52$$

and

$$(\bar{f}_w - G)^2 F'' + \lambda CF = 0 \quad 4.53$$

$$F(0) = 0 \quad 4.54$$

$$F(S_f) = 0 \quad 4.55$$

where λ is the separation constant. Eq. 4.52 gives the time behaviour of the fractional flow perturbation:

$$T(\tau) = e^{-\frac{\lambda}{N_c} \tau} \quad 4.56$$

Eqs. 4.53 to 4.55 constitute an eigenvalue problem of ordinary differential equations. To obtain nontrivial solutions, λ takes on specific discrete eigenvalues. Corresponding to each eigenvalue λ_n is an eigenfunction F_n . It turns out that Eqs. 4.53 to 4.55 constitute a special case of Sturm-Liouville system for which extensive theory exists (37).

Two properties of Eqs. 4.53 to 4.55 are of interest in the stability problem under consideration. These are the sign of the eigenvalues, and the orthogonality of the eigenfunctions. The sign of the eigenvalues determines the stability conclusion while the orthogonality of the eigenfunctions ensures that any arbitrary initial perturbation can be represented as an infinite series.

To determine the sign of the eigenvalues, Eq. 4.53 is first rearranged as

$$[F']' + \lambda \frac{C}{(\bar{f}_w - G)^2} F = 0 \quad 0 < S < S_f \quad 4.57$$

Let λ_n be an eigenvalue and F_n the corresponding eigenfunction.

Multiplying Eq. 4.57 by F_n and integrating between the limits, one obtains

$$\int_0^{S_f} F_n [F_n']' dS + \lambda_n \int_0^{S_f} \frac{C}{(\bar{f}_w - G)^2} F_n^2 dS = 0 \quad 4.58$$

Integrating the first term of Eq. 4.59 by parts yields

$$[F_n F_n']_0^{S_f} - \int_0^{S_f} F_n'^2 dS + \lambda_n \int_0^{S_f} \frac{C}{(\bar{f}_w - G)^2} F_n^2 dS = 0 \quad 4.59$$

Applying the homogeneous boundary conditions, Eq. 4.54 and 4.55, and rearranging gives

$$\lambda_n = \frac{\int_0^{S_f} F_n'^2 dS}{\int_0^{S_f} \frac{C}{(\bar{f}_w - G)^2} F_n^2 dS} \quad 4.60$$

Since $C/(\bar{f}_w - G)^2$, $F_n'^2$ and F_n^2 are all positive in the open interval $S(0, S_f)$, both the numerator and the denominator of Eq. 4.60 are positive numbers. Hence all the eigenvalues of the problem at hand are positive.

The orthogonality of the eigenfunctions may be proved as follows. Let λ_n and λ_m be two distinct eigenvalues with corresponding eigenfunctions F_n and F_m . Then from Eq. 4.57

$$[F_n']' + \lambda_n \frac{C}{(\bar{f}_w - G)^2} F_n = 0 \quad 4.61$$

and

$$[F_m']' + \lambda_m \frac{C}{(\bar{f}_w - G)^2} F_m = 0 \quad 4.62$$

Multiplying Eq. 4.61 by F_m and 4.62 by F_n and subtracting, leads to

$$F_m[F_n']' - F_n[F_m']' + (\lambda_n - \lambda_m) \frac{C}{(\bar{f}_w - G)^2} F_n F_m = 0 \quad 4.63$$

Integrating Eq. 4.64 between the limits,

$$\int_0^{S_f} [(F_n' F_m)' - (F_n F_m')'] dS + (\lambda_n - \lambda_m) \int_0^{S_f} \frac{C}{(\bar{f}_w - G)^2} F_n F_m dS = 0 \quad 4.64$$

Thus,

$$[F_n' F_m - F_n F_m']_0^{S_f} + (\lambda_n - \lambda_m) \int_0^{S_f} \frac{C}{(\bar{f}_w - G)^2} F_n F_m dS = 0 \quad 4.65$$

From the boundary conditions, the first term of Eq. 4.65 is zero.

Hence,

$$(\lambda_n - \lambda_m) \int_0^{S_f} \frac{C}{(\bar{f}_w - G)^2} F_n F_m dS = 0 \quad 4.66$$

Since λ_n and λ_m are distinct, then

$$\int_0^{S_f} \frac{C}{(\bar{f}_w - G)^2} F_n F_m dS = 0 \quad 4.67$$

Thus, the eigenfunctions are orthogonal with respect to the weight function, $C/(\bar{f}_w - G)^2$.

A general solution of the perturbation equation may now be expressed as an infinite series:

$$f_w^*(S, \tau) = \sum_{n=1}^{\infty} A_n F_n e^{-\frac{\lambda_n}{N_c} \tau} \quad 4.68$$

where A_n are coefficients yet to be determined. Application of the initial condition yields

$$\alpha_1(S) = \sum_{n=1}^{\infty} A_n F_n \quad 4.69$$

To determine A_n , Eq. 4.69 is multiplied by $F_m C / (\bar{f}_w - G)^2$ and integrated between the limits.

$$\int_0^{S_f} \frac{\alpha_1 C F_m}{(\bar{f}_w - G)^2} dS = \sum_{n=1}^{\infty} A_n \int_0^{S_f} \frac{F_n F_m C}{(\bar{f}_w - G)^2} dS \quad 4.70$$

Because of the orthogonality of the eigengunctions, all the terms in the right hand summation of Eq. 6.70 are zero except the one term for which n equals m . Hence,

$$\int_0^{S_f} \frac{\alpha_1 C F_m}{(\bar{f}_w - G)^2} dS = A_m \int_0^{S_f} \frac{F_m^2 C}{(\bar{f}_w - G)^2} dS \quad 4.71$$

Thus, A_n can in theory be calculated from

$$A_m = \frac{\int_0^{S_f} \frac{\alpha_1 C F_m}{(\bar{f}_w - G)^2} dS}{\int_0^{S_f} \frac{F_m^2 C}{(\bar{f}_w - G)^2} dS} \quad 4.72$$

This completes the formal solution of the linearized fractional flow perturbation equation in the frontal zone. Since all the eigenvalues are positive, the perturbation decays exponentially with time, resulting in a stable displacement.

In the trailing zone, the linearized perturbation equation is obtained from Eq. 4.22 as

$$\frac{\partial f_w^*}{\partial \tau} = 0 \quad S_f < S < 1 \quad 4.73$$

together with the auxilliary conditions expressed by Eqs. 4.23 to 4.25. Integration and application of the auxilliary conditions give

$$f_w^*(S, \tau) = \alpha_2(S) \quad 4.74$$

where

$$\alpha_2(S_f) = 0 \quad 4.75$$

$$\alpha_2(1) = 0 \quad 4.76$$

According to the linearized theory, therefore, the initial perturbation in the trailing zone will tend to persist with time, neither growing nor decaying.

4.2.4 Solution of the Linearized Lagrangian Equation

Linearization of the Lagrangian perturbation equation (Eq. 4.42) in the frontal zone gives the following nonhomogeneous partial differential equation

$$\begin{aligned} (\bar{f}_w - G)^2 \frac{\partial^2 X^*}{\partial S^2} + (\bar{f}_w - G)(\bar{f}_w - G)' \frac{\partial X^*}{\partial S} - N_c C \frac{\partial X^*}{\partial \tau} \\ = - (\bar{f}_w - G) \frac{\partial^2 \bar{X}}{\partial S^2} f_w^* \end{aligned} \quad 4.77$$

together with the initial and boundary conditions expressed by Eqs. 4.43 to 4.45. The term, f_w^* , which occurs on the right hand side of Eq. 4.77 is known to be an exponentially decaying function of time. It is given by Eq. 4.68.

In order to solve Eq. 4.77, it is first necessary to solve the related homogeneous problem:

$$(\bar{f}_w - G)^2 \frac{\partial^2 X^*}{\partial S^2} + (\bar{f}_w - G)(\bar{f}_w - G)' \frac{\partial X^*}{\partial S} - N_c C \frac{\partial X^*}{\partial \tau} = 0 \quad 4.78$$

with the conditions expressed by Eqs. 4.43 to 4.45. Separating variables as before leads to the following Sturm-Liouville system:

$$[(\bar{f}_w - G)X']' + \gamma \frac{C}{(\bar{f}_w - G)} X = 0 \quad 4.79$$

$$X(0) = 0 \quad 4.80$$

$$X(S_f) = 0 \quad 4.81$$

where γ is the separation constant. Proceeding in a manner completely analogous to that of the previous section, it can be shown that the eigenvalues of Eq. 4.78 are positive and the eigenfunctions orthogonal with respect to the weight function $C/(\bar{f}_w - G)$.

Returning to the nonhomogeneous problem of Eq. 4.77, a solution is proposed in the form

$$X^*(S, \tau) = \sum_{n=1}^{\infty} T_n(\tau) X_n(S) \quad 4.82$$

where T_n is a function of time yet to be determined and X_n , the eigenfunction of Eq. 4.79; that is, the eigenfunction of the related homogeneous problem. This proposal takes advantage of the ability of eigenfunctions to represent arbitrary functions in an infinite series.

The next step is to determine the equation for T_n . Multiplying Eq. 4.82 by $X_m C/(\bar{f}_w - G)$ and integrating between the limits, one obtains

$$\int_0^{S_f} \frac{X^* X_m C}{(\bar{f}_w - G)} dS = \sum_{n=1}^{\infty} T_n \int_0^{S_f} \frac{X_n X_m C}{(\bar{f}_w - G)} dS \quad 4.83$$

In view of the orthogonality of the eigenfunctions, Eq. 4.83 yields

$$T_m(\tau) = \frac{\int_0^{S_f} \frac{\chi^* \chi_m C}{(\bar{f}_w - G)} dS}{\int_0^{S_f} \frac{\chi_m^2 C}{(\bar{f}_w - G)} dS} \quad 4.84$$

Let

$$F^*(S, \tau) = -(\bar{f}_w - G) \frac{\partial^2 \bar{\chi}}{\partial S^2} f_w^* \quad 4.85$$

$F^*(S, \tau)$ can also be represented by a convergent series of the form

$$F^*(S, \tau) = \sum_{n=1}^{\infty} B_n(\tau) \chi_n(S) \quad 4.86$$

The coefficients B_n are exponentially decaying functions of time due to the nature of f_w^* . They may be obtained from orthogonality considerations as

$$B_m(\tau) = \frac{\int_0^{S_f} \frac{\bar{F}^* \chi_m C}{(\bar{f}_w - G)} dS}{\int_0^{S_f} \frac{\chi_m^2 C}{(\bar{f}_w - G)} dS} \quad 4.87$$

Substituting Eqs. 4.82 and 4.86 into 4.77, yields

$$\begin{aligned} (\bar{f}_w - G)^2 \sum_{n=1}^{\infty} T_n \chi_n'' + (\bar{f}_w - G)(\bar{f}_w - G)' \sum_{n=1}^{\infty} T_n \chi_n' \\ - N_C C \sum_{n=1}^{\infty} T_n' \chi_n = \sum_{n=1}^{\infty} B_n \chi_n \end{aligned} \quad 4.88$$

From Eq. 4.79,

$$(\bar{f}_w - G)^2 \chi_n'' = - [(\bar{f}_w - G)(\bar{f}_w - G)' \chi_n' + \gamma_n C \chi_n] \quad 4.89$$

Substituting Eq. 4.89 into 4.88 and rearranging, leads to

$$\sum_{n=1}^{\infty} X_n [N_c C T_n' + \gamma_n C T_n + B_n] = 0 \quad 4.90$$

For Eq. 4.90 to be satisfied for all X_n requires that

$$N_c C T_n' + \gamma_n C T_n + B_n = 0 \quad 4.91$$

The desired differential equation for T_n is then given by

$$T_n' + \frac{\gamma_n}{N_c} T_n = - \frac{1}{N_c C} B_n \quad 4.92$$

for $n > 1$

The appropriate initial condition is obtained from Eq. 4.84 as

$$T_n(0) = \frac{\int_0^{S_f} \frac{\beta_1 X_m C}{(\bar{F}_w - G)} dS}{\int_0^{S_f} \frac{X_m^2 C}{(\bar{F}_w - G)} dS} \quad 4.93$$

The solution of Eq. 4.92 is given by

$$T_n(\tau) = T_n(0) e^{-\frac{\gamma_n}{N_c} \tau} - \frac{1}{N_c C} e^{-\frac{\gamma_n}{N_c} \tau} \int_0^{\tau} B_n(t) e^{\frac{\gamma_n}{N_c} t} dt \quad 4.94$$

Both terms on the right hand side of Eq. 4.94 tend to zero as τ tends to ∞ . Therefore, the perturbations are damped with time, resulting in a stable displacement in the frontal zone.

Behind the front, the perturbation equation (Eq. 4.46) reduces to

$$\frac{\partial X^*}{\partial \tau} = 0 \quad 4.95$$

together with the auxilliary conditions of Eqs. 4.47 to 4.49.

Integrating and applying the conditions, one obtains

$$X^*(S, \tau) = \beta_2(S) \quad 4.96$$

where

$$B_2(S_f) = 0 \quad 4.97$$

$$B_2(1) = 0 \quad 4.98$$

Eq. 4.96 indicates that the initial perturbation behind the front will tend to persist in time, neither growing nor decaying.

4.2.5 The Effects of Rate and Mobility Ratio on the Stability Problem

The time behaviour of the fractional flow and displacement perturbations in the frontal zone of the Buckley-Leverett displacement model has been shown to comprise of exponentially decaying functions

of the form $e^{-\frac{\lambda_n}{N_c} \tau}$ and $e^{-\frac{\gamma_n}{N_c} \tau}$. The rate at which the perturbations are damped is therefore directly proportional to λ_n/N_c or γ_n/N_c . As this ratio increases with the mobility ratio and the displacement rate, adverse mobility ratios and high displacements will be beneficial to the stability of the displacement front.

4.2.6 Summary

A first order linear stability analysis has been conducted on the one-dimensional Buckley-Leverett equation by two methods to determine the stability of immiscible displacements that obey the Buckley-Leverett model. First order perturbations were introduced into the fractional flow and displacement equations. A formal solution of the resulting perturbation equations has led to the same stability conclusions. The perturbations in the frontal zone are damped whereas those behind the front are not. Moreover, adverse viscosity or mobility ratios and high displacement rates are

beneficial to stability. These conclusions are contrary to the reported observations regarding instability in connate water bearing systems. The reasons for the failure of the stability analysis based on the one-dimensional Buckley-Leverett equations to reveal instability will be discussed later.

4.3 EXTENSION OF THE STABILITY THEORY OF CHUOKE ET AL. (7)

4.3.1 Cylindrical Systems

In cylindrical coordinates, (r, θ, z) , the partial differential equation for the perturbed velocity potential (Eq. 3.19) is given by

$$\frac{\partial^2 \Phi}{\partial r^2} + \frac{1}{r} \frac{\partial \Phi}{\partial r} + \frac{1}{r^2} \frac{\partial^2 \Phi}{\partial \theta^2} + \frac{\partial^2 \Phi}{\partial z^2} = 0 \quad 4.99$$

As before, the constant rate displacement is assumed to be in the z -direction inclined at an angle α to the upward vertical.

Eq. 4.99 may be solved by separation of variables. Let

$$\Phi(r, \theta, z, t) = R(r)\Theta(\theta)Z(z)T(t) \quad 4.100$$

Substituting Eq. 4.100 into 4.99 and dividing through by $R\Theta ZT$ gives

$$\frac{R''}{R} + \frac{1}{r} \frac{R'}{R} + \frac{1}{r^2} \frac{\Theta''}{\Theta} + \frac{Z''}{Z} = 0 \quad 4.101$$

Introducing various separation constants into Eq. 4.101 leads to the following problems:

$$Z'' - \gamma^2 Z = 0 \quad -\infty < z < \infty \quad 4.102$$

$$\Theta'' + \mu^2 \Theta = 0 \quad -\pi < \theta < \pi \quad 4.103$$

$$\Theta(-\pi) = \Theta(\pi) \quad 4.104$$

$$\Theta'(-\pi) = \Theta'(\pi) \quad 4.105$$

and

$$(rR')' - \frac{\mu^2}{r} R + \gamma^2 r R = 0 \quad 0 < r < a \quad 4.106$$

$$R'(a) = 0 \quad 4.107$$

In Eqs. 4.102 to 4.107, γ and μ are separation constants and a , the radius of the cylindrical system. The boundary conditions expressed by Eqs. 4.104 and 4.105 ensure that there is no discontinuity at the artificial boundaries $\theta = \pm\pi$. Eq. 4.107 is a statement of the fact that the radial perturbed velocity must vanish at the wall.

Integrating Eq. 4.102 gives

$$Z = E_1 e^{\pm\gamma Z} \quad 4.108$$

Integration of Eq. 4.103 leads to

$$\Theta = A \sin \mu \theta + B \cos \mu \theta \quad 4.109$$

Applying the boundary conditions (Eqs. 4.104 and 4.105), one obtains

$$\mu B \sin \mu \pi = 0 \quad 4.110$$

and

$$A \sin \mu \pi = 0 \quad 4.111$$

Eq. 4.110 yields the following eigenvalue and corresponding eigenfunction:

$$\mu = 0, \quad \Theta = B = \text{constant} \quad 4.112$$

while Eq. 4.111 gives

$$\mu = m, \quad \Theta = B \cos m \theta \quad 4.113$$

where

$$m = 1, 2, 3, \dots$$

Eq. 4.106 is Bessel's equation with the general solution

$$R = C_1 J_\mu(\gamma r) + D_1 Y_\mu(\gamma r) \quad 4.114$$

Since Y_μ is singular when r is zero, to ensure that R is bounded,

D_1 must be zero. Hence, using Eq. 4.113,

$$R = C_1 J_m(\gamma r) \quad 4.115$$

Applying the boundary condition at the wall (Eq. 4.107) gives

$$J'_m(\gamma a) = 0 \quad 4.116$$

The zeros of J'_m are tabulated in various handbooks (38). The first few zeros are reproduced in Table 4.1.

Table 4.1
ZEROS OF BESSEL FUNCTION, $J'_m(x)$

$m = 0$	$m = 1$	$m = 2$	$m = 3$
0.0000	1.8412	3.0542	4.2012
3.8317	5.3314	6.7061	8.0152
7.0156	8.5363	9.9695	11.3459
10.1735	11.7060	13.1704	14.5859
13.3237	14.8636	16.3475	17.7888
16.4706	18.0155	19.5129	20.9725

The various solutions can now be assembled to give the perturbed velocity potential as

$$\Phi(r, \theta, z, t) = E_1 B C_1 e^{\pm \gamma z + nt} \cos m \theta J_m(\gamma r) \quad 4.117$$

The perturbed velocity potentials in the oil and water zones are therefore given by

$$\Phi_o = B_1 e^{-\gamma z + nt} \cos m \theta J_m(\gamma r) \quad 4.118$$

and

$$\Phi_w = B_2 e^{+\gamma z + nt} \cos m \theta J_m(\gamma r) \quad 4.119$$

The kinematic boundary condition at the perturbed interface gives

$$\frac{\partial \eta}{\partial t} + u_r^* \frac{\partial \eta}{\partial r} + \frac{1}{r} u_\theta^* \frac{\partial \eta}{\partial \theta} = u_z^* \quad 4.120$$

which upon linearization gives

$$\frac{\partial \eta}{\partial t} = u_z^* \quad \text{at } z = \eta \quad 4.121$$

which is the same as Eq. 3.49. The dynamic boundary condition is given by

$$(P_w - P_o)_{z=\eta} = -\sigma^* \left(\frac{\partial^2 \eta}{\partial r^2} + \frac{1}{r} \frac{\partial \eta}{\partial r} + \frac{1}{r^2} \frac{\partial^2 \eta}{\partial \theta^2} \right) + P_c(t) \quad 4.122$$

Proceeding in a manner completely analogous to the derivation of Chapter 3, the stability index is again given by

$$n = \frac{\gamma \left[\left(\frac{\mu_o}{K_{or}} - \frac{\mu_w}{K_{wr}} \right) V + (\rho_o - \rho_w) g \cos \alpha \right] - \sigma^* \gamma^3}{\left(\frac{\mu_o}{K_{or}} + \frac{\mu_w}{K_{wr}} \right)} \quad 4.123$$

It is convenient to rearrange Eq. 4.123 as

$$n = \frac{\gamma_i \sigma^*}{\left(\frac{\mu_o}{K_{or}} + \frac{\mu_w}{K_{wr}} \right) a^2} \left[\frac{(M - 1)(V - V_c) \mu_w a^2}{\sigma^* K_{wr}} - (\gamma_i a)^2 \right] \quad 4.124$$

where a is the core radius and the subscript i has been used to indicate that the eigenvalues, γ , can take on different discrete values. The displacement will be unstable whenever n is positive, i.e.,

$$\frac{(M - 1)(V - V_c) \mu_w a^2}{\sigma^* K_{wr}} - (\gamma_i a)^2 > 0 \quad 4.125$$

At the stability boundary,

$$\frac{(M - 1)(V - V_c) \mu_w a^2}{\sigma^* K_{wr}} - (\gamma_i a)^2 = 0 \quad 4.126$$

Several interesting observations and deductions may now be made regarding instability in cylindrical systems. The most probable wavelength, λ_m , is determined by the value of $(M - 1)(V - V_c) \mu_w a^2 / \sigma^* K_{wr}$. If this term is large as in a high rate displacement, then the eigenvalues, γ_i , will be large, resulting in numerous fingers with

short wavelengths. If it is small, as in a low rate displacement, then γ_i will be small, resulting in large fingers whose wavelengths may exceed the core diameter.

It should be noted that the possible discrete values of $\gamma_i a$ are given in Table 4.1. As $(M - 1)(V - V_c)\mu_w a^2 / \sigma^* K_{wr}$ is decreased, say by decreasing the displacement rate, $\gamma_i a$ takes on smaller and smaller values until at a sufficiently low rate, it attains the minimum nonzero value of 1.8412 at $m = 1$. Below this rate, there can be no instability.

Thus, at the onset of instability,

$$\left[\frac{(M - 1)(V - V_c)\mu_w a^2}{\sigma^* K_{wr}} \right]^{1/2} = (\gamma_i a)_{\text{minimum}} = 1.8412 \quad 4.127$$

The critical wavelength at the onset of instability is given by

$$\lambda_c = \frac{2\pi a}{1.8412} \quad 4.128$$

and the ratio of the critical wavelength to the core diameter, by

$$\frac{\lambda_c}{D} = \frac{\pi}{1.8412} = 1.7063 \quad 4.129$$

Eq. 4.127 may be employed to determine an appropriate scaling group to detect instability. At the onset of instability,

$$\frac{(M - 1)(V - V_c)\mu_w D^2}{C^* \sigma K_{wr}} = 13.56 \quad 4.130$$

The dimensionless group $(M - 1)(V - V_c)\mu_w D^2 / C^* \sigma K_{wr}$ therefore divides the displacement domain in a cylindrical core into a stable and an unstable region. When this group is less than 13.56, the displacement is stable, whereas when the group is greater than 13.56, the displacement is unstable. The breakthrough recovery data should

therefore be correlated with this group, if one wishes to detect instability in such data.

Several alternative forms of the scaling group may be derived. With the introduction of Chuoke's constant given by Eq. 3.82, Eq. 4.130 becomes

$$\frac{(M - 1)(V - V_c)\mu_w D^2}{C^2_{\sigma} K_{wr}} = \frac{3.39}{3\pi^2} \quad 4.131$$

In general, for any displacement for which there is instability,

$$\frac{(M - 1)(V - V_c)\mu_w D^2}{C^2_{\sigma} K_{wr}} = \frac{1}{3} \left(\frac{D}{\lambda_c}\right)^2 \quad 4.132$$

Thus when λ_c/D equals one,

$$\frac{(M - 1)(V - V_c)\mu_w D^2}{C^2_{\sigma} K_{wr}} = \frac{1}{3} \quad 4.133$$

or

$$\frac{(M - 1)(V - V_c)\mu_w D^2}{C^*_{\sigma} K_{wr}} = 4\pi^2 = 39.48 \quad 4.134$$

In a horizontal system, the critical rate, V_c , is zero.

If it may be assumed that K_{or} and K_{wr} are approximately equal to K , then Eq. 4.130 becomes

$$\left(\frac{\mu_o}{\mu_w} - 1\right) \frac{V_{\mu_w} D^2}{C^*_{\sigma} K} = 13.56 \quad 4.135$$

and a simpler working dimensionless group $(\mu_o/\mu_w - 1)V_{\mu_w} D^2/C^*_{\sigma} K$ results.

4.3.2 Rectangular Systems

In rectangular systems, the stability index given by Eq. 3.66 may be rearranged as

$$n = \frac{\gamma_{m_1 m_2} \sigma^*}{\frac{\mu_o}{K_{or}} + \frac{\mu_w}{K_{wr}}} \left[\frac{(M - 1)(V - V_c) \mu_w}{\sigma^* K_{wr}} - \pi^2 \left(\frac{m_1^2}{L_x^2} + \frac{m_2^2}{L_y^2} \right) \right] \quad 4.136$$

where the eigenvalues given by Eq. 3.42 have been substituted. As before, the minimum eigenvalues will determine the onset of instability. Thus at the onset of instability,

$$m_1 = m_2 = 1 \quad 4.137$$

and

$$\frac{(M - 1)(V - V_c) \mu_w L_x^2 L_y^2}{C^* \sigma K_{wr} (L_x^2 + L_y^2)} = 9.87 \quad 4.138$$

If as before, the system is horizontal and K_{or} and K_{wr} are approximately equal to K , then

$$\left(\frac{\mu_o}{\mu_w} - 1 \right) \frac{V \mu_w L_x^2 L_y^2}{C^* \sigma K (L_x^2 + L_y^2)} = 9.87 \quad 4.139$$

4.3.3 Summary

The stability theory of Chuoke et al. (7) has been extended to determine the onset of instability in cylindrical and rectangular systems. New dimensionless scaling groups have been derived which divide the displacement domain in both systems into stable and unstable regions. To apply these groups for predictive purposes requires that C and hence, C^* be estimated both in the

presence and absence of connate water saturation. The estimation of these numbers and the application of the new scaling groups will be undertaken in the experimental phase of this study.

CHAPTER 5

EXPERIMENTAL EQUIPMENT AND PROCEDURE

5.1 POROUS MEDIA

The porous media used in this study consisted of unconsolidated packs of 80 to 120 mesh Ottawa sand from Fisher Scientific. The cores were packed by tamping the sand filled tubes with a hammer until no visible settlement occurred. This packing procedure, which gave an average porosity of 38% and permeability of 18.5 darcys, was preferred over an earlier one in which the cores were vibrated for several days. In addition to expediting the core preparation, tamping with a hammer resulted in core properties that were comparable to those obtained by prolonged vibration.

Two core sizes were used: a short core of about 23 cm (the model) and a long one of approximately 112 cm (the prototype), each with a diameter of about 4.8 cm. The three short cores used were made of PVC pipe; of the five long cores, two were made of PVC and three of stainless steel. The stainless steel cores provided high pressure capability. Each long core had twelve pressure taps spaced 10 cm apart from the inlet to the outlet ends. The design details of similar coreholders have already been presented by Wiborg (32).

5.2 FLUIDS

Four fluids were used. These were Dow Corning 200, MCT 30, Kerosene and distilled water. Dow Corning 200, a clear silicon fluid available in a wide range of viscosities, is one of the few oils with

a density approximately equal to that of distilled water. This property made it well suited for the present viscous fingering experiments in which it was particularly necessary to minimize gravitational fingering. MCT 30 and Kerosene, on the other hand, being hydrocarbon oils are more representative of reservoir fluids than Dow Corning 200. MCT 30 is essentially lube oil which was obtained from Imperial Oil. Unlike Dow Corning fluid, MCT 30 and Kerosene have densities sufficiently lower than distilled water to permit gravitational segregation at low displacement rates. Two types of distilled water were employed. A clear distilled water was used to establish connate water saturation, while the same distilled water dyed with sodium fluorescein was used as the displacing phase.

The pertinent fluid properties are summarized in Table 5.1. The viscosities were measured with a Cannon Fenske viscometer, the densities with a Haake density meter, and the interfacial tensions by the spinning drop technique.

Table 5.1

FLUID PROPERTIES AT 21.5°C

Fluid Type	-	ρ (gm/cc)	μ (cp)	μ_o/μ_w	σ (dynes/cm)
Distilled Water		0.9910	1.028	-	-
Kerosene		0.7823	0.950	0.9	23.8
Dow Corning 200		0.9667	105.363	102.5	24.3
MCT 30		0.8799	310.532	302.1	26.4

Preliminary tests were performed on the model fluids to study their rheological properties. Presented in Figure 5.1. are the graphs of the shear stress as a function of shear rate for the two most viscous fluids, MCT 30 and Dow Corning 200. The linear relationships attest to the Newtonian character of the fluids. The shear stress and shear rate, measured with a Haake viscometer, are presented in Table B1 of Appendix B.

The fluids were further subjected to single phase flow in porous media and the pressure drops measured at various flow rates. The results, which may be found in Table B2 of Appendix B, are plotted in Figure 5.2. The linear relationships indicate that the model fluids were not only Newtonian but obeyed Darcy's law in porous media.

5.3 PUMPING SYSTEM

Central to the pumping system was a Ruska pump capable of fluid delivery at 24 constant rates, from 2.5 cc/hour to 1120 cc/hour. Five 2000 cc steel cylinders, each containing one of the fluids used in this study, were connected to the pump. The pump displaced mercury into these cylinders; the mercury in turn displaced the fluid of interest into the core.

5.4 PRESSURE RECORDING SYSTEM

Connected to each of the 12 pressure ports in the long cores were Validyne differential pressure transducers capable of sensing pressures up to 2000 psig. The continuous pressure signals were digitized and punched on paper tape by Doric's Digitrend 220 Data Acquisition System. This unit permitted the pressures to be sampled at frequencies ranging from one scan every two seconds to one scan

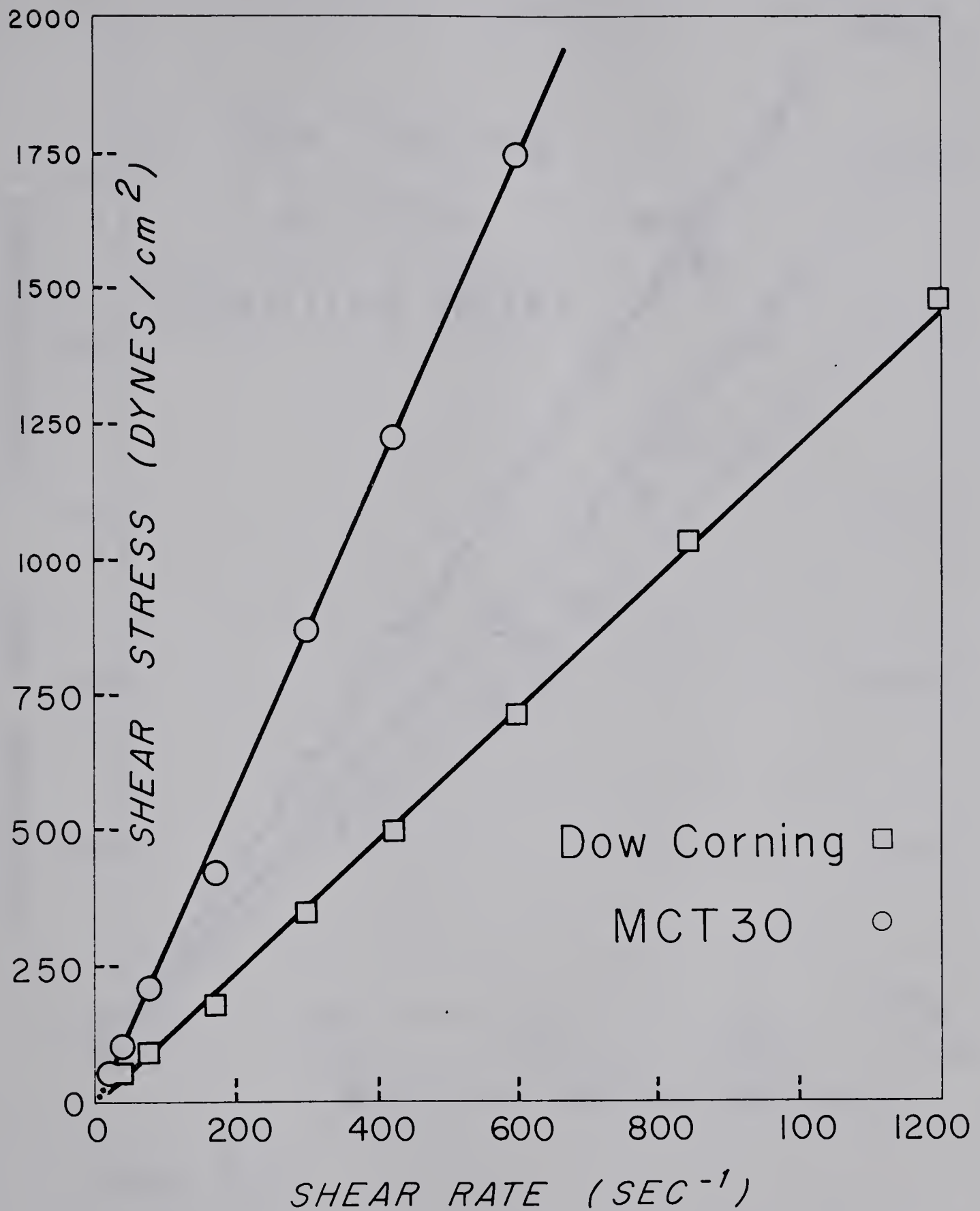


FIG. 5.1 Rheological Properties Of Model Fluids

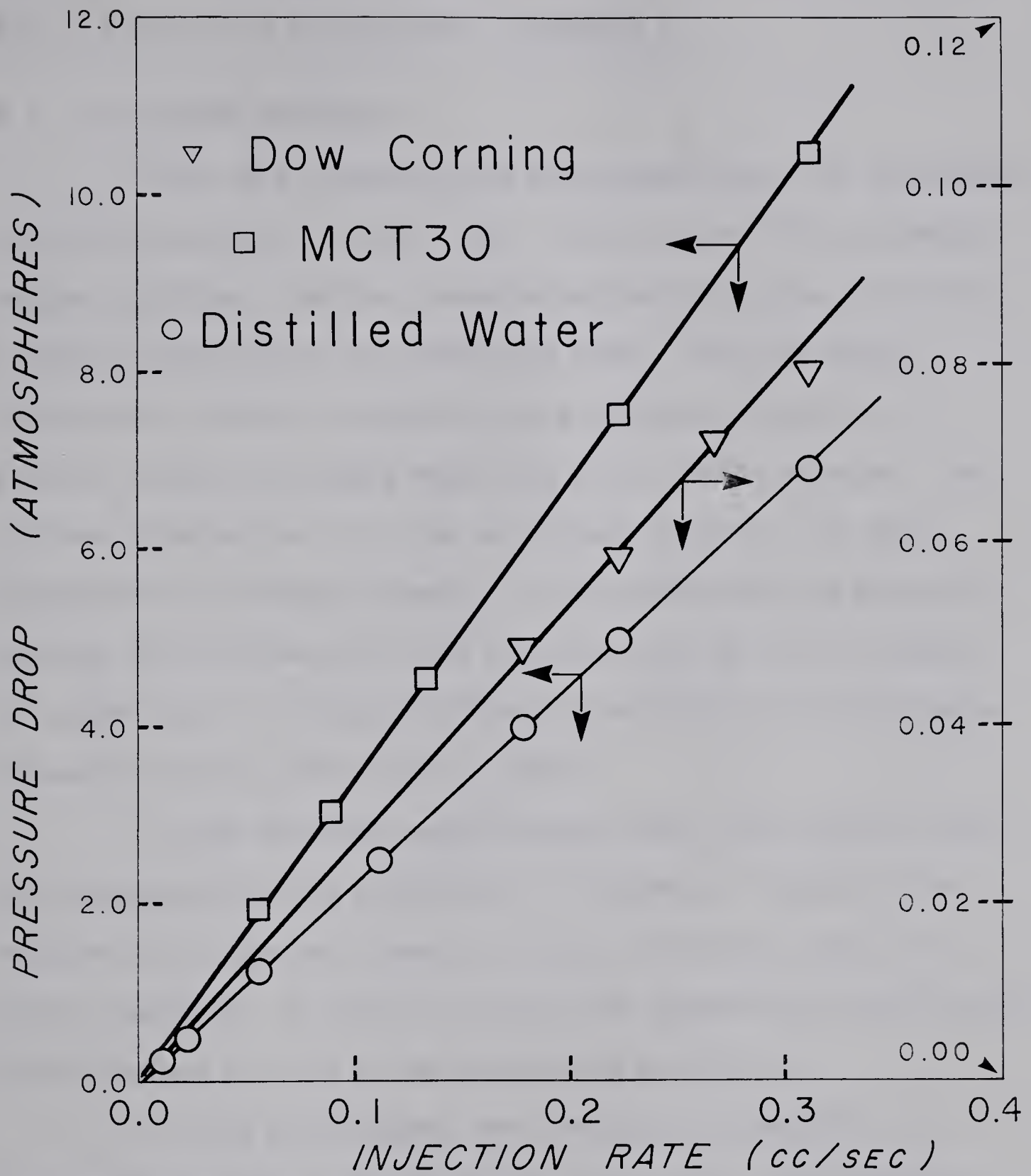


FIG. 5.2

VERIFICATION OF DARCY'S LAW

every hour. The Fortran program used to process the pressure records from the paper tape may be found in Appendix C.

5.5 DISPLACEMENT PROCEDURE

Tests were conducted with both connate water and nonconnate water bearing cores. In every case, the cores were first evacuated before saturation. For the connate water bearing systems, the first saturating fluid was a clear distilled water. The pore volume, porosity and absolute permeability were determined routinely by material balance and single phase flow of the distilled water. The pressure drops across the cores, which were generally low, were measured with a mercury manometer. After determining the core properties, the distilled water was displaced with the oil of interest at a high rate in a horizontal flood, to establish the connate water saturation and the initial oil in place.

In the nonconnate water bearing tests, the evacuated cores were saturated directly with the oil of interest. Because of the relatively high pressure drops, a pressure transducer rather than a mercury manometer was used in the absolute permeability determinations which involved the flow of Dow Corning 200 and MCT 30.

All the displacements were conducted horizontally in a constant temperature cabinet maintained at 21.5°C. The majority of the runs were terminated at water breakthrough, because this is the event most influenced by viscous fingering. However, a number of runs in which pressures were recorded continued beyond water breakthrough. In such runs, the produced effluent was collected in a bank of graduated test tubes. At the conclusion of each test, the

cores were cleaned, dried and repacked with new sand.

5.6 RETRIEVAL AND PHOTOGRAPHY OF CORE CROSS-SECTIONS

One of the objectives of this study was to attempt to obtain positive evidence of viscous fingering where this might exist in order to correlate the occurrence and nature of viscous fingering with the predictions of the various stability theories. To this end, a technique was developed whereby the flooded out core sections were examined for evidence of fingering.

At the termination of each test with a short core, sections of the porous media were retrieved from the coreholder at approximately 1.5 cm intervals and photographed. Under ultraviolet lighting, the areas of the cross-sections contacted by the fluorescent displacing water were bright yellow while the uncontacted areas were dark. The contrast between the two areas was further enhanced by the use of a yellow filter. By this means, several records of the displacement paths were successfully photographed during the course of this investigation.

CHAPTER 6

EXPERIMENTAL RESULTS AND OBSERVATIONS

6.1 GENERAL

Two types of experimental data were collected in this study. The first type consisted of the recovery data for each test at water breakthrough over a wide range of displacement rates, from 2.5 cc/hour to 1120 cc/hour. The choice of the breakthrough recoveries as the pertinent data was guided by three considerations. First, the moment of water breakthrough is the first observable event most influenced by instability and viscous fingering. Second, similar data abound in the literature, so that this choice will facilitate the comparison of the present findings with those of earlier researchers. Third, the breakthrough recovery data over a wide range of rates provide suitable data with which to study model scaling requirements for geometrically dissimilar cores.

The second type of experimental data consisted of the displacement records of the flooded out cores at water breakthrough. These were photographs of the core cross-sections showing areas invaded by the fluorescent displacing water. The photographs spanned the range of displacement rates studied. Even in the cases in which no photographs were taken, the core sections were examined visually at the conclusion of each test for evidence of viscous fingering.

The purpose was to use these records to verify the various stability theories, to make quantitative predictions regarding instability and viscous fingering and to determine the recovery

behaviour that may legitimately be attributed to viscous fingering during immiscible displacement.

As the literature seemed to indicate that the presence or absence of connate water saturation had some bearing on the displacement mechanism, it was decided to conduct the experimental tests on the two systems and to compare the results.

Most of the experiments, 26 out of 35 runs, were conducted with Dow Corning 200 at a viscosity ratio of 102.5. The rationale for this choice was to undertake a detailed study of a single adverse viscosity ratio displacement with a view to generalizing the results, rather than to undertake a cursory study of numerous viscosity ratio displacements from which generalization might be difficult. However, in order to verify the viscosity (or mobility) ratio requirement for instability, three tests were performed with Kerosene at a favourable viscosity ratio of 0.9. Furthermore, to ascertain whether the flood behaviour observed was peculiar to Dow Corning 200, which as pointed out earlier is not a hydrocarbon oil, six tests were conducted with MCT 30. These additional tests spanned the rates used in the Dow Corning experiments.

The experimental results have been condensed into Table 6.1 for the connate water bearing tests and Table 6.2 for the nonconnate water bearing floods. Shown in these tables are the pertinent core properties, the displacement rates and the breakthrough recovery data. Also tabulated are various dimensionless scaling or correlating parameters ranging from the conventional ratio of viscous to capillary forces, to new groups proposed in this study as being more suitable for presenting the experimental data collected on cores that are not

Table 6.1

SUMMARY OF DISPLACEMENT DATA WITH CONNATE WATER SATURATION

Run No.	L (cm)	D (cm)	φ (%)	K (darcy)	K _{or} (darcy)	S _{wi} (%)	Q (cc/hr)	$\frac{V_{\mu} L}{\sigma \sqrt{K \phi}}$	$\frac{V_{\mu} D}{\sigma \sqrt{K \phi}}$	$\frac{V_{\mu} D^2}{\sigma K}$	$\frac{\lambda_c}{D}$	$\frac{\mu_o - 1}{\mu_w} \frac{V_{\mu} D^2}{C \sigma K}$	Breakthrough Recovery (%IIP)
1*	22.9	4.809	38.98	16.43	15.82	11.20	2.5	1.475x10 ⁻³	3.097x10 ⁻⁴	2.307x10 ⁰	7.187x10 ⁰	7.645x10 ⁻¹	43.63
2	23.6	4.844	36.37	18.36	17.99	8.66	20.0	1.173x10 ⁻²	2.407x10 ⁻³	1.652x10 ¹	2.686x10 ⁰	5.475x10 ⁰	41.88
3	112.8	4.961	38.38	21.89	18.05	9.18	10.0	2.382x10 ⁻²	1.047x10 ⁻³	6.926x10 ⁰	4.148x10 ⁰	2.296x10 ⁰	43.68
4	23.7	4.809	38.94	18.93	18.33	11.34	160.0	9.096x10 ⁻²	1.846x10 ⁻²	1.281x10 ²	9.643x10 ⁻¹	4.245x10 ¹	35.32
5	110.5	4.825	38.91	20.52	18.50	10.83	50.0	1.265x10 ⁻¹	5.523x10 ⁻³	3.694x10 ¹	1.796x10 ⁰	1.224x10 ¹	40.30
6	110.0	4.805	37.61	21.91	19.40	10.48	100.0	2.499x10 ⁻¹	1.092x10 ⁻²	6.920x10 ¹	1.312x10 ⁰	2.294x10 ¹	41.10
7	23.6	4.844	37.49	14.19	11.03	15.26	480.0	3.153x10 ⁻¹	6.471x10 ⁻²	5.128x10 ²	4.820x10 ⁻¹	1.699x10 ²	30.40
8	116.1	4.961	34.66	18.28	15.57	8.32	160.0	4.516x10 ⁻¹	1.930x10 ⁻²	1.327x10 ²	9.476x10 ⁻¹	4.398x10 ¹	32.22
9	113.0	4.958	39.62	22.99	19.90	8.61	200.0	4.588x10 ⁻¹	2.013x10 ⁻²	1.319x10 ²	9.505x10 ⁻¹	4.371x10 ¹	30.89
10	115.9	4.958	35.86	19.22	15.49	12.53	240.0	6.492x10 ⁻¹	2.777x10 ⁻²	1.893x10 ²	7.934x10 ⁻¹	6.273x10 ¹	34.69
11*	22.8	4.843	37.52	16.23	15.19	11.20	1120.0	6.645x10 ⁻¹	1.411x10 ⁻¹	1.046x10 ³	3.375x10 ⁻¹	3.467x10 ²	23.94
12	110.4	4.805	37.46	20.85	18.48	10.00	480.0	1.237x10 ⁰	5.383x10 ⁻²	3.490x10 ²	5.843x10 ⁻¹	1.157x10 ²	26.81
13	115.9	4.972	37.80	18.54	15.53	9.29	480.0	1.280x10 ⁰	5.492x10 ⁻²	3.925x10 ²	5.510x10 ⁻¹	1.301x10 ²	33.24
14	110.0	4.805	38.11	22.50	18.62	8.91	800.0	1.961x10 ⁰	8.563x10 ⁻²	5.390x10 ²	4.702x10 ⁻¹	1.786x10 ²	28.62
15	112.8	4.972	35.48	22.72	20.90	9.92	1120.0	2.568x10 ⁰	1.132x10 ⁻¹	7.474x10 ²	3.993x10 ⁻¹	2.476x10 ²	33.43
16	23.4	4.843	34.61	14.51	9.58	11.03	10.0	6.698x10 ⁻³	1.386x10 ⁻³	9.617x10 ⁰	2.072x10 ⁰	9.454x10 ⁰	36.01
17	23.6	4.843	38.60	20.87	18.49	10.15	200.0	1.072x10 ⁻¹	2.200x10 ⁻²	1.337x10 ²	5.556x10 ⁻¹	1.314x10 ²	22.29
18	23.7	4.809	35.44	12.11	11.94	12.02	1120.0	8.345x10 ⁻¹	1.693x10 ⁻¹	1.291x10 ³	1.787x10 ⁻¹	1.269x10 ³	11.92

*Runs with photographic displacement record

Down Corning 200

MCT 30

Table 6.2
SUMMARY OF DISPLACEMENT DATA WITHOUT CONNATE WATER SATURATION

Run No.	L (cm)	D (cm)	φ (%)	K (darcy)	Q (cc/hr)	$\frac{V_{\mu_w} L}{\sigma \sqrt{K \phi}}$	$\frac{V_{\mu_w} D}{\sigma \sqrt{K \phi}}$	$\frac{V_{\mu_w} D^2}{\sigma K}$	$\frac{\lambda_c}{D}$	$\frac{\lambda_c}{\sqrt{DL}}$	$\frac{\mu_o}{\mu_w} - 1 \frac{V_{\mu_w} D^2}{C^* \sigma K}$	Breakthrough Recovery (%IIP)
19	22.9	4.809	41.33	17.26	2.5	1.396×10^{-3}	2.931×10^{-4}	2.196×10^0	9.825×10^{-1}	4.502×10^{-1}	4.080×10^1	69.91
20*	23.6	4.844	37.89	15.05	2.5	1.585×10^{-3}	3.254×10^{-4}	2.518×10^0	9.165×10^{-1}	4.152×10^{-1}	4.689×10^1	62.50
21	22.9	4.809	39.64	18.02	10.0	5.580×10^{-3}	1.172×10^{-3}	8.413×10^0	5.019×10^{-1}	2.300×10^{-1}	1.567×10^2	41.47
22	110.5	4.825	38.46	22.63	10.0	2.423×10^{-2}	1.059×10^{-3}	6.699×10^0	5.625×10^{-1}	1.175×10^{-1}	1.247×10^2	31.02
23*	23.5	4.843	38.25	16.20	40.0	2.425×10^{-2}	4.997×10^{-3}	3.743×10^1	2.380×10^{-1}	1.080×10^{-1}	6.971×10^2	22.46
24*	23.5	4.809	38.04	16.34	200.0	1.228×10^{-1}	2.514×10^{-2}	1.856×10^2	1.069×10^{-1}	4.835×10^{-2}	3.457×10^3	19.71
25	115.6	4.972	37.01	18.36	80.0	2.161×10^{-1}	9.296×10^{-3}	6.606×10^1	9.978×10^{-2}	2.069×10^{-2}	1.230×10^3	17.46
26*	23.7	4.809	38.20	15.62	480.0	3.033×10^{-1}	6.154×10^{-2}	4.659×10^2	6.745×10^{-2}	3.038×10^{-2}	8.677×10^3	16.05
27*	22.9	4.844	39.82	16.18	1120.0	6.486×10^{-1}	1.372×10^{-1}	1.049×10^3	4.494×10^{-2}	2.067×10^{-2}	1.954×10^4	16.66
28	110.0	4.825	38.13	24.79	800.0	1.852×10^0	8.124×10^{-2}	4.893×10^2	6.582×10^{-2}	1.379×10^{-2}	9.112×10^3	17.26
29	115.7	4.961	37.49	18.62	1120.0	3.002×10^0	1.286×10^{-1}	9.119×10^2	4.822×10^{-2}	9.985×10^{-3}	1.698×10^4	14.30
30	23.6	4.844	38.58	17.88	5.0	2.884×10^{-3}	5.919×10^{-4}	3.902×10^0	4.338×10^{-1}	1.965×10^{-1}	2.156×10^2	53.04
31	23.8	4.844	38.26	16.69	200.0	1.113×10^{-1}	2.265×10^{-2}	1.672×10^2	6.627×10^{-2}	2.990×10^{-2}	9.237×10^3	12.57
32	23.5	4.809	38.82	18.22	1120.0	6.445×10^{-1}	1.319×10^{-1}	8.578×10^2	2.926×10^{-2}	1.324×10^{-2}	4.739×10^4	13.70
33*	23.7	4.843	38.02	18.41	10.0	5.874×10^{-3}	1.200×10^{-3}	8.408×10^0				75.30
34	23.4	4.809	38.82	18.54	200.0	1.160×10^{-1}	2.384×10^{-2}	1.670×10^2				82.29
35*	23.5	4.843	37.31	18.20	1120.0	6.623×10^{-1}	1.365×10^{-1}	9.526×10^2				91.46

*Runs with photographic displacement records.

Dow Corning 200

MCT 30

Kerosene

geometrically similar. In calculating the dimensionless groups, the displacement rate was expressed in cm/sec, the viscosity in poise, the lengths in cm, the interfacial tension in dynes/cm and the permeability in cm^2 .

Each experimental run has been assigned a unique identification number which does not necessarily reflect the order in which the run was conducted. The runs with asterisks are those for which the displacement records are available.

6.2 DISPLACEMENT RECORDS

A complete displacement record consists of eighteen frames of photographs numbered sequentially from the inlet to the outlet ends of the core, Frame 1 being the inlet and Frame 18 the outlet end. The intervening frames are the cross-sections at equally spaced intervals between the inlet and outlet ends. Two displacement records may therefore be compared by comparing the corresponding frames in each record as these represent the cross-sections at the same dimensionless distances along each core.

In these pictures, the displacing water appears light while the bypassed oil is dark. A uniform light colour throughout the circular cross-section of the core indicates a uniform water invasion, the intensity of the lightness giving a qualitative indication of the displacing phase saturation at that cross-section. A spotty light colour, on the other hand, indicates the path left behind by viscous fingering.

6.2.1 No Connate Water Present

Plates 6.1 to 6.5 show the displacement records, in order of increasing rate, at a viscosity ratio of 102.5 in the absence of connate water saturation. Plate 6.1 which is the record at the lowest rate studied (2.5 cc/hour) presents two interesting features. First, although the displacement was uniform at most cross-sections, severe oil bypassing occurred in places. Such bypassing, evident in Frames 3, 4, 5, 6, 7, 8, 16, 17 and 18, is symptomatic of a possible instability even at this low displacement rate. Second, the oil bypassing at this low rate is clearly axially asymmetric.

As the rate increased to 40 cc/hour, the oil bypassing observed at 2.5 cc/hour took on the recognizable pattern of viscous fingering as shown on Plate 6.2, Frames 7 to 18. The dimensions of the fingers in Frames 9 to 18 may be used to estimate the most probable wavelength of instability at this rate.

As the rate increased to 200 cc/hour, Plate 6.3 shows that the fingering phenomenon became more spectacular and the fingers more numerous, resulting in smaller wavelengths than previously observed.

Finally, at the still higher rates of 480 cc/hour and 1120 cc/hour, the displacements were dominated by numerous tiny fingers of very short wavelengths, as shown in Plates 6.4 and 6.5, respectively. At these higher rates, the fingering pattern became more axially symmetric and showed some peripheral tendency towards the outlet ends of the cores.

Although no displacement records are shown, similar fingering patterns were observed with MCT 30 at a viscosity ratio



1 - Inlet
End



2



3



4

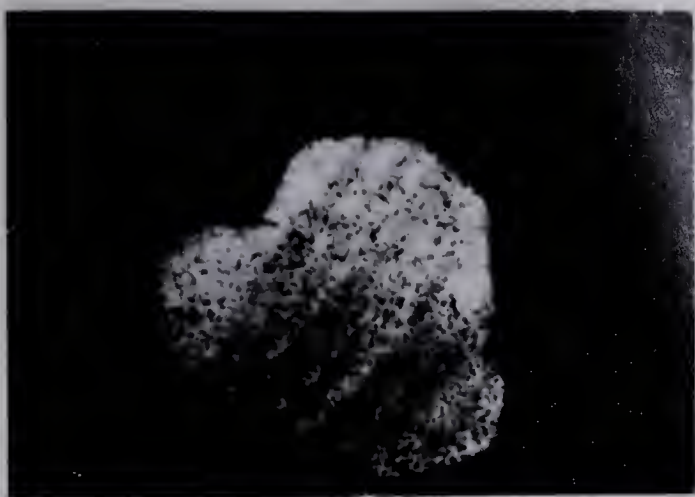


5

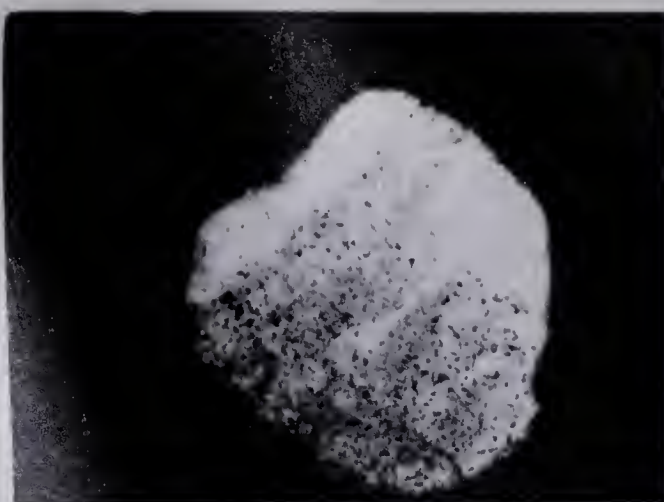


6

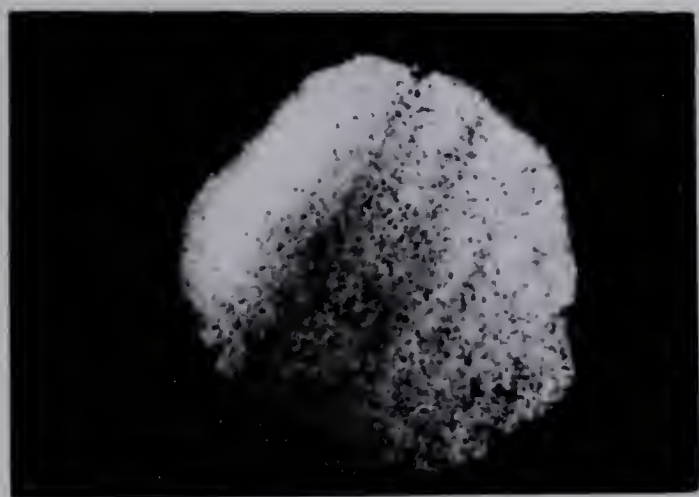
PLATE 6.1 DISPLACEMENT RECORD, RUN 20, NO CONNATE WATER
 $Q = 2.5$ CC/HOUR, VISCOSITY RATIO = 102.5



7



8



9



10

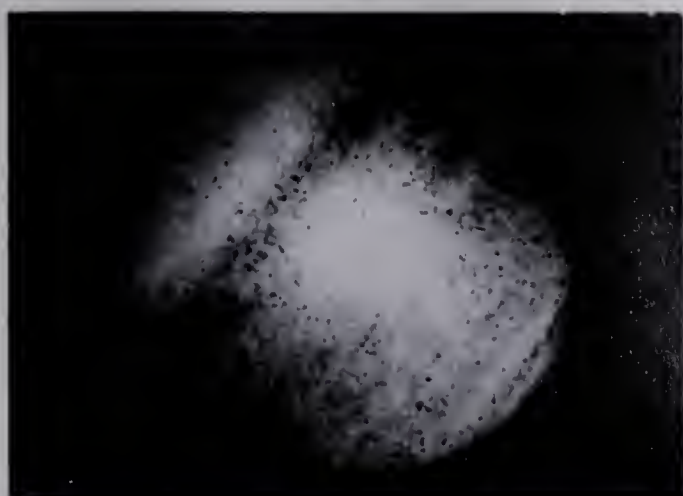


11



12

PLATE 6.1 CONTINUED



13



14



15



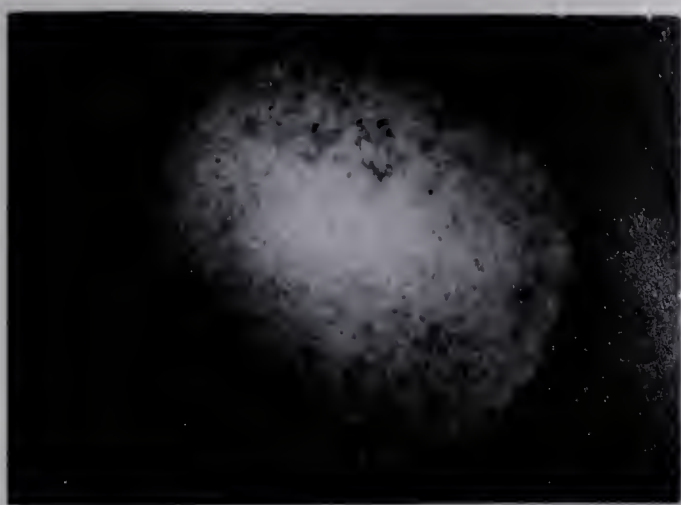
16



17

18 - Outlet
End

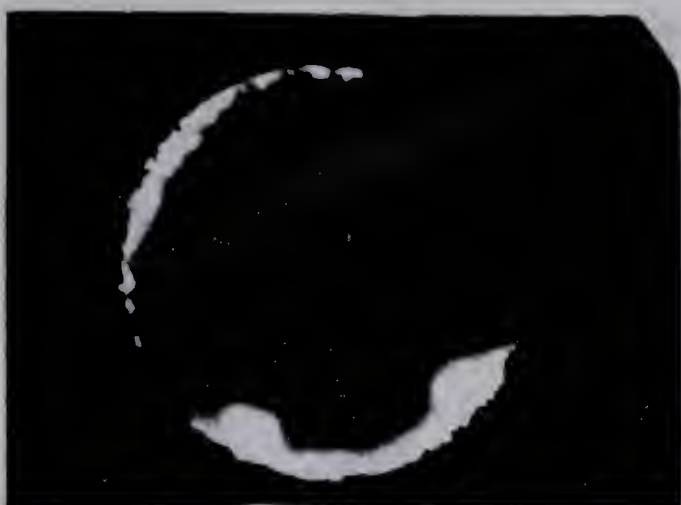
PLATE 6.1 CONTINUED



1 - Inlet
End



2



3



4



5



6

PLATE 6.2 DISPLACEMENT RECORD, RUN 23, NO CONNATE WATER
 $Q = 40$ CC/HOUR, VISCOSITY RATIO = 102.5



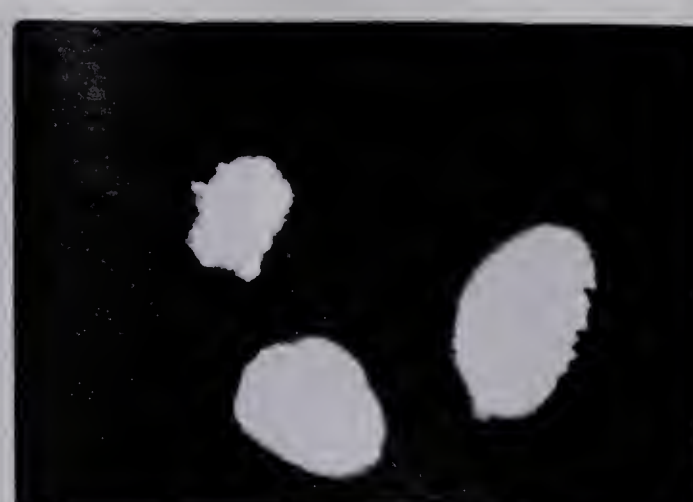
7



8



9



10



11



12

PLATE 6.2 CONTINUED



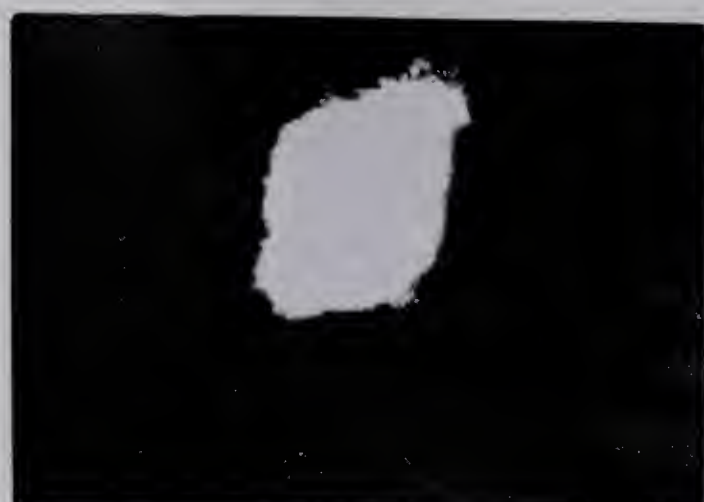
13



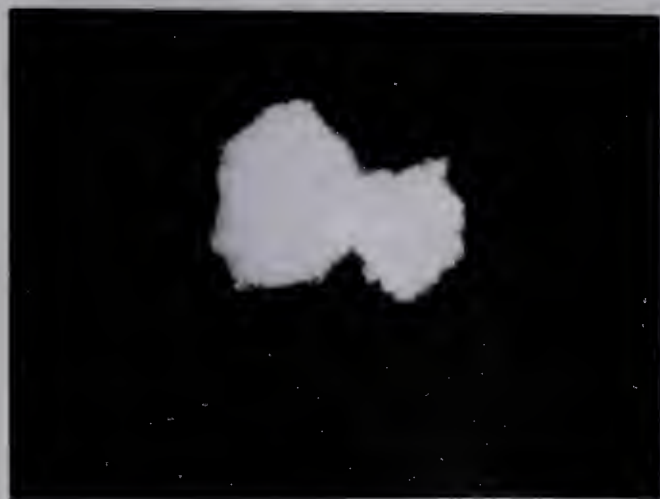
14



15



16



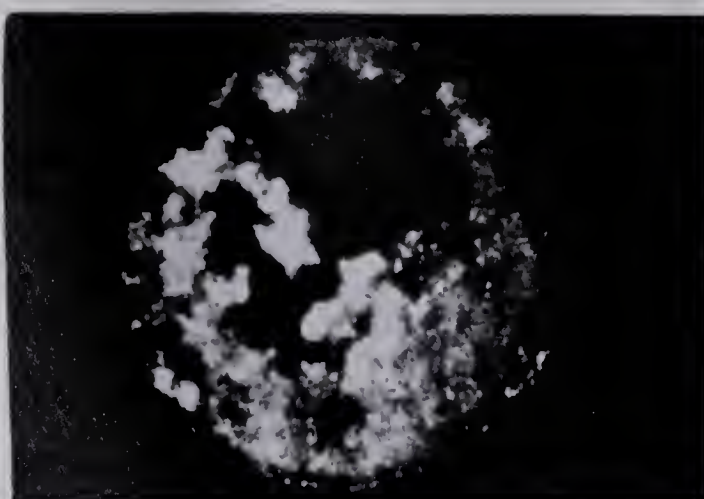
17

18 - Outlet
End

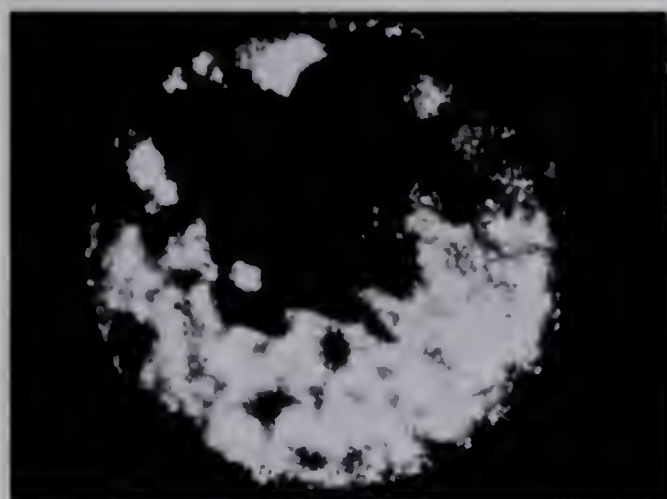
PLATE 6.2 CONTINUED



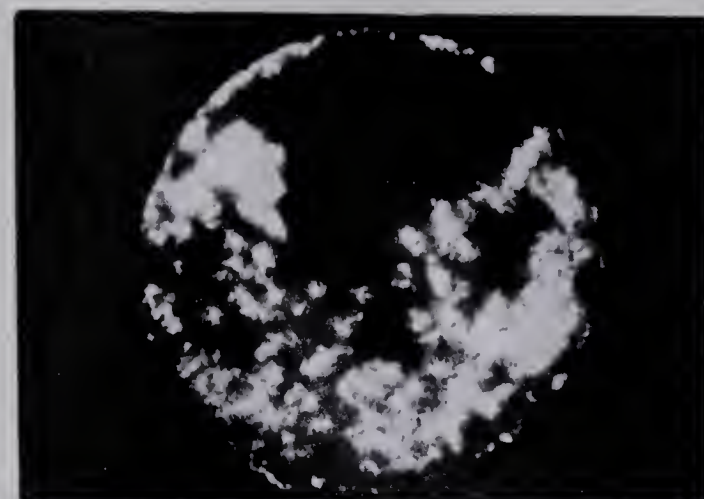
1 - Inlet
End



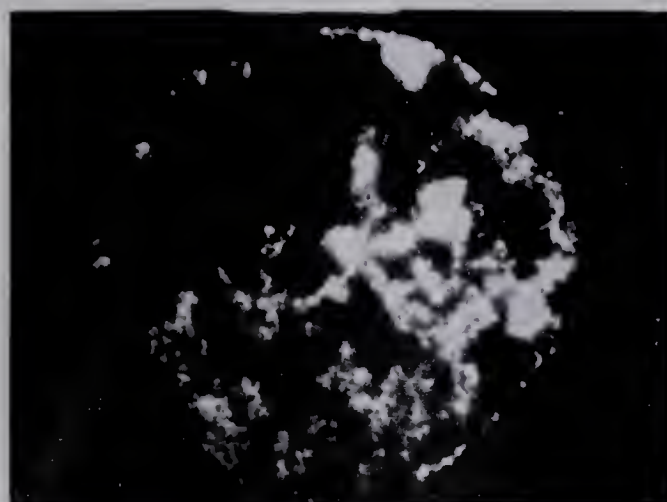
2



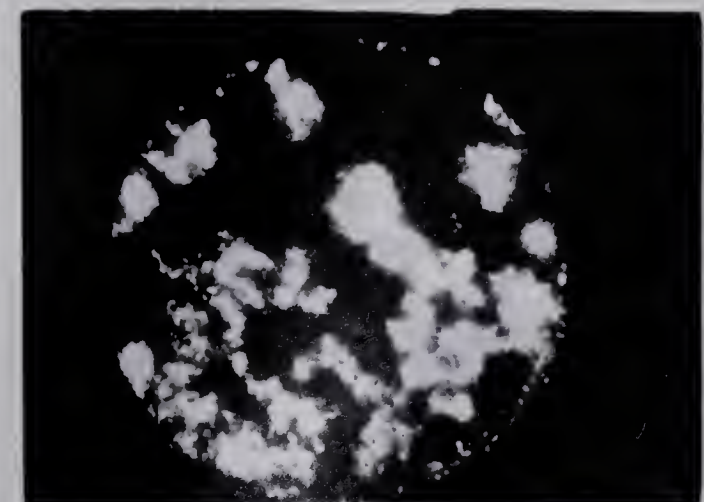
3



4

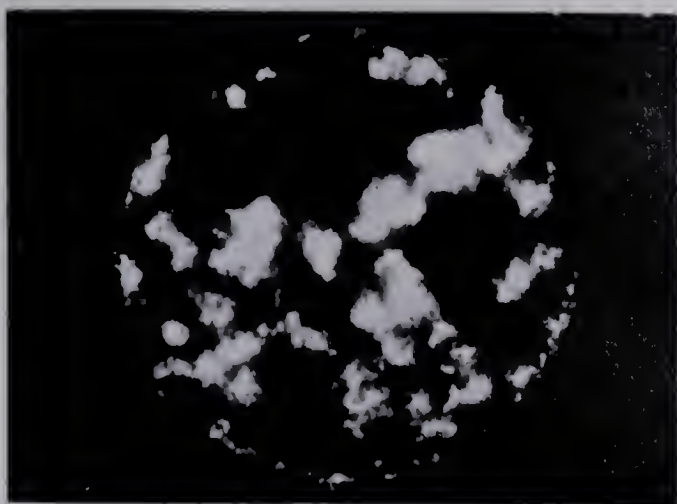


5



6

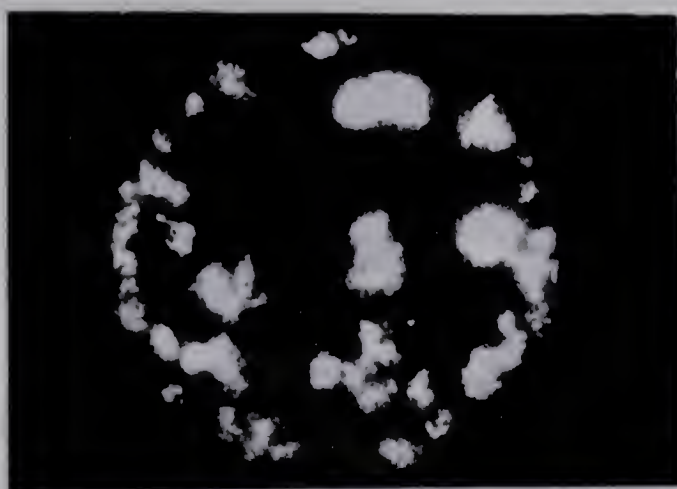
PLATE 6.3 DISPLACEMENT RECORD, RUN 24, NO CONNATE WATER
 $Q = 200$ CC/HOUR, VISCOSITY RATIO = 102.5



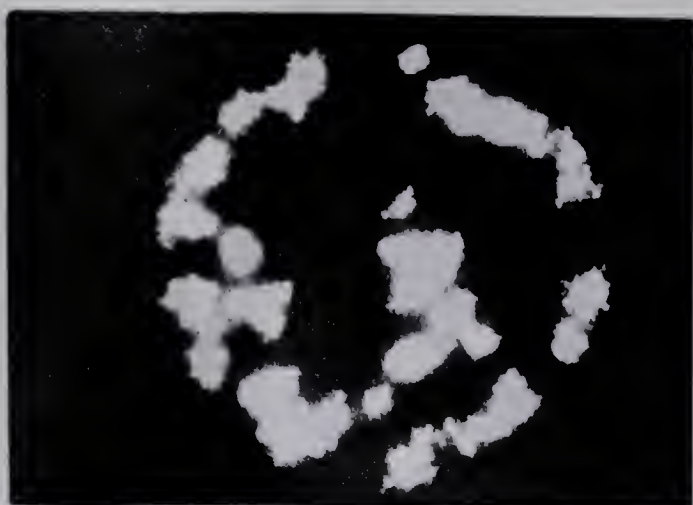
7



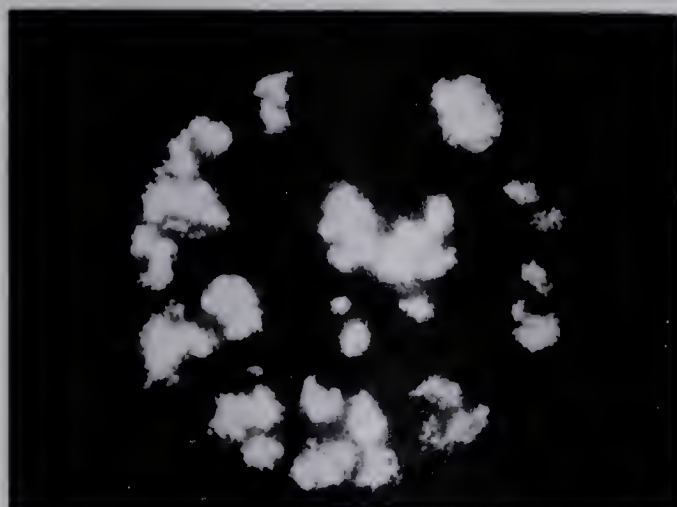
8



9



10

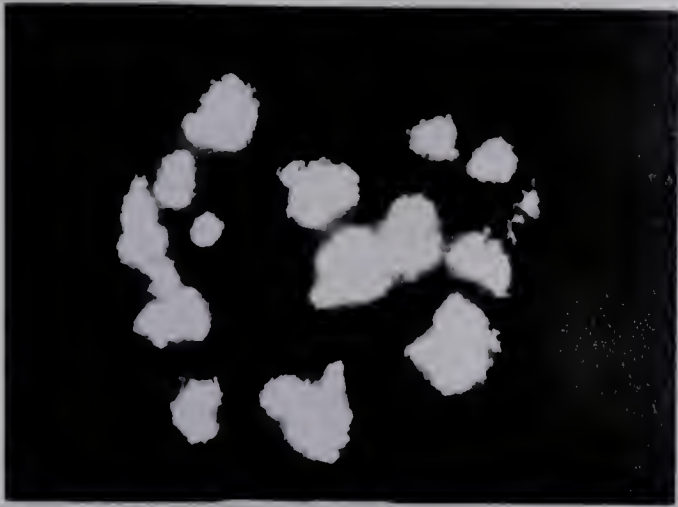


11



12

PLATE 6.3 CONTINUED



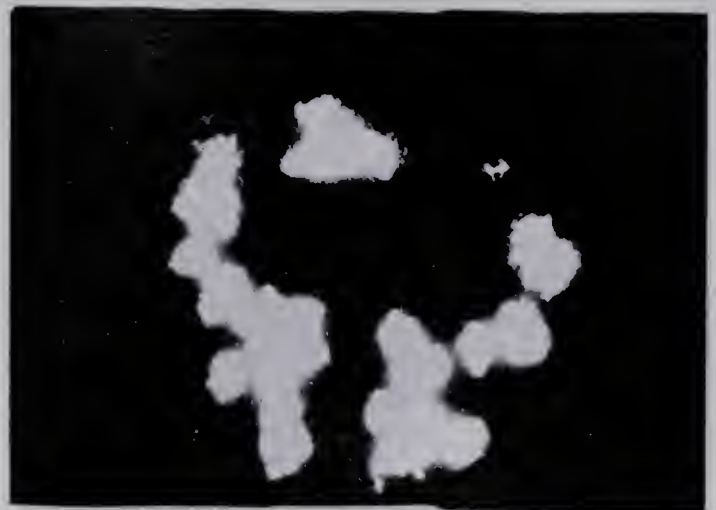
13



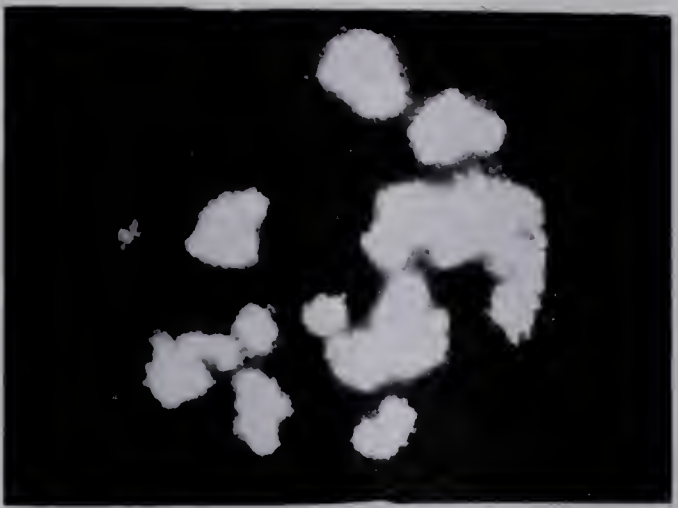
14



15



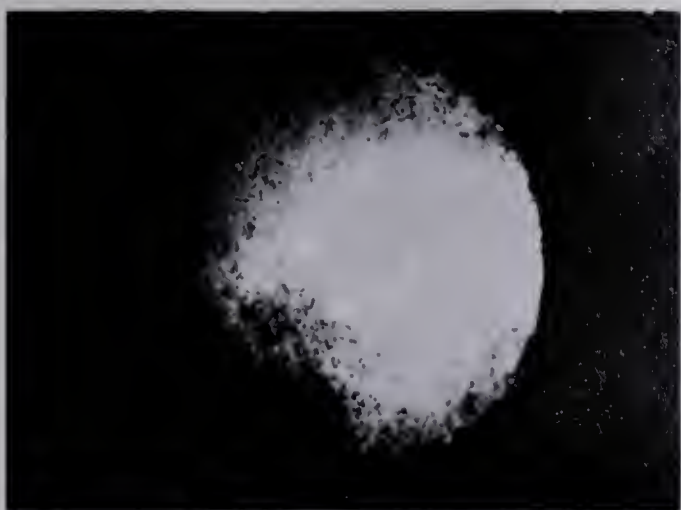
16



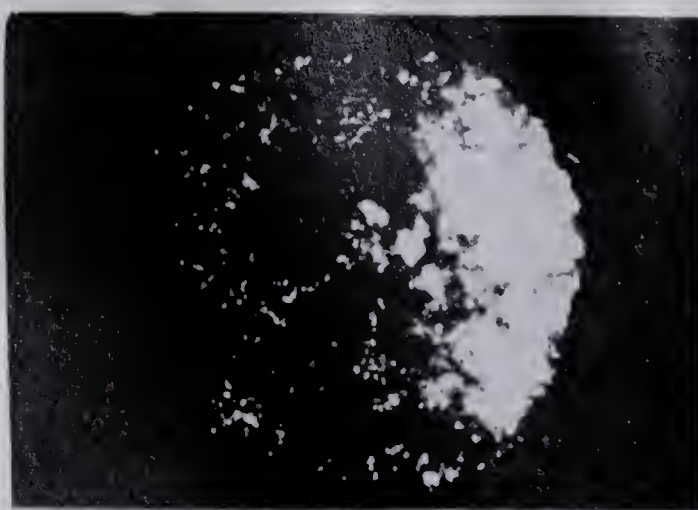
17



18 - Outlet
End



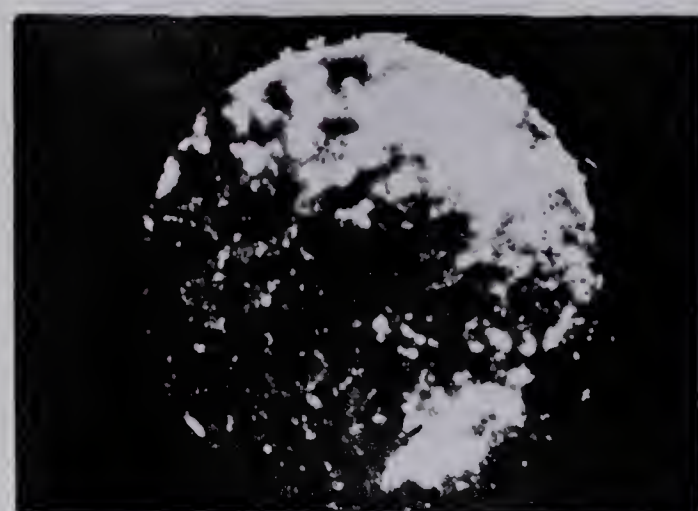
1 - Inlet
End



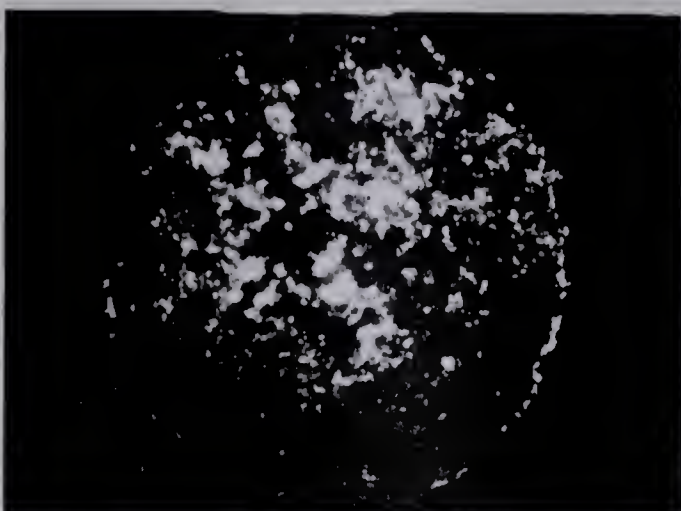
2



3



4



5

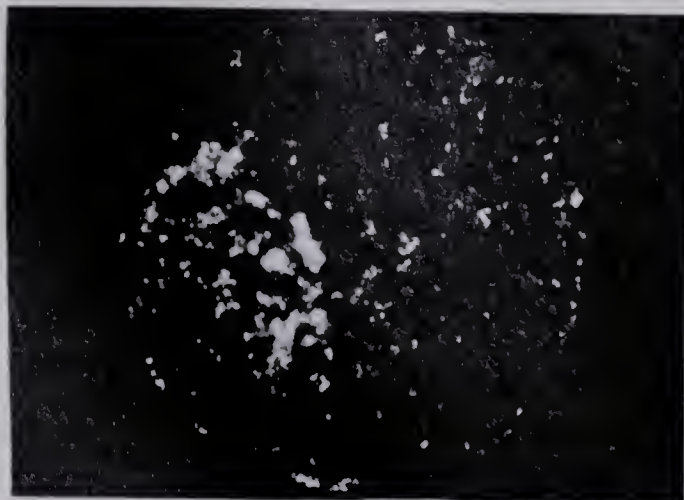


6

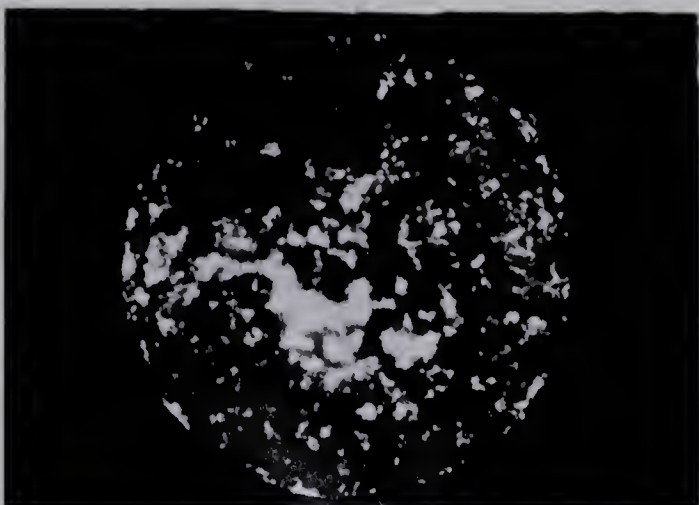
PLATE 6.4 DISPLACEMENT RECORD, RUN 26, NO CONNATE WATER
Q = 480 CC/HOUR, VISCOSITY RATIO = 102.5



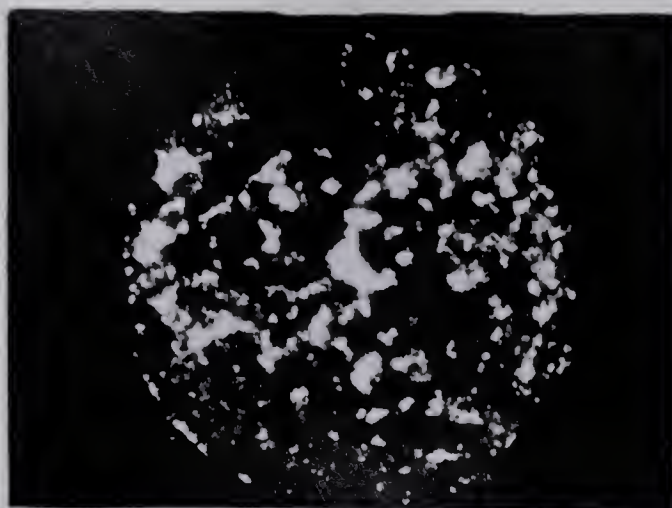
7



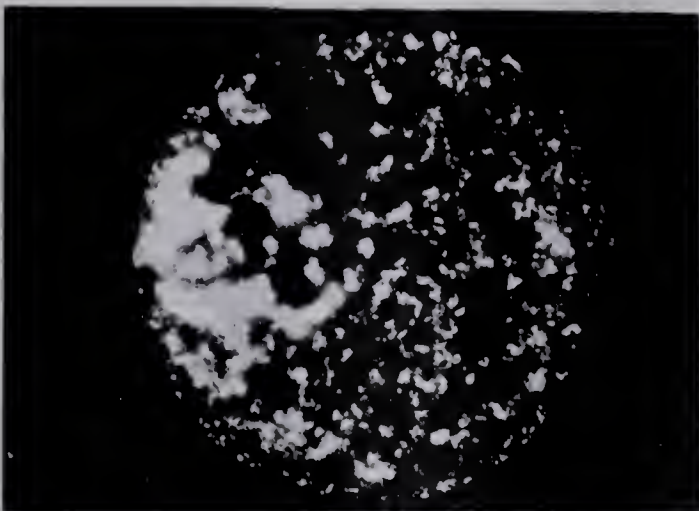
8



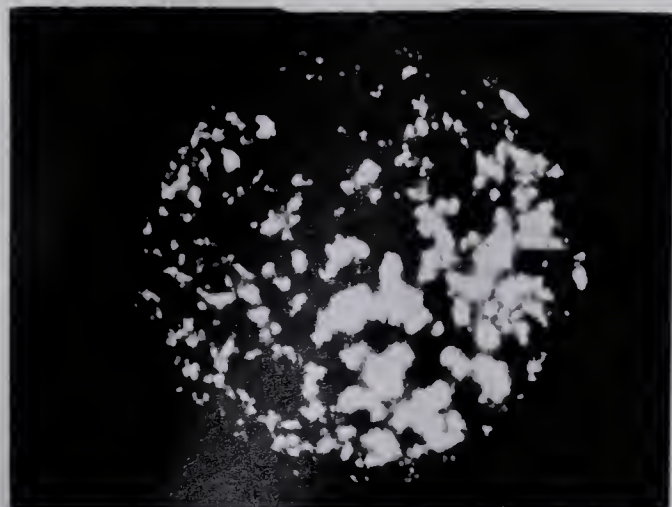
9



10

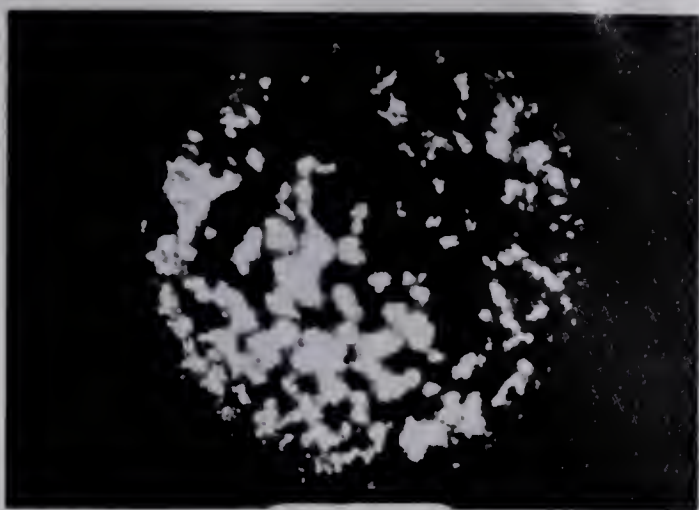


11



12

PLATE 6.4 CONTINUED



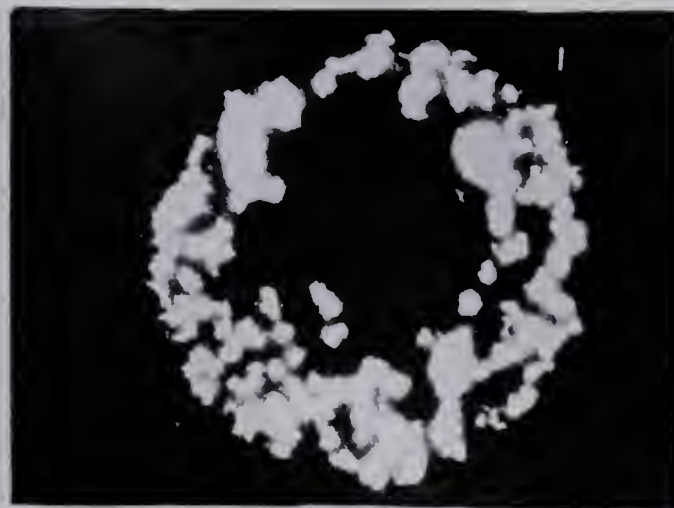
13



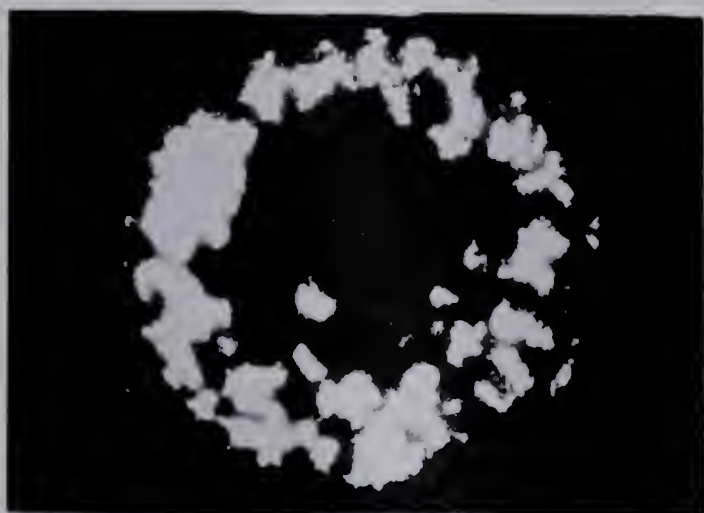
14



15



16



17

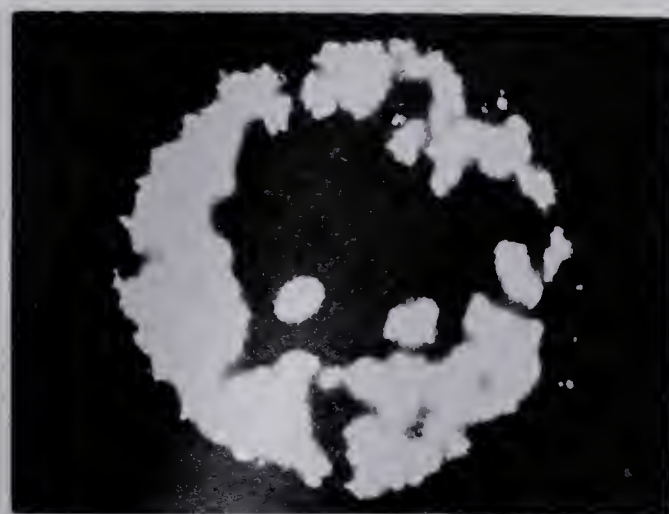
18 - Outlet
End

PLATE 6.4 CONTINUED



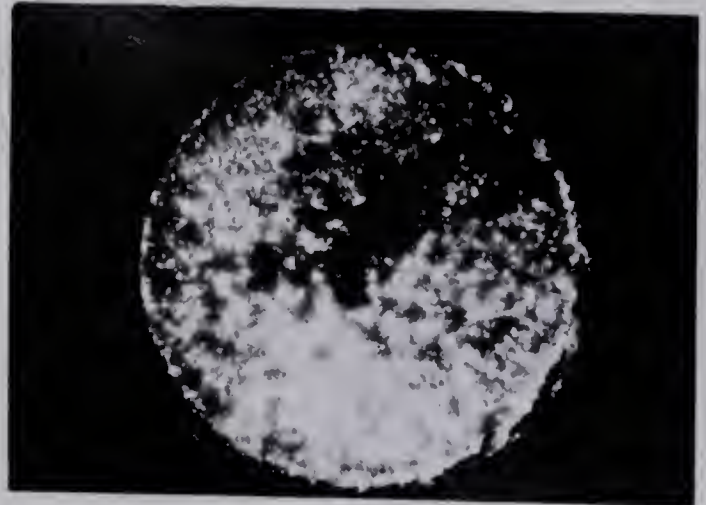
1 - Inlet
End



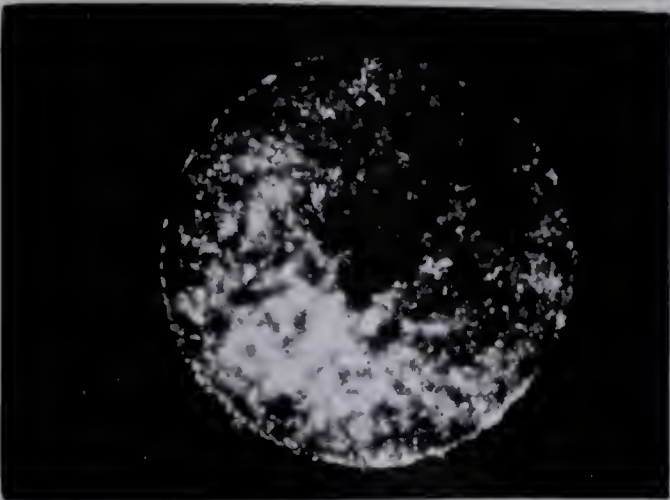
2



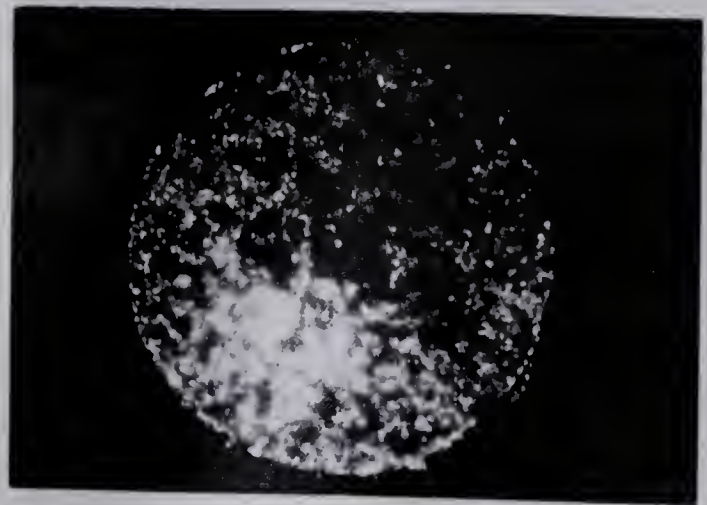
3



4

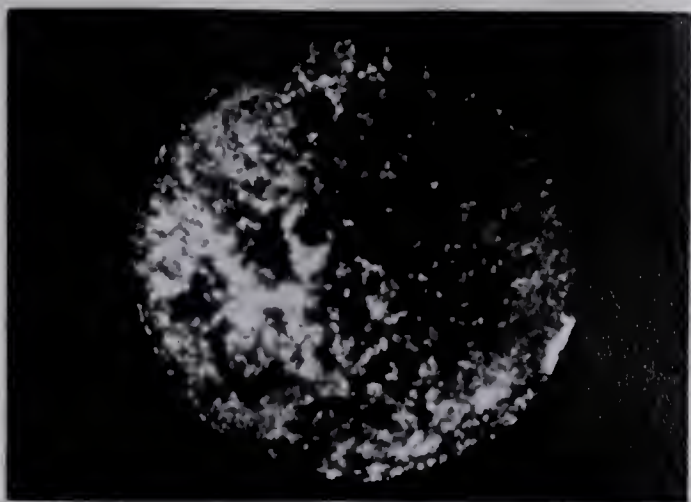


5



6

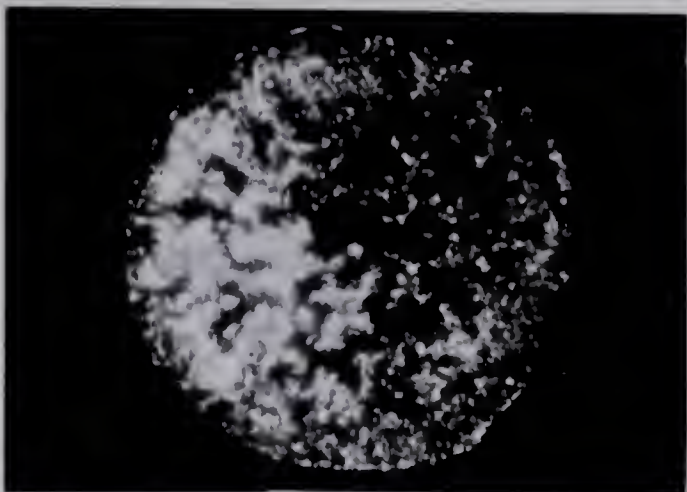
PLATE 6.5 DISPLACEMENT RECORD, RUN 27, NO CONNATE WATER
 $Q = 1120$ CC/HOUR, VISCOSITY RATIO = 102.5



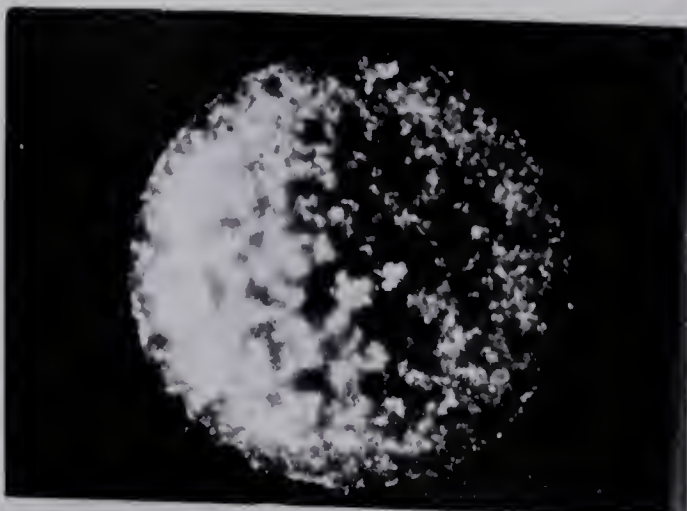
7



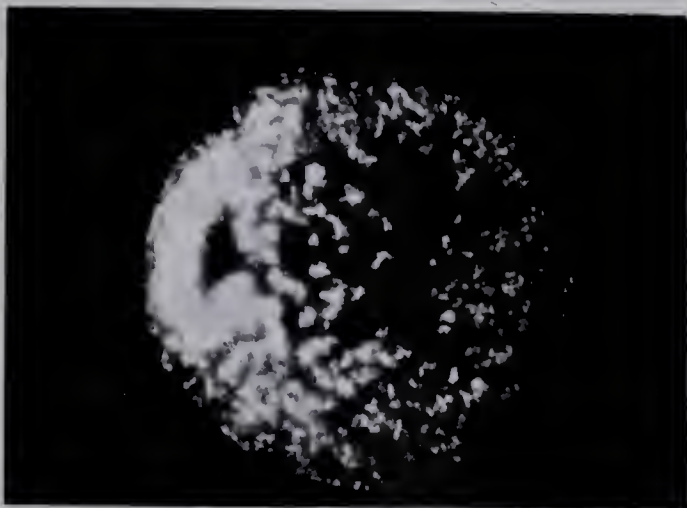
8



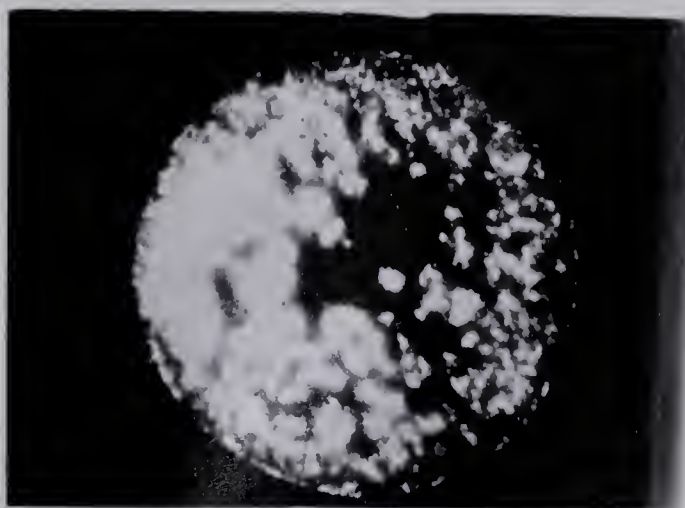
9



10

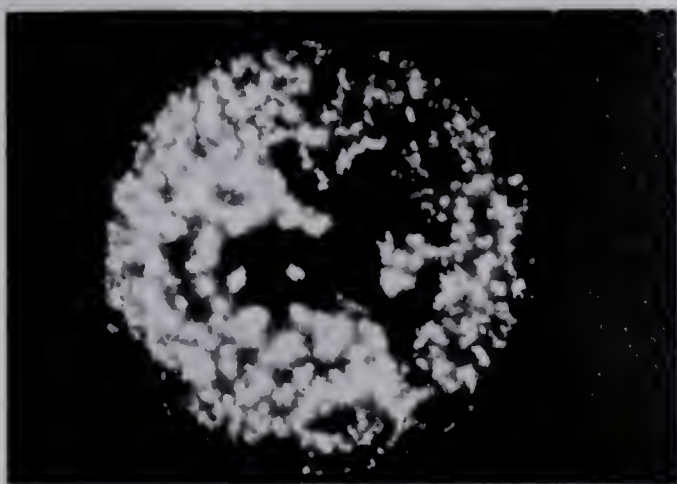


11



12

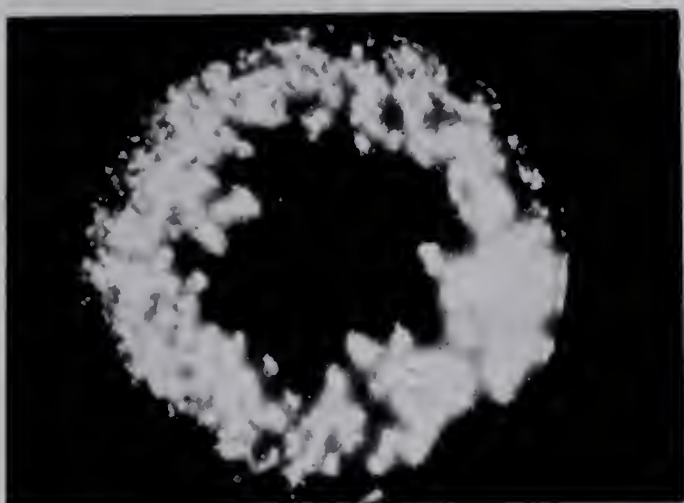
PLATE 6.5 CONTINUED



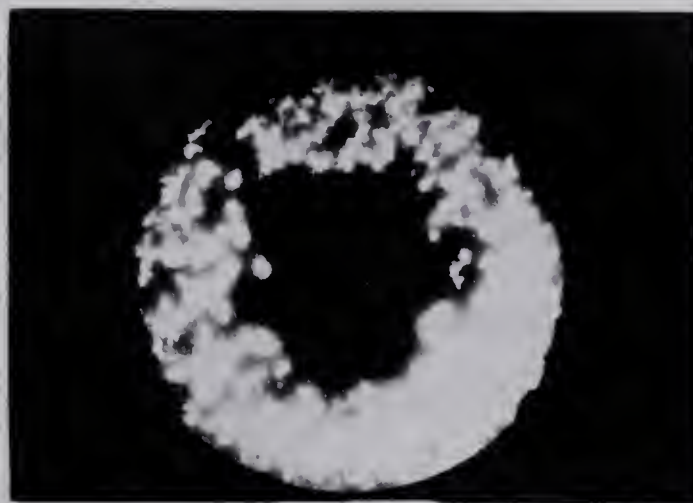
13



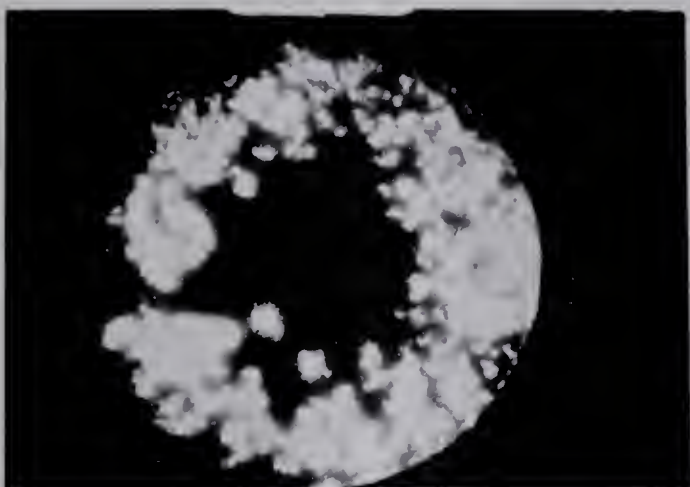
14



15



16



17

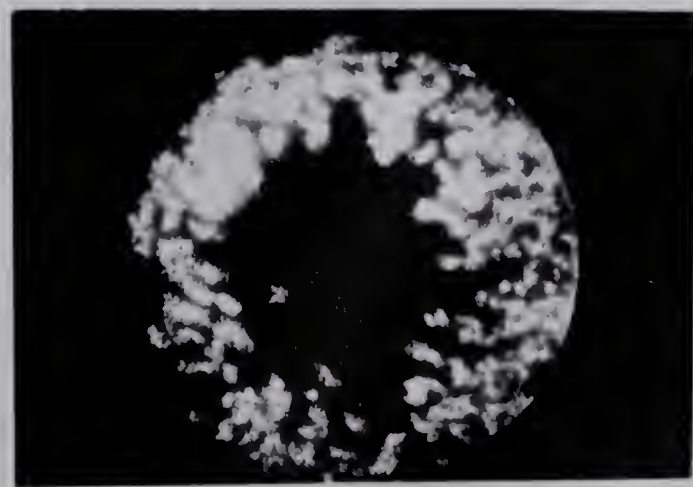
18 - Outlet
End

PLATE 6.5 CONTINUED

of 302.1. Superimposed upon the viscous fingering phenomenon was severe gravitational segregation. The displacement records of MCT 30 showed less contrast than the other oils due to the strongly fluorescent nature of MCT 30 itself under ultraviolet lighting. The fingering pattern with this oil was therefore observed visually under normal lighting in which the fingers could be clearly identified by the bright yellow colour of sodium fluorescein.

Shown on Plates 6.6 and 6.7 are the displacement records for two of the three tests carried out at a favourable viscosity ratio of 0.9. At the low rate of 10 cc/hour, Plate 6.6 indicates the formation of asymmetric oil pockets even at this favourable viscosity ratio. This oil bypassing at low rate might at first appear to be an indication of a possible instability. However, upon increasing the rate to 1120 cc/hour, the oil pockets were eliminated as may be seen on Plate 6.7, thus discounting the possibility of instability and viscous fingering at this viscosity ratio.

6.2.2 Connate Water Present

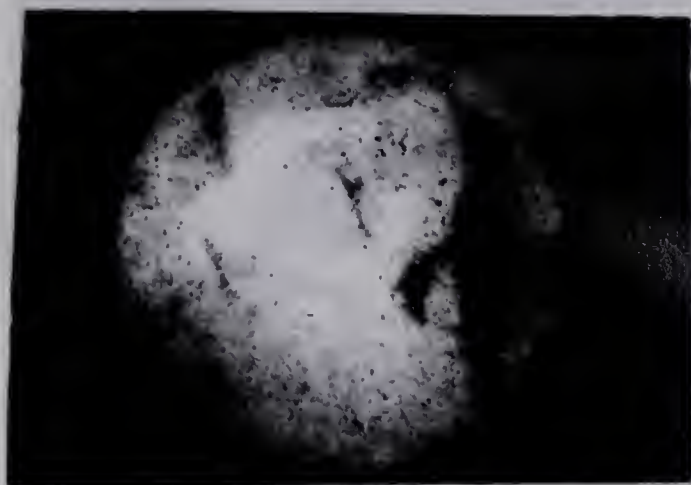
Plates 6.8 and 6.9 present the displacement records in the connate water bearing systems at the extreme rates of 2.5 cc/hour and 1120 cc/hour, for a viscosity ratio of 102.5. At 2.5 cc/hour, Plate 6.8 indicates uniform displacement with no fingering. At 1120 cc/hour, Plate 6.9 indicates uniform displacement up to Frame 6. Evident in Frames 7 to 18 is a prominent finger partially surrounded by bypassed oil. Because the edge of the finger is much more diffused, the finger is not as striking as was the case in the absence of connate water saturation. Nevertheless, the dimensions



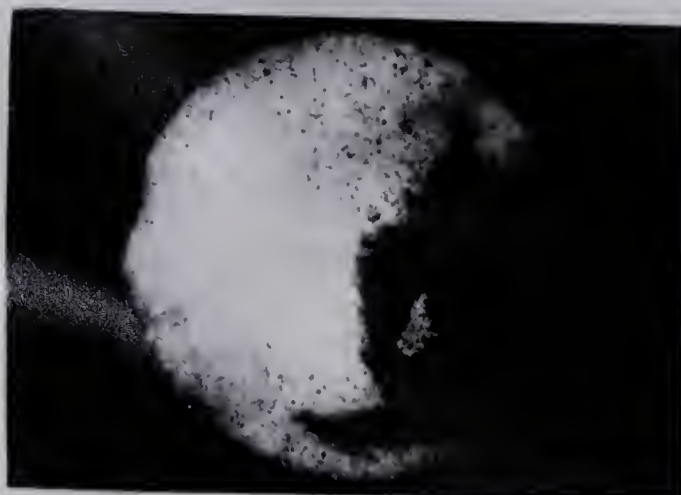
1 - Inlet
End



2



3



4



5



6

PLATE 6.6 DISPLACEMENT RECORD, RUN 33, NO CONNATE WATER
 $Q = 10 \text{ CC/HOUR}$, VISCOSITY RATIO = 0.92



7



8



9



10



11



12

PLATE 6.6 CONTINUED



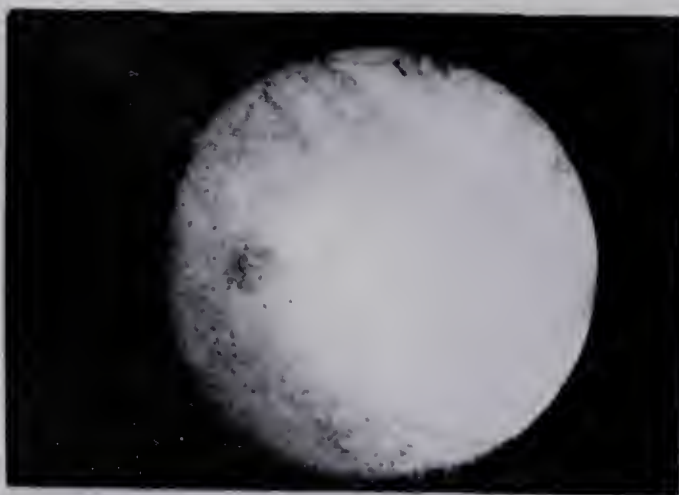
13



14



15



16



17

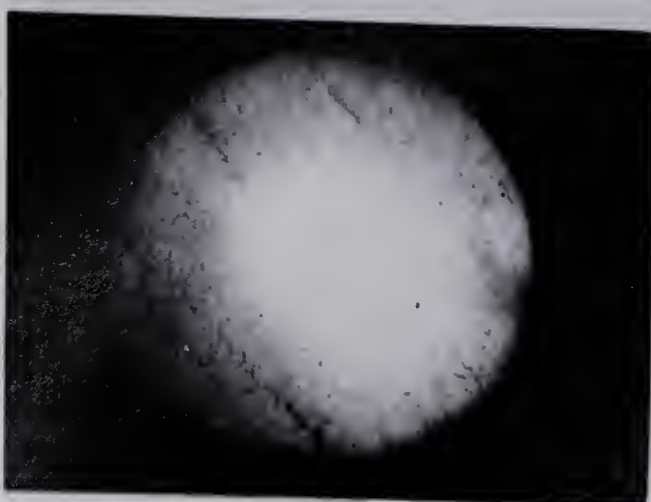
18 - Outlet
End

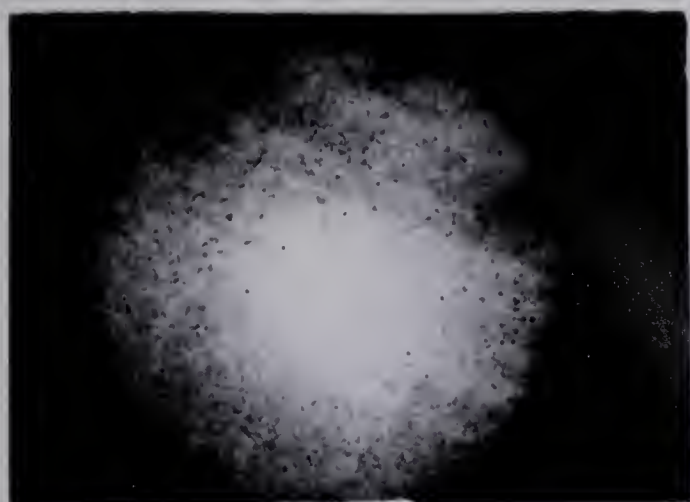
PLATE 6.6 CONTINUED



1 - Inlet
End



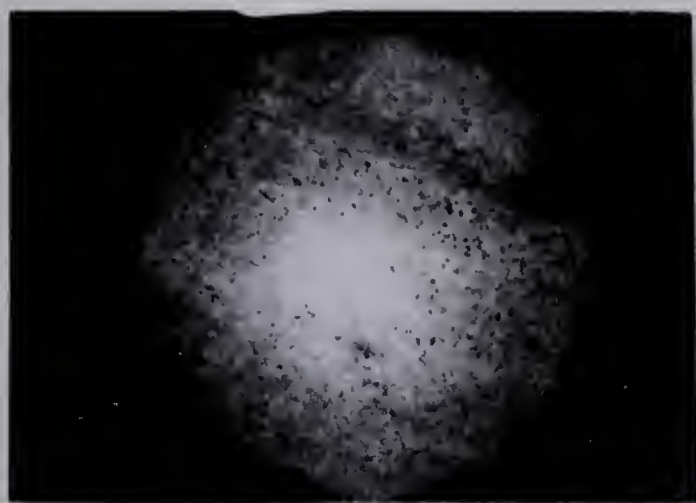
2



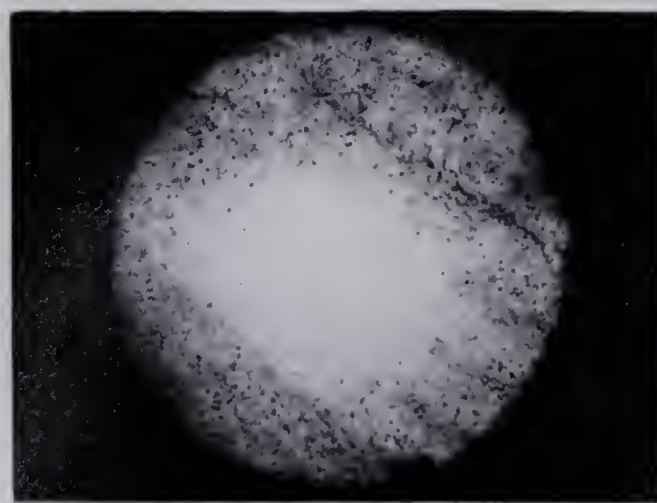
3



4

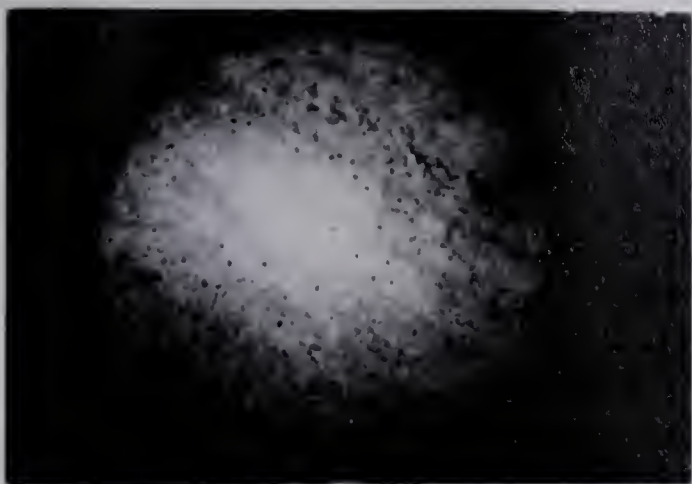


5

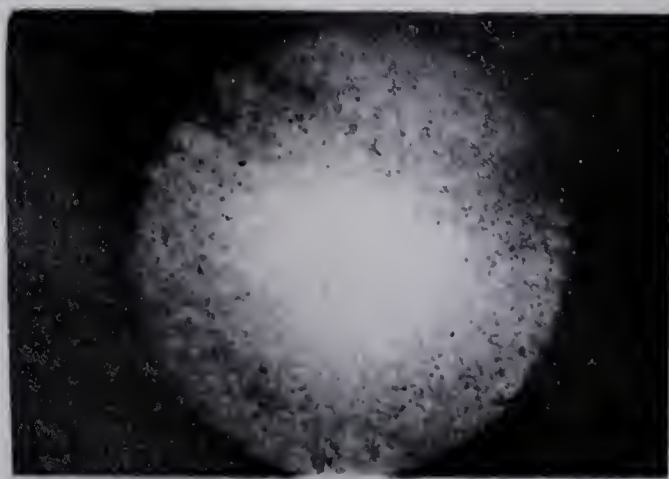


6

PLATE 6.7 DISPLACEMENT RECORD, RUN 35, NO CONNATE WATER
 $Q = 1120 \text{ CC/HOUR}$, VISCOSITY RATIO = 0.92



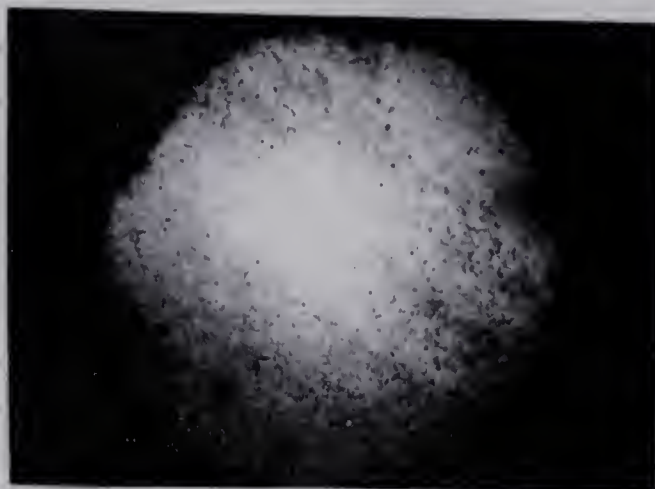
7



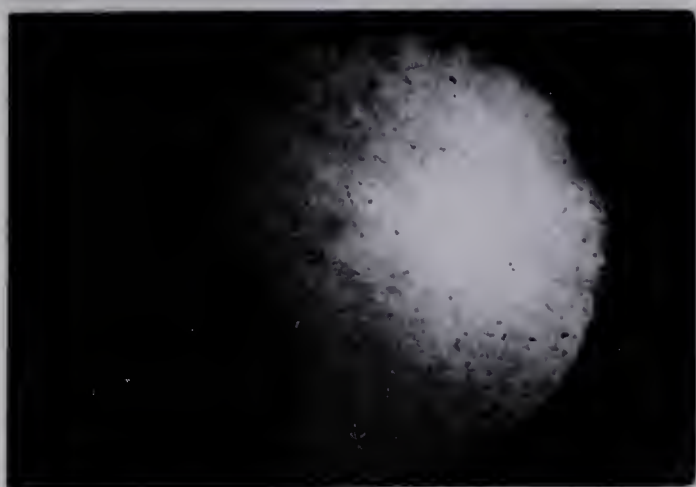
8



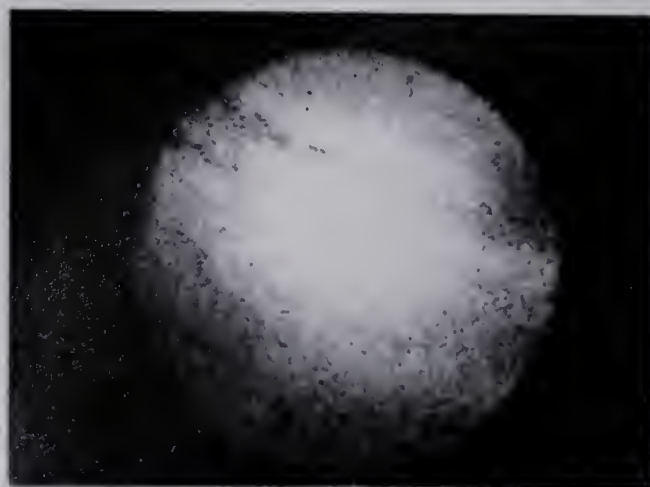
9



10

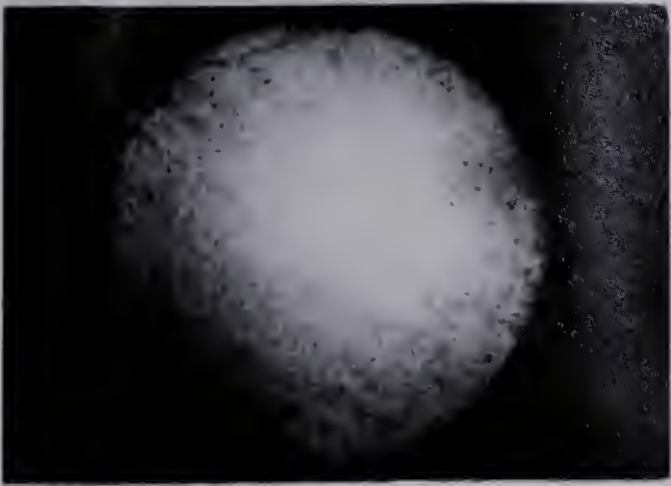


11



12

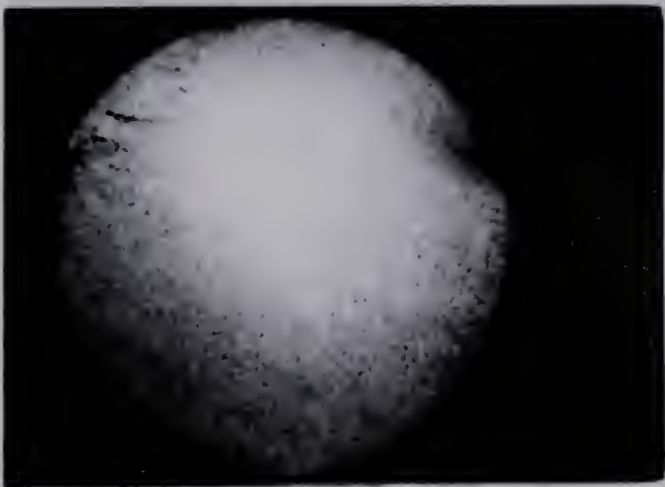
PLATE 6.7 CONTINUED



13



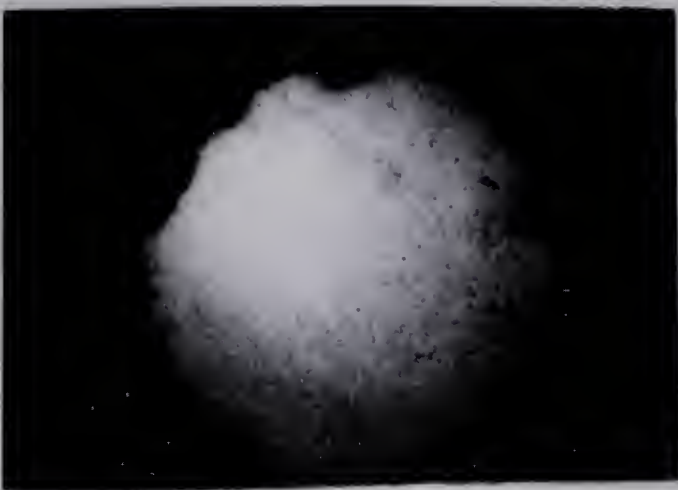
14



15



16



17



18 - Outlet
End



1 - Inlet
End



2



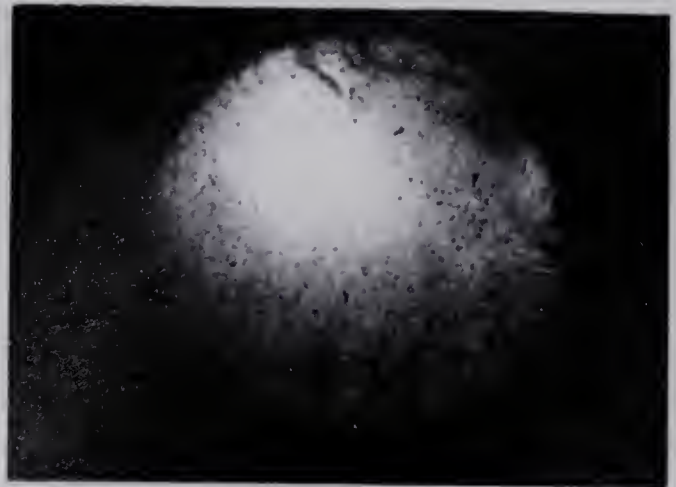
3



4

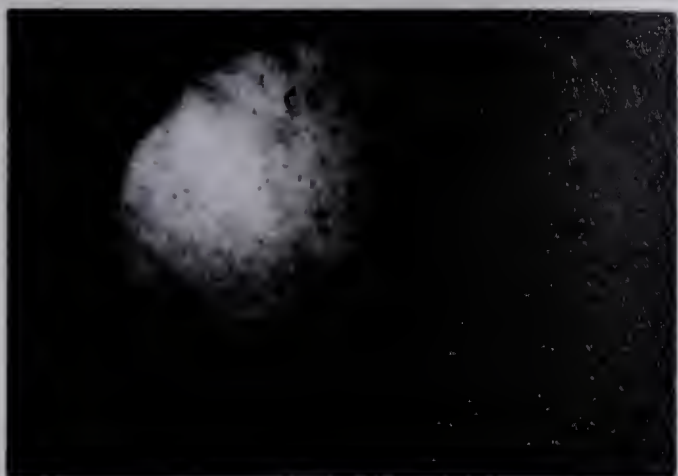


5



6

PLATE 6.8 DISPLACEMENT RECORD, RUN 1, CONNATE WATER PRESENT
Q = 2.5 CC/HOUR, VISCOSITY RATIO = 102.5



7



8



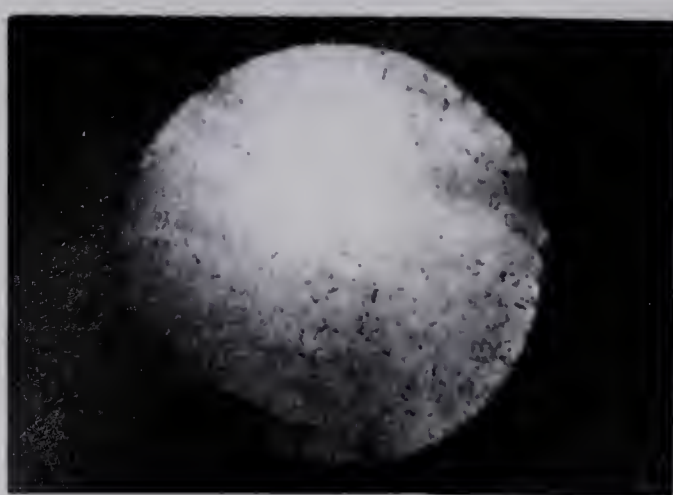
9



10



11

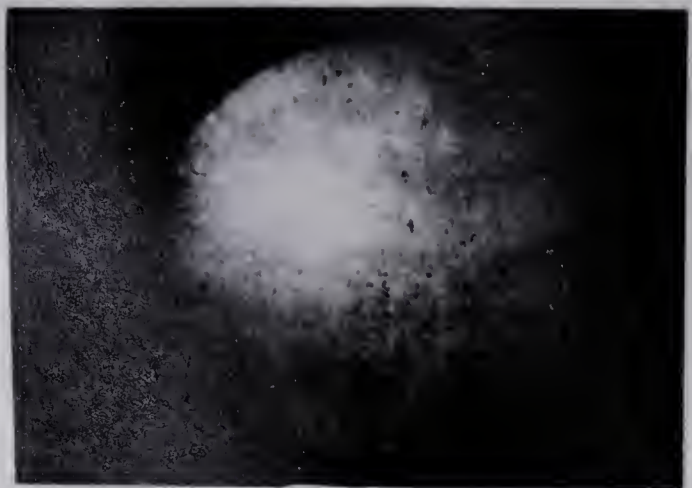


12

PLATE 6.8 CONTINUED



13



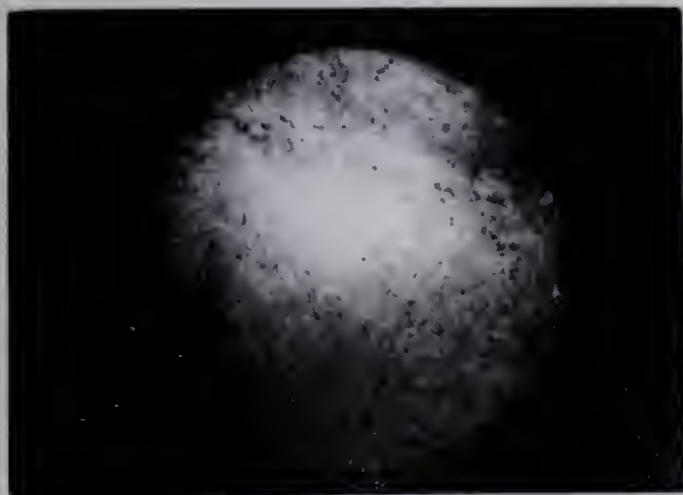
14



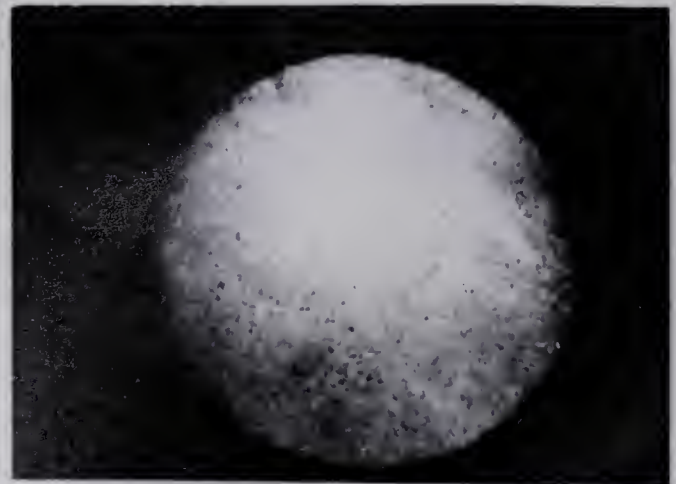
15



16



17



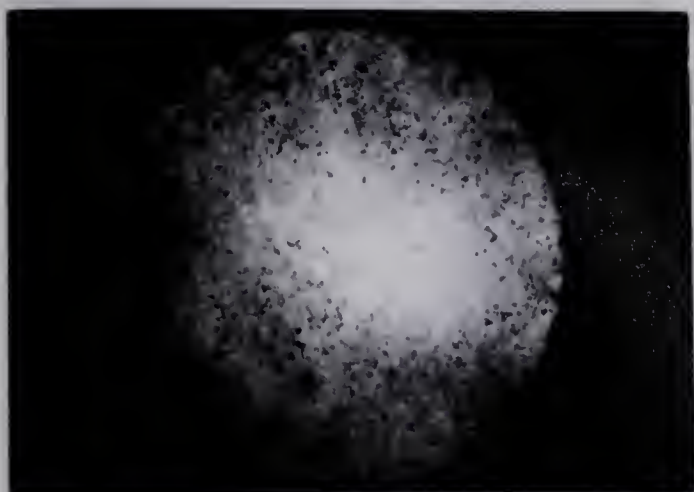
18 - Outlet
End



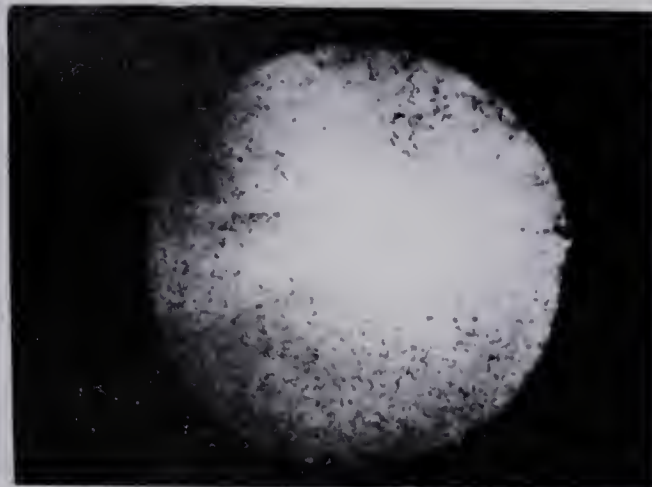
1 - Inlet
End



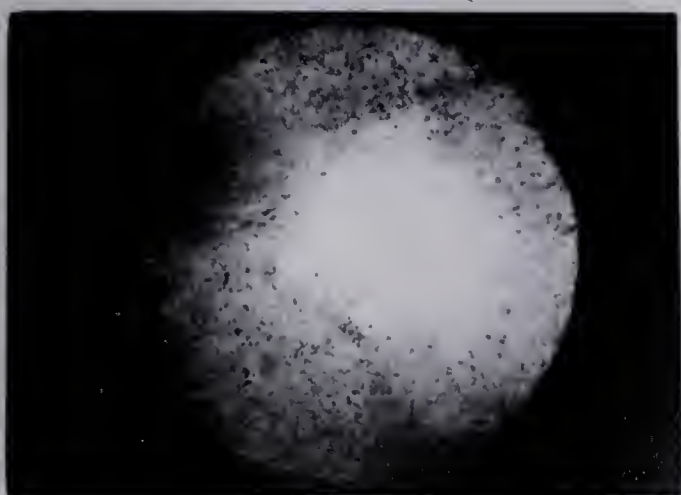
2



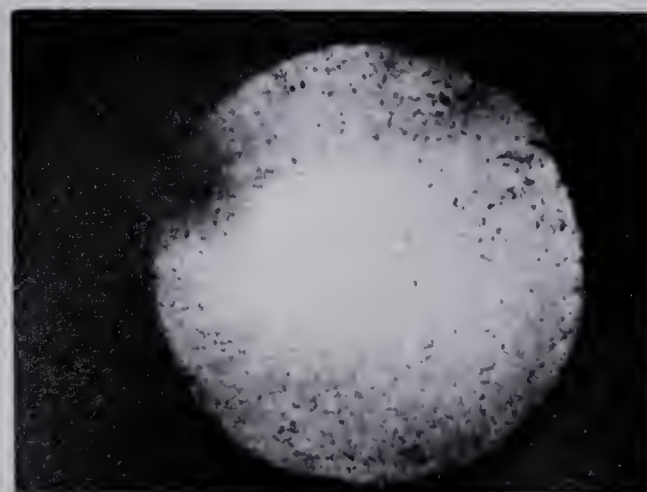
3



4



5



6

PLATE 6.9

DISPLACEMENT RECORD, RUN 11, CONNATE WATER PRESENT
 $Q = 1120$ CC/HOUR, VISCOSITY RATIO = 102.5



7



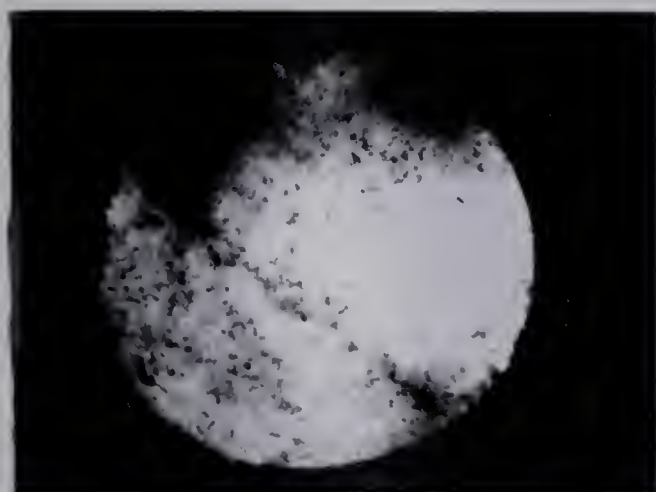
8



9



10



11



12

PLATE 6.9 CONTINUED



13



14



15



16



17

18 - Outlet
End

PLATE 6.9 CONTINUED

of the finger can still be measured for quantitative predictions.

The displacement records with MCT 30 showed a similar fingering pattern, but with gravitational underdrive.

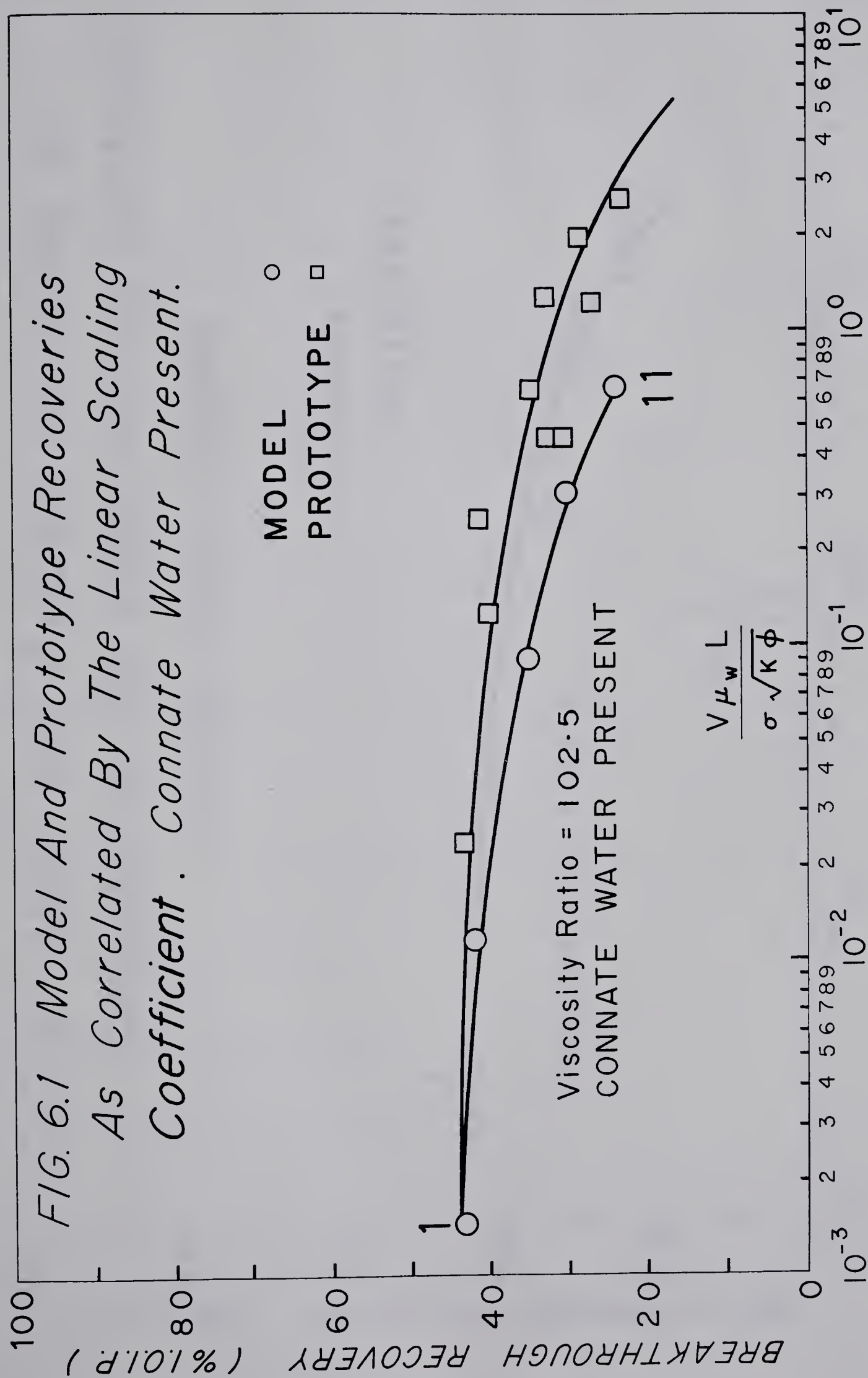
6.3 BREAKTHROUGH RECOVERY DATA

The recovery data were first correlated with the linear dimensionless scaling coefficient, $V_{\mu_W} L / \sigma \sqrt{K\phi}$, for both the model and the prototype. In the cases in which the two sets of data diverged, the data were replotted as a function of the radial scaling coefficient proposed in this study as being more suitable under the circumstance. The experimental points with numbers indicate those runs for which the displacement records are available.

6.3.1 Connate Water Present

Figure 6.1 presents the breakthrough recovery data for the model and the prototype as correlated by the linear scaling coefficient. As the data from the model and prototype diverge significantly, it is clear that this conventional scaling group is unsatisfactory for correlating the recovery data collected on geometrically dissimilar cores in the presence of connate water saturation. It is also clear that as matters now stand, the prototype recovery cannot be predicted by the model results over a wide range of the scaling number.

The same data were replotted in Figure 6.2 as a function of the radial scaling coefficient, $V_{\mu_W} D / \sigma \sqrt{K\phi}$. The result is that the experimental data from the model and prototype now plot as one curve. Under this scaling, the prototype recovery can be predicted using the model data.



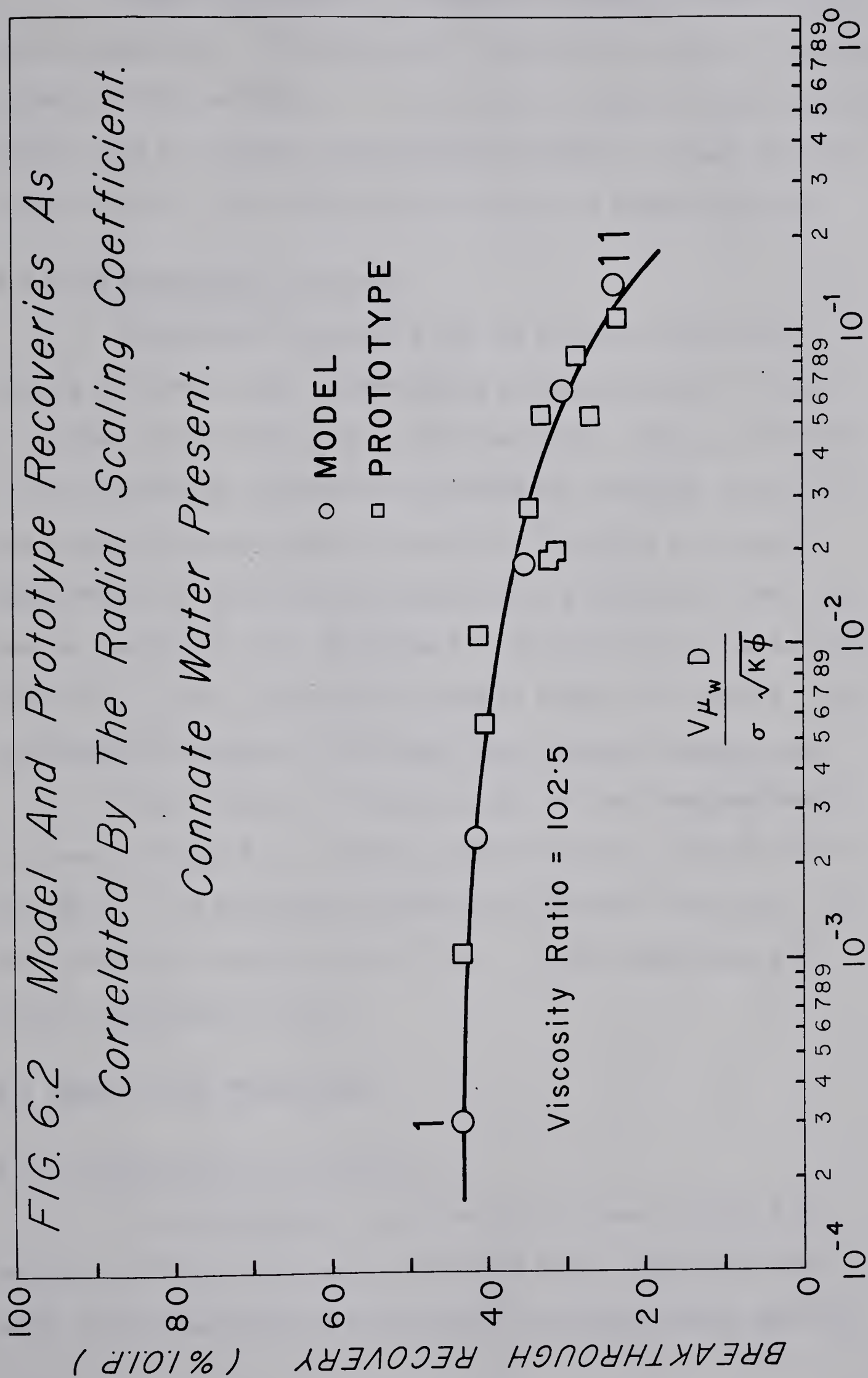


Figure 6.3 shows the influence of viscosity ratio on the recovery behaviour. Plotted on this figure are the data at viscosity ratios of 102.5 and 302.1. The recovery trends in both cases are similar; but as expected, the recovery efficiency is lower for the higher viscosity ratio flood at all the scaling numbers studied.

6.3.2 No Connate Water Present

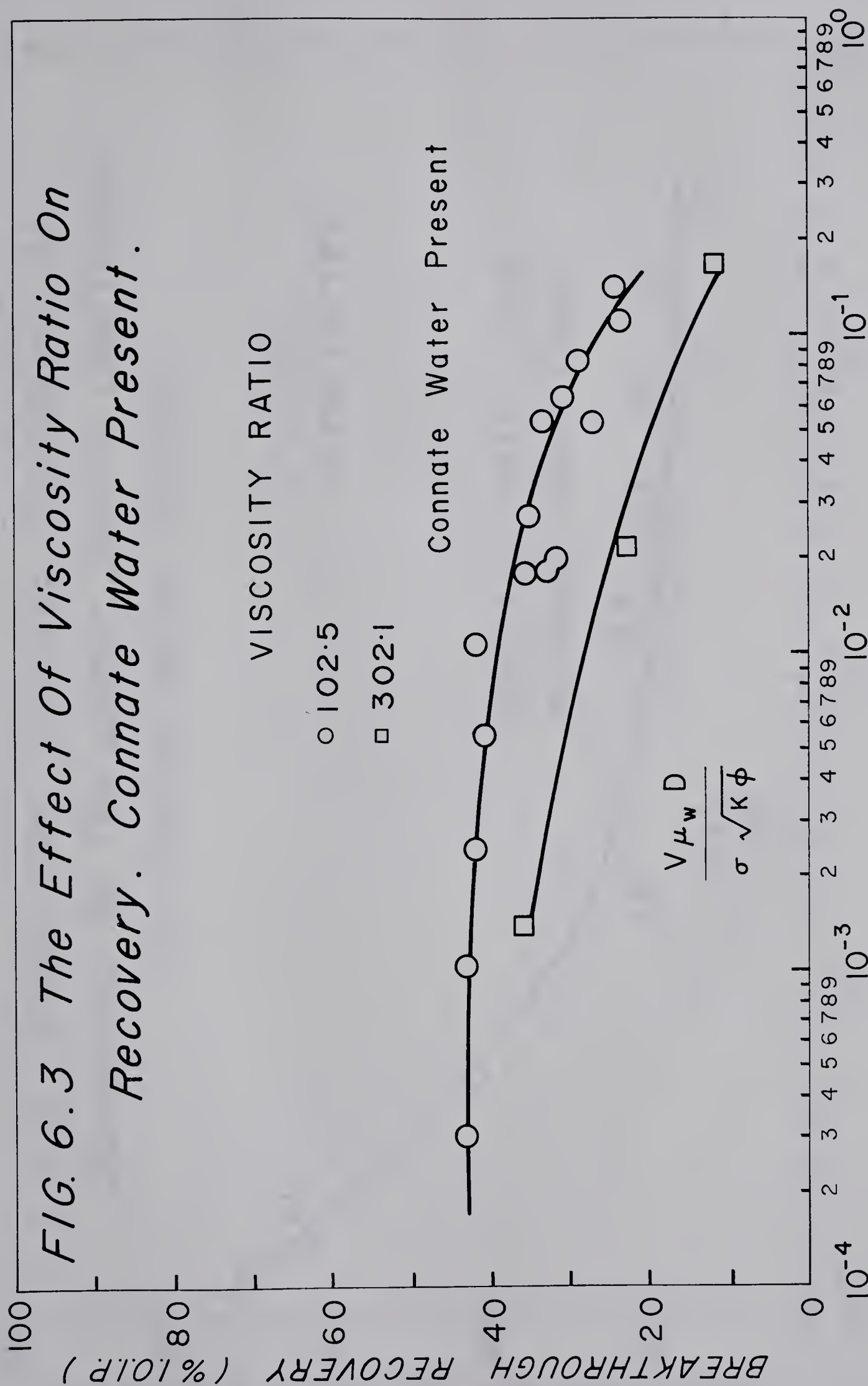
Presented in Figure 6.4 are the recovery data in the absence of connate water saturation at a viscosity ratio of 102.5. It is apparent from this figure that the linear scaling coefficient is satisfactory for correlating the model and prototype recovery in the absence of connate water saturation. That this is so may be demonstrated by replotting the same data as a function of the radial scaling coefficient that worked well in the presence of connate water saturation. Such a correlation, shown in Figure 6.5, results in an unacceptable divergence of the model and prototype recovery data.

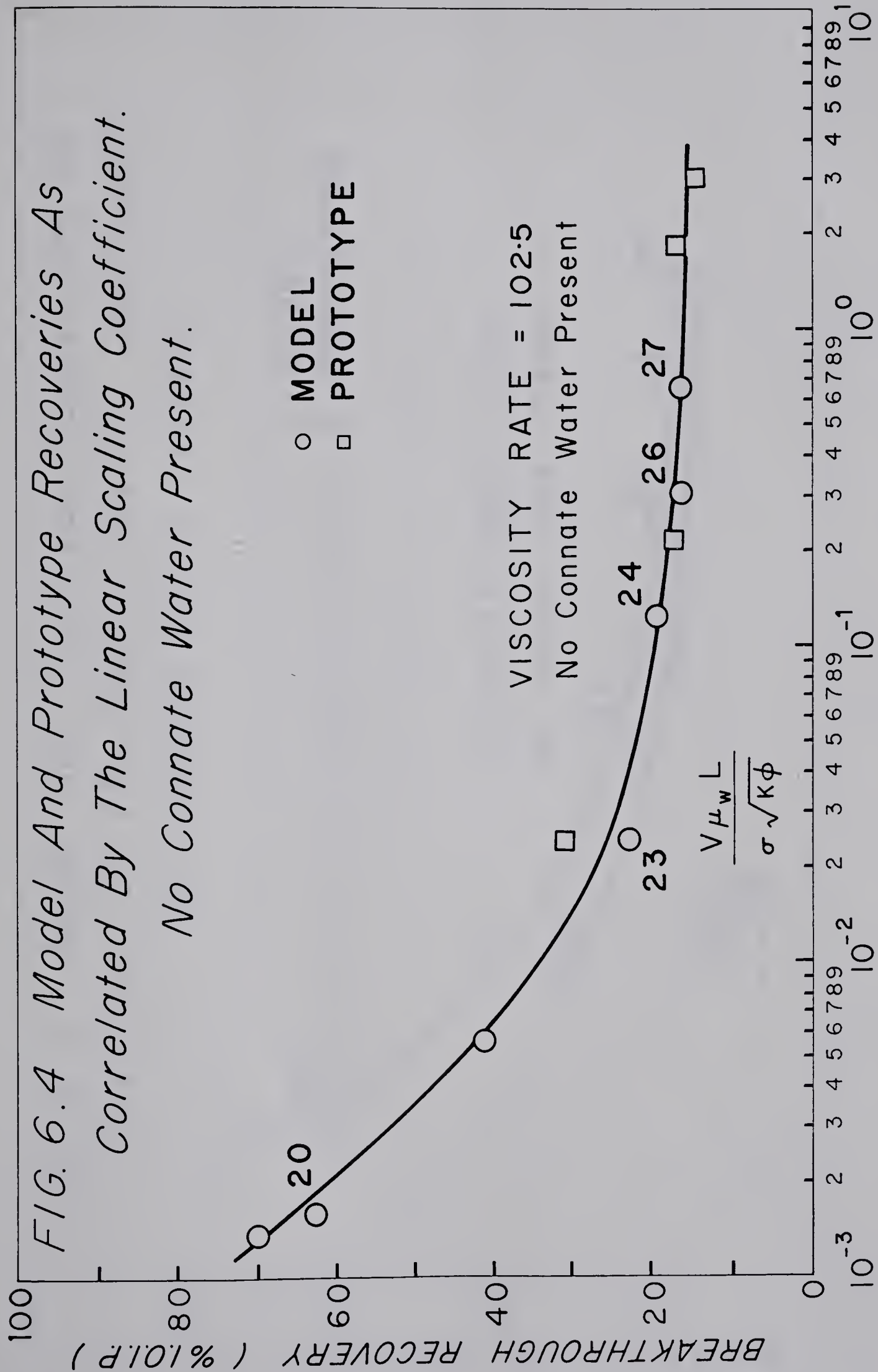
The influence of viscosity ratio on the flood performance is shown in Figure 6.6. For the adverse viscosity ratios of 102.5 and 302.1, the recoveries decreased significantly with rate. For the favourable viscosity ratio of 0.9, on the other hand, the recovery improved with rate.

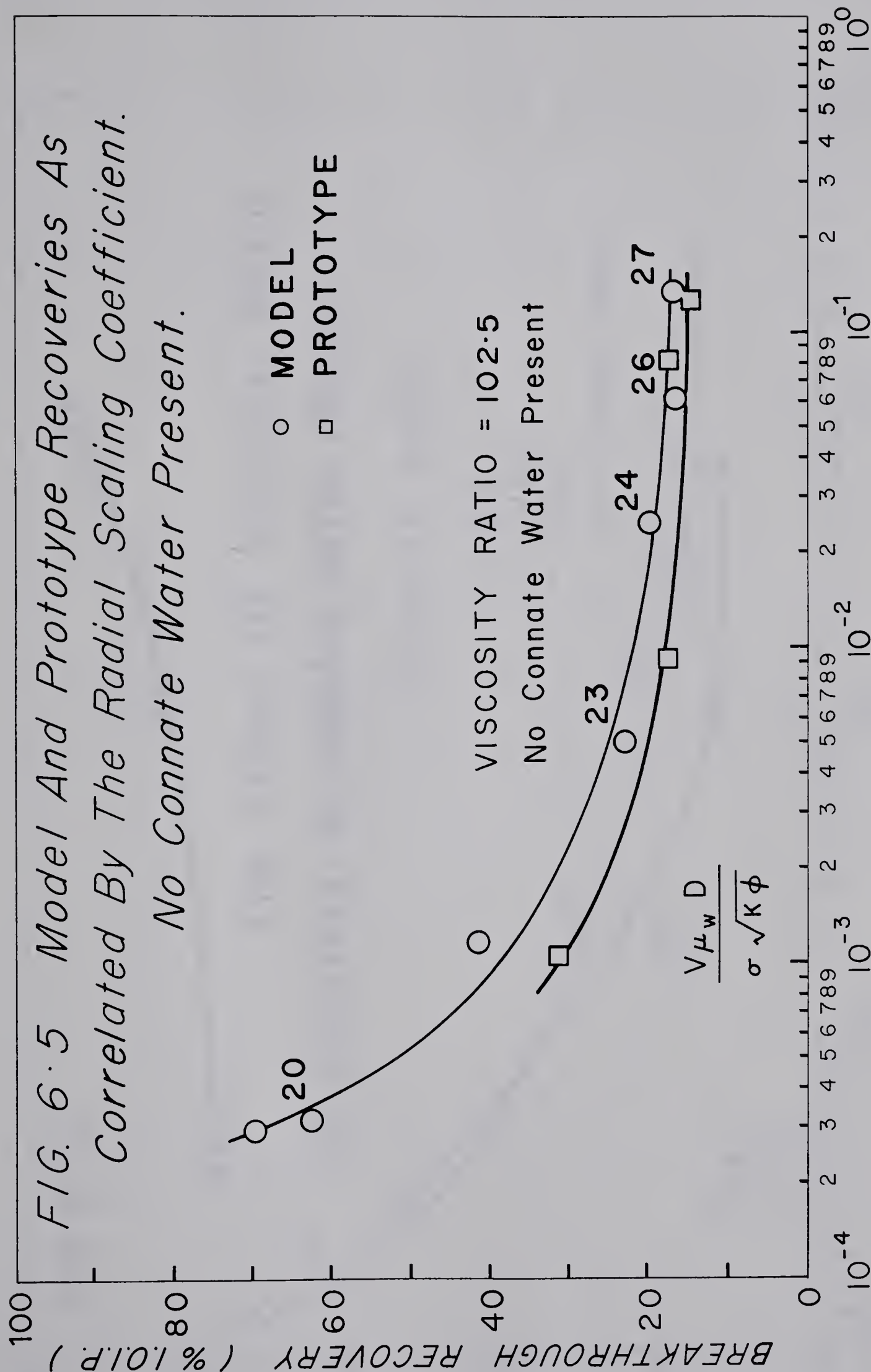
6.4 QUANTITATIVE PREDICTIONS

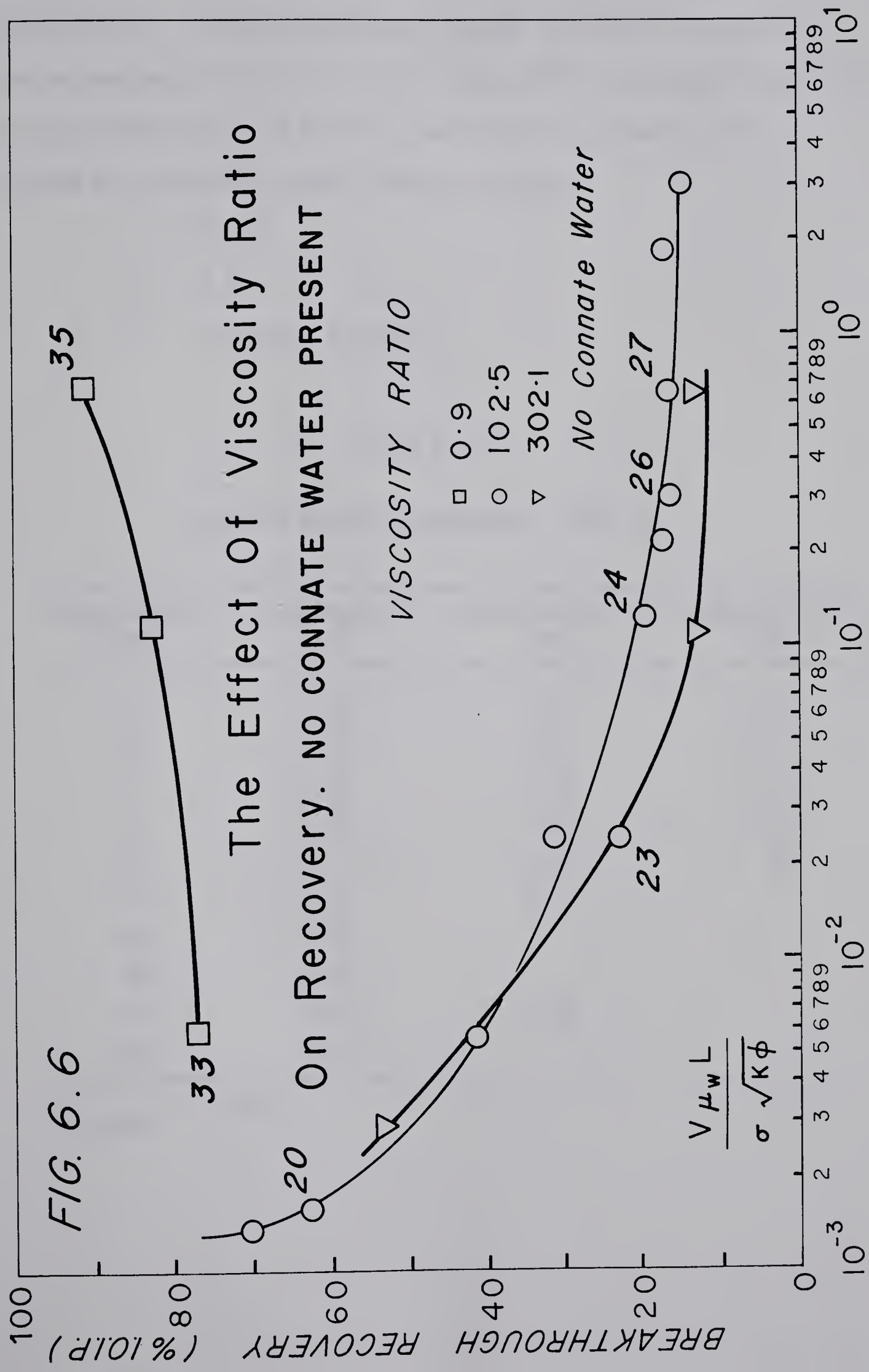
6.4.1 Estimation of C , C^* and σ^*

The displacement record for Run 23 shown on Plate 6.2 provides sufficient information about the finger wavelengths from which to make quantitative predictions in nonconnate water bearing









systems. The longest dimension of each of the fingers in Frames 9 to 18 was assumed to be the most probable wavelength of instability at 40 cc/hour. The measured values, shown in Table 6.3, give an average wavelength of 2.0 cm. Using Eqs. 3.83, 3.82 and 3.79, and the pertinent properties for Run 23, the following estimates were obtained for nonconnate water bearing systems:

$$C = 25.40$$

$$C^* = 5.45$$

$$\sigma^* = 1.324 \times 10^2 \text{ dynes/cm}$$

Table 6.3

MEASURED FINGER WAVELENGTHS - RUN 23

Photographic Frame	Wavelength #1 (cm)	Wavelength #2 (cm)	Wavelength #3 (cm)
9	1.00	1.59	2.67
10	1.34	1.67	2.17
11	1.42	2.34	2.17
12	1.50	2.00	2.67
13	1.67	2.84	1.59
14	1.67	2.17	
15	2.25		
16	3.09		
17	1.92	1.50	
18	2.67		
$\lambda_{\text{average}} = 2.00 \text{ cm}$			

Similar measurements of finger dimensions were made on Plate 6.9, Run 11, in the connate water bearing system. The measurements, tabulated in Table 6.4, gave an average wavelength of 2.84 cm. This resulted in the following estimates in connate water bearing systems:

$$C = 190.45$$

$$C^* = 306.25$$

$$\sigma^* = 7.442 \times 10^3 \text{ dynes/cm}$$

Table 6.4

MEASURED FINGER WAVELENGTHS - RUN 11

Photographic Frame	Wavelength (cm)
10	2.99
12	2.87
15	2.73
17	2.99
18	2.61

$$\lambda_{\text{average}} = 2.84 \text{ cm}$$

6.4.2 Estimation of the Finger Wavelengths for Run 24

With C now determined for both connate and nonconnate water bearing systems, the critical and most probable wavelengths at any displacement rate may be predicted. In particular, such a prediction was made for Run 24 for which fingers are available on Plate 6.3 for comparison. Using the experimental data pertaining to Run 24, the critical and most probable wavelengths were predicted as 0.51 cm and 0.89 cm, respectively. As shown in Table 6.5, the measured wavelengths were of the same order of magnitude as the predictions, with an average value of 0.72 cm. This value is in good agreement with 0.70 cm obtained by averaging the predicted critical and most probable wavelengths.

6.4.3 Prediction of the Onset of Instability

Using Eqs. 4.132 and 4.135 proposed in this study, the values of the dimensionless group $V_{\mu_w} D^2 / \sigma K$, at the onset of instability and the point at which λ_c / D equals one, were calculated. These predictions, shown in Table 6.6, are indicated on the recovery curves of Figure 6.7. It may be observed that for the same fluids and porous media the dimensionless rate for the onset of instability in the presence of connate water is about 56 times that in the absence of connate water saturation.

Table 6.5

MEASURED WAVELENGTHS IN CM - RUN 24

Frame 13	Frame 14	Frame 15
0.83	0.89	0.85
0.58	0.81	0.47
0.91	0.97	0.35
0.33	0.73	0.93
0.75	0.81	0.93
0.75	0.48	0.93
1.08	0.81	0.54
0.99	0.57	0.93
0.83	0.81	0.93
0.99	0.57	0.70
0.75	0.81	0.70
0.91	0.32	0.47
0.83	0.48	0.93
0.75	0.48	
0.83	0.48	
0.50	0.66	
0.50	0.57	

$$\lambda_{\text{average}} = 0.72 \text{ cm}$$

Table 6.6

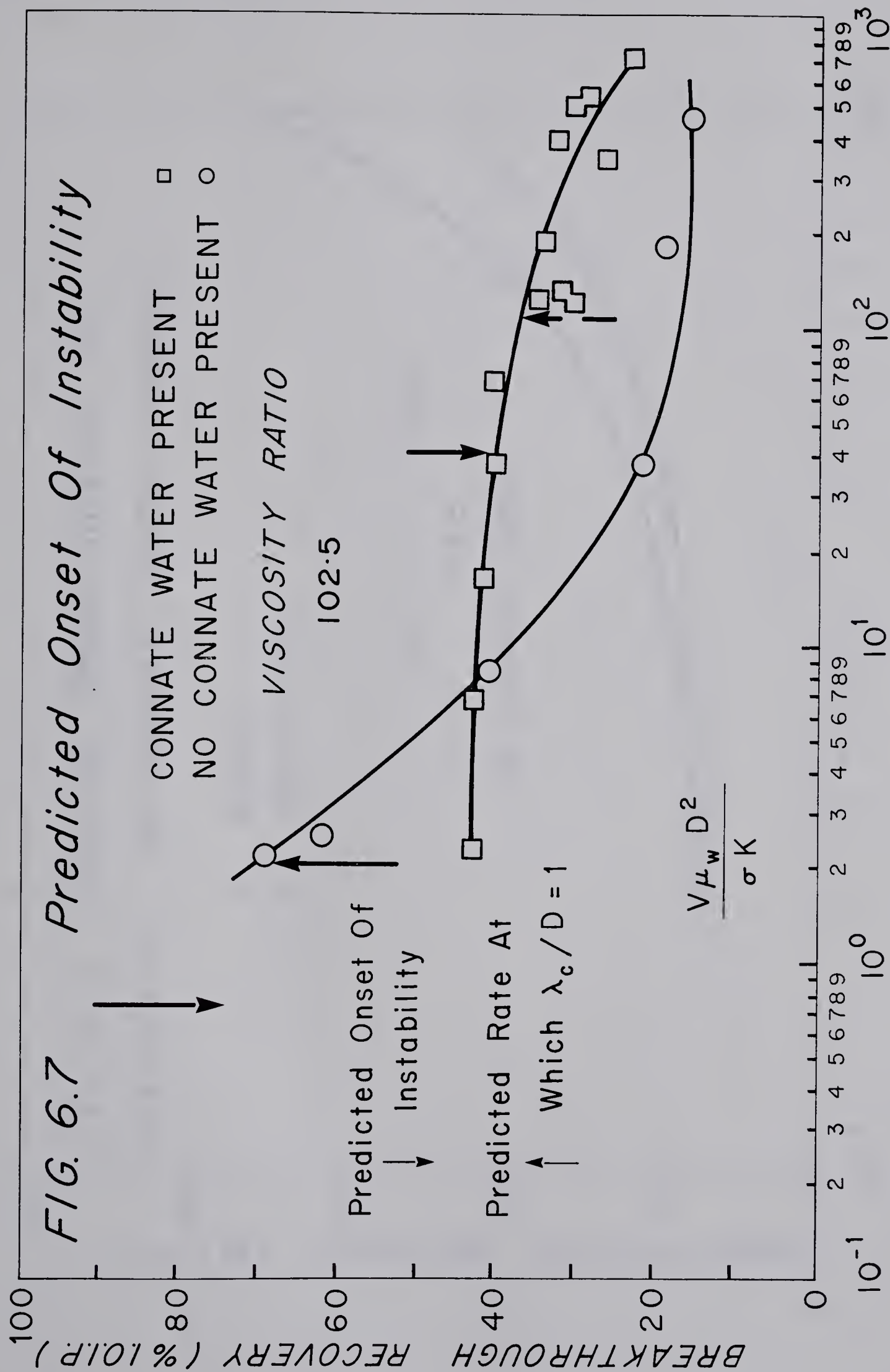
COMPARISON OF ONSET OF INSTABILITY IN THE
PRESENCE AND ABSENCE OF CONNATE WATER SATURATION
AT A VISCOSITY RATIO OF 102.5

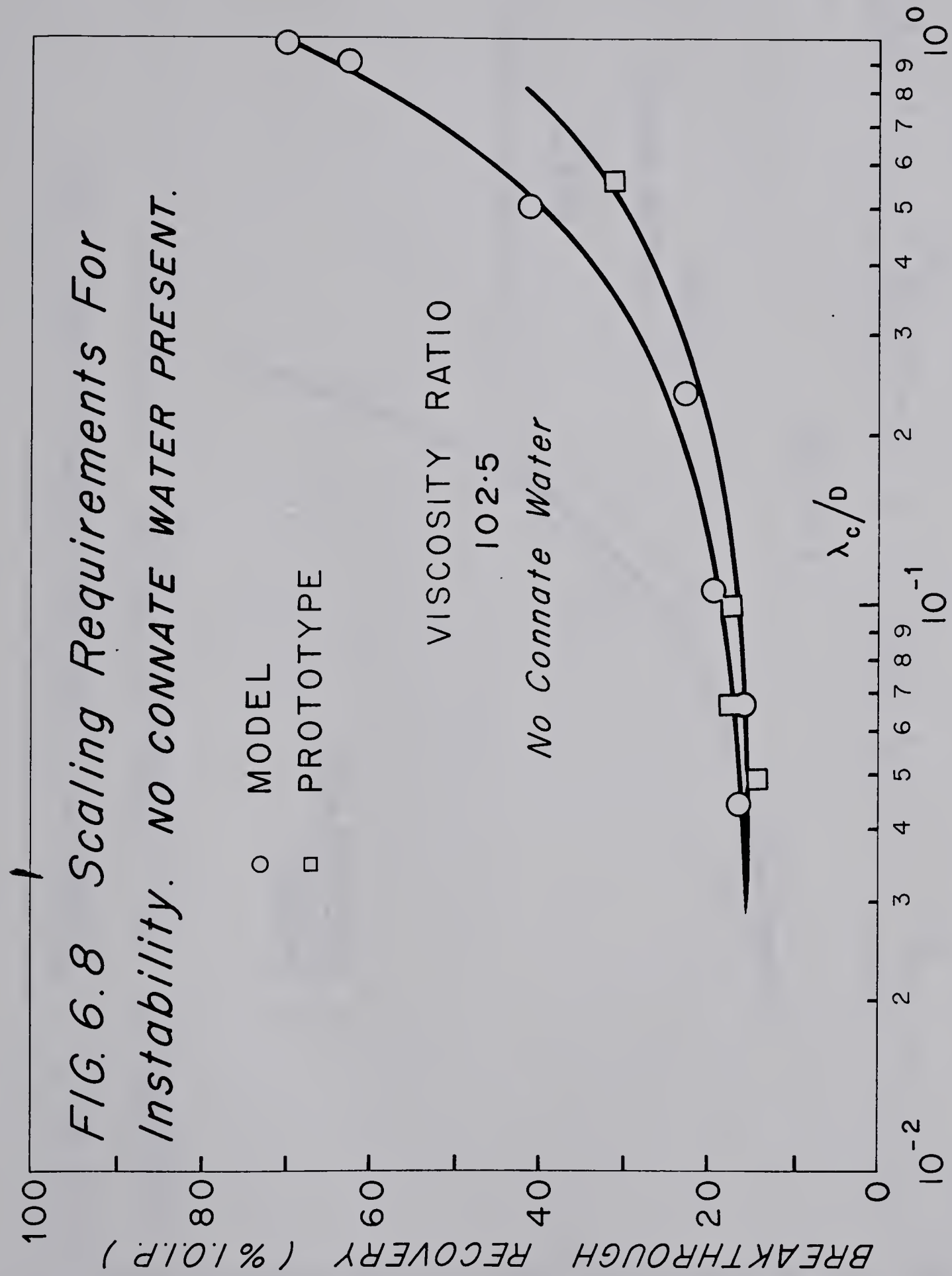
Dimensionless Group ($V_{\mu_w} D^2 / \sigma K$)		
	<u>Onset of Instability</u>	<u>$\lambda_c / D = 1$</u>
No Connate Water	0.73	2.12
Connate Water Present	40.92	119.13

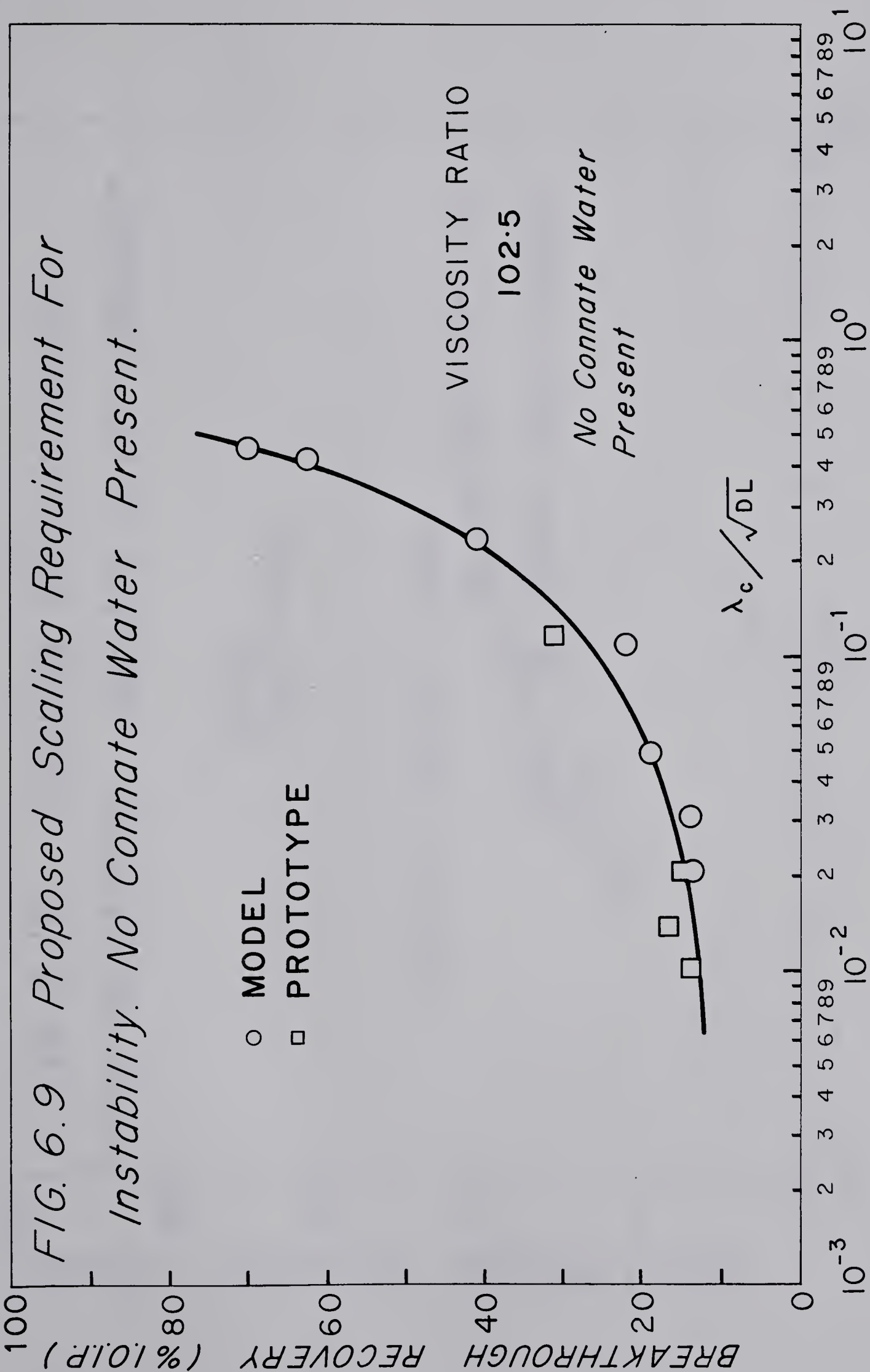
6.5 SCALING IN THE PRESENCE OF VISCOUS FINGERING

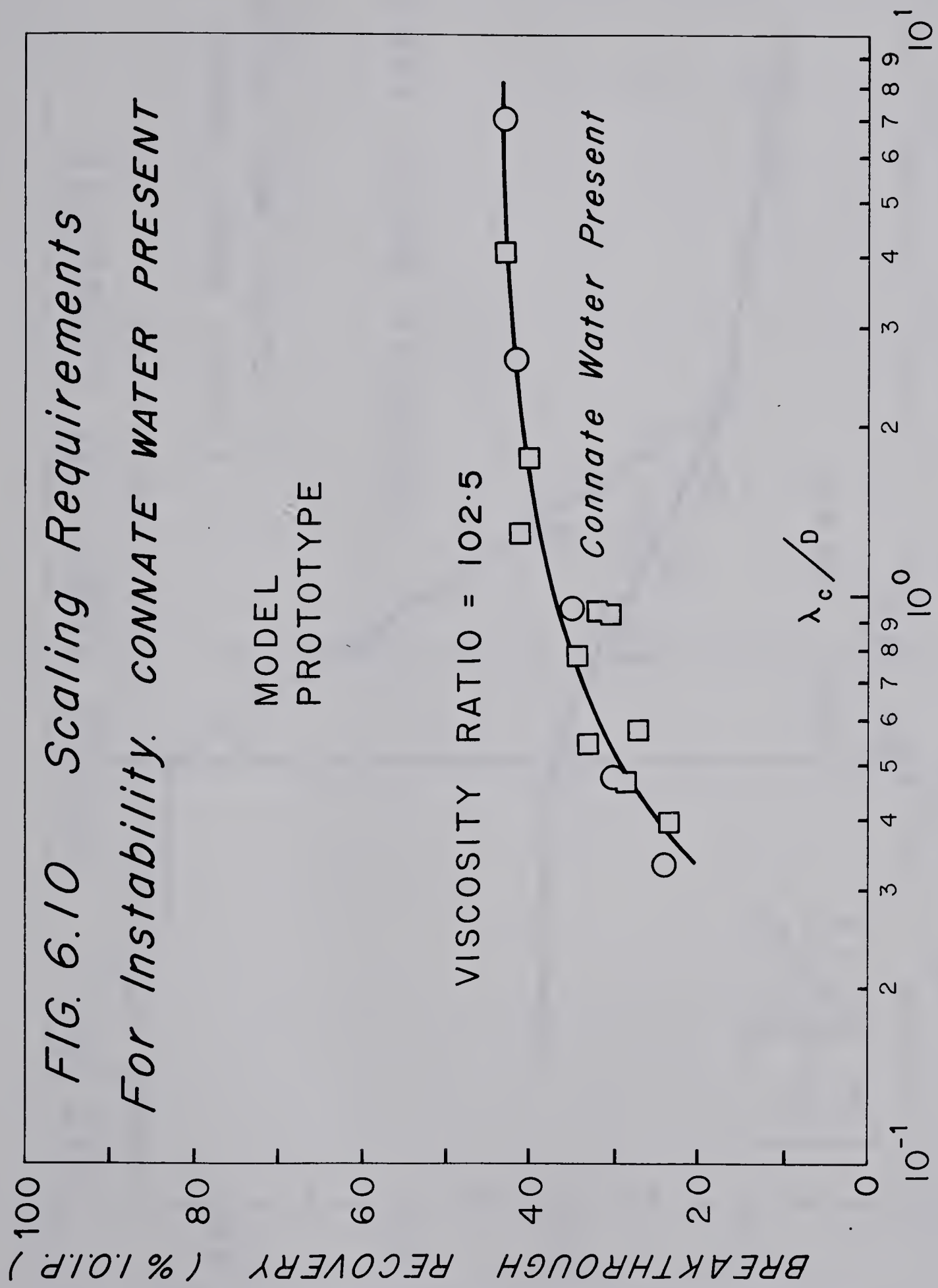
Presented in Figure 6.8 are the recovery data for the model and the prototype as a function of λ_c / D , in the absence of connate water saturation. The discrepancy between the two sets of data indicates that the results are not properly scaled. Introducing the linear dimension and replotting the same data as a function of λ_c / \sqrt{DL} resulted in a significant improvement in the correlation as indicated in Figure 6.9. In the presence of connate water saturation, however, the model and prototype results plotted as one curve when correlated with λ_c / D , as may be seen in Figure 6.10.

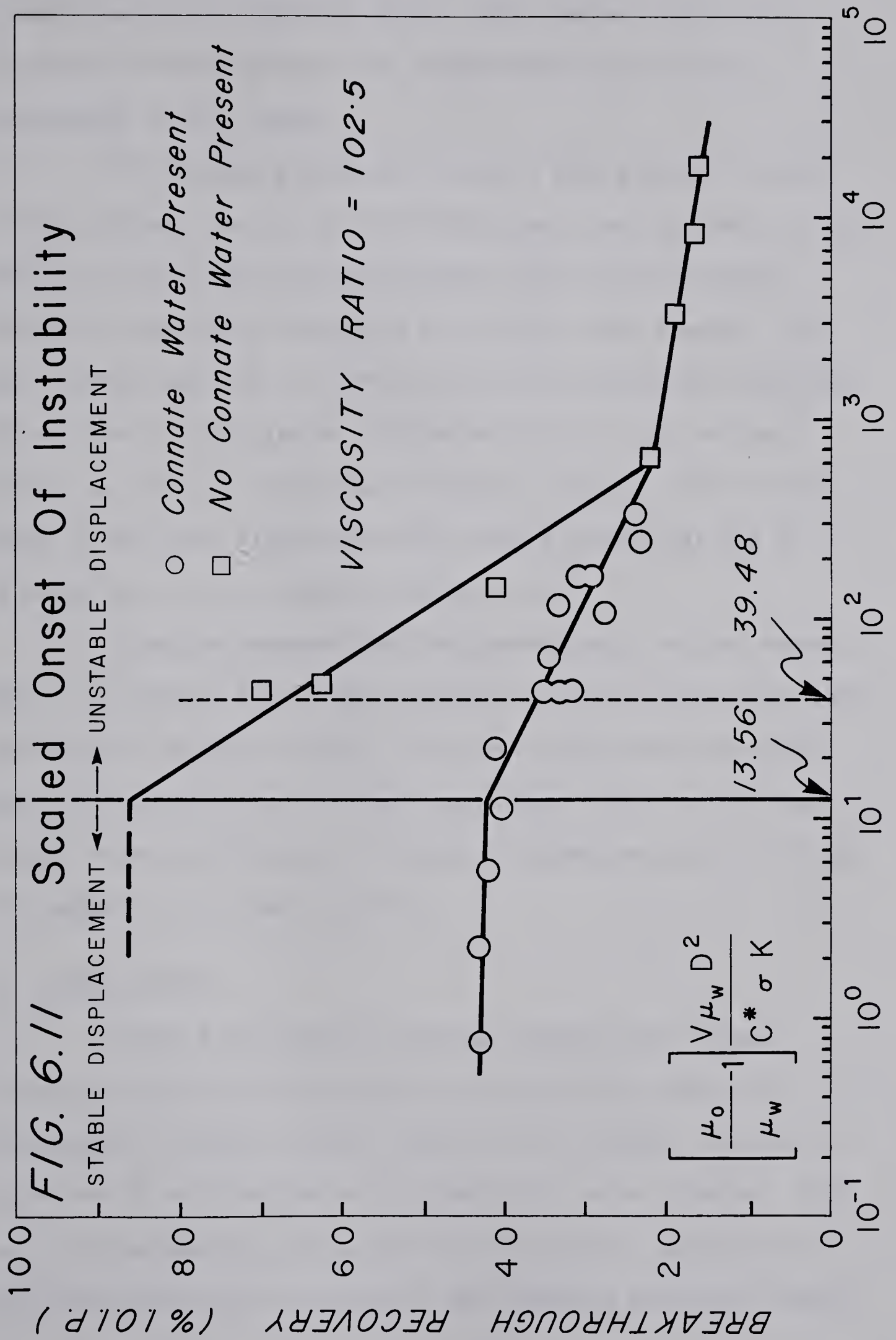
Figure 6.11 shows the breakthrough recovery data in the presence and absence of connate water saturation correlated against the dimensionless group $(\mu_o / \mu_w - 1) V_{\mu_w} D^2 / C^* \sigma K$. Plotted against this group, the connate water bearing data show a stabilized breakthrough recovery in the stable region and a declining recovery in the unstable region with a marked break in the two trends in the vicinity of 13.56











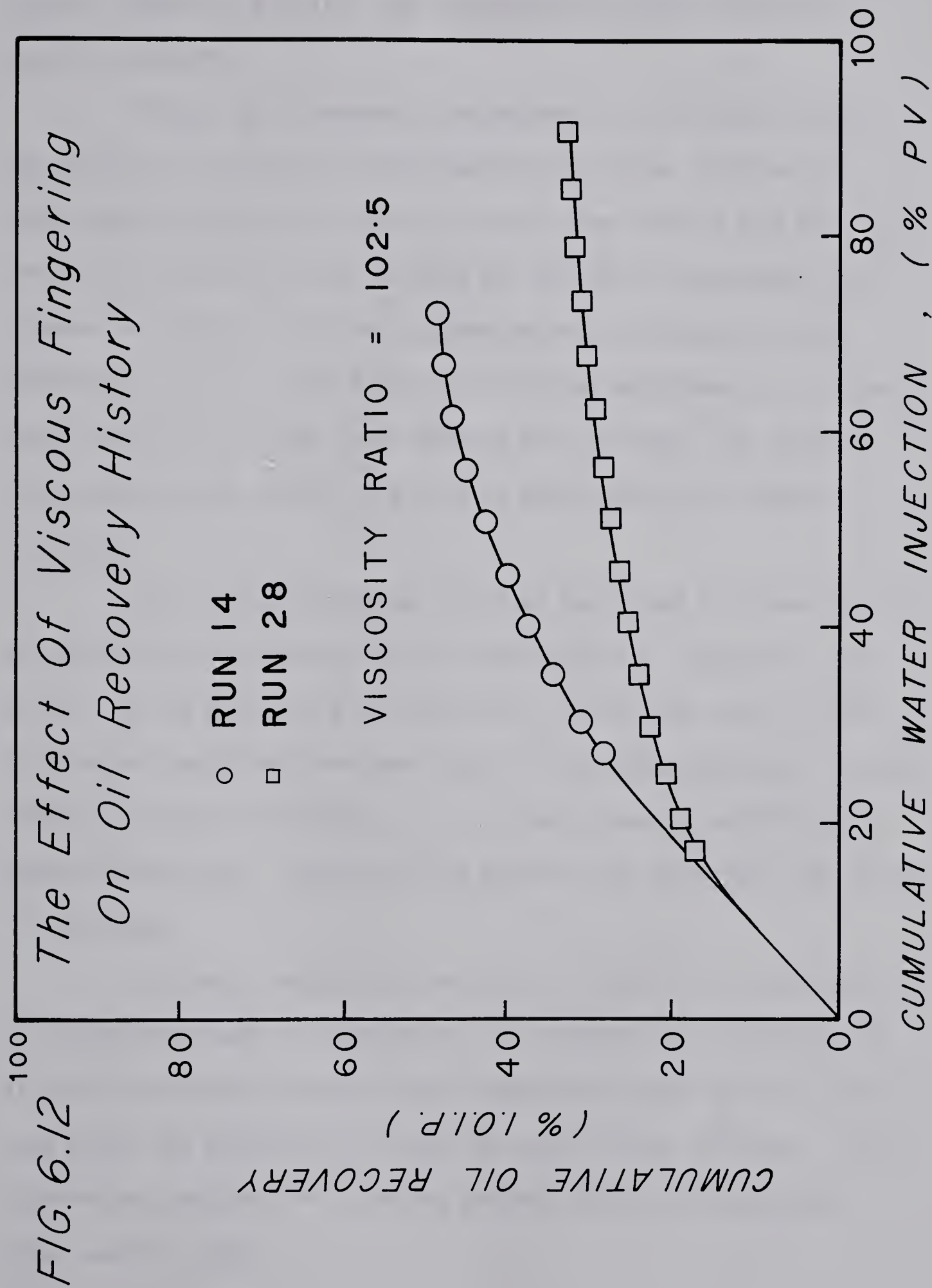
as predicted by the stability theory. The scatter in the data in the unstable region reflects the unpredictable nature of the displacement in this region.

The nonconnate water bearing data show a similar trend. For this system, however, all the displacements were unstable, a fact that is in accord with the displacement records which indicate instability and viscous fingering for all the rates studied. The steep recovery decline is a reflection of the spectacular fingering that occurred in this system. After the initial steep recovery decline, a region of slower decline seems to emerge. This is the region in which the fingers are sufficiently numerous as not to influence the recovery behaviour appreciably.

It may be observed that the connate water bearing recovery appears to approach that of the nonconnate water bearing system under conditions of extreme fingering. The two systems would therefore tend to be equivalent under these conditions. Finally, the breakthrough recovery performance in the two systems consists of straight line segments on the semi-log plot.

6.6 OTHER RESULTS

Figure 6.12 shows the permanent damage that viscous fingering can do to the oil recovery history during immiscible displacement. Plotted on this figure are the recovery histories of Runs 14 and 28 as a function of the cumulative water injected. Both runs were conducted on a long core at 800 cc/hour. Because Run 14 contained connate water saturation, the fingering phenomenon though



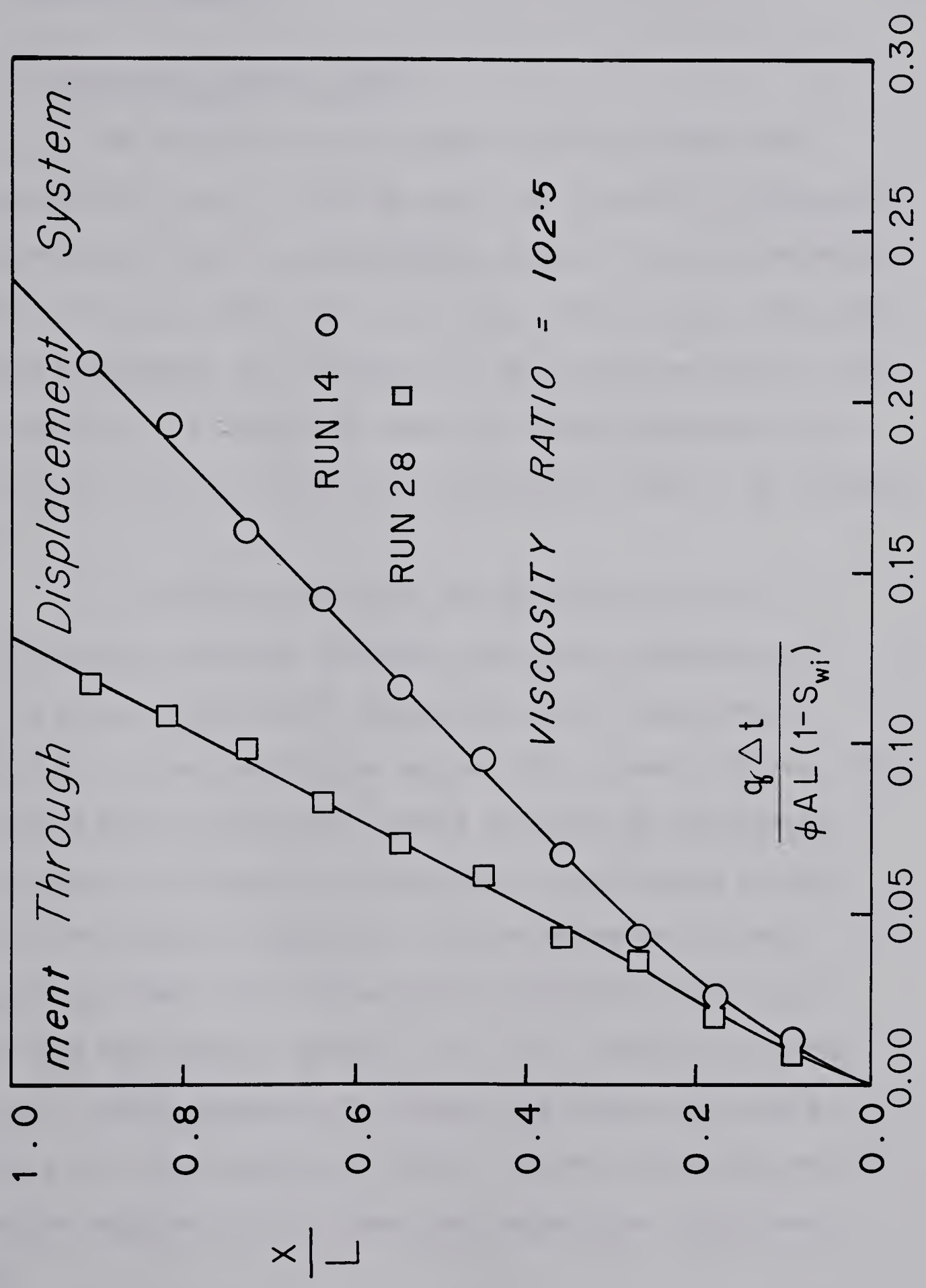
present was not as severe as in Run 28 without connate water saturation. Not only was the breakthrough recovery impaired by the severe fingering, but also the subsequent recovery history was equally impaired.

Figure 6.13 presents the estimates of the flood front positions as a function of the dimensionless time, obtained by analyzing the extensive pressure records from Runs 14 and 28. The arrival of the flood front at each of the twelve transducers was assumed to coincide with the maximum recorded pressure at each transducer. After a brief period of initial adjustment, the fronts propagated at a uniform speed through both systems, the speed of propagation being higher in Run 14 in which there was severe fingering.

The frontal positions, such as indicated in Figure 6.13, provided an indirect means of estimating the oil recovery at water arrival at the outlet end of the core. For all the runs in which the frontal positions were monitored, the estimated recovery at water arrival was generally found to be in good agreement with that at water breakthrough. Capillary end effects were therefore negligible in these runs.

Although instability resulted in significant differences in the breakthrough oil recoveries, the cumulative recoveries for all the runs carried beyond water breakthrough were generally the same after the injection of about two pore volumes of water. This observation was true for both the connate water and nonconnate water bearing tests.

FIG. 6.13 Effect Of Viscous Fingering On Frontal Move-



CHAPTER 7

DISCUSSION

7.1 STABILITY THEORIES

7.1.1 The Buckley-Leverett Model

The stability analysis based on the one-dimensional Buckley-Leverett model failed to reveal the instability that exists in connate water bearing displacements contrary to the experimental evidence of such instability found in the present study, and in the studies by Kloepper (31), Wiborg (32), Baird (33) and Hagoort (13). The source of this discrepancy seems to be the assumption of one-dimensional flow that was made at the outset in the Buckley-Leverett model.

An inspectional analysis of the multi-dimensional Buckley-Leverett equation revealed a transverse dimensionless scaling group, $V_{\mu_w} D^2 / \sigma^* L \sqrt{K\phi}$, in addition to the linear group, $V_{\mu_w} L / \sigma^* \sqrt{K\phi}$. It was anticipated on heuristic grounds that since this transverse group controls the lateral spreading of the injected fluid to prevent fingering, its magnitude should play a critical role in the onset of instability. As the assumption of one-dimensional linear flow eliminated this important dimensionless group from the stability analysis, it is not surprising that the analysis, though mathematically sound, gave results that are at variance with the experimental facts. A correct stability analysis therefore requires a multi-dimensional unperturbed displacement model.

It is, however, interesting to note that the present analysis led to conclusions similar to those of Rachford (12), in which adverse mobility ratios and high displacement rates were found to be beneficial to the stability of the displacement. Whether this agreement is fortuitous is not immediately apparent. Nevertheless the agreement would seem to suggest that although Rachford's (12) analysis was based on a multi-dimensional Buckley-Leverett model, his various assumptions and approximations of the perturbation equations may have been inappropriate.

Hagoort's (13) stability analysis involved a transverse dimensionless group, $V_{\mu_0} L_X / K_{or} \sigma \sqrt{\phi/K}$, which is pertinent to the stability problem. Because of the assumption of constant saturations behind and ahead of the front which effectively rendered his unperturbed model somewhat piston-like, his analysis was not based entirely on the Buckley-Leverett model. Hagoort (13) recognized this fact when he observed that any attempt at a stability theory based entirely on the Buckley-Leverett equations was bound to become mathematically intractable.

A successful stability theory of immiscible displacement founded on the Buckley-Leverett model is therefore still outstanding. The presence of the pertinent transverse scaling group in the multi-dimensional Buckley-Leverett model would seem to indicate that this model contains the essence of the displacement capable of instability. The lack of a successful stability theory to date may therefore be due to mathematical limitations rather than to the inadequacy of the model itself. A successful analysis will require

more powerful analytical techniques for coping with nonlinear partial differential equations in a multi-dimensional setting, than those employed to date.

7.1.2 Extended Theory of Chuoke et al. (7)

One of the significant achievements of the present study is the successful extension of the stability theory of Chuoke et al. (7) to predict the onset of instability in cylindrical cores. According to the present theory, the stability boundary in cylindrical cores is given by

$$\frac{(M - 1)(V - V_c)\mu_w D^2}{C^* \sigma K_{wr}} \leq 13.56 \quad 7.1$$

Though not verified experimentally, a similar stability boundary was derived for rectangular systems as

$$\frac{(M - 1)(V - V_c)\mu_w L_x^2 L_y^2}{C^* \sigma K_{wr} (L_x^2 + L_y^2)} \leq 9.87 \quad 7.2$$

The meaning of the equations is as follows. For any choice of displacement properties, if the dimensionless group on the left hand side of the equations is less than the pure number on the right hand side, then the displacement is stable. If the group exceeds the number, then the displacement is unstable, with the transition from one to the other occurring when the group equals the number.

It may be noted that the transverse or radial dimensionless group in cylindrical systems that was lost in the stability theory based on the one-dimensional Buckley-Leverett equation is retained in

the present theory. The radial group, $V_{\mu_w} D^2 / \sigma^* K_{wr}$, which appears on the left hand side of Eq. 7.1 is closely related to $V_{\mu_w} D^2 / \sigma^* L \sqrt{K\phi}$, found by an inspectional analysis of the Buckley-Leverett model. In addition to further highlighting the shortcoming of the linear flow assumption of the previous theory, this observation indicates that the present theory applies equally well to displacements of the Buckley-Leverett type. A successful stability theory based on the Buckley-Leverett model may therefore be expected to yield the same conclusions derived in the present theory.

Eqs. 7.1 and 7.2 embody the rate and mobility ratio conditions for instability as found by Chuoke et al. (7) and expressed by Eqs. 3.73 and 3.74. For example, instability in a cylindrical system requires that

$$\frac{(M - 1)(V - V_c)_{\mu_w} D^2}{C^* \sigma K_{wr}} > 13.56 \quad 7.3$$

Thus, if $V < V_c$, or $M < 1$, there can be no instability since the inequality expressed by Eq. 7.3 cannot be met. The present results, however, go beyond those of Chuoke et al. (7). Because the present analysis recognizes the special roles of the minimum eigenvalues in determining the onset of instability, quantitative predictions beyond those derived or anticipated by Chuoke et al. (7) are now possible. For example, in cylindrical systems, instability will occur whenever the ratio of the wavelength of the disturbance to core diameter is less than about 1.7.

Several useful deductions may be made from Eqs. 7.1 and 7.2. Gravity can have a stabilizing or a destabilizing effect on the displacement depending on the densities of the fluids concerned. If $\rho_w > \rho_o$, Eq. 3.69 indicates that V_c is positive, thus reducing the value of the scaling groups away from their stability boundaries. This is a stabilizing influence. If $\rho_w < \rho_o$, however, the opposite is true and gravity becomes a destabilizing force. In either case, the maximum influence of gravity is felt when the system is vertical and $\cos\alpha$ equals one. Other destabilizing influences are high mobility ratios, high displacement rates, large system dimensions, low interfacial tensions and low system permeabilities.

The need for stability boundaries such as those derived in this study has been felt for some time. The advent of high speed digital computers and recent advances in numerical techniques have permitted the large scale simulation of immiscible displacement in petroleum reservoirs. Perhaps, because of the lack of clear stability boundaries, these numerical simulators have often ignored the possibility of instability in the displacement being simulated. If the displacement is unstable, but the numerical prediction proceeded, as is often the case, as if the displacement were stable, then serious discrepancies may arise between the predicted and the observed behaviour. One such discrepancy is illustrated by Figure 2.6 which shows the breakthrough recovery trend predicted by the numerical solution of the one-dimensional Buckley-Leverett equation and Figure 6.11 which gives the recovery trend obtained experimentally. Figure 2.6 predicts a breakthrough recovery which increases with

rate until stabilization at high rates whereas Figure 6.11 indicates a breakthrough recovery that decreases with rate at high displacement rates due to instability, a recovery trend that disagrees with the mathematical prediction. Eqs. 7.1 and 7.2 provide a much needed guidance for determining the range of displacement parameters for which instability can no longer be ignored without seriously compromising the results of the mathematical prediction.

Instability introduces a certain element of uncertainty into the displacement behaviour which is difficult to simulate with the numerical solution of the deterministic equations of immiscible displacement. If one could numerically calculate the dynamics of the random viscous fingers, then the unstable displacement behaviour can in principle be simulated. But such a simulation would require a detailed knowledge of the distribution of the slight heterogeneities that initiate the viscous fingers. Such a complete knowledge of the porous medium is unlikely to be achieved in practice. Although the stability boundaries identified in this study provide no guidance on how to simulate an unstable displacement, they do provide a means of determining when such a simulation is necessary if one is to correctly predict the behaviour of the immiscible displacement.

7.2 EXPERIMENTAL VERIFICATION

7.2.1 Estimation of System Parameters

Before Eqs. 7.1 and 7.2 can be used for predictions, Chuoke's constant, C , and hence C^* , must be determined experimentally for both connate water and nonconnate water bearing systems.

The estimates of 25.40 and 5.45 of C and C^* obtained in the present study for nonconnate water bearing systems compare favourably with 30 and 6.66 obtained by Chuoke et al. (7). The values of 190.45 and 306.25 obtained for connate water bearing systems cannot be justifiably compared with available estimates by Wiborg (32) and Baird (33) since these were not obtained by measurements on actual fingers. A more meaningful comparison between the present results and those of these authors would be to scale their experimental recovery data using the C^* obtained in this study and to compare the resulting recovery trends with those of the present study. Such a comparison is particularly pertinent as the previous studies employed Dow Corning oil and Ottawa sand as well.

The good agreement between the estimates of C and C^* of the present study and those of Chuoke et al. (7) for nonconnate water bearing systems with widely different properties raises the possibility that C or C^* may in fact be universal constants that take on different values depending on the presence or absence of connate water saturation, at least for unconsolidated porous media. Chuoke et al. (7) obtained their estimate on a rectangular glass bead pack with a permeability of about 60 darcys while the present estimate was obtained on a cylindrical pack of Ottawa sand with a permeability of 16 darcys. More experimentation would, however, be required to substantiate this speculation.

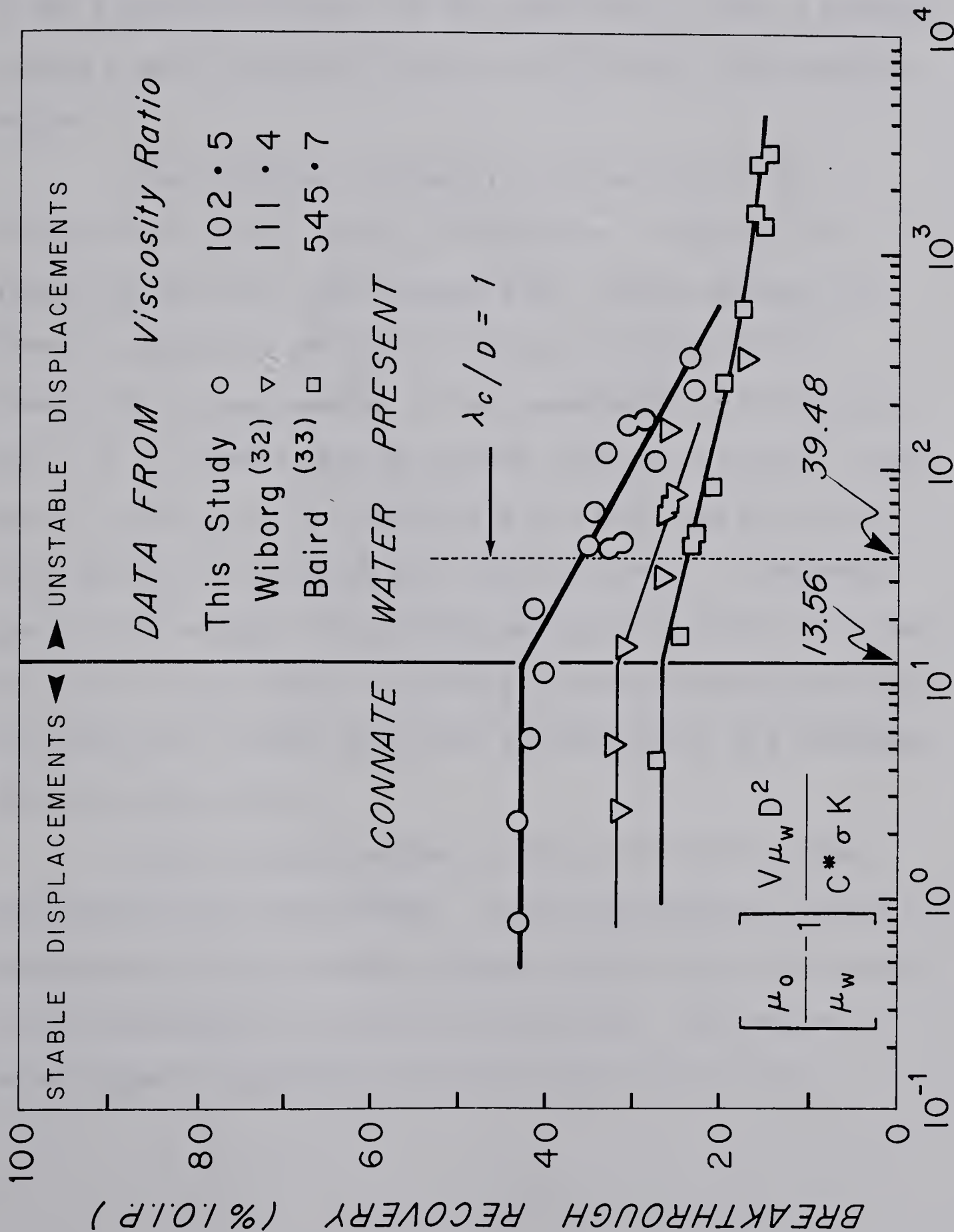
7.2.2 Prediction of the Onset of Instability

Figure 6.11 indicates that the present theory with the experimentally determined values of C^* successfully predicts the onset of instability in both connate water and nonconnate water bearing systems. To further test the theory and the applicability of the present estimates of C^* to other unconsolidated porous media, the experimental results of other investigators were scaled using the present estimates. These results are tabulated in Appendix E.

Figure 7.1 compares the scaled recovery data of Wiborg (32) and Baird (33) with those of the present study in the presence of connate water saturation. All three sets of data show a stabilized recovery behaviour in the stable region, and a declining recovery in the unstable region with a transition to instability occurring in the vicinity of 13.56 as predicted by the present theory. In addition to providing additional verification of the present theory, these observations indicate that C^* was approximately the same in all three studies. This fact is not surprising since the previous studies used Ottawa sand and Dow Corning oils similar to those of the present study.

The different recovery efficiencies in the three studies reflect the effect of mobility or viscosity ratio on the displacement behaviour in both stable and unstable regions. The higher the mobility ratio, the lower the recovery efficiency regardless of the stability of the displacement. Adverse mobility ratio therefore

FIG. 7.1 Prediction Of the Onset Of Instability In The Studies By Wiborg ⁽³²⁾ And Baird ⁽³³⁾



plays a dual role in the displacement process. First, it determines the breakthrough recovery efficiency, and second, it determines, in concert with other variables, the stability of the displacement. It may be observed that the high viscosity ratio of 545.7 employed by Baird (33) was sufficient to reveal a tendency towards a second region of recovery stabilization in the unstable region.

Also indicated on Figure 7.1 is the value of the dimensionless group at which λ_c/D equals one. Kloepper (31), Wiborg (32) and Baird (33) obtained their indirect estimates of Chuoke's constant by arbitrarily guessing the value of this dimensionless group based on a visual examination of the recovery data. It is apparent from the results presented in Figure 7.1 that there is nothing in the recovery data that might aid one in such a guess outside the framework of a stability theory. A successful guess of the correct value of 39.48 would have resulted in the same value of C in each study. The widely different estimates obtained by these authors suggest that their guesses were in fact different from the correct value.

A more reliable indirect estimate of C or C^* may be obtained from the present theory. Rather than seek the value of the dimensionless group at which λ_c/D equals unity, one should seek the value of the group at the onset of instability. This may be accomplished by correlating the recovery data against the

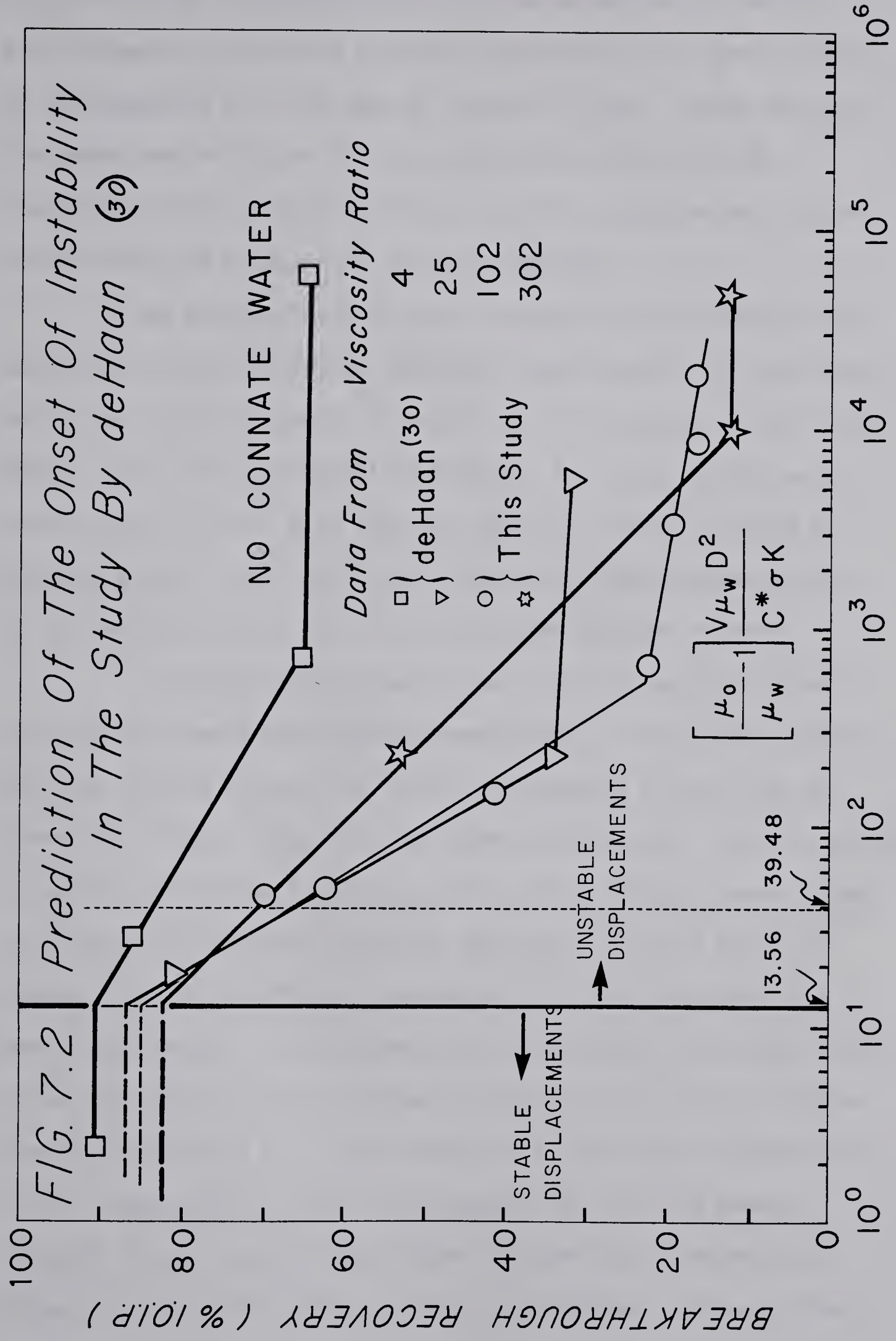
dimensionless group, $(\mu_o/\mu_w - 1)V\mu_w D^2/\sigma K$, on semi-log paper and identifying the point of intersection between the horizontal linear segment of the stable recovery and the inclined linear segment of the unstable recovery. The value of the scaling group at the point of intersection would then be equal to 13.56 times C^* .

Presented in Figure 7.2 is a comparison of the results of the present study with those of de Haan (30). As before, de Haan's results were rescaled using a C^* of 5.45 obtained in this study. Within the limits of the available experimental data, the predicted onset of instability is upheld. The influence of mobility ratio on the breakthrough recovery is again evident, and, in every case, a second region of stabilized recovery was obtained under conditions of extreme fingering.

The fact that the recovery profiles on a semi-log plot for both connate and nonconnate water bearing systems consist of linear segments suggests the possibility of deriving simple empirical formulas for predicting the breakthrough recovery in both stable and unstable region as a function of the scaling group and mobility ratio.

7.2.3 Qualitative Considerations

The technique of using a fluorescent displacing agent to capture viscous fingering proved particularly successful especially in the nonconnate water bearing tests. In these tests, each of the fingers was generally surrounded by a small halo or capillary fringe showing the small extent to which capillary forces succeeded in spreading the injected fluid beyond the main finger. This



observation was in marked contrast to the connate water bearing displacements in which the capillary spreading forces were so strong as to completely blur the edge of the main finger. There may also have been some diffusion of the highly water soluble sodium fluorescein from the injected fluid into the connate water further obliterating the evidence of viscous fingering.

The choice of the maximum dimension of the fingers as the wavelength of the disturbance deserves some comment. In the connate water bearing displacements in which there was only one major finger, one was left with no alternative choice. In the nonconnate water bearing displacements with numerous fingers, it may be argued on physical grounds that the finger dimension is more representative of the wavelength than the distance between adjacent fingers.

If the instability gave rise to closely packed fingers of the same wavelength distributed symmetrically at each cross section, then the spacing between the centres of adjacent fingers and the dimensions of each finger will be approximately equal. In this ideal situation, either the finger separation or the width of each finger will suffice as the characteristic wavelength. But in the real system, fingers of different wavelengths will be superposed in a complicated manner. This superposition may result in missing fingers at certain cross sections as shown in Plate 6.2 in which the three fingers of Frames 9 to 13 later merge into one finger in Frames 15 to 18. When certain fingers are missing, the distance between adjacent fingers may be greater than the wavelength, whereas the finger dimension will still provide a good estimate of the correct wavelength.

It should also be pointed out that the resolution of the disturbance into discrete wavelengths is a mathematical process and not a physical one. Therefore it will be difficult in the real system to recognize which of the measured wavelengths is the most probable at a particular displacement rate. The procedure whereby the average of the measured wavelengths was assumed to be the most probable wavelength, though not strictly correct, provided the most consistent treatment of the experimental data.

7.3 MODEL SCALING

The results of this study indicate that the breakthrough recovery data from a cylindrical model and prototype should be correlated with the radial dimensionless group in the presence of connate water saturation, but with the linear group in the absence of connate water, if the model is to successfully predict the prototype recovery. This difference in scaling requirement is due to the nature of instability and viscous fingering in the two systems.

In the stable regime, the transverse capillary forces are sufficient to prevent viscous fingering in both systems. As a result, the breakthrough recovery will be stabilized and independent of both scaling groups. Under this condition, the model and the prototype recoveries will plot as one curve, when correlated with either of the scaling groups.

Between the onset of instability and the region of a second stabilized recovery, the breakthrough recoveries in either

system are very sensitive to viscous fingering. In the connate water bearing cores, the fingering phenomenon is opposed by strong transverse spreading forces, modelled by the radial scaling group, to such an extent that only one prominent finger was observed in the present study. The model and prototype recoveries will therefore be determined by the radial group, regardless of the length of the cores. In the absence of connate water, the transverse forces in this transition regime is minimal. As a result, the displacement is dominated by several longitudinal fingers with little transverse spreading of the displacing phase. As this flow pattern closely approximates linear flow, the linear scaling group may be expected to be a suitable correlating group for models and prototypes operating in this regime.

In the second stabilized region, the model and prototype recoveries will again be independent of both groups and as a result, they will plot as one curve when correlated with either group.

The observed difference in scaling requirements in the presence and absence of connate water saturation is not without precedent. Using cores of the same diameter and permeability but different lengths, Moore and Slobod (29) found the best correlation of the breakthrough recovery data in strongly water-wet media with connate water when the core length was dropped from the conventional scaling group, and best correlation in oil-wet media when the core lengths were retained. They therefore successfully correlated their water-wet results collected on geometrically dissimilar cores with the dimensionless group, $V\mu_w/\sigma\cos\theta$, and the oil-wet results with

the dimensional group, $V_{\mu_W} L / \sigma \cos \theta$. These correlations are equivalent to using the radial and linear dimensionless groups of the present study.

The need to correlate the recovery data in the early stages of instability with the radial or linear scaling group depending on the presence or absence of connate water saturation is also evident in Figures 6.8 to 6.10. When the model and prototype data were scaled by λ_c / D as suggested by Chuoke et al. (7), the connate water bearing data showed good correlation, whereas the nonconnate water bearing data did not. However, the latter correlation was significantly improved by the introduction of the core length into the correlation as may be seen in Figure 6.9.

The advantage of the proper scaling of experimental results is demonstrated in Figure 6.11 which compares the recovery performance of the connate water and nonconnate water bearing displacements, properly scaled for instability. The data, presented in Figure 6.7, gave a rather confused picture of the relative recovery performance of the two systems. For example, it would appear that the displacements were more efficient in the presence of connate water saturation, over a wide range of the scaling group, $V_{\mu_W} D^2 / \sigma K$. But this scaling group compares in places, stable displacements with connate water with unstable displacements without connate water, a somewhat unfair comparison. Also, one may be tempted to place undue significance on the point of intersection of the two recovery curves in Figure 6.7.

The inadequacies of the correlation presented in Figure 6.7 are corrected by rescaling the data with the new group, $(\mu_o/\mu_w - 1)V\mu_w D^2/C^*\sigma K$, as shown in Figure 6.11. Under this rearrangement, both systems are compared in the stable and unstable regimes. With this scaling, a different picture of the relative performance of the two systems emerges. The nonconnate water bearing systems appear to be more efficient in both regimes. Furthermore, the previous intersection of the two curves which had no real significance is eliminated and the fact that both systems would tend to be equivalent under conditions of extreme fingering is emphasized.

7.4 CONNATE VERSUS NONCONNATE WATER BEARING SYSTEMS

Evident throughout this study has been a fundamental difference in the displacement behaviour of systems with and without connate water saturation. This difference has manifested itself in the ease with which instability occurs in one system as compared to the other, in the spectacular nature of the fingering in one system as compared to the other, and in the scaling requirements for the breakthrough recovery data collected on the two systems. One naturally wonders as to the cause of this difference in behaviour.

The cause seems to be in the level of capillary phenomena in the two system which is indicated by the values of C^* for each system. In the present study, C^* in the presence of connate water saturation was found to be over fifty times that in the absence of connate water saturation, for the same fluids and porous media.

In physical terms, C^* may be regarded as a wettability index. In strongly water-wet porous media with connate water

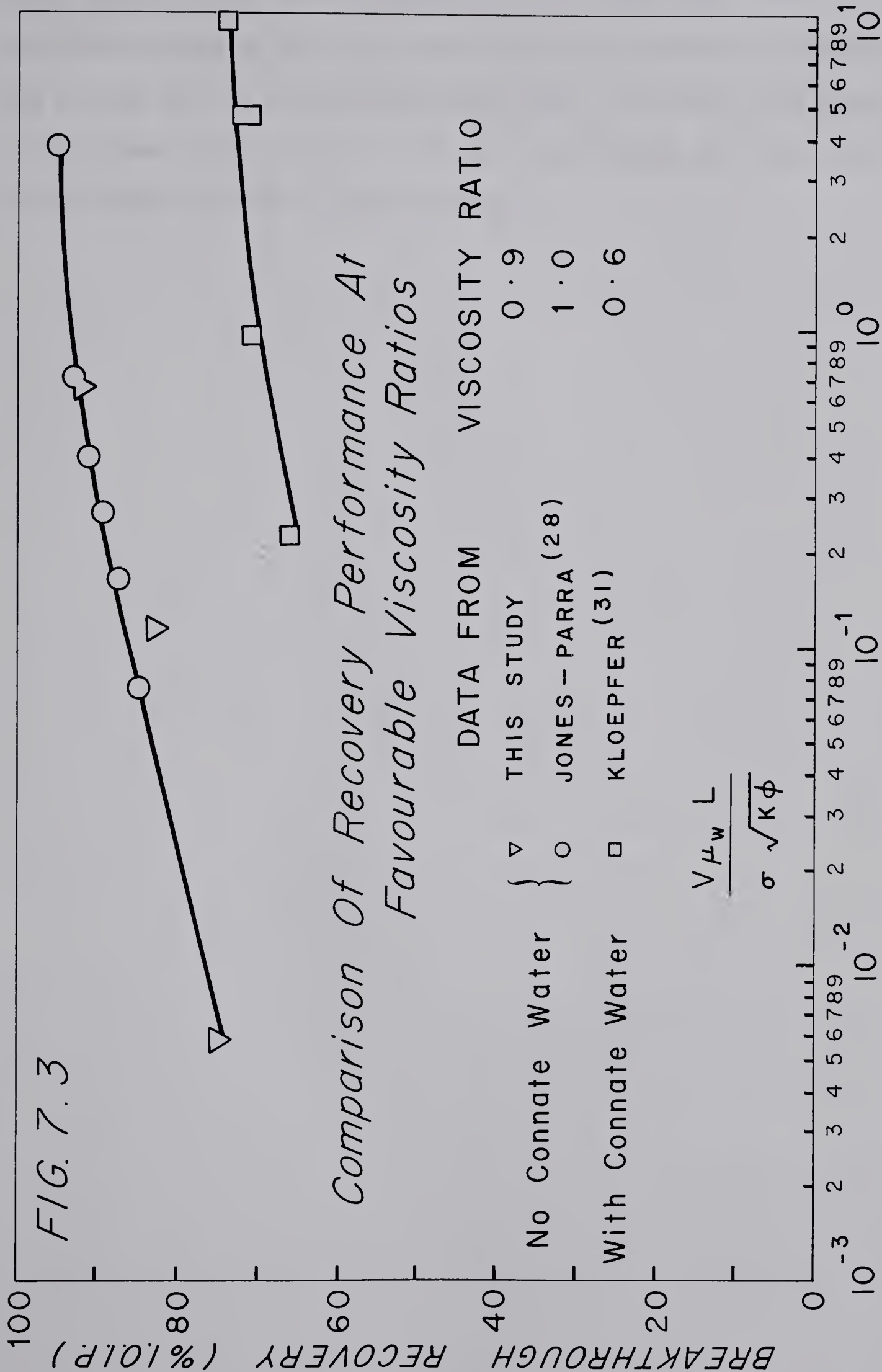
saturation, C^* will be high, whereas for oil-wet media, or in media without connate water saturation, it will be low. Between these extremes, will be C^* values representing intermediate or mixed wettability conditions. In strongly water-wet media therefore, the increased capillary phenomena consists of strong capillary imbibition which spreads the injected fluid in the transverse direction to prevent or delay the onset of instability. In oil-wet media, or in porous media without connate water saturation, there is little or no imbibition except at very low displacement rates. The absence of the beneficial influence of imbibition accounts for the ease with which instability can be induced in these systems.

7.5 OTHER RESULTS

Figure 7.3 compares the recovery behaviour of the present study with data from the literature at favourable viscosity ratios. As expected, there is no instability in either system. Instead, the recovery trends closely approximate those obtained by the numerical solution of the immiscible displacement equation presented in Figure 2.6.

It will be recalled that σ^* was employed in the definition of a universal capillary pressure curve in the form of a modified Leverett J-function. The estimate of σ^* by measurements on viscous fingers such as obtained in this study may therefore aid in the search for a universal capillary pressure function.

Finally, by requiring that the radial group, $V_{\mu_w} D^2 / \sigma^* L \sqrt{K\phi}$, obtained by an inspectional analysis, equals the group, $V_{\mu_w} D^2 / \sigma^* K$, obtained by a stability analysis, it can be shown that the length



which appears in the former group is of pore dimensions. This observation seems to be in agreement with that of Moore and Slobod (29) who claimed that in strongly water-wet media, the length that appears in the linear scaling group is not the system length but rather the grain or pore size of the porous medium.

CHAPTER 8

CONCLUSIONS AND RECOMMENDATIONS

8.1 SUMMARY AND CONCLUSIONS

A stability analysis was undertaken to predict the onset of instability that might lead to viscous fingering during immiscible displacement in porous media. The study revealed the existence of two distinct displacement systems depending on the presence or absence of connate water saturation. The analysis resulted in the theoretical predictions of the onset of instability in both systems for commonly encountered displacement geometries, which were verified by the available experimental data. A successful experiment was devised and implemented that gave further insight into the phenomenon of viscous fingering in the two systems. New dimensionless scaling groups were derived for presenting the water breakthrough recovery data to give them the widest possible application, and for differentiating stable from unstable displacements.

The theoretical and experimental results of this study have led to the following conclusions:

1. Instability resulting in viscous fingering during immiscible displacement in porous media occurs both in the presence and absence of connate water saturation.
2. The onset of instability occurs at a lower displacement rate in the absence of connate water saturation than in the presence of connate water saturation for the same fluids and porous media.

3. In both systems, instability results in an initial rapid decrease in breakthrough recovery, with a tendency towards an eventual recovery stabilization at a lower level than in the stable regime.
4. A stability theory based on the one-dimensional Buckley-Leverett displacement model will fail to reveal instability due to the loss, by assumption, of the transverse scaling group which determines the onset of instability.
5. A stability theory based on a piston-like model of the displacement suffices to predict the onset of instability even in the Buckley-Leverett type displacements.
6. The necessary and sufficient condition for the onset of instability in a cylindrical system is

$$\frac{(M - 1)(V - V_c)\mu_w D^2}{C^* \sigma K_{wr}} > 13.56$$

7. The necessary and sufficient condition for the onset of instability in a rectangular system is

$$\frac{(M - 1)(V - V_c)\mu_w L_x^2 L_y^2}{C^* \sigma K_{wr} (L_x^2 + L_y^2)} > 9.87$$

8. The constant C^* is 5.45 in the absence of connate water saturation and 306.25 in the presence of connate water saturation for an unconsolidated pack of Ottawa sand in which distilled water displaces Dow Corning oil. The corresponding Chuoke's constants are 25.40 and 190.45, respectively.

9. Laboratory breakthrough recovery data should be correlated with the dimensionless group, $(M - 1)(V - V_c)\mu_w D^2 / C^* \sigma K_{wr}$ for cylindrical systems, and $(M - 1)(V - V_c)\mu_w L_x^2 L_y^2 / C^* \sigma K_{wr} (L_x^2 + L_y^2)$ for rectangular systems in order to differentiate stable from unstable displacements.
10. Unstable breakthrough recovery data should be correlated with the radial group, $V\mu_w D / \sigma \sqrt{K\phi}$, in the presence of connate water saturation, and with the linear group, $V\mu_w L / \sigma \sqrt{K\phi}$, in the absence of connate water saturation to permit a meaningful comparison of data collected on geometrically dissimilar cores.

8.2 PRACTICAL APPLICATION OF THE RESULTS

The results of this study should be of interest to those involved in any aspect of immiscible displacement in porous media. The practicing engineer can use the simple equations derived in this study to determine the stability of his waterflood, for these equations apply to laboratory systems as well as to petroleum reservoirs of the same geometry.

The numerical simulation expert can use the results to determine the range of flood properties for which his numerical prediction technique should be modified to incorporate the influence of instability during immiscible displacement. This modification is necessary if the numerical model is to closely simulate the behaviour of an unstable displacement.

The laboratory technician will find the results of this study valuable in planning his relative permeability experiments. Because the procedure for computing relative permeabilities from

displacement data assumes stable displacements, the best results may be expected if the relative permeability tests are conducted in the stable region. However, because the technician often uses high displacement rates to minimize capillary end effects and adverse mobility ratios to obtain production histories suitable for relative permeability determinations, he runs the risk of instability. The stability boundaries derived in this study provide him with a practical guide for choosing the various displacement parameters to obtain stable displacements.

8.3 SUGGESTIONS FOR FURTHER STUDIES

The following studies should be undertaken to extend and complement the present one.

1. Extensive estimates of C^* should be undertaken for both unconsolidated and consolidated porous media in the presence and absence of connate water saturation. In making these estimates, direct measurements on viscous fingers are recommended over indirect estimates based on the breakthrough recovery data.
2. The extensive estimates of C^* should permit a more systematic verification of the theoretical onset of instability derived in this study for both cylindrical and rectangular systems. In conducting such a systematic study, attempts should be made to vary each of the pertinent variables in turn. The experiments should therefore be arranged to vary μ_o/μ_w , V , D , L_x , L_y , σ and K .
3. The connection between C^* and hence σ^* with a universal capillary pressure function should be further investigated.

4. Large field dimensions and low permeabilities may combine to ensure that field displacements are always unstable over most practical rates. Although the Buckley-Leverett equations cannot strictly be used to model unstable displacements, the second stabilized breakthrough recovery under conditions of extreme instability, may be simulated by the Buckley-Leverett equations if unstable relative permeability curves are available. It would therefore be of practical interest to investigate the possibility of obtaining relative permeability curves under conditions of extreme instability.
5. A stability theory based entirely on the Buckley-Leverett model is still outstanding. Although no new information is likely to be revealed by such a theory, its proper reconciliation with that based on the piston-like displacement model is still worthwhile. It should be attempted.

REFERENCES

1. Engelberts, W.F. and Klinkenberg, L.J.: "Laboratory Experiments on the Displacement of Oil by Water from Packs of Granular Materials", Proc. Third World Petroleum Congress, Sec.II, (1951), 544-554.
2. Betchov, R. and Criminale, W.O., Jr.: Stability of Parallel Flows. Academic Press, New York, 1967.
3. Chandrasekhar, S.: Hydrodynamic and Hydromagnetic Stability. Oxford Univ. Press, London, 1961.
4. Leipholz, H.: Stability Theory. Academic Press, 1970.
5. Lin, C.C.: The Theory of Hydrodynamic Stability. Cambridge University Press, 1955.
6. Eckhaus, W.: Studies in Non-Linear Stability Theory. Springer Tracts in Natural Philosophy, Vol.6, Springer-Verlag, 1965.
7. Chuoke, R.L., van Meurs, P. and van der Poel, C.: "The Instability of Slow, Immiscible, Viscous Liquid-Liquid Displacements in Permeable Media", Trans., AIME (1959) 216, 188-194.
8. Saffman, P.G. and Taylor, G.I.: "The Penetration of a Fluid Into a Porous Medium or Hele-Shaw Cell Containing a More Viscous Liquid", Proc. Roy. Soc., (1958) A245, 312-329.
9. Scheidegger, A.E.: "On the Stability of Displacement Fronts in Porous Media: A Discussion of the Muskat-Aronofsky Model", Can. Jour. of Physics (1960) 38, 153-162.
10. Outmans, H.D.: "Nonlinear Theory for Frontal Stability and Viscous Fingering in Porous Media", Soc. Pet. Eng. Jour. (June, 1962), 165-176.
11. Buckley, S.E. and Leverett, M.C.: "Mechanism of Fluid Displacement in Sands", Trans., AIME (1942) 146, 107-116.
12. Rachford, H.H., Jr.: "Instability in Water Flooding Oil from Water-Wet Porous Media Containing Connate Water", Trans., AIME (1964) 231, 133-148.
13. Hagoort, J.: "Displacement Stability of Water Drives in Water-Wet Connate-Water-Bearing Reservoirs", Soc. Pet. Eng. Jour. (Feb., 1974), 63-74.
14. Leverett, M.C.: "Capillary Behaviour in Porous Solids", Trans., AIME (1941) 142, 152-168.

15. Fayers, F.J. and Sheldon, J.W.: "The Effect of Capillary Pressure and Gravity on Two-Phase Fluid Flow in a Porous Medium", Trans., AIME (1959) 216, 147-155.
16. Bentsen, R.G.: "Scaled Fluid-Flow Models with Permeabilities Differing from that of the Prototype", Jour. of Can. Pet. Tech. (July-Sept., 1976) 15, 46-52.
17. Bentsen, R.G.: "Conditions Under Which the Capillary Term May Be Neglected", Jour. of Can. Pet. Tech. (Oct.-Dec., 1978) 17, 25-30.
18. Welge, H.J.: "A Simplified Method for Computing Oil Recoveries by Gas or Water Drive", Trans., AIME (1952) 195, 91-98.
19. Leverett, M.C., Lewis, W.B. and True, M.E.: "Dimensional-Model Studies of Oil-Field Behaviour", Trans., AIME (1942) 146, 175-193.
20. Rapoport, L.A.: "Scaling Laws for Use in Design and Operation of Water-Oil Flow Model", Trans., AIME (1955) 204, 143-150.
21. Croes, G.A. and Schwarz, N.: "Dimensionally Scaled Experiments and the Theories on the Water-Drive Process", Trans., AIME (1955) 204, 35-42.
22. Geertsma, J., Croes, G.A. and Schwarz, N.: "Theory of Dimensionally Scaled Models of Petroleum Reservoirs", Trans., AIME (1956) 207, 118-127.
23. Carpenter, C.W., Jr., Bail, P.T. and Bobek, J.E.: "A Verification of Waterflood Scaling in Heterogeneous Communicating Flow Models", Soc. Pet. Eng. Jour. (March, 1962), 9-12.
24. Perkins, F.M. and Collins, R.E.: "Scaling Laws for Laboratory Flow Models of Oil Reservoirs", Trans., AIME (1960) 219, 383-385,
25. Nielsen, R.L. and Tek, M.R.: "Evaluation of Scale-Up Laws for Two-Phase Flow Through Porous Media", Soc. Pet. Eng. Jour. (June, 1963), 164-176.
26. Greenkorn, R.A.: "Flow Models and Scaling Laws - Flow Through Porous Media", Ind. Eng. Chem. (1964) 56, 32-27.
27. Loomis, A.G. and Crowell, D.C.: "Theory and Application of Dimensional and Inspectional Analysis to Model Study Displacements in Petroleum Reservoirs", U.S. Bureau of Mines, Report of Investigations 6546, 1964.

28. Jones-Parra, J., Stahl, C.D. and Calhoun, J.C.: "A Theoretical and Experimental Study of Constant Rate Displacements in Water Wet Systems", Producers Monthly (Jan., 1954), 18-26.
29. Moore, T.F. and Slobod, R.L.: "The Effect of Viscosity and Capillarity on the Displacement of Oil by Water", Producers Monthly (Aug., 1956), 20-30.
30. de Haan, H.J.: "Effect of Capillary Forces in the Water-Drive Process", Proc. Fifth World Petroleum Congress (1959), Sec.II, Paper 25, 1-13.
31. Kloepper, J.G.: "Viscous Fingering in Unconsolidated Cores", M.Sc. Thesis, University of Alberta, 1975.
32. Wiborg, R.: "Frontal Instabilities When Waterflooding at Unfavourable Viscosity Ratios", M.Sc. Thesis, University of Alberta, 1976.
33. Baird, H.J.: "Waterflood Behaviour of Viscous Oils", M.Sc. Thesis, University of Alberta, 1978.
34. van Meurs, P.: "The Use of a Transparent Three Dimensional Model for Studying the Mechanism of Flow Processes in Oil Reservoirs", Trans., AIME (1957) 210, 295-301.
35. van Meurs, P. and van der Poel, C.: "A Theoretical Description of Water-Drive Processes Involving Viscous Fingering", Trans., AIME (1958) 213, 103-112.
36. Perkins, T.K. and Johnston, O.C.: "A Study of Immiscible Fingering in Linear Models", Soc. Pet. Eng. Jour (March, 1969), 39-45.
37. Morse, P.M. and Feshbach, H.: Methods of Theoretical Physics. McGraw-Hill, 1953.
38. Spiegel, M.R.: Mathematical Handbook. Schaum's Outline Series, McGraw-Hill Book Co., 1968.

BIBLIOGRAPHY

1. Abrams, A.: "The Influence of Fluid Viscosity, Interfacial Tension, and Flow Velocity on Residual Oil Saturation Left by Waterflood", Soc. Pet. Eng. Jour. (Oct., 1975), 437-447.
2. Baker, W.E., Westine, P.S. and Dodge, F.T.: Similarity Methods in Engineering Dynamics, Theory and Practice of Scale Modelling. Hayden Book Co., Inc., 1973.
3. Bear, J.: "Two-Liquid Flows in Porous Media", Advances in Hydrosience, Edited by V.T. Chow, Academic Press (1970) 6, 141-252.
4. Bear, J.: Dynamics of Fluids in Porous Media. American Elsevier Publishing Co., Inc., 1972.
5. Bellman, R. and Pennington, R.H.: "Effects of Surface Tension and Viscosity on Taylor Instability", Quart. Appl. Math. (1954) 12, 151-162.
6. Benham, A.L. and Olsen, R.W.: "A Model Study of Viscous Fingering", Soc. Pet. Eng. Jour. (June, 1963), 138-144.
7. Benner, F.C., Riches, W.W. and Bartell, F.E.: "Nature and Importance of Surface Forces in Production of Petroleum", API Drill. and Prod. Practice (1938), 442-446.
8. Blackwell, R.J., Rayne, J.R. and Terry, W.M.: "Factors Influencing the Efficiency of Miscible Displacement", Trans., AIME (1959) 216, 1-8.
9. Cardwell, W.T., Jr.: "The Meaning of the Triple Value in Noncapillary Buckley-Leverett Theory", Trans., AIME (1959) 216, 271-296.
10. Cellia Chung Chow and Scheidgger, A.E.: "Stability Conditions for Fingering Processes in Porous Media", Journal of Hydrology (1972) 15, 1-21.
11. Cheng Sin-I: "A Critical Review of Numerical Solution of Navier-Stokes Equations", Lecture Notes in Physics, Vol. 41, 78-225.
12. Chang, C.T.: "Dynamic Instability of Accelerated Fluids", Physics of Fluids (1959) 2, 656-663.
13. Chatenever, A. and Calhoun, J.C.: "Visual Examinations of Fluid Behaviour in Porous Media", Trans., AIME (1952) 195, 149-156.

14. Collins, R.E.: Flow of Fluids Through Porous Media. Reinhold Publishing Co., New York, 1961.
15. Corey, A.T.: Mechanics of Heterogeneous Fluids in Porous Media. Water Resources Publications, 1977.
16. Dietz, D.N.: "A Theoretical Approach to the Problem of Encroaching and Bypassing Edge Water", Proc., Koninkl. Ned. Akad. Wetenschap (1953)B56, 83-93.
17. Douglas, J., Blair, P.M. and Wagner, R.J.: "Calculation of Linear Waterflood Behaviour Including the Effects of Capillary Pressure", Trans., AIME (1958) 213, 96-102.
18. Douglas, J., Jr., Peaceman, D.W. and Rachford, H.H.: "A Method for Calculating Multi-Dimensional Immiscible Displacement", Trans., AIME (1959) 216, 297-308.
19. Dumoré, J.M.: "Stability Considerations in Downward Miscible Displacements", Soc. Pet. Eng. Jour. (Dec., 1964) 356-362.
20. Farouq Ali, S.M., Donohue, D.A.T. and Stahl, C.D.: "Fluid Flow in Porous Media - Problems in Relating Experiments to Field Projects", Proc. Seventh World Petroleum Congress (1967) 3, 159-168.
21. Flock, D.L., Peters, E.J., Baird, H., Wiborg, R. and Kloepper, J.: "The Influence of Frontal Instabilities During Viscous Oil Displacement", The Oil Sands of Canada - Venezuela (1977) CIM Special Vol.17, 380-385.
22. Gupta, S.P. and Greenkorn, R.A.: "An Experimental Study of Immiscible Displacement With an Unfavorable Mobility Ratio in Porous Media", Water Resources Research (April, 1974) 10, 371-374.
23. Hassler, G.L., Brunner, E. and Deahl, T.J.: "The Role of Capillarity in Oil Production", Trans., AIME (1944) 155, 155-174.
24. Hawthorne, R.G.: "Two-Phase Flow in Two-Dimensional Systems - Effects of Rate, Viscosity and Density on Fluid Displacement in Porous Media", Trans., AIME (1960) 219, 81-87.
25. Hiatt, W.N.: "Mathematical Basis of Two-Phase, Incompressible, Vertical Flow Through Porous Media and its Implications in the Study of Gravity-Drainage-Type Petroleum Reservoirs", Soc. Pet. Eng. Jour. (Sept., 1968), 225-230.
26. Hovanessian, S.A. and Fayers, F.J.: "Linear Water Flood with Gravity and Capillary Effects", Soc. Pet. Eng. Jour. (March, 1961), 32-36.

27. Ipsen, D.C.: Units, Dimensions and Dimensionless Numbers. McGraw-Hill Book Co., New York, 1960.
28. Joseph, D.D.: Stability of Fluid Motions I. Springer Tracts in Natural Philosophy, Vol.27, Springer-Verlag, 1976.
29. Joseph, D.D.: Stability of Fluid Motions II. Springer Tracts in Natural Philosophy, Vol.28, Springer-Verlag, 1976.
30. Kyte, J.R. and Rapoport, R.L.: "Linear Water Flood Behaviour and End Effects in Water-Wet Porous Media", Trans., AIME (1958) 213, 423-426.
31. Lamb, H.: Hydrodynamics. Dover Publications, New York, 1945.
32. Langhaar, H.L.: Dimensional Analysis and Theory of Models. John Wiley & Sons, Inc., New York, 1951.
33. Leach, R.O., Geffen, T.M. and Berry, V.J.: "Further Discussion of Wettability Versus Displacement in Water Flooding in Unconsolidated Sand Columns", Trans., AIME (1956) 207, 288-290.
34. Levich, V.G. and Krylov, V.S.: "Surface-Tension-Driven Phenomena", Annual Review Fluid Mech. (1969) 1, 293-316.
35. Lewis, D.J.: "The Instability of Liquid Surfaces when Accelerated in a Direction Perpendicular to their Planes II", Proc. Roy. Soc. (1950) A202, 81-96.
36. McEwen, C.R.: "A Numerical Solution of the Linear Displacement Equation with Capillary Pressure", Trans., AIME (1959) 216, 412-415.
37. Miller, F.G.: "A Laboratory Study of Water Encroachment in Oil-Filled Sand Columns", U.S. Bureau of Mines, Report of Investigation 2595, 1941.
38. Miller, R.D. and Miller, R.E.: "Physical Theory for Capillary Flow Phenomena", Jour. of Applied Physics (1956) 27, 324-332.
39. Morel-Seytoux, H.J.: "Introduction to Flow of Immiscible Liquids in Porous Media", Flow Through Porous Media, Ed. R.J.M. De Wiest, Academic Press, 1969.
40. Newcombe, J., McGhee, J. and Rzasa, M.J.: "Wettability Versus Displacement in Water Flooding in Unconsolidated Sand Columns", Trans., AIME (1955) 204, 227-232.
41. Outmans, H.D.: "Transient Interfaces During Immiscible Liquid-Liquid Displacement in Porous Media", Soc. Pet. Eng. Jour. (June, 1962), 156-164.

42. Outmans, H.D.: "On Unique Solutions for Steady-State Fingering in a Porous Medium", Jour. of Geophysical Res. (1963) 68, 5735-5737.
43. Perkins, F.M.: "An Investigation of the Role of Capillary Forces in Laboratory Water Floods", Trans., AIME (1957) 210, 409-411.
44. Perkins, T.K., Johnston, O.C. and Hoffman, R.N.: "Mechanics of Viscous Fingering in Miscible Systems", Trans., AIME (1965) 234, 301-317.
45. Perrine, R.L.: "The Development of Stability Theory for Miscible Liquid-Liquid Displacement", Trans., AIME (1961) 222, 17-25.
46. Perrine, R.L.: "Stability Theory and Its Use to Optimize Solvent Recovery of Oil", Trans., AIME (1961) 222, 9-16.
47. Perrine, R.L.: "A Unified Theory for Stable and Unstable Miscible Displacement", Soc. Pet. Eng. Jour. (Sept., 1963), 205-213.
48. Perrine, R.L. and Gay, G.M.: "Unstable Miscible Flow in Heterogeneous Systems", Soc. Pet. Eng. Jour. (Sept., 1966), 228-238.
49. Rapoport, L.A. and Leas, W.J.: "Properties of Linear Waterfloods", Trans., AIME (1953) 198, 139-148.
50. Richardson, J.G.: "Flow Through Porous Media", Handbook of Fluid Dynamics, Edited by V.L. Streeter, Section 16, McGraw-Hill, New York (1961), 16.1-16.112.
51. Rose, W.D.: "Some Problems Connected with the Use of Classical Description of Fluid/Fluid Displacement Processes", Fundamentals of Transport Phenomena in Porous Media, Elsevier Pub. Co. (1972), 229-240.
52. Scheidegger, A.E.: "Growth of Instabilities on Displacement Fronts in Porous Media", Physics of Fluids, (1960) 3, 94-104.
53. Scheidegger, A.E.: "General Spectral Theory for the Onset of Instabilities in Displacement Processes in Porous Media", Geofis. Pura. Appl. (1960) 47, 41-54.
54. Scheidegger, A.E. and Johnson, E.F.: "Statistical Behaviour of Instabilities in Displacement Processes in Porous Media", Can. Jour. of Physics (1961) 39, 326-334.

55. Scheidegger, A.E.: "Stability Conditions for Displacement Processes in Porous Media", Can. Jour. of Physics (1969) 47, 209-214.
56. Seve, B.J. and Pottier, J.: "French Engineers Review Soviet Modelling Practices", Jour. Pet. Tech. (June, 1963) 15, 581-588.
57. Stone, H.L. and Gardner, A.O., Jr.: "Analysis of Gas-Cap or Dissolved-Gas Reservoirs", Trans., AIME (1961) 22, 92-104.
58. Taylor, G.I.: "The Instability of Liquid Surfaces when Accelerated in a Direction Perpendicular to their Planes I", Proc. Roy. Soc. (1950) A201, 192-196.
59. Terwilliger, P.L., Wilsey, L.E., Hall, H.N., Bridges, P.M. and Morse, R.A.: "Experimental and Theoretical Investigation of Gravity Drainage Performance", Trans., AIME (1951) 192, 285-296.
60. Verma, A.P.: "Statistical Behaviour of Fingering in a Displacement Process in a Heterogeneous Porous Medium with Capillary Pressure", Can. Jour. of Physics (1969) 47, 319-324.
61. Verma, A.P.: "On Stabilization of Fingers in a Slightly Cracked Heterogeneous Porous Medium", Fundamentals of Transport Phenomena in Porous Media, Elsevier Pub. Co. (1972), 221-228.
62. Vossoughi, S.: "Viscous Fingering In Immiscible Displacement", Ph.D. Thesis, University of Alberta, 1976.
63. Wooding, R.A.: "The Stability of Viscous Liquid in a Vertical Tube Containing Porous Material", Proc. Roy. Soc. (1959) A252, 120-134.
64. Wooding, R.A.: "Instability of a Viscous Liquid of Variable Density in a Vertical Hele-Shaw Cell", Jour. of Fluid Mech. (1960) 7, 501-515.
65. Wooding, R.A.: "Growth of Fingers at an Unstable Interface in a Porous Medium or Hele-Shaw Cell", Jour. of Fluid Mech. (1969) 39, 477-495.
66. Wygal, R.J.: "Construction of Models that Simulate Oil Reservoirs", Trans., AIME (1963) 228, 281-286.
67. Yih, Chia-Shun: Dynamics of Nonhomogeneous Fluids. The Macmillan Co., New York, 1965.

APPENDIX A

NUMERICAL SOLUTION OF IMMISCIBLE DISPLACEMENT EQUATIONS


```

1      SUBROUTINE BMAT(N,TN,TW,PN,PW,F,A,B,C,X)
2      DIMENSION TN(1),TW(1),PN(1),PW(1),A(N,4),B(N,4),C(N,4),
3      *X(N,2),F(1)
4      C
5      C      CALCULATES THE ELEMENTS OF THE BLOCK TRIDIAGONAL MATRICES FOR
6      C      SIMULTANEOUS SOLUTION.
7      C
8      C      N - NUMBER OF GRID BLOCKS. NUMBER OF UNKNOWN IS N*2
9      C      TN - OIL TRANSMISSIBILITY VECTOR
10     C      TW - WATER TRANSMISSIBILITY VECTOR
11     C      PN - OIL PHASE PRESSURE VECTOR
12     C      PW - WATER PHASE PRESSURE VECTOR
13     C      A - MAIN DIAGONAL
14     C      B - LOWER DIAGONAL
15     C      C - UPPER DIAGONAL
16     C      X - R.H.S OF MATRIX EQUATION WITHOUT SOURCE TERMS
17     C      F - CAPILLARY COUPLING VECTOR
18     C
19     C      ALL VECTORS AND MATRICES HAVE BLOCK STRUCTURE WITH 2 BY 2
20     C      BLOCKS. THE ORDERING OF ELEMENTS IN BLOCKS IS
21     C
22     C           1      2      1
23     C           3      4      2
24     C           AND
25     C
26     NN=N-1
27     DO 1 I=2,NN
28     B(I,1)=TN(I-1)
29     B(I,2)=0.
30     B(I,3)=0.
31     B(I,4)=TW(I-1)
32     A(I,1)=F(I)-TN(I-1)-TN(I)
33     A(I,2)=-F(I)
34     A(I,3)=-F(I)
35     A(I,4)=F(I)-TW(I-1)-TW(I)
36     C(I,1)=TN(I)
37     C(I,2)=0.
38     C(I,3)=0.
39     C(I,4)=TW(I)
40     X(I,1)=-TN(I-1)*(PN(I-1)-PN(I))+TN(I)*(PN(I)-PN(I+1))
41     X(I,2)=-TW(I-1)*(PW(I-1)-PW(I))+TW(I)*(PW(I)-PW(I+1))
42     1  CONTINUE
43     A(1,1)=F(1)-TN(1)
44     A(1,2)=-F(1)
45     A(1,3)=-F(1)
46     A(1,4)=F(1)-TW(1)
47     C(1,1)=TN(1)
48     C(1,2)=0.
49     C(1,3)=0.
50     C(1,4)=TW(1)

```



```

51      B(N,1)=TN(N-1)
52      B(N,2)=0.
53      B(N,3)=0.
54      B(N,4)=TW(N-1)
55      A(N,1)=F(N)-TN(N-1)
56      A(N,2)=-F(N)
57      A(N,3)=-F(N)
58      A(N,4)=F(N)-TW(N-1)
59      X(1,1)=TN(1)*(FN(1)-PN(2))
60      X(1,2)=TW(1)*(PW(1)-PW(2))
61      X(N,1)=-TN(N-1)*(FN(N-1)-PN(N))
62      X(N,2)=-TW(N-1)*(PW(N-1)-PW(N))
63      RETURN
64      END
65      SUBROUTINE SOLVE(N,A,B,C,D,X)
66      DIMENSION A(N,4),B(N,4),C(N,4),D(N,2),X(N,2)
67      DIMENSION XAMDA(101,4),GAMMA(101,4)
68      C
69      C      SOLUTION OF BI-TRIDIAGONAL SYSTEM OF EQUATIONS
70      C
71      C      A - MAIN DIAGONAL
72      C      B - UPPER DIAGONAL
73      C      C - LOWER DIAGONAL
74      C      D - R.H.S. VECTOR
75      C      X - SOLUTION VECTOR
76      C      N - NUMBER OF GRID BLOCKS. NUMBER OF UNKNOWN IS N*2
77      C
78      C      ALL VECTORS AND MATRICES HAVE BLOCK STRUCTURE WITH 2 BY 2
79      C      BLOCKS. THE ORDERING OF ELEMENTS IN BLOCKS IS
80      C
81      C           1      2      1
82      C           3      4      AND
83      C           3      4      2
84      C
85      DO 10 I=1,N
86      BETA1=A(I,1)
87      BETA2=A(I,2)
88      BETA3=A(I,3)
89      BETA4=A(I,4)
90      IF(I.EQ.1)GOTO 20
91      BETA1=BETA1-C(I,1)*XAMDA(I-1,1)-C(I,2)*XAMDA(I-1,3)
92      BETA2=BETA2-C(I,1)*XAMDA(I-1,2)-C(I,2)*XAMDA(I-1,4)
93      BETA3=BETA3-C(I,3)*XAMDA(I-1,1)-C(I,4)*XAMDA(I-1,3)
94      BETA4=BETA4-C(I,3)*XAMDA(I-1,2)-C(I,4)*XAMDA(I-1,4)
95      20 XMI=BETA1*BETA4-BETA2*BETA3
96      XMIR=1./XMI
97      DELTA1=D(I,1)
98      DELTA2=D(I,2)
99      IF(I.EQ.1)GOTO 30
100     DELTA1=DELTA1-C(I,1)*GAMMA(I-1,1)-C(I,2)*GAMMA(I-1,2)

```



```

101      DELTA2=DELTA2-C(I,3)*GAMMA(I-1,1)-C(I,4)*GAMMA(I-1,2)
102      30      GAMMA(I,1)=(BETA4*DELTA1-BETA2*DELTA2)*XMIR
103      GAMMA(I,2)=(BETA1*DELTA2-BETA3*DELTA1)*XMIR
104      IF(I.EQ.N)GOTO 10
105      XAMDA(I,1)=(BETA4*B(I,1)-BETA2*B(I,3))*XMIR
106      XAMDA(I,2)=(BETA4*B(I,2)-BETA2*B(I,4))*XMIR
107      XAMDA(I,3)=(BETA1*B(I,3)-BETA3*B(I,1))*XMIR
108      XAMDA(I,4)=(BETA1*B(I,4)-BETA3*B(I,2))*XMIR
109      10      CONTINUE
110      X(N,1)=GAMMA(N,1)
111      X(N,2)=GAMMA(N,2)
112      NP1=N+1
113      DO 50 K=2,N
114      I=NP1-K
115      X(I,1)=GAMMA(I,1)-XAMDA(I,1)*X(I+1,1)-XAMDA(I,2)*X(I+1,2)
116      X(I,2)=GAMMA(I,2)-XAMDA(I,3)*X(I+1,1)-XAMDA(I,4)*X(I+1,2)
117      50      CONTINUE
118      RETURN
119      END
120      SUBROUTINE TRANS(N,M,RKN,RKW,A,DX,VN,VW,SWR,SNR,SW,TW,TN)
121      DIMENSION SW(1),TW(1),TN(1)
122      C
123      C      CALCULATES WATER AND OIL TRANSMISSIBILITIES
124      C
125      C      N - NUMBER OF GRID BLOCKS
126      C      M - EXPONENT OF RELATIVE PERMEABILITY MODEL
127      C      RKN - PERMEABILITY TO OIL AT INITIAL WATER SATURATION
128      C      RKW - PERMEABILITY TO WATER AT RESIDUAL OIL SATURATION
129      C      A - CROSS SECTIONAL AREA OF CORE
130      C      DX - LENGTH OF GRID BLOCK
131      C      VN - OIL VISCOSITY
132      C      VW - WATER VISCOSITY
133      C      SWR - INITIAL WATER SATURATION
134      C      SNR - RESIDUAL OIL SATURATION
135      C      SW - WATER SATURATION VECTOR
136      C      TW - WATER TRANSMISSIBILITY VECTOR
137      C      TN - OIL TRANSMISSIBILITY VECTOR
138      C
139      DO 1 I=1,N
140      S=(SW(I)-SWR)/(1.-SWR-SNR)
141      S=S**M
142      TW(I)=(A*RKW*S)/(DX*VW)
143      S=1.-S
144      TN(I)=(A*RKN*S)/(DX*VN)
145      1      CONTINUE
146      RETURN
147      END
148      SUBROUTINE CAPL(N,SWR,PCR,BPV,DT,Y)
149      DIMENSION Y(1)
150      C

```



```

151      C      CALCULATES THE CAPILLARY COUPLING VECTOR.
152      C      THIS EXAMPLE ASSUMES A LINEAR CAPILLARY VERSUS SATURATION
153      C      RELATIONSHIP. IF SOME OTHER CAPILLARY MODEL IS ASSUMED, THEN
154      C      THIS SUBROUTINE MUST BE MODIFIED ACCORDINGLY.
155      C
156      C      N - NUMBER OF GRID BLOCKS
157      C      SWR - INITIAL WATER SATURATION
158      C      PCR - CAPILLARY PRESSURE AT INITIAL WATER SATURATION
159      C      BPV - GRID PORE VOLUME
160      C      Y - CAPILLARY COUPLING VECTOR. Y IS CONSTANT FOR A LINEAR
161      C      CAPILLARY PRESSURE MODEL.
162      C
163      S=1.-SWR
164      DO 1 J=1,N
165      Y(J)=- (BPV*S)/(PCR*DT)
166      1  CONTINUE
167      RETURN
168      END
169      SUBROUTINE RAF(M,RKN,RKW,VN,VW,SF,R)
170      C
171      C      CALCULATES THE FRACTIONAL FLOW OF WATER IN THE LAST
172      C      GRID BLOCK USING WELGE'S TANGENT CONSTRUCTION.
173      C
174      C      M - EXPONENT OF RELATIVE PERMEABILITY MODEL
175      C      RKN - PERMEABILITY TO OIL AT INITIAL WATER SATURATION
176      C      RKW - PERMEABILITY TO WATER AT RESIDUAL OIL SATURATION
177      C      VN - OIL VISCOSITY
178      C      VW - WATER VISCOSITY
179      C      SF - NORMALIZED WATER SATURATION AT THE FRONT
180      C      R -- SLOPE OF TANGENT CONSTRUCTION
181      C
182      C      NEWTON-RAPHSON IS USED TO CALCULATE SF FOR THE CASE IN
183      C      WHICH M IS GREATER THAN 2.
184      C
185      B=RKN*VW
186      A=RKW*VN
187      SM=(B*(M-1))/(A-B)
188      IF(M-2)1,2,1
189      2  CONTINUE
190      SF=SQRT(SM)
191      GOTO 6
192      1  CONTINUE
193      X=.2
194      DO 4 I=1,20
195      Y=((M-1)*X**M+SM)/(M*X**(M-1))
196      E=ABS(Y-X)
197      IF(E-.000001)3,3,5
198      5  CONTINUE
199      X=Y
200      4  CONTINUE

```



```

201      3      CONTINUE
202      SF=Y
203      6      CONTINUE
204      R=(A*SF**(M-1))/(A*SF**M+B*(1.-SF**M))
205      RETURN
206      END
207      SUBROUTINE SAT(N,A,D,T,DP,R,DS)
208      DIMENSION T(1),DP(1),R(1),DS(1)
209      C
210      C      CALCULATES SATURATION CHANGES AT THE END OF A TIME STEP
211      C
212      C      N - NUMBER OF GRID BLOCKS
213      C      A - GRID PORE VOLUME
214      C      D - TIME STEP
215      C      T - TRANSMISSIBILITY VECTOR
216      C      DP - PRESSURE CHANGE VECTOR
217      C      R - R.H.S VECTOR OF MATRIX EQUATION
218      C      DS - SATURATION CHANGE VECTOR
219      C
220      NN=N-1
221      DO 1 I=1,NN
222      X=T(I-1)*(DP(I-1)-DP(I))-T(I)*(DP(I)-DP(I+1))
223      X=X-R(I)
224      DS(I)=(X*D)/A
225      1      CONTINUE
226      X=-T(1)*(DP(1)-DP(2))-R(1)
227      DS(1)=(X*D)/A
228      X=T(NN)*(DP(NN)-DP(N))-R(N)
229      DS(N)=(X*D)/A
230      RETURN
231      END
232      C
233      C
234      C      THE MAIN PROGRAM STARTS HERE
235      C
236      C      L - TIME STEP COUNTER AT WHICH PRINTED OUTPUT STARTS
237      C      KK - TIME STEP INCREMENT FOR PRINTED OUTPUT
238      C      M - SATURATION MODEL EXPONENT
239      C      N - NO OF GRID BLOCKS IN THE SIMULATOR
240      C      QH - DISPLACEMENT RATE IN CC/HOUR
241      C      SIG - WATER/OIL INTERFACIAL TENSION IN DYNES/CM
242      C      XL - CORE LENGTH IN CM
243      C      D - CORE DIAMETER IN CM
244      C      SWR - INITIAL WATER SATURATION
245      C      SNR - RESIDUAL OIL SATURATION
246      C      RKA - ABSOLUTE PERMEABILITY IN DARCYS
247      C      RKN - PERMEABILITY TO OIL AT INITIAL WATER SATURATION
248      C      RKW - PERMEABILITY TO WATER AT RESIDUAL OIL SATURATION
249      C      VN - OIL VISCOSITY IN CENTIPOISE
250      C      VW - WATER VISCOSITY IN CENTIPOISE

```



```

251      C      P - FRACTIONAL POROSITY
252      C      PCR - CAPILLARY PRESSURE AT INITIAL WATER SATURATION IN ATM
253      C      DTNOM - NORMALIZED DIMENSIONLESS TIME STEP
254      C      PRW - INITIAL WATER PRESSURE
255      C
256      C
257      DIMENSION TW(50),TN(50),SW(50),PW(50),PN(50),ALF(50)
258      DIMENSION A(50,4),B(50,4),C(50,4),X(50,2),Y(50,2)
259      DIMENSION XXW(50),XXN(50),DPWB(50),DPNB(50),DSW(50),DSN(50),SN(50)
260      L=100
261      KK=100
262      M=2
263      N=50
264      SIG=24.3
265      QH=1120.
266      Q=QH/3600.
267      XL=112.8
268      DX=XL/N
269      D=4.972
270      AX=3.141593*D*D/4.
271      SWR=.0992
272      SNR=.51
273      RKA=22.72
274      RKN=20.9
275      RKW=1.652
276      VN=105.363
277      VW=1.028
278      VR=VN/VW
279      EM=(RKW*VN)/(VW*RKN)
280      P=.3544
281      PCR=.05
282      PRW=1.
283      DTNOM=.001
284      FV=AX*XL*P
285      BPV=AX*DX*P
286      SNOM=1.-SWR-SNR
287      DT=(DTNOM*FV*SNOM)/Q
288      SCL=(Q*VW*.01*XL)/(AX*SIG*SQRT(RKA*9.869E-09*P))
289      SCD=SCL*D/XL
290      CUMN=0.
291      CUMJ=0.
292      CUMW=0.
293      K=0
294      SUM=0.
295      LT=0
296      27  CONTINUE
297      TIME=0.
298      DTIME=0.
299      DO 1 I=1,N
300      SW(I)=SWR

```



```

301      SN(I)=1.-SWR
302      PW(I)=PRW
303      PN(I)=PW(I)+PCR
304      1      CONTINUE
305      QIP=PV*(1.-SWR)
306      CALL RAF(M,RKN,RKW,VN,VW,SF,SLOPE)
307      2      CONTINUE
308      S=(SW(N)-SWR)/SNOM
309      IF(S-SF)3,3,4
310      3      CONTINUE
311      FW=SLOPE*S
312      GOTO 5
313      4      CONTINUE
314      FW=(RKW*VN*S**M)/(RKW*VN*S**M+RKN*VW*(1.-S**M))
315      5      CONTINUE
316      Q1=-Q
317      Q2=Q*FW
318      Q3=Q*(1.-FW)
319      6      CONTINUE
320      CALL CAPL(N,SWR,PCR,BPV,DT,ALF)
321      CALL TRANS(N,M,RKN,RKW,AX,DX,VN,VW,SWR,SNR,SW,TW,TN)
322      CALL BMAT(N,TN,TW,PN,PW,ALF,A,B,C,X)
323      X(1,2)=X(1,2)+Q1
324      X(N,1)=X(N,1)+Q3
325      X(N,2)=X(N,2)+Q2
326      CALL SOLVE(N,A,C,B,X,Y)
327      DO 7 I=1,N
328      XXN(I)=X(I,1)
329      XXW(I)=X(I,2)
330      DPNB(I)=Y(I,1)
331      DPWB(I)=Y(I,2)
332      7      CONTINUE
333      CALL SAT(N,BPV,DT,TW,DPWB,XXW,DSW)
334      CALL SAT(N,BPV,DT,TN,DPNB,XXN,DSN)
335      C
336      C      CHECK FOR EXCESSIVE SATURATION CHANGE AND
337      C      HALVE THE TIME STEP IF NECESSARY
338      C
339      DO 14 I=1,N
340      IF(ABS(DSW(I)).GT..1)GOTO 15
341      14     CONTINUE
342      SUM1=0.
343      DO 16 I=1,N
344      SUM1=SUM1+SW(I)
345      PW(I)=PW(I)+DPWB(I)
346      PN(I)=PN(I)+DPNB(I)
347      SW(I)=SW(I)+DSW(I)
348      SN(I)=SN(I)+DSN(I)
349      16     CONTINUE
350      C

```



```

351 C      CHECK FOR NEGATIVE SATURATION AND
352 C      HALVE THE TIME STEP IF NECESSARY
353 C
354      DO 17 I=1,N
355      IF(SW(I).LT.0.)GOTO 15
356 17    CONTINUE
357      GOTO 35
358 15    CONTINUE
359      DT=DT/2.
360      GOTO 6
361 35    CONTINUE
362      CUMN=CUMN+Q3*DT/OIP
363      CUMJ=CUMJ-Q1*DT/PV
364      CUMW=CUMW+Q2*DT/PV
365      WOR=Q2/Q3
366      IF(WOR.GT.1000.)GOTO 28
367      SUM2=0.
368      SUM3=0.
369      DO 18 I=1,N
370      SUM2=SUM2+SW(I)
371      SUM3=SUM3+(1.-SW(I))
372 18    CONTINUE
373      EINC=(BPV*(SUM2-SUM1)/(Q3*DT))-1.
374      ECUM=((OIP-BPV*SUM3)/(CUMN*OIP))-1.
375      EINC=EINC*100.
376      ECUM=ECUM*100.
377      K=K+1
378      TIME=TIME+DT
379      DTIME=DTIME+(DT*Q)/(PV*SNOM)
380      IF(K-L)2,19,19
381 19    CONTINUE
382      LT=LT+1
383      WRITE(6,20)LT,DTIME
384 20    FORMAT('1'//////////50X,'TABLE A',I1//
385      *31X,'SATURATION PROFILE AT A DIMENSIONLESS TIME OF',F4.1/)
386      WRITE(6,21)K,TIME,DTIME,CUMJ,CUMN,CUMW,WOR
387 21    FORMAT(' '///31X,'NO OF TIME STEPS',14X,'=',I10/
388      *31X,'ACTUAL TIME',19X,'=',F10.1,1X,'SECONDS'/
389      *31X,'DIMENSIONLESS TIME',12X,'=',F10.2/
390      *31X,'CUMULATIVE WATER INJECTED',5X,'=',F10.5,1X,'PORE VOLUMES'/
391      *31X,'CUMULATIVE OIL PRODUCED',7X,'=',F10.5,1X,'%IOIP'/
392      *31X,'CUMULATIVE WATER PRODUCED',5X,'=',F10.5,1X,'PORE VOLUMES'/
393      *31X,'WATER-OIL RATIO',15X,'=',F10.3)
394      WRITE(6,22)EINC,ECUM,QH,VR,EM,SCL,SCD
395 22    FORMAT(' ',30X,'INCREMENTAL MAT. BAL. ERROR',3X,'=',
396      *F10.5,1X,'PERCENT'/
397      *31X,'CUMULATIVE MAT. BAL. ERROR',4X,'=',F10.5,1X,'PERCENT'/
398      *31X,'VOLUMETRIC DISPLACEMENT RATE',2X,'=',F10.1,1X,'CC/HOUR'/
399      *31X,'OIL-WATER VISCOSITY RATIO',5X,'=',F10.3/
400      *31X,'END POINT MOBILITY RATIO',6X,'=',F10.3/

```



```

401      *31X,'LINEAR SCALING COEFFICIENT',4X,'=',1PE10.3/
402      *31X,'RADIAL SCALING COEFFICIENT',4X,'=',1PE10.3//)
403      WRITE(6,23)LT
404      23  FORMAT('1'///46X,'TABLE A',I1,1X,'CONTINUED'///
405      *43X,'GRID',10X,'NORMALIZED'/
406      *43X,'POINT',9X,'SATURATION'/
407      *43X,'-----')
408      DO 25 I=1,N
409      WATS=(SW(I)-SWR)/SNOM
410      OILS=(SN(I)-SNR)/SNOM
411      WRITE(6,24)I,WATS
412      24  FORMAT(' ',40X,I4,F21.6)
413      IF(0.-WATS)26,29,29
414      26  CONTINUE
415      25  CONTINUE
416      29  CONTINUE
417      IF(K.EQ.600)GOTO 28
418      L=L+KK
419      GOTO 2
420      31  FORMAT(' ',10X,2F20.8)
421      32  CONTINUE
422      28  CONTINUE
423      END

```


TABLE A1

SATURATION PROFILE AT A DIMENSIONLESS TIME OF 0.1

NO OF TIME STEPS	=	100	
ACTUAL TIME	=	97.5	SECONDS
DIMENSIONLESS TIME	=	0.10	
CUMULATIVE WATER INJECTED	=	0.03908	PORE VOLUMES
CUMULATIVE OIL PRODUCED	=	0.04338	%IOIP
CUMULATIVE WATER PRODUCED	=	0.0	PORE VOLUMES
WATER-OIL RATIO	=	0.0	
INCREMENTAL MAT. BAL. ERROR	=	-0.00576	PERCENT
CUMULATIVE MAT. BAL. ERROR	=	0.01926	PERCENT
VOLUMETRIC DISPLACEMENT RATE	=	1120.0	CC/HOUR
OIL-WATER VISCOSITY RATIO	=	102.493	
END POINT MOBILITY RATIO	=	8.101	
LINEAR SCALING COEFFICIENT	=	2.713E+00	
RADIAL SCALING COEFFICIENT	=	1.196E-01	

TABLE A1 CONTINUED

GRID POINT	NORMALIZED SATURATION
1	0.873659
2	0.753178
3	0.655888
4	0.576467
5	0.508925
6	0.448366
7	0.390471
8	0.329971
9	0.258077
10	0.159340
11	0.044100
12	0.001494
13	0.000000
14	0.0

TABLE A2

SATURATION PROFILE AT A DIMENSIONLESS TIME OF 0.2

NO OF TIME STEPS	=	200	
ACTUAL TIME	=	195.0	SECONDS
DIMENSIONLESS TIME	=	0.20	
CUMULATIVE WATER INJECTED	=	0.07816	PORE VOLUMES
CUMULATIVE OIL PRODUCED	=	0.08677	%IOIP
CUMULATIVE WATER PRODUCED	=	0.0	PORE VOLUMES
WATER-OIL RATIO	=	0.0	
INCREMENTAL MAT. BAL. ERROR	=	0.00401	PERCENT
CUMULATIVE MAT. BAL. ERROR	=	0.00973	PERCENT
VOLUMETRIC DISPLACEMENT RATE	=	1120.0	CC/HOUR
OIL-WATER VISCOSITY RATIO	=	102.493	
END POINT MOBILITY RATIO	=	8.101	
LINEAR SCALING COEFFICIENT	=	2.713E+00	
RADIAL SCALING COEFFICIENT	=	1.196E-01	

TABLE A2 CONTINUED

GRID POINT	NORMALIZED SATURATION
1	0.964274
2	0.901123
3	0.833208
4	0.770066
5	0.713933
6	0.664091
7	0.619748
8	0.579807
9	0.543253
10	0.509460
11	0.477379
12	0.446501
13	0.415835
14	0.384250
15	0.350069
16	0.310117
17	0.258123
18	0.181037
19	0.071854
20	0.005666
21	0.000012
22	0.0

TABLE A3

SATURATION PROFILE AT A DIMENSIONLESS TIME OF 0.3

NO OF TIME STEPS	=	300	
ACTUAL TIME	=	292.5	SECONDS
DIMENSIONLESS TIME	=	0.30	
CUMULATIVE WATER INJECTED	=	0.11724	PORE VOLUMES
CUMULATIVE OIL PRODUCED	=	0.13015	%IDIP
CUMULATIVE WATER PRODUCED	=	0.0	PORE VOLUMES
WATER-OIL RATIO	=	0.0	
INCREMENTAL MAT. BAL. ERROR	=	-0.00087	PERCENT
CUMULATIVE MAT. BAL. ERROR	=	0.00687	PERCENT
VOLUMETRIC DISPLACEMENT RATE	=	1120.0	CC/HOUR
OIL-WATER VISCOSITY RATIO	=	102.493	
END POINT MOBILITY RATIO	=	8.101	
LINEAR SCALING COEFFICIENT	=	2.713E+00	
RADIAL SCALING COEFFICIENT	=	1.196E-01	

TABLE A3 CONTINUED

GRID POINT	NORMALIZED SATURATION
1	0.989482
2	0.960207
3	0.917461
4	0.869984
5	0.823333
6	0.779427
7	0.739090
8	0.702167
9	0.668258
10	0.637305
11	0.608446
12	0.581756
13	0.556717
14	0.533046
15	0.510479
16	0.488862
17	0.467823
18	0.447109
19	0.426462
20	0.405434
21	0.383369
22	0.359465
23	0.332047
24	0.298250
25	0.251923
26	0.180327
27	0.074823
28	0.006540
29	0.000018
30	0.0

TABLE A4

SATURATION PROFILE AT A DIMENSIONLESS TIME OF 0.4

NO OF TIME STEPS	=	400	
ACTUAL TIME	=	390.0	SECONDS
DIMENSIONLESS TIME	=	0.40	
CUMULATIVE WATER INJECTED	=	0.15631	PORE VOLUMES
CUMULATIVE OIL PRODUCED	=	0.17353	%IOIP
CUMULATIVE WATER PRODUCED	=	0.0	PORE VOLUMES
WATER-OIL RATIO	=	0.0	
INCREMENTAL MAT. BAL. ERROR	=	-0.00576	PERCENT
CUMULATIVE MAT. BAL. ERROR	=	0.00572	PERCENT
VOLUMETRIC DISPLACEMENT RATE	=	1120.0	CC/HOUR
OIL-WATER VISCOSITY RATIO	=	102.493	
END POINT MOBILITY RATIO	=	8.101	
LINEAR SCALING COEFFICIENT	=	2.713E+00	
RADIAL SCALING COEFFICIENT	=	1.196E-01	

TABLE A4 CONTINUED

GRID POINT	NORMALIZED SATURATION
1	0.996921
2	0.984784
3	0.961039
4	0.928667
5	0.892404
6	0.855307
7	0.819475
8	0.785528
9	0.753642
10	0.724180
11	0.696506
12	0.670900
13	0.646837
14	0.624330
15	0.603029
16	0.582973
17	0.563940
18	0.545629
19	0.528210
20	0.511390
21	0.495035
22	0.479139
23	0.463470
24	0.448019
25	0.432537
26	0.416879
27	0.400684
28	0.383742
29	0.365394
30	0.344723
31	0.320114
32	0.288462
33	0.243268
34	0.171130
35	0.066219
36	0.004856
37	0.000009
38	0.0

TABLE A5

SATURATION PROFILE AT A DIMENSIONLESS TIME OF 0.5

NO OF TIME STEPS	=	500	
ACTUAL TIME	=	487.5	SECONDS
DIMENSIONLESS TIME	=	0.50	
CUMULATIVE WATER INJECTED	=	0.19539	PORE VOLUMES
CUMULATIVE OIL PRODUCED	=	0.21691	%IOIP
CUMULATIVE WATER PRODUCED	=	0.0	PORE VOLUMES
WATER-OIL RATIO	=	0.0	
INCREMENTAL MAT. BAL. ERROR	=	-0.00576	PERCENT
CUMULATIVE MAT. BAL. ERROR	=	0.00448	PERCENT
VOLUMETRIC DISPLACEMENT RATE	=	1120.0	CC/HOUR
OIL-WATER VISCOSITY RATIO	=	102.493	
END POINT MOBILITY RATIO	=	8.101	
LINEAR SCALING COEFFICIENT	=	2.713E+00	
RADIAL SCALING COEFFICIENT	=	1.196E-01	

TABLE A5 CONTINUED

GRID POINT	NORMALIZED SATURATION
1	0.999105
2	0.994478
3	0.982760
4	0.963013
5	0.937130
6	0.907698
7	0.877247
8	0.846932
9	0.817570
10	0.789832
11	0.763408
12	0.738676
13	0.715296
14	0.693364
15	0.672522
16	0.652936
17	0.634444
18	0.616647
19	0.599889
20	0.583809
21	0.568389
22	0.553595
23	0.539219
24	0.525442
25	0.512032
26	0.498991
27	0.486106
28	0.473558
29	0.461187
30	0.448826
31	0.436503
32	0.424074
33	0.411360
34	0.398293
35	0.384477
36	0.369653
37	0.353178
38	0.334040
39	0.310504
40	0.279119
41	0.232611
42	0.156481
43	0.052005
44	0.002650
45	0.000002
46	0.0

TABLE A6

SATURATION PROFILE AT A DIMENSIONLESS TIME OF 0.6

NO OF TIME STEPS	=	600
ACTUAL TIME	=	584.9 SECONDS
DIMENSIONLESS TIME	=	0.60
CUMULATIVE WATER INJECTED	=	0.23447 PORE VOLUMES
CUMULATIVE OIL PRODUCED	=	0.25969 ZIDIP
CUMULATIVE WATER PRODUCED	=	0.00054 PORE VOLUMES
WATER-OIL RATIO	=	0.177
INCREMENTAL MAT. BAL. ERROR	=	0.10595 PERCENT
CUMULATIVE MAT. BAL. ERROR	=	0.00324 PERCENT
VOLUMETRIC DISPLACEMENT RATE	=	1120.0 CC/HOUR
OIL-WATER VISCOSITY RATIO	=	102.493
END POINT MOBILITY RATIO	=	8.101
LINEAR SCALING COEFFICIENT	=	2.713E+00
RADIAL SCALING COEFFICIENT	=	1.196E-01

TABLE A6 CONTINUED

GRID POINT	NORMALIZED SATURATION
1	0.999739
2	0.998076
3	0.992833
4	0.982023
5	0.965283
6	0.943639
7	0.919202
8	0.893269
9	0.867053
10	0.841522
11	0.816635
12	0.793046
13	0.770441
14	0.749136
15	0.728711
16	0.709466
17	0.691271
18	0.673717
19	0.657193
20	0.641385
21	0.626244
22	0.611760
23	0.597734
24	0.584368
25	0.571441
26	0.559035
27	0.546773
28	0.535091
29	0.523704
30	0.512488
31	0.501625
32	0.490958
33	0.480406
34	0.470057
35	0.459826
36	0.449443
37	0.439341
38	0.429048
39	0.418625
40	0.407966
41	0.396935
42	0.385346
43	0.372935
44	0.359294
45	0.343777
46	0.325285
47	0.301834
48	0.269468
49	0.219550
50	0.105721

Table A7

BREAKTHROUGH RECOVERY PREDICTED BY
ONE-DIMENSIONAL NUMERICAL SIMULATOR

$V_{\mu_w} L / \sigma \sqrt{K\phi}$	Breakthrough Recovery (%IOIP)	
	M = 1.922	M = 8.101
6.055×10^{-3}	16.36	14.97
1.211×10^{-2}	20.11	17.35
4.844×10^{-2}	28.46	21.69
1.211×10^{-1}	33.84	22.52
2.422×10^{-1}	36.66	23.38
4.844×10^{-1}	38.18	23.90
1.211×10^0	39.08	24.25
1.938×10^0	39.17	24.34
2.713×10^0	39.35	24.38

APPENDIX B

RHEOLOGICAL PROPERTIES OF MODEL FLUIDS

Table B1

SUMMARY OF VISCOMETER TESTS

Dow Corning 200		MCT 30	
Shear Rate (Sec ⁻¹)	Shear Stress (dynes/cm ²)	Shear Rate (Sec ⁻¹)	Shear Stress (dynes/cm ²)
2.34	8.95	2.34	8.95
4.68	14.20	4.68	14.20
9.36	25.00	9.36	26.85
18.72	35.80	18.72	53.40
37.44	53.40	37.44	107.10
74.88	89.20	74.88	214.20
169.42	178.40	169.42	428.10
299.52	347.85	299.52	874.10
423.54	499.40	423.54	1230.90
599.04	713.60	599.04	1748.50
847.08	1034.90		
1198.08	1480.90		

Table B2

VERIFICATION OF DARCY'S LAW

Fluid Type	L cm	d cm	μ cp	Q cc/sec	ΔP atm
Distilled Water	112.8	4.961	1.028	0.3111	0.0803
				0.2667	0.0724
				0.2222	0.0592
				0.1778	0.0487
				0.0000	0.0000
Dow Corning 200	115.6	4.972	105.363	0.3111	10.4650
				0.2222	7.5303
				0.1333	4.5439
				0.0889	3.0573
				0.0556	1.9284
				0.0014	0.0476
MCT 30	23.6	4.844	310.532	0.0000	0.0000
				0.3111	6.9275
				0.2222	4.9697
				0.1778	3.9860
				0.1111	2.4920
				0.0556	1.2486
				0.0222	0.4878
				0.0111	0.2426
				0.0000	0.0000

APPENDIX C

COMPUTER PROGRAM FOR PROCESSING
PRESSURE RECORDS FROM PAPER TAPE


```

1  C*****C
2  C
3  SUBROUTINE RDSCAN(TIME,TRNDCR,IOU,WRK,*,*)
4  C
5  C--- RDSCAN reads one complete scan stored in a single record
6  C--- and converts the scan data to the internal processing form.
7  C--- The time of each scan is returned in seconds. The transducer
8  C--- readings are returned in volts. Error readings are set to
9  C--- the maximum negative number, i.e. bit pattern X'FFFFFFFF'.
10 C
11 C--- If an End-of-File condition occurs while reading, this routine
12 C--- RETURNS to the statement label replacing the first "*" in the
13 C--- parameter list. If an Error condition occurs while reading,
14 C--- the routine RETURNS to the second statement label.
15 C
16 C    TIME    - time of scan in seconds (real variable).
17 C    TRNDCR  - transducer readings in volts (real vector).
18 C    IOU     - logical input unit to which data file is attached.
19 C    WRK     - work area same length as TRNDCR (integer vector).
20 C
21 C*****C
22 REAL*4 TRNDCR(1),MAXNEG/ZFFFFFFFF/
23 INTEGER*2 WRK(1),ALARM/'* '/
24 C
25 C-- Read a complete scan - next input record.
26 READ(IOU,1000,END=91,ERR=92) IHR,MIN,ISEC,
27 * (WRK(2*I-1),TRNDCR(I),WRK(2*I),I=1,12)
28 1000 FORMAT(2X,3(I2,1X),5(A1,3X,F6.0,I1),2X,6(A1,3X,F6.0,I1),
29 * 2X,A1,3X,F6.0,I1)
30 C
31 C-- Compute the time of scan in seconds.
32 TIME=3600*IHR+60*MIN+ISEC
33 C
34 C-- Compute the transducer values.
35 DO 50 I=1,12
36 IF (WRK(2*I-1).EQ.ALARM) GOTO 45
37 INT=-WRK(2*I)
38 TRNDCR(I)=TRNDCR(I)*10.**INT
39 GOTO 50
40 45 TRNDCR(I)=MAXNEG
41 50 CONTINUE
42 RETURN
43 C
44 C-- If end-of-file on input, return to first statement in list.
45 91 RETURN1
46 C
47 C-- If error on input, return to second statement in list.
48 92 RETURN2
49 END

```



```

50      REAL X(12),Y(12)
51      INTEGER M(12),INT(12)
52      DO 1 J=1,12
53          M(J)=J
54          X(J)=0.
55          Y(J)=0.
56      1  CONTINUE
57          L=0
58          T1=0.
59          WRITE(6,2)
60      2  FORMAT('1'////////53X,'TABLE D2'//
61          *45X,'PRESSURE HISTORY - RUN 14'////
62          *T25,'INLET',T112,'OUTLET'//)
63          WRITE(6,3)(M(J),J=1,12)
64      3  FORMAT(' ',5X,'TIME (SECS.)',12I8//)
65          WRITE(6,8)T1,(Y(J),J=1,12)
66      8  FORMAT(' ',6X,F8.0,5X,12F8.2,I10)
67          CALL RDSCAN(T1,X,4,INT,&44,&44)
68          N=600
69      12 CONTINUE
70          L=L+1
71          CALL RDSCAN(T2,Y,4,INT,&44,&55)
72          T2=T2-T1
73          DO 9 J=1,12
74              Y(J)=(Y(J)-X(J))*200.
75              S=Y(J)
76              Y(J)=ABS(S)
77      9  CONTINUE
78          WRITE(6,8)T2,(Y(J),J=1,12)
79          IF(L.LT.N)GOTO 12
80      44 CONTINUE
81          GOTO 57
82      55 CONTINUE
83          WRITE(6,56)
84      56 FORMAT(' ',20X,'ENCOUNTERED DIFFICULTIES IN READING DATA ')
85      57 CONTINUE
86      END

```


APPENDIX D

RECOVERY AND PRESSURE DATA FOR RUNS 14 AND 28

TABLE D1

PRODUCTION HISTORY - RUN 14

TIME SECS	TOTAL PROD CC	INCR WATER PROD CC	INCR OIL PROD CC	CUM FLUID PROD CC	CUM WATER PROD CC	CUM OIL PROD CC	CUM FLUID INJE VOL	CUM WATER PROD VOL	CUM OIL PROD CENT IOIP
0.0	0.0	0.0	0.0	0.0	0.0	0.0	0.0	0.0	0.0
922.5	205.0	0.0	205.0	205.0	0.0	205.0	0.269	0.0	28.6
1035.9	25.2	6.0	19.2	230.2	6.0	224.2	0.302	0.008	31.3
1195.6	35.5	11.5	24.0	265.7	17.5	248.2	0.348	0.023	34.7
1368.9	38.5	16.5	22.0	304.2	34.0	270.2	0.399	0.045	37.7
1545.7	39.3	21.0	18.3	343.5	55.0	288.5	0.450	0.072	40.3
1733.8	41.8	23.0	18.8	385.3	78.0	307.3	0.505	0.102	42.9
1914.3	40.1	23.0	17.1	425.4	101.0	324.4	0.558	0.132	45.3
2101.5	41.6	28.0	13.6	467.0	129.0	338.0	0.612	0.169	47.2
2281.5	40.0	32.5	7.5	507.0	161.5	345.5	0.665	0.212	48.2
2464.2	40.6	35.0	5.6	547.6	196.5	351.1	0.718	0.258	49.0

TABLE D2
PRESSURE HISTORY - RUN 14

TIME (SECS.)	INLET											OUTLET	
	1	2	3	4	5	6	7	8	9	10	11	12	12
0.	0.0	0.0	0.0	0.0	0.0	0.0	0.0	0.0	0.0	0.0	0.0	0.0	0.0
8.	0.89	0.55	0.10	0.02	0.02	0.08	0.04	0.02	0.08	0.05	0.06	0.00	0.00
13.	4.36	1.38	1.45	1.98	0.65	0.33	0.85	0.12	0.30	0.22	0.14	0.03	0.03
41.	70.26	63.15	57.28	52.09	46.77	38.88	33.74	26.47	21.99	13.97	6.05	0.14	0.14
71.	96.86	89.57	81.30	74.03	67.33	57.71	49.28	40.29	32.01	20.50	9.10	0.16	0.16
76.	98.74	91.75	83.00	75.65	68.75	58.93	50.04	41.23	32.78	21.12	9.17	0.18	0.18
81.	100.04	93.17	84.16	76.89	69.75	59.85	50.95	41.89	33.25	21.31	9.44	0.14	0.14
86.	101.10	94.43	85.20	77.79	70.53	60.63	51.59	42.53	33.64	21.60	9.60	0.13	0.13
91.	101.68	95.09	86.02	78.47	71.35	61.39	52.11	43.06	34.05	21.87	9.66	0.20	0.20
97.	102.42	95.79	86.72	79.13	71.97	61.91	52.51	43.37	34.29	22.04	9.75	0.17	0.17
102.	102.76	96.53	87.24	79.71	72.45	62.41	52.77	43.75	34.58	22.09	9.87	0.19	0.19
107.	102.86	96.91	87.62	79.97	72.73	62.65	53.07	43.95	34.72	22.28	9.90	0.12	0.12
112.	103.10	97.23	87.94	80.23	72.99	62.89	53.31	44.05	34.77	22.30	9.98	0.16	0.16
117.	102.86	97.45	88.12	80.43	73.25	63.11	53.53	44.14	34.93	22.33	9.84	0.24	0.24
122.	102.84	97.53	88.26	80.61	73.41	63.11	53.51	44.27	34.85	22.48	10.03	0.13	0.13
127.	102.90	97.67	88.44	80.65	73.41	63.33	53.59	44.27	35.04	22.46	9.91	0.10	0.10
132.	102.76	97.85	88.52	80.79	73.59	63.35	53.61	44.50	35.08	22.54	9.98	0.14	0.14
138.	102.70	97.89	88.64	80.93	73.61	63.37	53.71	44.53	35.03	22.56	9.99	0.10	0.10
143.	102.54	97.89	88.74	80.91	73.79	63.61	53.89	44.54	35.12	22.57	9.94	0.15	0.15
148.	102.18	97.83	88.76	80.93	73.81	63.49	53.95	44.62	35.14	22.55	10.10	0.21	0.21
153.	101.96	97.93	88.86	81.11	73.83	63.61	53.87	44.65	35.24	22.64	10.08	0.18	0.18
158.	101.70	97.91	88.90	81.11	73.91	63.71	53.97	44.77	35.14	22.60	10.03	0.19	0.19
163.	101.34	97.81	88.92	81.27	73.97	63.75	54.07	44.65	35.30	22.69	10.18	0.10	0.10
168.	101.52	97.83	88.98	81.25	74.03	63.83	54.13	44.68	35.26	22.73	10.10	0.23	0.23
173.	101.20	97.67	89.10	81.35	74.11	63.97	54.05	44.68	35.37	22.63	10.03	0.01	0.01
178.	101.00	97.51	89.16	81.57	74.07	63.77	54.17	44.73	35.40	22.98	10.13	0.07	0.07
184.	100.72	97.67	89.22	81.31	74.21	63.77	53.99	44.71	35.15	22.72	9.99	0.25	0.25
189.	100.46	97.47	89.20	81.59	74.29	64.05	54.19	44.83	35.46	22.99	10.08	0.20	0.20
194.	100.26	97.19	89.32	81.59	74.31	63.93	54.27	44.87	35.45	22.77	10.06	0.09	0.09
199.	99.82	97.07	89.26	81.59	74.25	63.99	54.31	44.99	35.57	22.79	10.23	0.16	0.16
204.	99.56	96.63	89.28	81.61	74.49	63.95	54.49	44.96	35.45	22.72	10.30	0.31	0.31
209.	99.28	96.53	89.14	81.61	74.53	63.91	54.07	44.77	35.37	22.94	10.03	0.17	0.17
214.	98.82	96.19	89.16	81.51	74.23	64.03	54.17	44.98	35.18	22.99	10.09	0.14	0.14

224.	98.28	95.81	88.94	81.43	74.27	63.75	54.15	44.88	35.57	22.72	10.30	0.17
229.	97.96	95.69	88.88	81.29	74.13	63.67	54.27	44.92	35.11	22.59	9.92	0.09
234.	97.72	95.39	88.72	81.41	74.19	63.83	53.95	44.89	35.40	22.78	10.11	0.24
240.	97.32	94.97	88.66	81.39	74.17	63.87	54.23	44.91	35.27	22.93	10.04	0.17
245.	97.02	94.77	88.64	81.59	74.43	63.77	54.29	44.98	35.33	22.80	10.03	0.17
250.	96.20	94.35	88.58	81.55	74.27	64.07	54.11	44.95	35.28	22.78	10.17	0.06
255.	96.28	94.49	88.34	81.51	74.31	63.87	54.15	44.88	35.42	22.86	10.13	0.21
260.	96.18	94.25	88.24	81.51	74.23	63.99	54.09	44.92	35.43	22.79	10.18	0.17
265.	95.74	93.81	88.08	81.55	74.27	63.97	54.17	44.91	35.50	22.90	10.21	0.18
270.	95.38	93.61	87.96	81.39	74.31	64.01	54.23	44.90	35.56	22.86	10.15	0.18
275.	95.20	93.39	87.86	81.53	74.33	63.91	54.19	44.90	35.48	22.93	10.20	0.12
280.	94.78	93.03	87.68	81.45	74.29	63.99	54.23	44.99	35.45	22.97	10.15	0.18
286.	94.56	92.77	87.54	81.49	74.35	63.93	54.31	44.98	35.41	22.97	10.35	0.05
291.	94.44	92.63	87.56	81.45	74.35	64.03	54.17	45.01	35.35	22.85	10.30	0.11
296.	94.06	92.25	87.20	81.23	74.33	63.81	54.37	45.01	35.32	22.86	10.41	0.14
301.	93.68	91.91	86.94	81.33	74.33	64.11	54.25	44.82	35.30	22.81	10.21	0.17
306.	93.34	91.43	86.80	81.07	74.13	63.99	54.17	45.00	35.39	22.85	10.11	0.15
311.	93.18	91.19	86.50	81.21	74.39	64.07	54.35	45.02	35.36	22.80	10.19	0.21
316.	92.80	91.05	86.38	81.03	74.35	63.99	54.39	45.04	35.50	22.91	10.27	0.16
321.	92.30	90.79	86.08	80.95	74.47	63.89	54.23	44.94	35.54	22.81	10.11	0.18
326.	92.10	90.23	85.98	80.75	74.19	63.95	54.39	44.96	35.65	23.03	10.12	0.19
331.	91.75	90.11	85.70	80.73	74.23	63.81	54.31	44.90	35.53	22.82	10.11	0.13
337.	91.50	89.79	85.44	80.61	74.25	63.99	54.25	44.95	35.44	22.90	10.19	0.21
342.	91.04	89.41	85.24	80.45	74.29	63.93	54.21	44.86	35.34	22.88	10.15	0.17
347.	90.78	89.31	84.94	80.17	74.31	64.27	54.37	44.88	35.29	22.86	10.27	0.13
352.	90.66	88.95	84.90	80.31	74.33	63.93	54.09	44.90	35.48	22.89	10.08	0.22
357.	90.30	88.55	84.68	80.13	74.17	63.79	54.55	45.03	35.60	22.89	10.13	0.26
362.	89.98	88.25	84.44	80.09	74.13	63.93	54.17	44.97	35.52	22.97	10.13	0.27
367.	89.54	88.13	84.26	79.97	74.11	63.93	54.31	45.02	35.47	22.90	10.17	0.09
372.	89.46	87.85	84.03	79.85	74.07	63.97	54.33	45.05	35.53	22.90	10.23	0.14
377.	89.16	87.47	83.82	79.69	74.01	63.95	54.29	44.89	35.44	23.03	10.20	0.21
382.	88.64	87.13	83.48	79.51	73.79	63.61	54.33	45.10	35.57	22.94	10.24	0.18
388.	88.36	86.79	83.24	79.13	73.75	63.83	54.31	44.96	35.48	22.88	10.21	0.16
393.	87.90	86.47	82.96	79.03	73.81	63.87	54.19	44.97	35.50	22.85	10.31	0.16
398.	87.74	86.17	82.70	78.91	73.67	63.85	54.31	44.85	35.52	23.04	10.20	0.20
403.	87.44	85.89	82.56	78.75	73.69	63.85	54.21	44.91	35.43	22.91	10.16	0.17
408.	87.26	85.59	82.26	78.51	73.57	63.99	54.31	44.85	35.52	22.86	10.12	0.14
413.	86.58	85.23	81.98	78.27	73.43	63.83	54.21	44.93	35.48	22.94	10.16	0.18
418.	86.42	85.01	81.74	78.05	73.33	63.75	54.23	44.90	35.55	23.00	10.15	0.23
423.	86.16	84.57	81.42	77.89	73.21	63.71	54.19	44.94	35.51	22.86	10.20	0.22
428.	85.78	84.37	81.18	77.77	73.13	63.73	54.27	44.91	35.47	22.88	10.18	0.19
433.	85.48	83.87	80.84	77.51	72.91	63.69	54.15	44.96	35.40	22.84	10.17	0.16
439.	85.34	83.65	80.68	77.31	72.81	63.65	54.29	44.96	35.47	22.97	10.23	0.18
444.	84.92	83.43	80.40	77.17	72.69	63.67	54.17	44.94	35.49	22.96	10.14	0.18
449.	84.54	83.11	80.12	76.81	72.53	63.61	54.27	44.91	35.43	22.97	10.14	0.25
454.	84.16	82.71	79.76	76.65	72.39	63.45	54.25	44.96	35.52	23.01	10.22	0.17
459.	83.66	82.47	79.52	76.43	72.29	63.43	54.33	44.92	35.42	23.07	10.19	0.21
464.	83.70	82.17	79.24	76.27	72.05	63.43	54.23	45.04	35.45	23.13	10.19	0.16
469.	83.34	81.91	78.98	75.99	71.95	63.33	54.21	44.90	35.56	23.02	10.28	0.20
474.	82.90	81.57	78.66	75.81	71.79	63.21	54.31	44.97	35.58	23.09	10.11	0.15

479.	82.46	81.13	78.42	75.53	71.57	63.11	54.21	44.96	35.60	23.06	10.16	0.19
485.	82.28	80.85	78.08	75.29	71.41	63.01	54.31	45.05	35.52	23.13	10.18	0.13
490.	81.98	80.51	77.74	74.93	71.15	62.99	54.17	44.94	35.50	23.00	10.11	0.17
495.	81.60	80.11	77.48	74.67	71.05	62.81	54.09	44.90	35.44	23.08	10.20	0.14
500.	81.16	79.75	77.12	74.35	70.91	62.69	54.09	44.98	35.28	23.03	10.27	0.21
505.	80.82	79.43	76.76	74.21	70.65	62.63	54.01	45.02	35.49	23.04	10.15	0.23
510.	80.52	78.89	76.46	73.77	70.23	62.33	54.01	44.97	35.56	23.08	10.26	0.17
515.	80.20	78.77	76.22	73.63	70.21	62.25	53.99	44.96	35.43	23.06	10.17	0.21
520.	79.68	78.47	75.80	73.35	70.03	62.25	53.95	44.92	35.45	23.08	10.21	0.21
525.	79.38	78.17	75.48	73.01	69.75	62.13	53.91	44.91	35.53	23.14	10.16	0.12
530.	79.18	77.77	75.22	72.79	69.53	61.89	53.87	44.94	35.48	23.22	10.23	0.23
536.	78.76	77.43	74.96	72.51	69.35	61.89	53.75	44.90	35.50	23.18	10.19	0.23
541.	78.56	77.11	74.62	72.29	69.17	61.73	53.71	44.92	35.51	23.13	10.17	0.16
546.	78.30	76.81	74.32	72.05	68.93	61.57	53.61	44.97	35.52	23.15	10.18	0.22
551.	77.82	76.59	74.08	71.77	68.73	61.53	53.57	45.02	35.52	23.18	10.24	0.23
556.	77.50	76.17	73.74	71.53	68.53	61.37	53.53	45.03	35.59	23.16	10.22	0.26
561.	77.12	75.73	73.36	71.11	68.21	61.13	53.27	44.95	35.49	23.15	10.18	0.12
566.	76.60	75.41	73.08	70.95	67.93	61.07	53.25	44.87	35.47	23.12	10.13	0.15
571.	76.34	74.91	72.66	70.67	67.69	60.69	53.11	44.84	35.55	23.12	10.02	0.19
576.	75.94	74.55	72.34	70.07	67.51	60.59	53.03	44.75	35.47	23.19	10.10	0.16
582.	75.60	74.13	72.06	69.85	67.15	60.41	53.03	44.74	35.62	23.23	10.18	0.14
587.	75.16	73.85	71.60	69.67	66.87	60.15	52.81	44.86	35.33	23.05	10.17	0.23
592.	74.98	73.49	71.38	69.33	66.59	59.87	52.61	44.69	35.61	23.27	10.34	0.21
597.	74.56	73.13	70.98	68.95	66.23	59.83	52.53	44.57	35.60	23.13	10.16	0.31
602.	74.10	72.81	70.62	68.71	65.95	59.69	52.49	44.51	35.54	22.99	10.16	0.22
607.	73.76	72.35	70.14	68.31	65.63	59.23	52.31	44.38	35.49	23.16	10.20	0.17
612.	73.34	72.01	70.02	67.93	65.45	59.03	52.11	44.32	35.45	23.16	10.20	0.25
617.	73.08	71.67	69.66	67.71	65.17	58.91	51.97	44.23	35.52	23.17	10.16	0.17
622.	72.72	71.45	69.26	67.31	64.99	58.63	51.75	44.33	35.33	23.20	10.16	0.26
628.	72.38	71.03	68.94	67.11	64.75	58.77	51.75	44.30	35.49	23.02	10.12	0.13
633.	71.96	70.77	68.72	66.85	64.37	58.25	51.57	44.03	35.42	23.23	10.22	0.15
638.	71.82	70.41	68.40	66.47	64.07	58.05	51.59	44.03	35.40	23.19	10.32	0.10
643.	71.38	69.83	68.04	66.07	63.77	57.65	51.23	43.87	35.30	23.16	10.32	0.15
648.	71.04	69.55	67.70	65.95	63.43	57.63	51.31	43.88	35.20	23.42	10.24	0.23
653.	70.60	69.13	67.26	65.31	63.05	57.43	51.09	43.44	35.18	23.05	10.29	0.15
658.	70.20	68.99	67.06	64.93	62.77	57.11	50.59	43.51	35.24	23.03	10.21	0.29
663.	69.84	68.27	66.58	64.65	62.51	56.71	50.55	43.42	35.06	23.17	10.21	0.22
668.	69.38	68.03	66.00	64.39	62.23	56.53	50.37	43.25	35.07	23.08	10.21	0.32
673.	68.92	67.73	65.86	64.03	61.87	56.29	50.14	43.09	35.01	23.09	10.08	0.18
678.	68.76	67.21	65.46	63.81	61.61	55.89	49.92	43.04	34.91	23.04	10.20	0.16
684.	68.42	67.05	65.10	63.49	61.23	55.79	49.73	42.86	34.98	23.15	10.20	0.23
689.	67.98	66.55	64.88	63.11	60.95	55.45	49.48	42.67	34.77	23.06	10.08	0.14
694.	67.58	66.21	64.48	62.87	60.45	55.11	49.38	42.58	34.88	23.05	10.11	0.23
699.	67.16	65.65	64.00	62.39	60.33	54.93	49.17	42.41	34.63	23.09	10.22	0.13
704.	66.98	65.35	63.76	62.19	60.03	54.65	48.89	42.28	34.50	23.05	10.17	0.25
709.	66.42	64.91	63.28	61.95	59.61	54.23	48.60	42.04	34.21	22.94	10.02	0.25
714.	66.08	64.83	63.02	61.45	59.37	53.93	48.50	42.08	34.11	23.08	10.09	0.21
719.	65.70	64.43	62.70	60.95	59.15	53.99	48.14	41.89	34.27	22.97	10.26	0.22
724.	65.38	63.85	62.38	60.85	58.67	53.43	48.02	41.56	34.10	23.05	10.22	0.20
729.	65.04	63.49	62.06	60.45	58.33	53.29	47.89	41.49	34.06	23.09	10.08	0.01

734.	64.56	63.25	61.60	60.07	58.11	53.19	47.62	41.26	33.87	22.71	10.13	0.25
740.	64.26	62.81	61.34	59.57	57.53	52.57	47.39	40.99	33.70	22.70	10.14	0.25
745.	63.78	62.41	60.86	59.31	57.35	52.21	47.07	40.90	33.62	22.67	10.14	0.19
750.	63.40	61.93	60.48	59.19	56.99	51.77	46.85	40.66	33.39	22.56	10.18	0.14
755.	62.86	61.45	60.08	58.63	56.63	51.63	46.58	40.53	33.25	22.46	10.25	0.20
760.	62.66	61.09	59.64	58.25	56.37	51.27	46.26	40.34	33.09	22.48	10.17	0.25
765.	62.20	60.59	59.42	57.95	55.83	51.21	46.13	39.95	32.83	22.15	10.23	0.27
770.	61.86	60.37	58.82	57.39	55.73	50.83	45.76	39.94	32.87	22.18	10.22	0.21
775.	61.38	59.81	58.52	56.99	55.37	50.47	45.33	39.85	32.70	22.30	10.10	0.15
780.	61.10	59.27	58.16	56.69	54.85	50.32	45.20	39.45	32.36	21.99	10.11	0.06
785.	60.72	58.87	57.98	56.47	54.55	49.73	45.05	39.39	32.31	21.79	10.13	0.28
790.	60.26	58.09	57.46	56.05	54.25	49.27	44.69	39.22	31.98	21.73	9.93	0.15
795.	59.92	58.33	57.06	55.93	53.95	49.22	44.44	38.77	32.12	21.68	9.99	0.21
800.	59.48	57.95	56.80	55.59	53.65	48.84	44.03	38.61	31.85	21.52	9.89	0.22
810.	58.80	57.31	56.10	54.79	52.99	48.30	43.61	38.18	31.65	21.23	9.97	0.36
816.	58.38	57.13	55.76	54.13	52.65	48.09	43.28	38.06	31.50	21.14	9.95	0.28
821.	58.08	56.61	55.26	54.05	52.31	47.71	43.05	37.74	31.16	21.08	9.87	0.34
826.	57.64	56.37	54.96	53.65	51.87	47.20	42.85	37.69	31.28	21.28	9.77	0.22
831.	57.26	55.91	54.66	53.33	51.69	46.97	42.54	37.27	30.90	20.92	9.62	0.20
836.	56.88	55.37	54.26	52.83	51.03	46.47	41.96	37.19	30.66	20.64	9.69	0.22
841.	56.48	54.73	53.80	52.61	50.63	46.26	41.78	36.77	30.53	20.86	9.61	0.17
846.	56.06	54.63	53.42	51.99	50.69	46.17	41.51	36.88	30.30	20.52	9.46	0.28
851.	55.68	54.35	53.08	51.79	50.19	45.76	41.36	36.33	30.13	20.50	9.45	0.09
856.	55.34	53.79	52.64	51.63	49.87	45.33	41.08	36.13	29.85	20.39	9.38	0.22
861.	54.90	53.57	52.42	51.31	49.46	45.09	40.70	36.02	29.91	20.09	9.46	0.23
867.	54.50	52.97	51.84	50.81	49.19	45.02	40.25	35.73	29.56	20.02	9.28	0.23
872.	54.16	52.41	51.54	50.47	48.83	44.41	40.28	35.36	29.13	19.83	9.32	0.15
877.	53.74	52.17	51.22	50.23	48.54	44.23	39.84	35.19	29.00	19.55	9.00	0.16
882.	53.42	52.11	50.88	49.67	48.03	43.93	39.68	34.91	28.91	19.54	9.10	0.15
887.	53.04	51.71	50.52	49.75	47.68	43.49	39.34	34.74	28.89	19.44	9.01	0.03
892.	52.64	51.13	49.94	49.30	47.53	43.16	39.08	34.58	28.58	19.21	8.93	0.23
897.	52.34	51.09	49.80	48.79	47.13	43.04	38.87	34.31	28.50	19.24	9.02	0.29
902.	52.00	50.67	49.54	48.42	46.82	42.85	38.44	34.10	28.26	19.23	8.84	0.27
907.	51.64	49.99	49.22	48.24	46.44	42.32	38.39	33.94	27.94	19.34	8.82	0.16
912.	51.32	49.77	48.78	47.77	46.54	42.30	37.90	33.88	28.20	19.23	8.53	0.18
918.	51.04	49.49	48.56	47.72	46.01	42.11	37.75	33.70	27.90	18.97	8.56	0.18
923.	50.68	49.47	48.24	47.12	45.66	41.58	37.82	33.45	27.74	18.66	8.36	0.13
928.	50.24	48.90	47.95	46.88	45.28	41.30	37.47	33.01	27.40	18.83	8.47	0.07
933.	50.00	48.53	47.76	46.78	45.09	40.95	37.14	32.82	27.54	18.41	8.23	0.17
938.	49.64	48.27	47.11	46.60	44.88	40.85	36.68	32.65	26.99	18.33	8.46	0.17
943.	49.44	47.82	46.83	46.33	44.49	40.26	36.57	32.60	27.06	18.18	8.34	0.11
948.	49.08	47.63	46.51	46.02	44.44	40.15	36.55	32.33	27.00	18.47	8.48	0.17
953.	48.72	47.34	46.34	45.71	44.14	39.98	36.07	32.14	26.78	18.20	8.34	0.29
958.	48.46	47.00	46.10	45.32	43.75	39.84	35.98	31.80	26.84	17.95	8.39	0.33
963.	48.22	46.79	45.65	45.05	43.69	39.56	35.67	31.60	26.69	17.83	8.42	0.22
968.	47.88	46.56	45.66	44.68	43.31	39.40	35.64	31.63	26.34	17.77	8.36	0.18
973.	47.64	46.22	45.33	44.45	43.09	39.17	35.25	31.36	26.11	17.81	8.27	0.26
978.	47.39	45.86	45.21	44.27	42.94	38.94	35.03	31.11	26.00	17.66	8.13	0.23
983.	47.01	45.70	44.83	44.06	42.64	38.70	35.01	30.97	25.87	17.63	8.17	0.18
989.	46.69	45.36	44.45	43.75	42.41	38.49	34.60	30.83	25.74	17.55	8.05	0.14

994.	46.43	45.18	44.11	43.52	42.20	38.37	34.20	30.60	25.70	17.41	7.94	0.25
999.	46.30	44.82	43.86	43.41	41.85	37.99	34.31	30.35	25.42	17.37	7.81	0.25
1004.	45.78	44.55	43.65	42.95	41.63	37.71	33.98	30.28	25.18	17.24	7.83	0.18
1009.	45.71	44.29	43.36	42.71	41.49	37.58	33.77	30.18	25.19	17.19	7.67	0.25
1014.	45.50	43.97	43.15	42.36	41.20	37.38	33.59	29.91	25.07	16.90	7.68	0.24
1019.	45.07	43.65	42.78	42.10	40.93	37.08	33.34	29.57	24.82	16.76	7.69	0.15
1025.	44.71	43.38	42.61	41.94	40.59	36.99	33.19	29.50	24.64	16.80	7.61	0.25
1030.	44.62	43.21	42.34	41.68	40.41	36.66	33.03	29.32	24.66	16.65	7.72	0.16
1035.	44.46	42.99	42.17	41.59	40.25	36.52	32.92	29.31	24.68	16.40	7.75	0.15
1075.	42.32	41.03	40.34	39.91	38.67	34.94	31.45	28.19	23.45	15.97	7.41	0.20
1181.	37.90	36.72	36.47	35.97	35.15	32.30	28.40	25.73	21.45	14.65	6.61	0.31
1337.	32.54	31.52	31.50	31.35	30.53	28.24	25.49	22.64	18.93	12.77	6.07	0.26
1397.	31.21	29.99	30.01	29.67	29.06	26.52	24.17	21.62	17.74	11.80	5.59	0.16
1457.	30.00	28.67	28.38	28.18	27.68	25.38	23.15	20.91	17.29	11.52	4.93	0.24
1517.	29.10	27.94	27.65	27.61	27.21	24.80	22.81	21.06	17.58	11.43	5.34	0.24
1577.	28.06	26.96	26.68	26.67	26.14	23.89	21.95	20.49	17.62	11.82	4.90	0.28
1637.	26.98	26.11	25.84	25.64	25.28	23.03	21.08	20.00	17.52	12.14	5.09	0.16
1697.	25.96	24.66	24.76	24.83	24.15	22.14	20.38	19.04	16.92	12.28	5.49	0.39
1757.	24.35	23.18	23.19	23.22	22.80	20.84	18.95	17.82	15.94	11.69	5.59	0.20
1817.	22.67	21.42	21.49	21.55	21.09	19.30	17.35	16.33	14.45	10.67	5.35	0.21
1877.	20.77	19.76	19.60	19.64	19.27	17.42	15.64	14.75	13.13	9.35	4.73	0.20
1937.	19.02	17.91	18.06	18.06	17.50	15.72	14.10	13.01	11.31	8.14	4.22	0.22
1997.	17.56	16.40	16.39	16.32	15.94	14.58	12.89	11.64	9.86	7.18	3.45	0.21
2057.	16.36	15.31	15.39	15.43	14.79	13.33	11.65	10.56	9.04	6.24	2.94	0.18
2117.	15.57	14.81	14.60	14.66	14.15	12.57	10.96	9.88	8.31	5.70	2.58	0.17
2177.	15.04	13.96	14.03	14.25	13.59	12.06	10.60	9.44	8.28	5.41	2.44	0.28
2237.	14.56	13.77	13.51	13.50	12.95	11.50	10.14	8.99	7.75	5.10	2.27	0.16
2297.	14.07	13.26	13.25	13.34	12.63	11.27	9.74	8.69	7.44	5.10	2.15	0.14
2357.	13.78	13.06	12.96	12.98	12.43	11.05	9.51	8.57	7.32	4.87	2.08	0.40
2417.	13.39	12.49	12.68	12.65	12.00	10.71	9.18	8.32	7.10	4.69	1.98	0.10

TABLE D3
PRODUCTION HISTORY - RUN 28

TIME SECS	TOTAL PROD CC	INCR WATER PROD CC	INCR OIL PROD CC	CUM FLUID PROD CC	CUM WATER PROD CC	CUM OIL PROD CC	CUM FLUID INJE VOL	CUM WATER PROD VOL	CUM OIL PROD PER CENT IOIP
0.0	0.0	0.0	0.0	0.0	0.0	0.0	0.0	0.0	0.0
598.5	133.0	0.0	133.0	133.0	0.0	133.0	0.173	0.0	17.3
706.5	24.0	11.0	13.0	157.0	11.0	146.0	0.204	0.014	18.9
866.3	35.5	22.5	13.0	192.5	33.5	159.0	0.250	0.043	20.6
1033.2	37.1	19.8	17.3	229.6	53.3	176.3	0.298	0.069	22.9
1217.7	41.0	31.0	10.0	270.6	84.3	186.3	0.351	0.109	24.2
1397.7	40.0	30.5	9.5	310.6	114.8	195.8	0.403	0.149	25.4
1581.3	40.8	32.0	8.8	351.4	146.8	204.6	0.456	0.191	26.6
1766.7	41.2	33.0	8.2	392.6	179.8	212.8	0.510	0.233	27.6
1957.9	42.5	34.4	8.1	435.1	214.2	220.9	0.565	0.278	28.7
2155.9	44.0	36.7	7.3	479.1	250.9	228.2	0.622	0.326	29.6
2344.0	41.8	34.6	7.2	520.9	285.5	235.4	0.676	0.371	30.6
2533.0	42.0	36.0	6.0	562.9	321.5	241.4	0.731	0.417	31.3
2729.2	43.6	37.5	6.1	606.5	359.0	247.5	0.787	0.466	32.1
2936.7	46.1	41.5	4.6	652.6	400.5	252.1	0.847	0.520	32.7
3137.4	44.6	40.0	4.6	697.2	440.5	256.7	0.905	0.572	33.3

TABLE D4
PRESSURE HISTORY - RUN 28

TIME (SECS.)	INLET							OUTLET				
	1	2	3	4	5	6	7	8	9	10	11	12
0.	0.0	0.0	0.0	0.0	0.0	0.0	0.0	0.0	0.0	0.0	0.0	0.0
5.	4.25	3.01	2.90	1.48	2.09	1.52	1.55	0.71	0.74	0.68	0.39	0.01
10.	12.38	9.93	9.15	7.02	7.40	5.95	5.12	2.90	2.98	1.94	0.96	0.02
15.	23.55	19.83	17.72	15.25	14.45	11.98	10.03	7.18	6.19	3.65	1.90	0.07
21.	36.11	30.97	27.35	24.02	22.00	18.31	15.43	11.87	9.44	5.81	2.77	0.09
26.	47.16	41.04	36.04	31.81	28.85	24.05	20.41	16.04	12.52	7.68	3.66	0.04
31.	55.72	48.60	42.91	38.00	34.21	28.66	24.12	19.13	14.78	9.10	4.21	0.14
36.	59.26	51.99	45.90	40.72	36.98	31.20	26.53	21.35	16.63	10.30	4.82	0.18
41.	63.14	55.73	49.22	44.19	39.87	33.47	28.29	22.62	17.42	10.86	5.03	0.20
46.	66.94	59.13	52.06	46.40	41.84	35.17	29.61	23.69	18.30	11.35	5.26	0.20
51.	69.72	61.57	54.16	48.15	43.38	36.44	30.70	24.55	18.89	11.73	5.45	0.14
56.	71.70	63.49	55.80	49.53	44.64	37.45	31.55	25.18	19.41	11.88	5.53	0.15
62.	73.46	64.95	57.16	50.71	45.70	38.24	32.27	25.70	19.72	12.16	5.67	0.21
67.	74.64	66.13	58.12	51.57	46.41	38.88	32.76	26.10	20.00	12.40	5.72	0.17
72.	75.64	67.11	58.96	52.21	47.07	39.27	33.12	26.35	20.35	12.61	5.84	0.10
77.	76.40	67.67	59.50	52.71	47.42	39.73	33.47	26.65	20.39	12.57	5.82	0.16
82.	77.12	68.39	60.04	53.21	47.87	39.97	33.75	26.84	20.50	12.72	5.91	0.19
87.	77.74	68.71	60.34	53.53	48.17	40.25	33.89	27.09	20.61	12.80	5.86	0.19
92.	77.84	69.09	60.68	53.79	48.33	40.49	34.11	27.22	20.79	12.84	5.95	0.20
97.	78.02	69.61	61.00	54.17	48.64	40.72	34.28	27.30	20.90	12.95	5.98	0.20
102.	78.04	69.87	61.38	54.43	48.87	40.88	34.41	27.45	21.02	13.01	6.07	0.18
107.	77.86	70.23	61.58	54.61	49.08	41.04	34.63	27.54	21.10	13.04	6.04	0.20
113.	77.24	70.41	61.90	54.83	49.29	41.15	34.76	27.60	21.19	13.18	6.08	0.19
118.	76.70	70.61	62.04	54.97	49.49	41.35	34.79	27.70	21.19	13.11	6.06	0.18
123.	76.16	70.79	62.24	55.21	49.52	41.43	34.92	27.80	21.27	13.24	6.15	0.15
128.	75.62	70.57	62.30	55.27	49.70	41.53	35.02	27.83	21.32	13.12	6.09	0.26
133.	75.02	70.21	62.32	55.21	49.70	41.56	35.02	27.90	21.35	13.20	6.13	0.15
138.	74.50	69.99	62.44	55.39	49.73	41.69	35.05	27.96	21.33	13.21	6.12	0.17
143.	73.62	69.61	62.48	55.43	49.89	41.77	35.16	27.88	21.44	13.23	6.11	0.22
148.	73.12	69.13	62.56	55.47	49.81	41.74	35.10	28.00	21.46	13.27	6.19	0.16
153.	72.56	68.65	62.48	55.45	49.93	41.72	35.15	27.99	21.39	13.28	6.19	0.10
158.	71.78	68.15	62.38	55.47	49.87	41.70	35.11	27.97	21.44	13.24	6.18	0.25
164.	71.06	67.57	62.20	55.57	49.89	41.70	35.09	28.00	21.47	13.28	6.15	0.23

169.	70.62	67.09	62.04	55.59	49.89	41.74	35.20	27.95	21.45	13.22	6.13	0.18
174.	70.18	66.73	61.88	55.51	49.84	41.79	35.08	28.03	21.38	13.25	6.21	0.17
179.	69.52	66.19	61.72	55.57	49.95	41.72	35.11	27.96	21.44	13.16	6.20	0.18
184.	69.12	65.79	61.54	55.65	49.91	41.78	35.20	28.09	21.44	13.30	6.23	0.18
189.	68.58	65.41	61.40	55.55	50.06	41.89	35.25	28.04	21.44	13.32	6.19	0.21
194.	67.90	64.91	61.02	55.59	50.10	41.95	35.25	28.15	21.49	13.25	6.20	0.27
199.	67.38	64.39	60.80	55.59	50.08	41.87	35.30	28.06	21.57	13.22	6.19	0.13
204.	66.84	63.85	60.32	55.55	50.02	41.87	35.24	28.03	21.57	13.30	6.18	0.23
210.	66.44	63.35	60.00	55.47	50.05	41.92	35.25	28.14	21.49	13.31	6.13	0.03
215.	65.98	63.01	59.58	55.39	50.02	41.96	35.30	28.16	21.61	13.24	6.22	0.20
220.	65.56	62.39	59.30	55.17	50.14	41.95	35.28	28.02	21.56	13.42	6.13	0.14
225.	64.90	61.83	58.88	55.05	50.11	41.89	35.34	28.04	21.56	13.31	6.29	0.22
230.	64.22	61.41	58.48	54.73	50.15	41.86	35.38	28.18	21.55	13.36	6.26	0.17
235.	63.66	60.91	58.02	54.53	50.17	41.90	35.37	28.18	21.59	13.35	6.20	0.17
240.	63.24	60.37	57.60	54.13	50.09	42.06	35.33	28.17	21.56	13.38	6.22	0.16
245.	62.86	59.87	57.08	53.83	50.00	42.04	35.31	28.11	21.55	13.40	6.21	0.22
250.	62.22	59.25	56.68	53.45	50.06	41.93	35.28	28.10	21.61	13.30	6.18	0.15
255.	61.54	58.85	56.32	53.17	49.91	41.90	35.42	28.16	21.52	13.30	6.25	0.22
260.	61.10	58.37	55.90	52.81	49.69	41.83	35.38	28.08	21.55	13.30	6.23	0.21
265.	60.58	57.69	55.38	52.39	49.43	41.94	35.30	28.20	21.55	13.33	6.18	0.17
271.	59.88	57.19	54.98	52.09	49.26	41.93	35.39	28.14	21.59	13.40	6.14	0.16
276.	59.54	56.69	54.58	51.69	49.02	42.03	35.36	28.17	21.60	13.37	6.23	0.12
281.	58.96	56.27	54.20	51.41	48.71	42.04	35.40	28.23	21.56	13.39	6.23	0.16
286.	58.36	55.77	53.74	51.03	48.37	42.10	35.42	28.15	21.62	13.32	6.29	0.17
291.	57.98	55.23	53.28	50.75	48.14	41.95	35.34	28.19	21.62	13.31	6.21	0.15
296.	57.50	54.85	52.88	50.33	47.89	41.81	35.48	28.22	21.61	13.39	6.29	0.18
301.	56.94	54.37	52.40	49.97	47.48	41.69	35.50	28.26	21.67	13.36	6.23	0.16
306.	56.36	53.77	51.98	49.51	47.21	41.49	35.46	28.23	21.65	13.35	6.16	0.17
311.	55.94	53.53	51.54	49.07	46.75	41.29	35.46	28.27	21.65	13.40	6.24	0.19
317.	55.44	52.95	51.06	48.60	46.47	40.99	35.49	28.26	21.67	13.38	6.23	0.13
322.	54.88	52.43	50.58	48.18	46.16	40.74	35.55	28.30	21.65	13.47	6.26	0.20
327.	54.36	51.87	50.10	47.81	45.75	40.42	35.54	28.22	21.68	13.43	6.27	0.21
332.	53.92	51.53	49.60	47.31	45.42	40.11	35.49	28.28	21.63	13.40	6.22	0.12
337.	53.22	50.91	49.14	46.91	44.95	39.82	35.37	28.30	21.64	13.43	6.21	0.14
342.	52.94	50.43	48.63	46.52	44.56	39.44	35.19	28.23	21.70	13.34	6.23	0.20
347.	52.16	49.91	48.21	45.94	44.13	39.03	35.01	28.35	21.70	13.38	6.24	0.21
352.	51.76	49.30	47.75	45.52	43.74	38.71	34.72	28.35	21.70	13.48	6.28	0.18
357.	51.28	48.84	47.13	45.18	43.32	38.41	34.54	28.37	21.63	13.36	6.26	0.12
362.	50.60	48.29	46.73	44.71	42.92	38.02	34.29	28.37	21.74	13.40	6.31	0.20
368.	50.22	47.82	46.26	44.39	42.55	37.78	33.96	28.41	21.71	13.45	6.16	0.25
373.	49.82	47.23	45.79	43.87	42.07	37.33	33.62	28.34	21.79	13.47	6.29	0.16
378.	49.15	46.77	45.20	43.42	41.75	36.96	33.26	28.22	21.75	13.45	6.21	0.17
383.	48.54	46.23	44.80	42.91	41.24	36.58	32.99	28.04	21.75	13.44	6.29	0.13
388.	48.03	45.71	44.33	42.47	40.80	36.14	32.62	27.97	21.76	13.44	6.23	0.15
393.	47.55	45.23	43.85	41.97	40.36	35.83	32.43	27.67	21.77	13.48	6.32	0.15
398.	47.11	44.69	43.38	41.60	39.89	35.41	31.96	27.44	21.80	13.46	6.27	0.20
403.	46.57	44.18	42.95	41.15	39.54	35.15	31.71	27.29	21.82	13.44	6.33	0.19
408.	45.97	43.70	42.48	40.76	39.11	34.68	31.38	27.00	21.87	13.45	6.30	0.15
414.	45.50	43.12	41.89	40.28	38.64	34.20	31.03	26.68	21.77	13.51	6.38	0.16
419.	44.93	42.68	41.46	39.69	38.26	33.90	30.60	26.39	21.68	13.46	6.26	0.19

424.	44.49	42.14	40.92	39.24	37.82	33.50	30.26	26.08	21.57	13.53	6.26	0.24
429.	43.88	41.66	40.43	38.75	37.27	33.03	29.82	25.82	21.32	13.51	6.29	0.23
434.	43.41	41.17	39.98	38.30	36.83	32.62	29.47	25.39	21.16	13.49	6.39	0.20
439.	42.81	40.58	39.40	37.74	36.26	32.18	29.08	25.09	20.96	13.53	6.33	0.19
444.	42.33	40.05	38.91	37.35	35.90	31.68	28.79	24.82	20.64	13.56	6.23	0.13
449.	41.81	39.55	38.49	36.89	35.49	31.35	28.28	24.53	20.49	13.54	6.33	0.22
454.	41.26	39.07	38.00	36.48	34.98	30.95	27.86	24.06	20.23	13.54	6.26	0.15
460.	40.78	38.62	37.54	36.03	34.58	30.48	27.56	23.80	19.97	13.44	6.34	0.18
465.	40.25	38.01	36.91	35.46	34.04	30.02	27.11	23.39	19.67	13.44	6.31	0.19
470.	39.69	37.48	36.44	35.01	33.54	29.52	26.70	23.08	19.29	13.26	6.28	0.21
475.	39.21	36.97	35.90	34.44	33.03	29.17	26.25	22.68	19.03	13.04	6.35	0.22
480.	38.68	36.48	35.41	33.99	32.59	28.76	25.94	22.38	18.66	12.86	6.34	0.17
485.	38.09	35.94	35.03	33.55	32.13	28.27	25.48	21.92	18.30	12.65	6.34	0.23
490.	37.61	35.41	34.48	33.07	31.69	27.86	25.07	21.61	18.00	12.35	6.29	0.17
495.	37.07	34.93	33.99	32.53	31.18	27.36	24.67	21.09	17.69	12.05	6.40	0.23
500.	36.50	34.34	33.48	32.04	30.72	26.77	24.12	20.72	17.21	11.75	6.39	0.14
506.	35.88	33.79	32.93	31.50	30.15	26.45	23.71	20.27	16.75	11.46	6.18	0.13
511.	35.33	33.23	32.34	31.01	29.69	25.91	23.18	19.85	16.34	11.11	5.94	0.23
516.	34.87	32.70	31.93	30.53	29.21	25.43	22.82	19.53	16.14	10.87	5.78	0.15
521.	34.30	32.18	31.33	30.02	28.72	24.96	22.35	19.08	15.72	10.58	5.58	0.20
526.	33.91	31.65	30.90	29.53	28.23	24.43	21.94	18.66	15.27	10.13	5.41	0.15
531.	33.33	31.16	30.35	29.05	27.75	24.04	21.50	18.29	14.95	9.88	5.26	0.21
536.	32.75	30.65	29.92	28.64	27.24	23.59	21.14	17.90	14.62	9.64	4.99	0.20
541.	32.30	30.19	29.38	28.13	26.87	23.20	20.72	17.54	14.24	9.37	4.82	0.22
546.	31.73	29.73	28.98	27.78	26.45	22.77	20.30	17.15	13.95	9.12	4.56	0.26
551.	31.28	29.30	28.55	27.31	26.02	22.46	20.01	16.86	13.64	8.91	4.38	0.20
556.	30.88	28.83	28.17	26.89	25.65	22.12	19.61	16.56	13.36	8.73	4.26	0.18
562.	30.61	28.48	27.77	26.48	25.24	21.71	19.35	16.14	13.11	8.38	4.28	0.16
567.	30.15	28.10	27.34	26.23	24.92	21.46	19.05	15.99	12.84	8.37	4.12	0.19
572.	29.71	27.72	27.00	25.94	24.64	21.17	18.87	15.83	12.73	8.16	4.04	0.19
577.	29.46	27.39	26.91	25.61	24.31	20.92	18.52	15.74	12.60	8.07	3.95	0.08
582.	28.97	27.13	26.54	25.38	24.10	20.59	18.44	15.42	12.41	8.09	3.97	0.07
587.	28.89	26.87	26.04	25.26	23.84	20.47	18.30	15.29	12.22	7.87	3.87	0.17
592.	28.60	26.59	26.10	25.01	23.73	20.26	18.02	14.99	12.10	7.81	3.77	0.21
597.	28.38	26.45	25.79	24.73	23.54	20.13	17.91	14.93	12.02	7.78	3.70	0.15
602.	28.17	26.13	25.52	24.48	23.21	19.98	17.55	14.77	11.91	7.78	3.84	0.17
608.	27.85	25.99	25.36	24.43	23.14	19.65	17.53	14.65	11.92	7.48	3.68	0.17
613.	27.63	25.63	25.12	24.01	22.76	19.52	17.39	14.56	11.59	7.47	3.77	0.07
618.	27.36	25.49	24.88	23.75	22.66	19.52	17.13	14.33	11.46	7.46	3.68	0.19
623.	27.30	25.17	24.63	23.60	22.53	19.06	16.96	14.39	11.26	7.58	3.52	0.17
628.	27.01	25.09	24.52	23.64	22.22	19.12	17.00	14.40	11.23	7.13	3.45	0.23
633.	26.66	24.87	24.32	23.32	22.05	18.91	16.74	14.24	11.24	7.39	3.53	0.12
638.	26.60	24.76	24.07	23.17	21.85	18.72	16.63	13.73	11.09	6.97	3.62	0.08
643.	26.45	24.33	23.94	23.00	21.77	18.44	16.66	13.84	11.04	7.00	3.29	0.11
648.	26.15	24.32	23.98	22.77	21.46	18.64	16.40	13.72	10.79	7.11	3.59	0.13
653.	25.95	24.14	23.66	22.51	21.44	18.43	16.27	13.48	10.91	6.96	3.37	0.27
658.	25.81	23.79	23.50	22.55	21.32	18.25	16.12	13.40	10.86	7.03	3.41	0.25
663.	25.67	23.81	23.32	22.42	21.19	18.28	16.06	13.26	10.61	6.60	3.23	0.17
669.	25.46	23.71	23.09	22.01	21.20	17.96	15.93	13.23	10.48	6.57	3.23	0.15
674.	25.24	23.45	22.90	22.09	20.84	17.80	15.81	13.16	10.57	6.73	3.23	0.25

679.	25.15	23.18	22.78	21.72	20.60	17.64	15.67	12.97	10.46	6.75	3.23	0.05
684.	25.14	22.99	22.54	21.54	20.42	17.83	15.68	12.78	10.19	6.60	3.10	0.22
689.	24.70	22.88	22.38	21.49	20.45	17.61	15.62	12.79	10.35	6.79	3.09	0.25
694.	24.56	22.57	22.29	21.25	20.12	17.44	15.06	12.58	9.92	6.45	3.20	0.15
699.	24.35	22.60	22.08	21.07	19.98	16.98	15.04	12.74	10.24	6.31	3.15	0.12
704.	24.36	22.39	21.91	20.91	19.90	16.97	15.09	12.50	10.06	6.41	3.23	0.14
709.	24.03	22.15	21.82	21.05	19.74	17.07	14.85	12.41	9.81	6.19	3.05	0.19
715.	23.88	22.10	21.88	20.65	19.73	16.80	14.92	12.23	9.85	6.27	3.09	0.25
720.	23.93	21.97	21.61	20.80	19.43	16.66	14.60	12.20	9.61	6.18	3.03	0.18
725.	23.55	21.83	21.48	20.62	19.46	16.58	14.50	12.00	9.76	6.10	2.87	0.11
730.	23.38	21.72	21.42	20.49	19.37	16.45	14.64	12.06	9.67	6.22	3.01	0.19
735.	23.34	21.55	21.20	20.33	19.35	16.28	14.48	11.83	9.53	6.13	2.95	0.16
740.	23.21	21.30	21.08	20.19	19.09	16.29	14.43	11.81	9.40	6.07	2.99	0.18
745.	23.10	21.21	20.88	19.94	19.01	16.31	14.20	11.79	9.38	6.09	2.99	0.11
750.	22.96	21.08	20.92	20.16	18.84	15.89	14.06	11.68	9.35	5.86	2.88	0.15
755.	22.86	21.04	20.63	19.76	18.79	15.81	14.12	11.61	9.24	5.99	2.76	0.19
760.	22.61	20.93	20.46	19.61	18.73	15.92	14.01	11.50	9.19	5.85	2.90	0.16
766.	22.55	20.76	20.42	19.75	18.70	15.89	14.06	11.33	9.14	5.90	2.76	0.10
771.	22.48	20.55	20.47	19.61	18.67	15.60	13.67	11.44	9.11	5.86	2.99	0.07
776.	22.30	20.50	20.30	19.43	18.36	15.61	13.68	11.37	9.13	5.77	2.74	0.09
781.	22.04	20.45	19.93	19.37	18.21	15.34	13.57	11.36	8.95	5.48	2.66	0.15
786.	21.97	20.28	19.87	19.11	18.42	15.30	13.68	11.22	9.05	5.64	2.83	0.16
791.	22.00	20.15	19.83	19.24	18.16	15.33	13.49	11.11	9.02	5.77	2.60	0.15
796.	22.00	20.00	19.73	18.89	17.97	15.04	13.38	11.06	8.97	5.81	2.71	0.12
801.	21.75	19.89	19.74	18.97	17.84	15.19	13.40	10.93	8.78	5.55	2.82	0.16
806.	21.53	19.61	19.52	18.78	17.82	15.03	13.26	10.89	8.73	5.54	2.71	0.27
812.	21.42	19.56	19.42	18.65	17.68	14.97	13.24	10.88	8.69	5.50	2.72	0.10
817.	21.32	19.67	19.34	18.57	17.71	14.97	13.18	10.80	8.64	5.45	2.63	0.16
822.	21.28	19.47	19.30	18.53	17.54	14.81	13.05	10.76	8.63	5.41	2.66	0.13
827.	21.10	19.36	19.18	18.40	17.40	14.70	12.96	10.63	8.48	5.45	2.61	0.15
832.	21.00	19.25	18.96	18.30	17.37	14.69	12.96	10.56	8.44	5.36	2.64	0.15
837.	20.88	19.10	18.99	18.24	17.27	14.62	12.88	10.53	8.41	5.35	2.61	0.12
842.	20.81	19.08	18.88	18.18	17.21	14.54	12.78	10.52	8.30	5.31	2.60	0.21
847.	20.73	18.95	18.76	18.06	17.11	14.46	12.73	10.41	8.39	5.28	2.57	0.12
852.	20.61	18.87	18.69	18.01	17.01	14.41	12.70	10.41	8.28	5.25	2.54	0.11
857.	20.50	18.82	18.63	17.94	16.97	14.39	12.53	10.33	8.27	5.24	2.57	0.15
863.	20.43	18.68	18.56	17.82	16.83	14.21	12.55	10.25	8.20	5.14	2.53	0.06
868.	20.36	18.61	18.39	17.74	16.75	14.10	12.48	10.15	8.09	5.16	2.48	0.10
873.	20.21	18.32	18.30	17.57	16.68	14.08	12.41	10.15	8.18	5.13	2.52	0.16
878.	20.12	18.23	18.26	17.51	16.57	13.93	12.34	10.13	8.08	5.10	2.48	0.17
883.	19.99	18.27	18.08	17.39	16.56	13.95	12.29	10.01	8.00	5.08	2.48	0.12
888.	19.87	18.18	18.05	17.34	16.41	13.84	12.20	9.96	7.99	5.07	2.47	0.14
893.	19.76	18.06	17.92	17.30	16.43	13.84	12.21	9.91	8.02	5.06	2.47	0.19
898.	19.73	18.03	17.89	17.14	16.29	13.76	12.09	9.86	7.95	5.02	2.45	0.14
904.	19.66	18.01	17.89	17.20	16.26	13.65	12.06	9.83	7.92	4.96	2.44	0.07
909.	19.60	17.80	17.69	17.03	16.19	13.61	12.05	9.79	7.82	4.96	2.39	0.13
914.	19.50	17.79	17.55	17.06	16.16	13.61	11.88	9.75	7.80	4.94	2.37	0.06
919.	19.45	17.62	17.55	16.85	16.06	13.48	11.82	9.68	7.77	4.90	2.35	0.13
924.	19.37	17.39	17.48	16.86	15.97	13.41	11.87	9.67	7.72	4.86	2.37	0.10
929.	19.25	17.54	17.38	16.81	15.96	13.34	11.88	9.67	7.72	4.87	2.37	0.11

935.	19.14	17.68	17.37	16.64	15.81	13.32	11.75	9.57	7.64	4.83	2.39	0.15
940.	19.14	17.54	17.38	16.66	15.86	13.33	11.71	9.52	7.60	4.85	2.33	0.20
945.	18.99	17.19	17.19	16.64	15.66	13.24	11.67	9.45	7.53	4.71	2.36	0.17
950.	18.89	17.25	17.13	16.52	15.58	13.09	11.61	9.42	7.53	4.78	2.32	0.14
955.	18.83	17.25	17.05	16.31	15.56	13.09	11.54	9.32	7.48	4.75	2.35	0.10
960.	18.77	16.88	17.02	16.29	15.47	13.02	11.49	9.33	7.44	4.69	2.26	0.18
965.	18.68	17.00	16.92	16.27	15.46	12.94	11.49	9.29	7.40	4.66	2.32	0.15
970.	18.61	16.89	16.82	16.22	15.38	12.88	11.38	9.21	7.44	4.69	2.30	0.10
976.	18.46	16.75	16.83	16.11	15.33	12.85	11.33	9.23	7.44	4.64	2.25	0.14
981.	18.47	16.77	16.69	16.05	15.29	12.75	11.30	9.16	7.41	4.65	2.24	0.18
986.	18.35	16.68	16.63	16.05	15.18	12.76	11.23	9.14	7.36	4.64	2.25	0.10
991.	18.30	16.51	16.60	15.90	15.11	12.66	11.23	9.03	7.32	4.57	2.30	0.15
996.	18.26	16.70	16.57	15.85	15.10	12.60	11.16	9.06	7.34	4.54	2.17	0.17
1001.	18.21	16.29	16.48	15.79	15.05	12.63	11.14	8.99	7.23	4.48	2.21	0.10
1006.	18.15	16.39	16.36	15.81	14.94	12.47	11.11	8.98	7.22	4.60	2.22	0.14
1011.	18.04	16.48	16.31	15.65	14.91	12.49	11.02	8.89	7.14	4.51	2.16	0.01
1017.	17.98	16.42	16.20	15.63	14.80	12.45	10.99	8.89	7.10	4.50	2.16	0.16
1022.	17.86	16.29	16.26	15.58	14.77	12.35	10.93	8.87	7.15	4.52	2.20	0.15
1027.	17.86	16.13	16.21	15.52	14.68	12.29	10.91	8.83	7.05	4.50	2.16	0.22
1032.	17.83	16.18	16.05	15.49	14.64	12.27	10.82	8.77	7.05	4.51	2.16	0.16
1037.	17.72	16.07	16.02	15.42	14.65	12.22	10.87	8.76	6.99	4.37	2.11	0.15
1042.	17.63	16.05	15.91	15.33	14.57	12.21	10.79	8.71	6.95	4.36	2.16	0.08
1047.	17.51	15.80	15.90	15.37	14.56	12.14	10.78	8.72	6.97	4.38	2.19	0.14
1052.	17.46	15.75	15.82	15.37	14.45	12.10	10.73	8.63	6.91	4.39	2.14	0.05
1057.	17.45	15.76	15.75	15.18	14.53	12.03	10.61	8.60	6.91	4.41	2.19	0.12
1062.	17.36	15.72	15.67	15.15	14.34	11.95	10.61	8.53	6.87	4.32	2.12	0.15
1067.	17.32	15.56	15.63	15.03	14.29	11.98	10.55	8.47	6.86	4.35	1.94	0.28
1073.	17.21	15.46	15.66	14.98	14.23	11.87	10.58	8.44	6.87	4.33	2.15	0.03
1078.	17.18	15.46	15.48	15.02	14.30	11.88	10.51	8.54	6.78	4.30	2.11	0.16
1142.	16.48	14.84	14.91	14.37	13.69	11.41	10.09	8.07	6.50	4.13	2.00	0.16
1202.	15.87	14.32	14.33	13.84	13.07	10.92	9.65	7.83	6.16	3.96	1.90	0.13
1262.	15.27	13.76	13.83	13.34	12.66	10.52	9.34	7.42	6.06	3.79	1.84	0.10
1322.	14.72	13.26	13.38	12.90	12.28	10.18	9.04	7.16	5.75	3.68	1.74	0.16
1382.	14.26	12.87	12.88	12.59	11.84	9.44	8.70	6.89	5.64	3.51	1.67	0.12
1442.	13.09	12.31	12.53	12.23	11.53	9.44	8.46	6.64	5.40	3.43	1.68	0.09
1502.	13.44	11.91	12.20	11.80	11.18	9.22	8.18	6.45	5.21	3.27	1.64	0.08
1562.	13.02	11.49	11.70	11.53	10.84	9.00	7.93	6.28	5.19	3.23	1.52	0.15
1622.	12.70	11.16	11.48	11.15	10.65	8.67	7.73	6.09	4.94	3.18	1.52	0.14
1682.	12.38	10.89	11.19	10.93	10.36	8.42	7.59	5.82	4.81	3.01	1.47	0.19
1742.	12.07	10.70	10.89	10.65	10.06	8.12	7.40	5.68	4.61	2.95	1.43	0.14
1802.	11.68	10.36	10.59	10.41	9.82	7.92	7.19	5.52	4.61	2.79	1.38	0.17
1862.	11.31	10.09	10.36	10.27	9.56	7.84	7.01	5.44	4.50	2.66	1.24	0.18
1922.	11.12	9.77	10.12	10.06	9.41	7.86	7.00	5.15	4.32	2.84	1.24	0.04
1982.	10.84	9.57	9.82	9.72	9.05	7.53	6.63	5.06	4.19	2.70	1.19	0.11
2042.	10.74	9.44	9.65	9.64	8.98	7.27	6.49	5.06	4.05	2.65	1.23	0.17
2102.	10.45	9.23	9.31	9.38	8.70	7.04	6.39	4.89	4.02	2.48	1.32	0.16
2162.	10.18	8.98	9.24	9.33	8.62	6.98	6.24	4.72	4.06	2.42	1.16	0.16
2222.	9.90	8.73	9.07	9.03	8.53	6.69	6.14	4.69	3.88	2.29	1.14	0.12
2282.	9.87	8.65	8.93	8.95	8.26	6.54	5.98	4.56	3.75	2.32	1.11	0.12
2342.	9.50	8.40	8.73	8.74	8.22	6.42	5.87	4.46	3.67	2.25	1.06	0.10

Table D5

ESTIMATION OF FLOOD FRONT ARRIVAL AT
THE PRESSURE TRANSDUCERS

Transducer No.	$\frac{x}{L}$	Run 14		Run 28	
		t (secs)	$\frac{q(t - t_o)}{AL(1 - S_{wi})}$	t (secs)	$\frac{q(t - t_o)}{AL(1 - S_{wi})}$
1	0.00	112	0.000	102	0.000
2	0.09	153	0.013	133	0.009
3	0.18	194	0.026	169	0.019
4	0.27	245	0.043	225	0.036
5	0.36	321	0.067	250	0.043
6	0.45	408	0.095	311	0.061
7	0.55	474	0.116	347	0.071
8	0.64	556	0.142	388	0.083
9	0.73	617	0.162	439	0.098
10	0.82	714	0.193	475	0.108
11	0.91	770	0.211	506	0.117
12	1.00	-	-	-	-

APPENDIX E

EXPERIMENTAL RESULTS FROM THE LITERATURE

Table E1

EXPERIMENTAL RESULTS FROM WIBORG (32)

$$\begin{aligned}\mu_o/\mu_w &= 111.4 & \phi &= 37.1\% \\ K &= 16.7 \text{ darcys} & D &= 5.08 \text{ cm} \\ \sigma &= 34.5 \text{ dynes/cm} & & \text{Dow Corning Oil}\end{aligned}$$

Run No.	S_{wi} %	Q cc/hr	$\left(\frac{\mu_o}{\mu_w} - 1\right) \frac{V\mu_w D^2}{C^* \sigma K}$	Breakthrough Recovery (%IOIP)
1	9.6	160.0	1.636×10^2	25.9
2	10.0	80.0	8.180×10^1	25.0
3	10.5	5.0	5.113×10^0	32.8
4	10.8	15.0	1.534×10^1	31.2
5	9.5	30.0	3.187×10^1	26.7
6	9.2	2.5	2.556×10^0	31.6
7	10.2	20.0	2.043×10^0	29.9
8	9.7	60.0	6.135×10^1	26.6
9	9.5	320.0	3.272×10^2	17.3

Table E2

EXPERIMENTAL RESULTS FROM BAIRD (33)

Dow Corning Oil

$$\mu_o/\mu_w = 545.7$$

$$\sigma = 34 \text{ dynes/cm}$$

Run No.	L (cm)	D (cm)	ϕ (%)	K (darcy)	K _{or} (darcy)	S _{wi} (%)	Q (cc/hr)	$(\frac{\mu_o}{\mu_w} - 1) \frac{V_{\mu_w} D^2}{C^* \sigma K}$	Breakthrough Recovery (%IOIP)
1	107.15	4.96	36.5	15.40	13.35	9.80	2.5	4.378×10^0	27.22
2	107.95	4.96	36.9	17.34	13.55	11.26	10.0	1.556×10^1	24.41
3	108.61	4.96	36.7	16.39	14.31	11.45	160.0	2.632×10^2	19.74
4	107.73	4.96	37.2	13.75	12.12	12.50	300.0	5.882×10^2	16.98
5	107.75	4.96	36.0	8.43	7.30	11.44	800.0	2.558×10^3	16.28
6	107.31	4.92	36.1	7.56	6.66	10.58	20.0	7.134×10^1	25.87
7	107.72	4.96	36.8	8.54	8.18	11.86	560.0	1.768×10^3	16.17
8	106.92	4.96	38.0	16.72	14.95	12.46	50.0	8.065×10^1	20.90
9	107.81	4.92	35.5	8.66	8.18	9.70	15.0	4.671×10^1	23.77
10	107.34	9.73	37.1	18.28	15.73	10.80	40.0	5.902×10^1	25.11
11	107.01	9.73	37.4	11.33	10.09	11.73	600.0	1.428×10^3	15.20
12	107.17	9.73	36.2	10.39	9.89	10.34	1120.0	2.097×10^3	15.10

Table E3

EXPERIMENTAL RESULTS FROM de HAAN (30)

$\mu_o/\mu_w = 4$ $\phi = 33\%$
 $K = 200 \text{ darcys}$ $D = 6 \text{ cm}$
 $\sigma = 30\text{-}50 \text{ dynes/cm}$

No connate water present

$\left(\frac{\mu_o}{\mu_w} - 1\right) \frac{V\mu_w D^2}{C^* \sigma K}$	Breakthrough Recovery (%IOIP)
2.308×10^0	90
2.885×10^1	86
6.929×10^2	65
5.771×10^4	66
$\mu_o/\mu_w = 25$	
1.846×10^1	81
2.308×10^2	34
5.544×10^3	32

B30243